Max-Planck-Institut für Festkörperforschung

Stuttgart

Computational determination of the low-temperature parts of phase diagrams on ab initio level

Ilya Pentin

Dissertation an der Universität Stuttgart

Stuttgart, 2009

Computational determination of the low-temperature parts of phase diagrams on ab initio level

Von der Fakultät Chemie der Universität Stuttgart
zur Erlangung der Würde eines
Doktors der Naturwissenschaften (Dr. rer. nat.)
genehmigte Abhandlung

Vorgelegt von

Ilya Pentin

aus Moskau, Russland

Hauptberichter:	**Prof. Dr. Martin Jansen**
Mitberichter:	**Prof. Dr. Günter Petzow**
Prüfungsvorsitzender:	**Prof. Dr. Thomas Schleid**

Tag der mündlichen Prüfung: 18.12.2008

Max-Planck-Institut für Festkörperforschung, Stuttgart
Universität Stuttgart
2009

Acknowledgements

This thesis would not be possible without the support from many people. First of all I would like to thank **Prof. Dr. Dr. h.c. M. Jansen**, for the opportunity to join his team, providing me with the necessary financial support and his interest in my research. I would like particularly to thank **Prof. Dr. J.C. Schön**, for the intensive support, patience and constant readiness for discussion, his enthusiasm for my topic, as well as a careful proofreading of my dissertation. Furthermore, I thank **Prof. Dr. Dr. h.c. Günter Petzow** and **Prof. Dr. Thomas Schleid** for being co-examiners. I extend my thanks to the Max-Planck society for a stipend.

The working group members I would like thank for the friendly atmosphere. Special thanks go to my colleague **Dr. Ž. Čančarević** for many scientific discussion and support. Moreover I would like to express my thanks to many close friends and colleagues.

Needless to say, a thousand thanks go directly to my family for their patience and support.

Contents

Acknowledgements iii

Abstract ix

I Introduction 1

1 Introduction and Outline 3
- 1.1 Introduction . . . 3
- 1.2 Outline . . . 5

II Theoretical background 7

2 Energy landscape and modeling of solids 9
- 2.1 Energy landscape . . . 9
  - 2.1.1 General aspects . . . 9
  - 2.1.2 Global optimization methods . . . 15
  - 2.1.3 Exploration of the barrier structure . . . 18

3 Methods of electronic structure calculations 21
- 3.1 General remarks . . . 21
- 3.2 Hartree-Fock method . . . 22
  - 3.2.1 Hartree-Fock algorithm . . . 23
- 3.3 Density Functional Theory (DFT) . . . 25
- 3.4 Basis sets . . . 28
  - 3.4.1 Basis sets types . . . 28
  - 3.4.2 Basis set superposition error . . . 29

4 Calculation of phase diagrams 31
- 4.1 Calculation of the phase equilibrium . . . 31
  - 4.1.1 General definitions . . . 32
  - 4.1.2 Multicomponent system . . . 32
  - 4.1.3 Sublattice model . . . 34
- 4.2 Construction of phase diagrams: Convex hull method . . . 35
  - 4.2.1 Convex hull algorithm . . . 36

III Methods 39

5 Method **41**
5.1 General approach 41
5.2 Ab initio calculations and global exploration: technical details 43
5.3 Computation of the enthalpy of formation 44
5.4 Construction of the phase diagram 44

IV Systematic application to selected chemical systems **47**

6 Quasi-binary alkali halogenide systems **49**
6.1 Introduction 49
6.2 General remarks 50
6.3 Phase diagrams with miscibility gaps 50
6.3.1 NaCl-LiCl, NaBr-LiBr and NaCl-KCl 50
6.3.2 KBr-NaBr, KCl-RbCl and KBr-RbBr 54
6.3.3 The MBr-MI systems, where M = Li, Na, K, Rb or Cs 58
6.3.4 The MBr-MCl systems, where M = Li, Na or K 66
6.4 Phase diagrams with ordered crystalline phases 71
6.4.1 Introduction 71
6.4.2 The CsX-LiX systems, where X = F, Cl, Br, I 71
6.4.3 The LiX-RbX systems, where X = Cl or Br 83
6.5 Critical discussion 88
6.6 Conclusion 92

7 Quasi-binary and quasi-ternary semiconductors in $A^{III}B^{V}$ systems (A = Al, Ga or In; B = As or Sb) **93**
7.1 Introduction 93
7.2 General remarks 94
7.3 Results and Discussion 94
7.4 Conclusion 100

8 Quasi-binary lanthanum halogenide systems **103**
8.1 Introduction 103
8.2 General remarks 103
8.3 Results and Discussion 104
8.3.1 Binary halides LaX_3 (X = F, Cl, Br or I) 104
8.3.2 Quasi-binary halides LaX_3-LaY_3 (X,Y = F, Cl, Br, I) 104
8.4 Conclusion 123

V Summary **125**

9 Summary **127**

VI Zusammenfassung **129**

10 Zusammenfassung **131**

VII Appendix **133**

A Quasi-binary alkali halogenide systems **135**
A.1 Alkali halogenides: auxiliary data 135
A.1.1 General data 135
A.1.2 The CsX-LiX systems, where X = F, Cl, Br or I 137
A.1.3 The LiX-RbX systems, where X = Cl or Br 138

B Quasi-binary and quasi-ternary semiconductors **143**
B.1 Semiconductors: $A^{III}B^{V}$: auxiliary data 143

C Quasi-binary lanthanum halogenide systems **145**
C.1 Lanthanum halides: auxiliary data 145

D List of publications **147**

VIII Bibliography **149**

Bibliography **151**

IX Formalia **159**

Abstract

From the point of view of thermodynamic, materials are found as thermodynamically stable (equilibrium) or metastable phases. These can be characterized via functions of state that depend uniquely on the given state variables such as temperature, pressure and composition. The graphical representations of all thermodynamically stable phases that exist or co-exist at equilibrium is called the phase diagram of the chemical system as function of the thermodynamic variables.

The knowledge of equilibrium phases of chemical compounds as function of thermodynamic parameters and their thermodynamic stability lies at the foundation of our understanding of the properties and processes of modern materials. From the point of view of experimental methods, the determination of the thermodynamic functions and the equilibria between phases is an enormous task, especially at low temperature. For that reason it has become common practice to support the experimental research by a variety of theoretical calculations. Thus, in the seventies the project CALPHAD was started where different phenomenological models and general rules for the analysis and calculation of the phase diagrams were implemented. Over the past few years, calculations of phase diagrams and thermodynamic properties of materials have appeared in the literature, where typically information from experiment, such as the known existence of various ordered crystalline or solid solution-like phases, was combined with quantum mechanical computations. Clearly, such ab initio calculations can be very useful for the validation of existing phase diagrams. However, the reliance on experimental data is often a serious limitation, especially if one attempts to predict a phase diagram or is interested in competing metastable phases that might occur during the synthesis of new materials. Thus, it is necessary to develop a method to compute phase diagrams without experimental information.

The general approach to the analysis of the low-temperature part of a (equilibrium) phase diagram without recourse to experimental data proceeds in several stages. First, structure candidates are identified via global explorations of the energy landscape for different compositions for a given chemical system. This is followed by a local optimization of the candidates on *ab initio* level. Next, one can calculate the enthalpies of formation for selected candidates, using the ideal entropy of mixing write the Gibbs energy function and calculate the low-temperature part of the phase diagram.

The goal of this thesis has been to develop a general strategy to analyze and to predict the low-temperature parts of phase diagrams without any input of experimental data, and to apply this method to a number of chemical system.

These chemical systems have been selected and investigated with several aims in mind:

- For the purpose of validation of our methodology, we have chosen systems where enough thermodynamic data are available for a comparison between theory and experiment, and which are sufficiently simple to be studied systematically while still allowing for the possibility of reasonably complex phase diagrams.
- Analysis of systems where the thermodynamic data are incomplete.
- Prediction of the low-temperature part of the phase diagram including not-yet-synthesized phases for chemical systems where no solid compounds are known so far or even the whole phase diagram is unknown.

Thus, the following chemical systems were investigated in this thesis: quasi-binary alkali metal halides, quasi-binary lanthanum halides, quasi-binary and quasi-ternary semiconductors $A^{III}B^{V}$.

Part I

Introduction

1 Introduction and Outline

1.1 Introduction

The availability of high-quality phase diagrams of chemical systems is of great importance in materials science and engineering (1). However, in many instances, it is both very time-consuming and difficult to determine the full phase diagram from experiment alone (2). In particular the low-temperature part is often nearly impossible to access, since the time scales on which equilibration to the thermodynamically stable phase takes place exceed the time available for the experiment. Nevertheless, e.g. information about the existence of a thermodynamically stable crystalline phase that will form by very slow transformation processes from, say, a solid solution-like phase, is crucial for deciding whether this compound is suitable for practical applications.

Thus, theoretical methods have been called upon for a long time to supplement the experiments in deriving phase diagrams. Since the beginning of the seventies, these calculations have been brought together in the CALPHAD-project (2). The methods proposed in the CALPHAD-project have found wide applications in the field of phase diagrams calculations (3; 4) of different types of systems, such as intermetallics (5; 6), semiconductors (7; 8; 9) or ceramic materials (10; 11). While originally phenomenological models and empirical interpolation functions had been employed to interpolate between experimental data, during the past decade, first-principle calculations combined with statistical thermodynamic theories have become widely used to assist in the construction and validation of phase diagrams (12; 13; 14; 15; 16). Recently, ab initio calculations of the thermodynamic properties and phase diagrams have appeared in the literature (17; 18; 19; 20; 21; 22; 23; 24; 25; 26; 27). For instance, the thermodynamic properties of Al, Ni, NiAl and Ni_3Al were obtained through ab initio methods (28). And in other work (29), the stability of different phases (fcc vs. bcc vs. hcp) of 78 pure elemental solids based on ab initio calculations was compared with the stability deduced via standard CALPHAD methods. Other authors (30) investigated phase stability and enthalpies of formation for 69 intermetallics in the Al-M (where M = Ti, Zr or Hf) systems.

Clearly, for validation of existing phase diagrams, such ab initio calculations can be very useful. However, if one attempts to fill in white spots in a phase diagram, there remains a fundamental problem: Unless one knows that a solid solution-like phase or an ordered crystalline phase exists, ab initio methods lack a starting point. An increasing number of groups have attempted to deal with this issue by comparing the energies of several hypothetical modifications of a chemical compound for a composition of interest (31; 32;

33; 34; 35; 36; 37; 38), where the structures of these modifications have been chosen from among the known structure types compiled in the ICSD (39). But this approach is not really satisfactory for several reasons: For one, experience has shown that there still exists a plethora of possible crystalline structure types which have not yet been discovered (40). Secondly, the decision of postulating the super-structure of a solid solution-like phase is similarly arbitrary, unless some experimental information is available. Both these reasons point to the final, and in some way most fundamental concern: None of these approaches represent a way to compute the phase diagram starting only from the constituent elements without any prior experimental information.

Since the early nineties, in the department of Prof. Jansen a new general methodology (40; 41; 42; 43) has been developed that allows one to determine such hypothetical stable and metastable compounds that have not yet been synthesized in a chemical system, without any recourse to prior experimental information. The central piece of this approach has been the global exploration of the potential energy landscapes of the chemical system, in order to determine the local minima on these landscapes and the barriers around them, since for sufficiently high barriers, these minimum configurations correspond to (meta)-stable modifications of the system. In previous works, the prediction of not-yet-synthesized compounds for a fixed chemical composition (44; 45; 46; 47; 48) was the main goal of the investigations; however, possible structure candidates were already analyzed also as function of composition in several systems, $CaBr_2/Ca_2Si$ (49), MgO/MgF_2 (50) and Li_3N/Na_3N (51). In all these cases, the $T \approx 0$ region of the phase diagram was studied, without any regard to additional phases that might be thermodynamically stable at elevated temperatures such as solid solution-like phases.

In this earlier work, a general technique (and computational power) had been lacking which would have allowed to decide whether formation of a solid solution could take place or single ordered crystalline phases will appear, and furthermore to compute the free enthalpy associated with this respective phase. Thus, in this work, we have developed an approach which allows us to determine the behaviour of the system in the subsolidus region and predict the phase diagram at low temperatures.

In the general modular approach on which this thesis is based, the following procedure is applied: First, we perform a global search on the energy landscape for structure candidates for given compositions of the quasi-binary or quasi-ternary system under investigation using an empirical Coulumb-plus-Lennard-Jones potential for the potential energy contribution to the enthalpy. Second, we perform a local optimization of the selected candidates on *ab initio* level. From the computed E(V) curves and the structural features of the candidates one can suggest whether ordered crystalline phases or a solid solution-like phase will be found in the system. Finally, we calculate the enthalpies of formation for selected candidates and construct the low-temperature part of the phase diagrams using the so-called Convex-hull method (52). A large number of systems were investigated to show the capability of our approach: twenty quasi-binary alkali metal halides, six quasi-binary and two quasi-ternary semiconductors, and the six quasi-binary lanthanum halogenide systems.

1.2 Outline

The thesis is divided into several parts: (I) **Introduction**, (II) **Theoretical background**, (III) **Methods**, (IV) **Systematic application to selected chemical systems**, (V) **Summary**, (VI) **Zusammenfassung**, followed by an (VII) **Appendix**.

In **Part** II: **Theoretical background**, we review some aspects of the theoretical approaches to the "Energy landscape and modeling of solids", *ab initio* calculations and background of the methods and models of phase diagram calculations.

In **Part** III: **Methods**, we present our new strategy to the analysis of the low-temperature part of phase diagrams: from the exploration of an energy landscape of a given chemical system to the construction of the low-temperature part of phase diagrams.

Part IV: **Systematic application to selected chemical systems**, describes studies of three different systems: (1) "*Quasi-binary alkali halogenide systems*", (2) "*Quasi-binary and quasi-ternary semiconductor* $A^{III}B^{V}$ *systems*", (3) "*Quasi-binary lanthanum halogenide systems*".

Chapter 6, "Quasi-binary alkali halogenide systems", is split into two parts. First, in the Section: *Phase diagrams with miscibility gaps* (Section 6.3), we investigate the low-temperature part of the phase diagrams for alkali halide systems exhibiting solid-solution behaviour. We found good agreement with available data and predicted several miscibility curves for those systems where there is a lack of thermodynamic data. Next, in the Section: *Phase diagrams with ordered crystalline phases* (Section 6.4), we investigated alkali halide systems that exhibit ordered crystalline phases at low-temperatures. We show, that our method can be successfully used not only for systems where solid solution-like behaviour is stable, but also for systems with crystalline phases. We found all known phases and predicted several new ones.

In **Chapter** 7: "*Quasi-binary and quasi-ternary semiconductors in* $A^{III}B^{V}$ *systems (A = Al, Ga or In; B = As or Sb)*", we investigate the low-temperature parts of the phase diagrams for the six quasi-binary systems, MX-M'X, where M,M' = Al, Ga, In and X = Sb or As; and two quasi-ternary systems AlX-GaX-InX where X = Sb or As. The locations of the miscibility gaps for all eight systems were predicted.

In **Chapter** 8: "*Quasi-binary lanthanum halogenide systems*", we investigate the low-temperature parts of the phase diagrams for the six mixed lanthanum halide systems, LaX_3-LaY_3, where X,Y - F, Cl, Br or I. We found that in all systems under investigation ordered crystalline phases might exist and that there is no solid solution-like behaviour.

Part II

Theoretical background

2 Energy landscape and modeling of solids

Nowadays, the goals of modern solid-state chemistry are no longer to perform purely exploratory synthesis in a chemical system, but to actually predict and subsequently synthesize new crystalline compounds (53; 54). Collaboration between theory and experiment becomes especially important, when one tries to obtain the possible (meta)stable compounds in a chemical system which have not yet been synthesized in the first place. Similarly, in many chemical systems, the amount of information gained from experiments is not sufficient to allow the determination[1] of the structure of a new crystalline compound, as well as understanding the dynamics of transformations among various (meta)stable modifications. In these cases, theory, and in particular computational modeling, has to come to the assistance (55; 56). The fundamental quantity that describes a chemical system and its dynamics from the theoretical point of view is the energy as a function of the ionic degrees of freedom (57).

2.1 Energy landscape

2.1.1 General aspects

Every arrangement of the atoms in a solid or molecule can be described in the classical limit by the position vectors in 3D space of all the N atoms belonging to the system. These N position vectors $\mathbf{x}_i$ can be combined into a $3N$-dimensional vector $\mathbf{X} = (\mathbf{x}_1, \ldots, \mathbf{x}_N)$. In this case, each atomic configuration is represented by a point in a $3N$-dimensional Euclidean space, called configuration space. To get the full classical description of a solid, one should add to each atom its velocity vector $\mathbf{v}_i$ (which can also be combined to $\mathbf{V} = (\mathbf{v}_1, \ldots, \mathbf{v}_N)$ or momenta $\mathbf{P} = (\mathbf{p}_1, \ldots, \mathbf{p}_N)$, $\mathbf{p}_i = m_i \mathbf{v}_i$), which results in a $6N$-dimensional space of both the N position vectors $\mathbf{X}$ and N velocity vectors $\mathbf{V}$, the so-called phase space. For simplicity, we will often replace this vector and an infinitesimal cube in phase space around it by a state i and the integral over phase space by summation over i (55; 56). The energy of such classical systems $E = E(\mathbf{X}, \mathbf{V})$ can be split into two parts:

---

[1] Sometimes 'structure determination' is also called 'structure solution'. Also in the older literature, work that should be classified as 'structure determination' is sometimes advertised as 'structure prediction'. However, since the knowledge of e.g. the cell coordinates together with the composition massively restricts the range of feasible structures, 'prediction' of atom positions when given this information really should be termed 'structure determination' (55; 56).

$$E = E(\mathbf{X}, \mathbf{V}) = E_{pot}(\mathbf{X}) + E_{kin}(\mathbf{V}), \tag{2.1}$$

where $E_{pot}(\mathbf{X})$ is the potential energy and $E_{kin}(\mathbf{V}) = 1/2\sum_i m_i \mathbf{v}_i^2$ is the kinetic energy, respectively. The time evolution of such a system is governed by Newton's equations:

$$\frac{d\mathbf{x}_i}{dt} = \frac{\mathbf{p}_i}{m_i} = \mathbf{v}_i \tag{2.2}$$

$$\frac{d\mathbf{p}_i}{dt} = \mathbf{F}_i = -\frac{\partial E_{pot}(\mathbf{X})}{\partial \mathbf{x}_i} \tag{2.3}$$

In principle these equations can be solved and yield a unique solution (trajectories $(\mathbf{X}(t), \mathbf{V}(t))$ for every physically valid choice of initial conditions $(\mathbf{X}_0, \mathbf{V}_0)$.

In general, an energy landscape possesses a multitude of local minima and a complicated barrier structure. The minima represent stable configurations at zero temperature, and the height of barriers around them are the measure of the stability of these configurations at non-zero temperatures. Thus, the explorations of the energy landscape give us the information which configurations are associated with (meta)stable compounds of the chemical system under investigation (41). Once the local minima on the energy hypersurface are known, one can switch to the further analysis and phase diagram prediction.

The definition of a general (mathematical) landscape requires three elements: A configuration space of states (or solutions of an optimization problem), energy (or cost) function given as a real function over configuration space, and a neighborhood relation (topology). Energy landscapes of atomic configurations usually have 'natural' neighborhoods given by the topology of $\mathbb{R}^{3N}$, but for optimizations problem we have to explicitly define such a neighborhood relation (called moveclass).

In the case of employing global landscape exploration methods, the use of simple empirical potentials is essential, because energy calculations on the *ab initio* level are still computationally very expensive[2]. Especially since no information about cell geometry and atom positions is available, the configurational space that needs to be investigated is greatly enlarged due to the necessary variation of the simulation cell compared to only an adjustment of atomic coordinates. This enforces a trade-off between the speed and accuracy of the energy calculation. In such a case, the global optimization requires appropriate approximations of energy functions. The resulting local minima are (only) structure candidates and need to be refined employing local optimizations on *ab initio* level.

The time evolution of the classical system, its trajectory in phase space (see Fig. 2.2), is determined by the positions and velocities of all the atoms at some initial time t_1, together

---

[2] Recently, new methods appeared in the literature (58) which allow one to explore energy landscapes on the *ab initio* level.

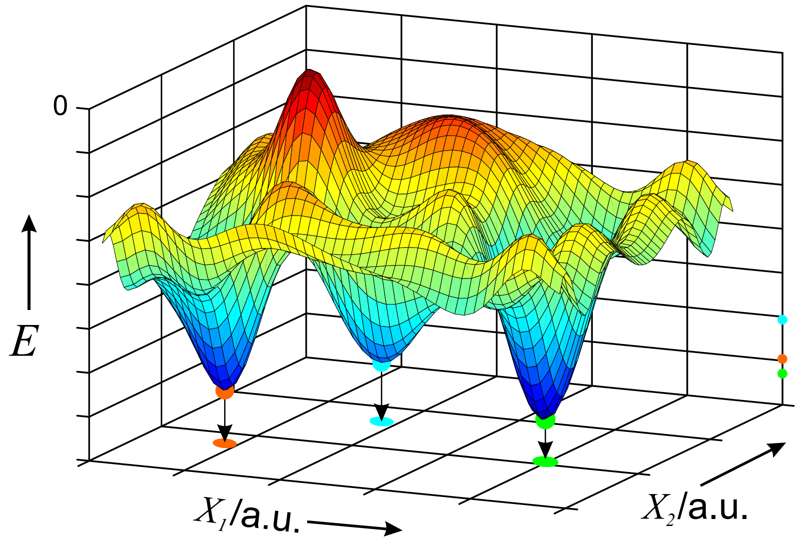

Figure 2.1: Schematic representation of a cut through a configuration space for a single-component system with fictive coordinates X_1 and X_2 (40).

with Newton's equations and the energy function of the system, from which the forces on the atoms can be calculated. A physical measurement consists of the average of some observable O,

$$\langle O \rangle = \frac{1}{t_{obs}} \int_{t_1}^{t_2} O\left(\mathbf{X}\left(t'\right), \mathbf{V}\left(t'\right)\right) dt' \tag{2.4}$$

over a time interval $[t_1, t_2]$ of length $t_{obs} = t_2 - t_1$ along this trajectory. In many cases the properties are essentially independent of the starting point t_1 of the trajectory in phase/configuration space, $\langle O \rangle_{t_1,t_2} = \langle O \rangle_{t_{obs}=t_1-t_2}$. In particular, if a system can reach equilibrium, with respect to the observable O, faster than we perform measurements, $t_{obs} > t_{eq}(O)$, the so-called ensemble average,

$$\langle O \rangle_{ens}(T) = \frac{\int O\left(\mathbf{V}, \mathbf{X}\right) e^{-\frac{E(\mathbf{V},\mathbf{X})}{k_B T}} d\mathbf{V} d\mathbf{X}}{\int e^{-\frac{E(\mathbf{V},\mathbf{X})}{k_B T}} d\mathbf{V} d\mathbf{X}} \tag{2.5}$$

equals the time average within an accuracy a_m,

$$\left| \langle O \rangle_{t_{obs}} - \langle O \rangle_{ens} \right| < a_m. \tag{2.6}$$

If this is the case, we call the system (globally) ergodic, with respect to the observable O, on the time scale t_{obs} and up to the accuracy a_m. Proving that a system is ergodic is a non-trivial task, but in many cases, the assumption of ergodicity turns out to be justified.

There exists a third important time scale (beside t_{obs} and t_{eq}), the so-called escape time t_{esc}. The escape time tells us, for how long the system remains in the locally ergodic region $\mathscr{R}$ (59; 60). The concept of local ergodicity is an extension of the (global) ergodicity concept, and refers to the fact that only a subset $\mathscr{R}$ of the energy landscape may be ergodic. If we can get a reproducible diffractogram of a modification associated with $\mathscr{R}$

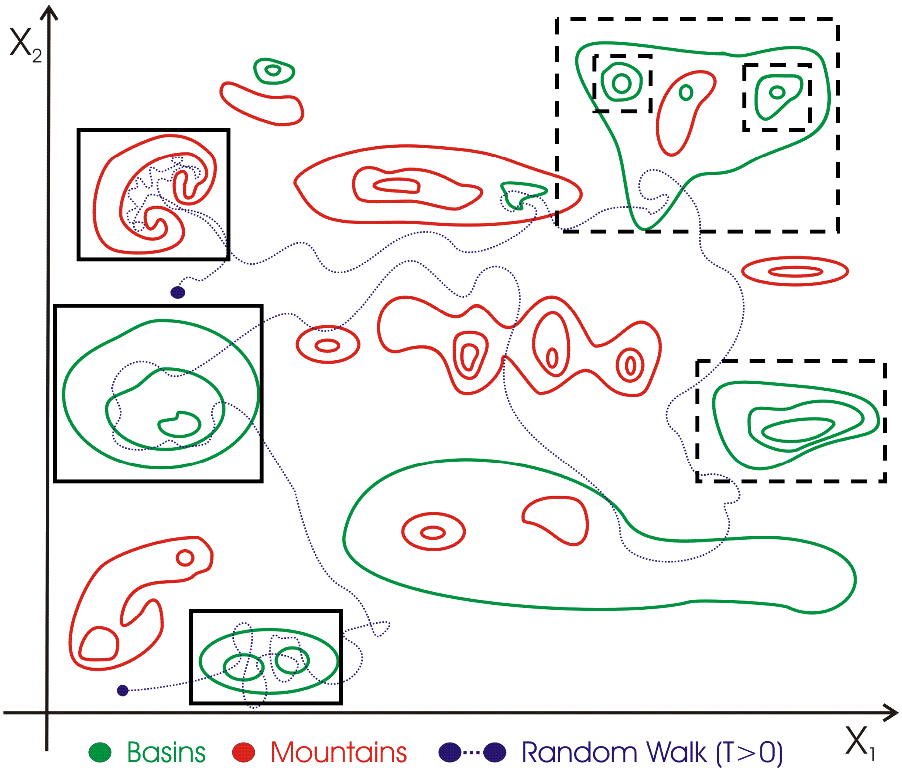

Figure 2.2: 2D-projection of 3N-dimensional landscape. The blue line shows the trajectory of the time evolution of a system on the landscape. This applies both to a trajectory of a real system and one simulated on the computer. Blue dots indicate equal time steps, e.g. two dots might be separated in time by one minute (for a real system) or one nanosecond (for a simulated system). Measurements correspond to time averages of observables along the trajectory over a time interval (e.g. encompassing 4 minutes). Note that the trajectory spends more time in certain regions than in others. In particular, some regions are 'explored' rather thoroughly, i.e. one could replace the time average along the trajectory within such a region by a (weighted) average over all states in the region, without making too much of an error. If that is feasible, one says that this region of the landscape is 'locally ergodic'. The regions enclosed in black rectangles are such regions that have been observed along the trajectory shown (e.g. during a Monte Carlo simulation). The dashed rectangles are those locally ergodic region that exist, but that have not been found during this particular simulation run.

before the substance disintegrates or transforms to another modification, $t_{esc}(\mathscr{R};O) > t_{obs} > t_{eq}(\mathscr{R};O)$, then we are dealing with a metastable compound on our observation scale t_{obs}. If we are dealing with a system that is not an isolated solid but a system in contact with an external heat bath at constant temperature, then the temperature serves as an indicator that the solid has equilibrated with respect to its surrounding. In this case one cannot perform reproducible experiments on a time scale that is shorter than the temperature equilibration time[3] t_{eq}^{T}.

Both equilibrium time and escape time are temperature dependent. In particular the escape time can vary by many orders of magnitude, according to the Arrhenius[4] law,

$$t_{esc} \propto e^{\frac{E_{barrier}}{k_B T}} \tag{2.7}$$

Once the locally ergodic regions $\mathscr{R}_i$ have been found (for a given temperature and t_{obs}), one can compute the local free energy of each region (see Section 2.1.3). The kinetic stability of the modification one associates with such a region is given by the escape time t_{esc}.

Temperature and other thermodynamic parameters like pressure, and external fields (electric $\mathbf{E}$, magnetic $\mathbf{B}$, etc.) act on the energy landscape in very different ways. Temperature, for example, changes the dynamics of the landscape in a stochastic fashion via the average kinetic energy ($\langle E_{kin}\rangle = 3/2Nk_BT$). The pressure p modifies the energy function itself:

$$E(p=0,\mathbf{E}=\mathbf{0},\ldots) = E_{pot} \rightarrow E(p\neq 0,\mathbf{E}\neq\mathbf{0},\ldots) = E_{pot} + pV + \mathbf{EP} + \ldots. \tag{2.8}$$

But, as long as these external parameters are time-independent, we are still dealing with a fixed time-independent energy landscape, and these modifications do not pose any real difficulties. We can perform the exploration of this modified landscape $E(p\neq 0,\ldots)$ analogously to the one of the potential energy landscape $E(p=0,\ldots)$.

In any case, the first step in the exploration of an energy landscape is the determination of the locally ergodic regions. At low temperatures, such region correspond to single local minima and the escape times are controlled by energy barriers, and will increase exponentially according to the Arhenius law (Eqn. (2.7)). Experience shows that in many instances these barriers are actually high enough for local ergodicity to hold even at much higher temperatures (55; 56). On the other hand, at intermediate temperatures there also can exist locally ergodic regions that contain many local minima, with rather small energy barriers between them. That allows the system to switch between these minima on relatively short time scales. This behaviour is often found in chemical systems where structure families exist. Such families consist of a number of candidates where different types of atoms are randomly distributed on one of the sublattices keeping within the limits of one overall structure type.

---

[3] Temperature is proportional to the expectation value of the kinetic energy in classical statistical mechanics.

[4] There exist no real proof for this rule, but one can, for locally ergodic regions and temperatures $T << E_{barrier}$, use a simple probabilistic argument to define an appropriate escape time.

2.2.1.1. High quality empirical potentials and ab initio methods

Nowadays, there are a large number of quite accurate empirical potentials of ever increasing complexity that have been employed to model ionic compounds. The list goes from simple two-body potentials like the Buckingham-potential (61), the Born-Huggins-Meyer-potential (62), the simple robust potential we have been using (see the Section 5.2) or a refined version thereof with environment dependent radii (49; 50), over dipole (63) and quadrupole (64) shell models, to various kinds of breathing potentials (65; 66; 67; 68; 69; 70; 71; 72; 73; 74; 75; 76; 77; 78; 79) of increasing levels of refinement. The latter ones are discussed more fully in several reviews (80; 81; 82). Examples include Gordon-Kim type approaches (modified electron gas, or MEG, potential induced breathing, or PIB, variationally induced breathing known as VIB, and self-consistent charge deformation model - SCAD), and Slater-Koster type tight-binding methods. As long as these potentials can be fast evaluated, they can be considered for use in global explorations.

While the more refined potentials typically allow us to compute at least some properties of a given material with relatively high accuracy, it is not clear, whether their use during the global optimization would be worth the cost as long as we are only interested in identifying possible structure candidates in a chemical system. For one, such potentials tend to be much more complicated and computationally expensive than the simple potentials we usually employ. Secondly, the number of parameters involved typically increases with the complexity of the potential, which makes it very difficult, to construct such a potential without detailed a priori experimental knowledge of the system. However, this contradicts the premise of our approach, i.e., to identify the stable and metastable modifications of a chemical system without any prior information except the identity of the participating atoms. Of course, one can attempt to fit the parameters of the empirical potential to *ab initio* calculations in the system, but this typically involves a large amount of effort. Finally, we have found that many of these potentials are not globally applicable. They strongly favor the structure(s) to which they have been fitted, and even successfully reproduce their properties. But at the same time, these potentials often weaken or even eliminate the minima representing important alternative modifications on the landscape of the chemical system.

Regarding the ranking of structure candidates by energy using such empirical potentials, one should bear in mind that potentials have often been fitted to a particular modification, which could bias the results. Thus, one needs to go beyond empirical potentials and employ various *ab initio* methods at least during the local optimization to achieve the right results. Nowadays, two different general approaches are common - density functional methods (DFT) and the Hartree-Fock approximation (HF) (for basic background see Chapter (3)).

2.2.1.2. Energy functions with building units and molecules

Generally, each atom of a chemical system has complete freedom of movement. It means that we need 3N parameters to describe the system. However, in many situation, the problem at hand can be described with a reduced set of coordinates. This is especially the case if we are dealing with chemical reactions in which part of or the whole molecule can be treated as rigid (building group). These constraints, of course, affect the barrier structure of the energy landscape under investigation, by preventing certain atomic movement. The cost one pays to reduce the number of the system's degrees of freedom is a slightly more complicated description of the interaction of the building units with the rest of the system. But the reduction in the number of parameters usually outweighs this cost, especially, if one is satisfied with an approximately correct packing of the molecules during a global optimization. In the second step (local optimization) the atom positions can be refined (42; 83).

In the study of the landscape of extended solids, one also often replaces some of the atoms with more or less rigid building units, depending strongly on the question one tries to address. If the structure candidates that contain building units all correspond to high-lying minima (compared to the structures formed upon free movement of all atoms), the only way to access these minima is via kinetic control. Another reason for the use of building units is the fact that typically building units are held together by mostly covalent forces. But, the interaction of building units with the rest of the system is mainly via ionic or van-der-Waals forces which are easier to model and control. In this work, such building units are not employed.

2.1.2 Global optimization methods

Quite often the problems confronting scientists can be formulated in terms of searching for the minimum or maximum of a cost function defined over a space of acceptable solutions. A multitude of methods have been developed to deal with this issue. They can, in general, be divided into global and local approaches, usually called *global optimization* and *local optimization* techniques.

Global optimization is a branch of applied mathematics and numerical analysis that deals with the optimization of a function or a set of functions according to some criteria. The most common form is the minimization of one real-valued function $f(\mathbf{x})$ in the configuration/solution space. In addition, the states $\vec{x}$ may have to fulfill one or several constraints $C(\mathbf{x}) = 0$. In real-life problems, functions of many variables have a large number of local minima and maxima. Finding an arbitrary local optimum is relatively straightforward by using *local optimization* methods. Finding the global maximum or minimum of a function is a lot more challenging and has been impossible for many problems so far. The maximization of a real-valued function $g(x)$ can be regarded as the minimization of the transformed function $f(x) = (-1) \cdot g(x)$ (84; 85; 86; 87). Typical examples of global optimization applications include: Structure prediction (minimize the energy/free energy function), traveling salesman problem and circuit design (minimize the path length) (88), chemical engineering (e.g., analyzing the Gibbs free energy), safety verification, safety engineering (e.g., of mechanical structures, buildings), worst case analysis, mathematical problems (e.g., the Kepler conjecture), spin glasses, etc (87).

There are several approaches: deterministic (the most successful are branch and bound methods and methods based on real algebraic geometry), stochastic (several Monte-Carlo-based algorithms exist such as simulated annealing (SA), direct Monte-Carlo sampling, stochastic tunneling, parallel tempering, Monte-Carlo with minimization), and heuristics and metaheuristics. The latter approaches include heuristic strategies to explore the search space in a (more or less) intelligent way, including evolutionary algorithms (e.g., genetic algorithms), swarm-based optimization algorithms (e.g., particle swarm optimization and ant colony optimization), memetic algorithms, and algorithms combining global and local search strategies (84; 85; 86; 87; 89; 90; 91; 92; 93; 94).

The energy landscape of a chemical system is a special case of cost functions which require a clever combination of *global optimization* and *local optimization* methods, since in many instances the energy landscape possesses extremely many minima and a very complicated barrier structure (see Fig. 2.2).

2.2.2.1. Monte-Carlo methods

Monte Carlo (MC) methods are a class of computational algorithms for simulating the behavior of various physical and mathematical systems. They are distinguished from other simulation methods (such as molecular dynamics) by being stochastic, i.e. non-deterministic in some manner - usually by using random numbers (or more often pseudo-random numbers) - as opposed to deterministic algorithms (87; 95). In these stochastic algorithms one (or many) walker at configuration i at time step t chooses one of the neighbor configurations as test configuration j. If this configuration fulfills an acceptance criterion, the walker moves to j; else, it remains at i. In the classical MC, one usually employs the ratio of the Boltzmann-factors of configurations i and j as acceptance criterion (the so-called Metropolis criterion (96)). If the energy of state j is equal to or below the one of state i, the move is accepted. If $E(j) > E(i)$, the move is only accepted with probability $\exp(-(E(j) - E(i))/C)$, where C is a control parameter. Such a weighted random walk can be used in order to simulate the ensemble average of the chemical system at temperature $T = C/k_B$. In the case of a stochastic quench, only downhill moves are accepted ($T = C = 0$).

In the simulated annealing (89; 90; 93) (SA) global optimization method, every point of the search space corresponds to a state of some physical system, and the function $E(s)$ to be minimized is interpreted as the internal energy of the system in that state. Therefore the goal is to bring the system, from an arbitrary initial state, to a state with the minimum possible energy. At each step, the SA heuristic considers some neighbor s' of the current state s, and, as in the MC simulations described above, decides between moving the system to state s' or staying put in state s. Upon lowering the temperature, the ensemble one samples becomes more concentrated at low energies. The sequence of temperatures is chosen such that the system ultimately tends to move to states of lower energy. One can prove that for a sufficiently slow decrease in the control parameter C, the random walk will end up in the global minimum, or at least in some of the low-lying local minima (97). Typically this step is repeated until the system reaches a state which is good enough for the particular application, or until a given computation budget has been exhausted.

2.2.2.2. Gradient-based methods

The simple stochastic methods described above are very general. They can be applied to both discrete and continuous landscapes. On the other hand, these algorithms do not take available local information such as the derivatives of the cost function into account. Such information is used in those classes of algorithms that follow the gradient downhill (such as gradient descent[5], line search) or take, in addition, second derivatives into account (conjugate gradient[6], Newton-Raphson, etc. (85; 86; 87)).

2.2.2.3. Genetic algorithms

The third class of global optimization methods are the so-called genetic algorithms (98; 99). A genetic algorithm is a search technique used in computer science to find approximate solutions to optimization and search problems. Genetic algorithms are a particular class of evolutionary algorithms that use techniques inspired by evolutionary biology such as inheritance, mutation, natural selection, and recombination (or crossover) (87; 100).

Genetic algorithms are typically implemented as a computer simulation in which a population of abstract representations (called chromosomes) of candidate solutions (called individuals) to an optimization problem evolves toward better solutions. Traditionally, solutions are represented in binary fashion as strings of 0s and 1s, but different encodings are also possible. The evolution starts from a population of completely random individuals and proceeds in generations. In each generation, the fitness of the whole population is evaluated, multiple individuals are stochastically selected from the current population (based on their fitness), and modified (mutated or recombined) to form a new population, which becomes the current one in the next iteration of the algorithm (87; 100).

---

[5] Gradient descent is an optimization algorithm that approaches a local minimum of a function by taking steps proportional to the negative of the gradient (or the approximate gradient) of the function at the current point. If instead one takes steps proportional to the gradient, one approaches a local maximum of that function; the procedure is then known as gradient ascent. Gradient descent is also known as steepest descent, or the method of steepest descent. When called the latter, gradient descent should not be confused with the method of steepest descent for approximating integrals (85; 86; 87).

[6] In mathematics, the conjugate gradient method is an algorithm for the numerical solution of particular systems of linear equations, namely those whose matrix is symmetric and positive definite. The conjugate gradient method is an iterative method, so it can be applied to sparse systems which are too large to be handled by direct methods involving the computation of the full matrix of second derivatives.

Applied in the framework of the exploration of energy landscapes, this means that an ensemble of configurations with the lowest energy survives preferentially from one generation to the next. The selection criteria can vary between two extremes: only those configurations with the lowest energy survive, or all new configurations always survive (at least for one generation). Between these two extremes one uses probabilistic criteria analogous to the Metropolis criterion.

2.1.3 Exploration of the barrier structure

In most cases, identifying low-lying states, in particular local energy minima, is completely sufficient. However, for structure prediction it is also very important to know to which extent the local minimum found exhibits a high degree of stability. Knowledge of the barrier structure around minima[7] gives some useful information to judge the stability of the corresponding structure candidates. Investigations of the barrier structure can be accomplished by employing both stochastic and deterministic approaches.

2.2.3.1. Threshold algorithm

The threshold algorithm (101; 102) is a stochastic approach. As soon as a local minimum is found one can chose a sequence of energy lids L_k ($L_k > \mathrm{E}_{min}$), and for a given lid L_k perform long Monte Carlo (MC) walks, where every move is accepted, unless it exceeds the energy of the lid. Every n_q moves, one performs one or many quenches into the closest local minima. Then, one repeats the procedure with another lid. From the energy lids, where new minima are first found during one of the quenches, one deduces an estimate for the barrier height between the starting minimum and other minima. From the distribution of energies encountered during the runs at various lids, one can deduce the local density of states within the basin of the starting minimum. Next, one can repeat the whole procedure for all other local minima observed.

The transition probabilities determined by this algorithm between the local minima include both energetic, entropic and kinetic contributions. As a result, we identify the lowest energy lids at which a transition between two minima can occur, yielding an estimate of the (free)energy barrier between minima.

---

[7] The dynamics of relaxations and transformation is controlled by the energetic and entropic barriers around and among the local minima.

2.2.3.3. Free energy

If we are on a time scale where many locally ergodic regions can equilibrate among each other, the one we are most likely to observe for a given experiment is the one with the lowest free energy (Eqn. (2.9)).

$$F\left(\mathscr{R}\right) = -k_B T ln Z\left(\mathscr{R}\right) \tag{2.9}$$

Thus, we would need to perform a minimization of the local free energy over all locally ergodic regions. The space of locally ergodic regions consists of exceedingly many but isolated 'points' (see Fig. 2.2). Mathematically we do not have the local free energy as a continuous function of $\mathscr{R}$. If we write down a continuous order parameter $\mathbf{M}$, which allows us to parametrize the full configurational space, we can then calculate the free energy as a function of the order parameter. But, in this case the region of the landscape that corresponds to a given value of this parameter $\mathbf{M}$ is usually not locally ergodic. In the best case, we can divide the coordinates into two groups: those with degrees of freedom that equilibrate very quickly, and the remaining ones that vary more slowly (so-called reaction coordinates). If the number of the fast degrees of freedom that are decoupled exceeds (vastly) the number of reaction coordinates, then we can approximate the full free energy on short time scales, by computing F only with respect to the fast degrees of freedom.

At low temperatures, the most important contribution to the local free energy of insulators is due to the lattice vibrations (phonons), while metals also exhibit a contribution due to the electrons at the Fermi level.

2.2.3.4. Configuration entropy and entropy of mixing

An idea of the physical nature of entropy can be gained from statistical thermodynamics. In terms of statistical thermodynamics configuration entropy can be evaluated using an adaption of the Boltzmann formula:

$$S = k_B \ln W(E, V, N) \tag{2.10}$$

where k_B is the Boltzmann's constant and $W(E, V, N)$ is the number of configurations in which the components can be arranged for a particular macrostate of the system consistent with the thermodynamic variables E, V and N. Assuming equal probability for all microstates, W is a measure of the disorder of the system, and the maximum entropy is associated with the greatest disorder. The full entropy of a system contains many contributions, due to lattice vibrations around a minimum configuration, defects, etc. One particular contribution is the so-called configurational entropy, which accounts for the fact that a macrostate can include many local minima of the energy, each of which adds a very similar amount of vibrational entropy to the total entropy of the system. Thus, one can write $W(E, V, N) = W_{conf}(E, V, N) W_{phon}(E, V, N)$, where W_{conf} equals the number of such minima or "configurations" of the system. Thus, $S_{total} = S_{phon} + S_{conf}$, where $S_{conf} = k_B \ln W_{conf}$.

In the case of a mixture of several components, we deal with the so-called entropy of mixing, which can be easily derived from Eqn. (2.10). For a multi-component system, W is equal to the number of permutations given by

$$W = \frac{N!}{\prod_i n_i!} \tag{2.11}$$

where $N = \sum_i n_i$, n_i is the number of atoms of type i and N is the total number of atoms in the system. For one mole of atoms, N is equal to Avogadro's number (N_A). Using Stirling's approximation, we can rewrite the equation for the configurational entropy as follows:

$$S = -Nk_B \sum_i \frac{n_i}{N} \ln \frac{n_i}{N} = -k_B \sum_i n_i \ln \frac{n_i}{N} \tag{2.12}$$

The ideal molar entropy of mixing then is given by:

$$S = -N_A k_B \sum_i x_i \ln x_i \tag{2.13}$$

where $x_i = n_i/N$ is the mole fraction of component i. In the a case of two-component system, we can write:

$$\Delta S = -R(x_1 \ln x_1 + x_2 \ln x_2) \tag{2.14}$$

where $R = N_A k_B$ is the gas constant and x_i is the mole fraction of component i.

2.2.3.5. Landscape representation

When using energy landscapes to understand the behavior of chemical systems, one faces the problem that the energy landscapes are complicated high-dimensional objects. Finding appropriate low-dimensional representations of the energy landscape that can be used to distinguish relevant regions of the landscape or help to analyze specific properties is a very important issue. There are many ways to address this problem. One of the most useful pictorial descriptions is the so-called tree graph representation of an energy landscape.

In computer science, a tree is a widely-used computer data structure that emulates a tree structure with a set of linked nodes. It is a special case of a graph. Each node has zero or more child nodes, which are below it in the tree (in computer science, unlike in nature, trees grow down, not up). A node that has a child is called the child's parent node. A child has at most one parent; a node without a parent is called the root node (or root). Nodes with no children are called leaf nodes (87; 103).

Applied to the energy landscape it means that we have to focus on the minima of the energy landscape and their connectivity. By employing the threshold algorithm, we start from the local minima, extend edges up in energy, which merge at the lowest energy where a transition between two minima has been observed. We continue in this fashion until all minima are connected. For low temperatures, this tree graph contains the full dynamics of the energy landscape, since all escape times are larger than the equilibration times, and the escape times are energy barrier dominated (55; 56).

3 Methods of electronic structure calculations

3.1 General remarks

In the previous chapter we briefly discussed the concept of the energy landscape of the chemical system. Since in the present work we deal with ideal periodic solids, the short overview of some aspects of the theory of ideal solids will be given in the present chapter.

In 1926 Schrödinger wrote down his famous equation:

$$\mathbf{H}\Psi = E\Psi, \tag{3.1}$$

where $\mathbf{H}$ is the Hamiltonian of a system, Ψ - wave functions and E - energy. The Hamiltonian of a chemical system is represented by the following formula:

$$\begin{aligned} H_{total} &= \sum_A \frac{p_A^2}{2M_A} + \sum_i \frac{p_i^2}{2m_i} \\ &+ \frac{1}{2}\sum_{A,B} \frac{ZZ'e^2}{|\mathbf{R}_A - \mathbf{R}_B|} + \frac{1}{2}\sum_{i,j} \frac{e^2}{|\mathbf{r}_i - \mathbf{r}_j|} \\ &+ \frac{1}{2}\sum_{A,i} \frac{Ze^2}{|\mathbf{R}_A - \mathbf{r}_i|} + \text{relativistic corrections} \\ &= T_A + T_e + V_{AB} + V_{ee} + V_{Ae}, \end{aligned} \tag{3.2}$$

where Z and Z' are ion charges (in units of electron charge e) numbers labeled by A and B, respectively. $\mathbf{R}_A$ and $\mathbf{r}_i$ are position vectors of the ion A and electron i, respectively; M_A and m_i are the masses of ion A and electron i, respectively.

The wave function of a system must be a solution of the Schrödinger equation obeying the condition that electrons are fermions[1], and the nuclei are either fermions or bosons[2]. Since the mass of an ion is much bigger than the mass of an electron, - $\mathrm{m}_i/\mathrm{M}_A << 1$, one can separate the electronic and the ionic degrees of freedom - the so-called the Born-Oppenheimer approximation. As a result, we are able to solve the equation for electrons in a static lattice potential of fixed ions. Afterwards we determine the movement of the nuclei around constant average positions and finally take the electron-phonon interaction into account.

---

[1] Fermions are particles with half-integer spin, named after Enrico Fermi.

[2] Bosons are particles with integer spin, named after Satyendra Nath Bose.

Note that no excited electronic states are accessible within the Born-Oppenheimer approximation, or, if one started with an excited electronic state, the system would not relax due to the electronic motion, but only adiabatically on its own time scale. From the assumption that the ions do not move at the electronic time scale follows the Ansatz:

$$\Psi\left(\mathbf{X},\mathbf{x}\right)=\chi\left(\mathbf{X}\right)\psi\left(\mathbf{x};\mathbf{X}\right) \tag{3.3}$$

Here, $\mathbf{X}$ and $\mathbf{x}$ are the ionic and the electronic degrees of freedom, respectively. Inserting Eqn. (3.3) into the Schrödinger equation given by the Hamiltonian in Eqn. (3.2), and assuming that $\chi T_I\psi$ and $(\vec{\nabla}\chi)(\vec{\nabla}\psi)$ are small compared to $\chi T_e\psi$ and can be omitted, one can write

$$H\Psi=\psi\left(T_I+V_{II}\right)\chi+\left(H_e\psi\right)\chi=E\Psi, \tag{3.4}$$

where $H_e=T_e+V_{ee}+V_{eI}$. H_e cannot be written as a sum of one electron terms due to V_{ee}. If we neglect V_{ee} or replace it by a particle independent function $V_{ee}\left(\mathbf{x}\right)$ which is the same for all electrons, all electrons see the same, average, potential. In this case, we can replace the many-particle equation by N identical independent one-particle equations, the so-called band-approximation. Here, the only "remnant" of the many-body nature of the problem is the Pauli-principle, i.e. no electronic state can be occupied by two electrons.

However, usually, the first major approximation when dealing with the electrons is the one-electron approximation, which leads to the Hartree- and the Hartree-Fock approximations. This results in N one-particle equations, where each electron sees a different average potential generated by the other $N-1$ electrons. We now have to solve each one-particle equation separately, and feed the N one-particle ground state wave functions back into V_{ee}, until self-consistency is reached.

3.2 Hartree-Fock method

In the end of the 1920s, D.R. Hartree introduced a procedure, which he called the self-consistent field method, to calculate approximate wavefunctions and energies for atoms and ions. Hartree sought to do away with empirical parameters and solve the many-body time-independent Schrödinger equation from fundamental physical principles. In 1930 Slater and V.A. Fock independently pointed out that the Hartree method did not respect the principle of antisymmetry of the wavefunctions. The Hartee method used the Pauli exclusion principle in its older formulation, forbidding the presence of two electrons in the same quantum state. However, this was shown to be fundamentally incomplete in its neglect of quantum statistics.

Then, it was shown that the Slater determinant, a determinant of one-particle orbitals first used by Heisenberg and Dirac in 1926, trivially satisfies the antisymmetric property of the exact solution and hence is a suitable Ansatz for applying variational principles. The original Hartree method can then be viewed as an approximation to the Hartree-Fock method by neglecting exchange (87).

We will discuss only the Restricted Hartree-Fock (RHF) method, where the solid is a closed-shell system with all orbitals doubly occupied (two spin states are possible for each electron). Open shell systems, where some of the electrons are not paired, can be dealt with using the Restricted Open-shell Hartree-Fock (ROHF) or Unrestricted Hartree-Fock (UHF) Hartree-Fock method.

3.2.1 Hartree-Fock algorithm

The Hartree-Fock method is typically used to solve the time-independent Schrödinger equation for a multi-electron atom, molecule or solid described in the fixed-nuclei approximation by the electronic Hamiltonian. Because of the complexity of the differential equations, the problem is usually impossible to solve analytically, and so the numerical technique of iteration is applied. The method makes five major simplifications in order to deal with this task:

- The Born-Oppenheimer approximation is inherently assumed.
- Typically, relativistic effects are completely neglected.
- The wave function is approximated by a single Slater determinant.
- The basis set is composed of a finite number of orthogonal functions.
- The effects of electron correlation are completely neglected (by “definition”).

According to the variational theorem, for a time-independent Hamiltonian operator, any trial wavefunction will have an energy expectation value that is greater than or equal to the true ground state wavefunction corresponding to the given Hamiltonian. As a consequence, the Hartree-Fock energy is an upper bound to the true ground state energy of a given molecule or solid. The limit of the Hartree-Fock energy, as the basis set becomes infinite, is called the Hartree-Fock limit and it is a unique set of one-electron orbitals, and their eigenvalues (87). The difference between the Hartree-Fock limit and the true energy of the ground state is often defined as the correlation energy.

The starting point for the Hartree-Fock method is a set of approximate one-electron orbitals. For an atomic calculation, these are typically the orbitals for a hydrogen-like atom (an atom with only one electron, but the appropriate nuclear charge). For a molecular or crystalline calculation, the initial approximate one-electron wavefunctions are typically linear combinations of atomic orbitals (LCAO). This gives a collection of one electron orbitals that, due to the fermionic nature of electrons, must be antisymmetrized. In order to deal with this problem, Fock and Slater introduced the anti-symmetry from the outset, by using a Slater-determinant instead of a single product. At this point, a new approximate Hamiltonian operator, called the Fock operator, is constructed.

Finding a ground state is actually an optimization problem, where we minimize $\int \psi^* H\psi d\mathbf{x}$ with the conditions that only anti-symmetric wave functions are admissible, because of the Pauli-principle[3], and that these wave functions are normalized,

$$\int |\psi|^2 \, d\mathbf{x} = 1. \tag{3.5}$$

Within the one-determinant-Hartree-Fock approximation one first takes the functional derivative of $\int \psi^* H\psi d\mathbf{x}$, and sets this equal to zero, taking Eqn. (3.5) into account. After some calculation one can derive the so-called Hartree-Fock Hamiltonian:

$$H_{HF}\left(i\right) = T_e\left(i\right) + V_{eI}\left(i\right) + \left(V_c - V_{ex}\right), \tag{3.6}$$

The first terms in this Hamiltonian are a sum of kinetic energy operators for each electron, the internuclear repulsion energy, and a sum of Coulombic attraction terms between nuclei and electrons. The final set of terms models the Coulombic repulsion terms between each pair of electrons within the sum. The sum is composed of a net repulsion energy for each electron in the system, which is calculated by treating all of the other electrons within the molecule or solid as a smooth distribution of negative charge. This is the major simplification inherent in the Hartree-Fock method.

Note that Eqn. (3.6) only refers to the ground state wave function, and does not produce any excited states of the many-particle Hamiltonian. A non-local term, V_{ex}[4], reflects the fact that electrons with the same spin "repel" each other.

The newly constructed Fock operator is then used as the Hamiltonian in the time-independent Schrödinger equation. Solving the equation yields a new set of approximate one-electron orbitals. This new set of orbitals is then used to construct a new Fock operator. The procedure is stopped when the change in total electronic energy is negligible between two iterations. In this way, a set of so-called "self-consistent" one-electron orbitals are calculated. The Hartree-Fock electronic wavefunction is then equal to the Slater determinant of these approximate one-electron wavefunctions.

In modern Hartree-Fock calculations, the one-electron wavefunctions are approximated by a linear combination of atomic orbitals (LCAO), in the form of Slater-type orbitals. It is also very common for the atomic orbitals (AO) to be composed of a linear combination (LC) of one or more Gaussian-type orbitals, rather than Slater-type orbitals, in the interest of saving considerable computational time. Various basis sets are used in practice, most of which are composed of Gaussian functions, due to reasons mentioned above.

One should note, however, that the requirement of self-consistency introduces non-linearity back into the system. Thus, in principle, several solutions can exist, and one has to analyze the solutions with respect to their properties, in order to decide, whether one has determined the correct one. An alternative route are the so-called density functional theories (DFT), of which the simplest ones introduce semi-phenomenological factors and terms, in order to simplify the model and its solution.

---

[3] By requiring that each "orbital" is occupied only by one electron.

[4] Only appears in the Hartree-Fock approximation.

3.3 Density Functional Theory (DFT)

The fundamental tenet of density functional theory is that any property of a system of many interacting particles can be viewed as a functional of the ground state density $n_0(\mathbf{r})$; that is, one scalar function of position $\mathbf{r}$, $n_0(\mathbf{r})$ determines all information in the many-body wavefunctions for the ground state and all excited states (104).

The original DFT of quantum systems is the method of Thomas (105) and Fermi (106) proposed in 1927. Although their approximation is not accurate enough for present-day electronic structure calculations, the approach illustrates the way density functional theory works. In the original method the kinetic energy of the system of electrons is approximated as an explicit functional of the density, idealized as non-interacting electrons in a homogeneous gas with density equal to the local density at any given point. Both Thomas and Fermi neglected exchange and correlation among the electrons; however, their approximation was extended by Dirac (107) in 1930, who formulated the local approximation for exchange which is still in use today. The attraction of DFT is evident by the fact that one equation for the density is considerably simpler than the full many-body Schrödinger equation that involves 3N degrees of freedom for N electrons. However, the Thomas-Fermi approach starts with approximations that are too crude, missing essential physics and chemistry, such as shell structures of atoms and binding of molecules. Thus it falls short of the goal of a useful description of electrons in matter.

The approach of Hohenberg and Kohn is to formulate DFT as an exact theory of a many-body system. The formulation applies to any system of interacting particles in an external potential $V_{ext}(\mathbf{r})$, including any problem of electrons and fixed nuclei, where the Hamiltonian for the electrons can be written:

$$\hat{H} = -\frac{\hbar^2}{2m_e}\sum_i \nabla_i^2 + \sum_i V_{ext}(\mathbf{r}_i) + \frac{1}{2}\sum_{i\neq j}\frac{e^2}{|\mathbf{r}_i - \mathbf{r}_j|} \tag{3.7}$$

DFT is based upon two theorems:

- **Theorem I:** For any system of interacting particles in an external potential $V_{ext}(\mathbf{r})$, the potential $V_{ext}(\mathbf{r})$ is determined uniquely, except for a constant, by the ground state particle density $n_0(\mathbf{r})$.

- **Theorem II:** A universal functional for the energy E[n] in terms of the density $n(\mathbf{r})$ can be defined, valid for any external potential $V_{ext}(\mathbf{r})$. For any particular $V_{ext}(\mathbf{r})$, the exact ground state energy of the system is the global minimum value of this functional, and the density $n(\mathbf{r})$ that minimizes the functional is the exact ground state density $n_0(\mathbf{r})$.

The most common implementation of DFT is through the Kohn-Sham method. The main idea of this approach is to replace a difficult interacting many-body system obeying the Hamiltonian with a different auxiliary system that can be solved more easily. Since there is no unique prescription for choosing the simpler auxiliary system, this is an Ansatz. The Ansatz of Kohn and Sham assumes that the ground state density of the original interacting system is equal to that of some chosen non-interacting system. This leads to independent-particle equations for the non-interacting system that can be considered exactly soluble with all the difficult many-body terms incorporated into an exchange-correlation functional of the density. By solving the equations one finds the ground state density and energy of the original interacting system with accuracy limited only by the approximations in the exchange-correlation functional.

The Kohn-Sham Ansatz rests upon two assumptions:

1. The exact ground state density can be represented by the ground state density of an auxiliary system of non-interacting particles. This is called ”non-interacting V representability”.

2. The auxiliary Hamiltonian is chosen to have the usual kinetic operator and an effective local potential $V^{\sigma}_{eff}(\mathbf{r})$ acting on an electron of spin σ at point $\mathbf{r}$. The local form is not essential, but it is an extremely useful simplification that is often taken as the defining characteristic of the Kohn-Sham approach. The auxiliary effective potential $V^{\sigma}_{eff}(\mathbf{r})$ must depend upon spin in order give the correct density for each spin, except in cases that are spin symmetric.

Thus, the Kohn-Sham approach to the full interacting many-body problem can be written as follows:

$$E_{KS} = T_s[n] + \int d\mathbf{r} V_{ext}(\mathbf{r}) n(\mathbf{r}) + E_{Hartree}[n] + E_{II} + E_{xc}[n]. \tag{3.8}$$

Here $V_{ext}(\mathbf{r})$ is the external potential due to the nuclei and any other external fields (assumed to be independent of spin) and E_{II} is the interaction between the nuclei. Thus the sum of the terms involving V_{ext}, $E_{Hartree}$, and E_{II} forms a neutral grouping that is well defined. The independent-particle kinetic energy T_s is given explicitly as a functional of the orbitals; however, T_s for each spin σ must be a unique functional of density $n(\mathbf{r}, \sigma)$ by application of the Hohenberg-Kohn arguments to the independent-particle Hamiltonian. All many-body effects of exchange and correlation are grouped into the exchange-correlation energy E_{xc}, which can be written as follows:

$$E_{xc}[n] = \left\langle \hat{T} \right\rangle - T_s[n] + \left\langle \hat{V}_{int} \right\rangle - E_{Hartree}[n]. \tag{3.9}$$

Here [n] denotes a functional of the density $n(\mathbf{r}, \sigma)$ which depends upon both position in space $\mathbf{r}$ and spin σ. The sum of $\left\langle \hat{T} \right\rangle$ and $\left\langle \hat{V}_{int} \right\rangle$ includes all internal energies, kinetic and potential, of the interacting electron system. Basically, E_{xc} is the difference of the kinetic and the internal interaction energies of the true interacting many-body system from those of the fictitious independent-particle system with electron-electron interactions replaced by the Hartree energy. If the universal functional E_{xc}[n] defined in (3.9) were known, then the exact ground state energy and density of the many-body electron problem could be found by solving the Kohn-Sham equation for independent-particles. To the extent that an approximation for E_{xc}[n] describes the true exchange-correlation energy, the Kohn-Sham method provides a feasible approach to calculating the ground state properties of a many-body electron system.

The major problem with DFT is that the exact functionals for the exchange and correlation are not known except for the free electron gas. Already in their seminal paper, Kohn and Sham proposed making the local density approximation (LDA) or more generally the local spin density approximation (LSDA), in which the exchange-correlation energy is simply an integral over all space with the exchange-correlation energy density at each point, to be the same as in a homogeneous electron gas with that density,

$$\begin{aligned} E_{xc}^{LSDA}[n^{\uparrow}, n^{\downarrow}] &= \int d^3 r n(\mathbf{r}) \epsilon_{xc}^{hom}(n^{\uparrow}(\mathbf{r}), n^{\downarrow}(\mathbf{r})) \\ &= \int d^3 r n(\mathbf{r}) [\epsilon_{x}^{hom}(n^{\uparrow}(\mathbf{r}), n^{\downarrow}(\mathbf{r})) + \epsilon_{c}^{hom}(n^{\uparrow}(\mathbf{r}), n^{\downarrow}(\mathbf{r}))] \end{aligned} \tag{3.10}$$

Once one has made the local Ansatz of the L(S)DA, then all the rest follows. Since the functional $E_{xc}[n^{\uparrow}, n^{\downarrow}]$ is universal, it follows that it is exactly the same as for the homogeneous gas. The only information needed is the exchange-correlation energy of the homogeneous gas as a function of density; the exchange energy of the homogeneous gas can be written in a simple analytic form and the correlation energy can be calculated with great accuracy, e.g. using the Monte-Carlo method.

The success of the LSDA has led to the development of various generalized gradient approximations (GGAs). Generalized gradient approximations are still local but also take into account the gradient of the density at the same coordinate. Using GGA, very good results for molecular geometries and ground state energies have been achieved. Many further incremental improvements have been made to DFT by developing better representations of the functionals.

DFT has been very popular for calculations in solid state physics since the 1970s. In many cases DFT with the local-density approximation gives quite satisfactory results for solid-state calculations in comparison to experimental data, at relatively low computational costs when compared to other ways of solving the quantum mechanical many-body problem. However, it was not considered accurate enough for calculations in quantum chemistry until the 1990s, when the approximations used in the theory were greatly refined to better model the exchange and correlation interactions. DFT is now a leading method for electronic structure calculations in both fields. But, despite the improvements in DFT, there are still difficulties in using density functional theory to properly describe intermolecular interactions, especially van der Waals forces (dispersion), or in calculations of the band gap in semiconductors (87; 108; 109; 110; 111).

In practice, Kohn-Sham theory can be applied in several distinct ways depending on what is being investigated. A popular functional is known as BLYP (from the names Becke, Lee, Yang and Parr). Even more widely used is B3LYP (112; 113; 114) which is a hybrid method in which the DFT exchange functional, in this case from BLYP, is combined with the exact exchange functional from Hartree-Fock theory. Unfortunately, although the results obtained with these functionals are usually sufficiently accurate for most applications, there is no systematic way of improving them. Hence in the current DFT approach it is not possible to estimate the error of the calculations without comparing them to other methods or experiment (87; 108; 109; 110; 111).

HF and DFT, as well as other methods such as quantum Monte Carlo dealing with the ideal solid at $T = 0$, are applicable for fixed positions of the ions, treated as a complicated external static field. In the past years, there have been attempts to include the movements of the ions in the calculations. The scheme proposed by Car and Parrinello proceeds by performing a molecular dynamics of the ions with partially relaxed electronic degrees of freedom, taking into account that electrons stay relatively close to the Born-Oppenheimer surface.

3.4 Basis sets

Quantum chemical calculations are typically performed using a finite set of basis functions. It is common to use a basis composed of a finite number of atomic orbitals, centered at each atomic nucleus within the solid (linear combination of atomic orbitals, LCAO)[5]. Initially, these atomic orbitals were typically Slater orbitals, which corresponded to a set of functions which decayed exponentially with distance from the nuclei. Later, it was realized that these Slater-type orbitals could in turn be approximated as linear combinations of Gaussian orbitals instead. Because it is easier to calculate overlap and other integrals with Gaussian basis functions, this led to huge computational savings (87; 108; 109; 110; 111; 115).

3.4.1 Basis sets types

There are many types of basis sets composed of Gaussian-type orbitals (GTOs). The basis sets that contain only occupied orbitals are called minimal basis sets. They are typically composed of the minimum number of basis functions required to represent all of the electrons on each atom. Even in this case some of the largest basis sets can contain literally dozens of basis functions on each atom. In order to achieve some flexibility within the basis set, so-called polarization functions can be added. These, the most common addition to minimal basis sets, are auxiliary functions with one additional node. This is an important addition when considering accurate representations of bonding between atoms. Another common addition to basis sets is the addition of diffuse functions. These additional basis functions can be important when considering anions and other large, ”soft” molecular systems (87; 108; 109; 110; 111; 116).

A common naming convention for minimal basis sets is STO-XG, where X is an integer. This X value represents the number of Gaussian primitive functions. In these basis sets, the same number of Gaussian primitives comprise core and valence orbitals. Minimal basis sets typically give rough results but are much cheaper than their larger counterparts (87; 108; 109; 110; 111; 116; 117).

---

[5] A number of DFT-programs (e.g. WIEN, VASP) employ very large plane-wave sets. Those are often combined with pseudopotentials, because the wave functions of the inner electrons are very expensive to describe using only plane waves.

The valence electrons usually contribute most of the bonding in molecules and solids. In recognition of this fact, it is common to represent valence orbitals by more than one basis function, (each of which can in turn be composed of a fixed linear combination of primitive Gaussian functions). The notation for these split-valence basis sets is typically X-YZg. In this case, X represents the number of primitive Gaussians comprising each core atomic orbital basis function. The Y and Z indicate that the valence orbitals are composed of two basis functions each. The first one is composed of a linear combination of Y primitive Gaussian functions, and the other is composed of a linear combination of Z primitive Gaussian functions (87; 116).

Basis sets in which there are multiple basis functions corresponding to each atomic orbital, including both valence orbitals and core orbitals or just the valence orbitals, are called double, triple, or quadruple-zeta basis sets.

3.4.2 Basis set superposition error

If we use a finite basis set in our calculations, the interaction energies are susceptible to basis set superposition error (BSSE). As the atoms of interacting molecules (or of different parts of the same molecule or solid) approach one another, their basis functions overlap. If the total energy is minimized as a function of the system geometry, the short-range energies from the mixed basis sets must be compared with the long-range energies from the unmixed sets, and this mismatch introduces an error (87; 108; 109; 110; 111; 116; 117).

4 Calculation of phase diagrams

Phase diagrams are graphical representations of all thermodynamically stable phases in a chemical system at given temperature, pressure and composition. The main goal of phase equilibrium calculations is the determination of the amount and chemical mixture of each part of a mixture of heterogeneous substances. As a starting point, one needs to know the characteristic functions, e.g. the Gibbs energy function[1], for all possible phases in the system even at conditions where those phases are metastable or even unstable. Conclusions about the stability of phases can usually be derived from calculations, of course. Once the Gibbs energy for all feasible phases and their combinations is known as function of the thermodynamic parameters, minimization of the Gibbs energy yields the phase diagram of the system. Nowadays, the main rules and methods of phase diagram calculations and constructions have been formalized in the CALPHAD (CALculation of PHAse Diagrams) project, and represented by an organization and a journal of the same name.

4.1 Calculation of the phase equilibrium

In general, there are two ways to determine the characteristic function of a complex system: via experiment or by performing theoretical calculations usually based on a model of the internal constitution of the system and the known properties of its parts. In this presentation, we are not going to discuss the issues associated with the experimental determination of the Gibbs energy; instead we will focus on the theoretical approach. The main advantage of the theoretical method is that one does not need to know the real chemical and phase compositions of the equilibrium system beforehand, since those compositions at equilibrium can be derived from the calculations. In the following, we are going to describe the most basic methods currently employed to compute phase diagrams, where they can either be based on experiment or calculations or on a combination of both.

---

[1] Nowadays, in the literature the term Gibbs free energy is often shortened to Gibbs energy. This is the result of a 1988 IUPAC meeting to set unified terminologies for the international scientific community, in which the adjective "free" was supposedly banished (87).

4.1.1 General definitions

In thermodynamics, and especially in the field of phase diagram calculations, the Gibbs energy plays the main role. It is defined as follows:

$$G = U + pV - TS, \tag{4.1}$$

where U is the internal energy, p is the pressure, V is the volume, T is the temperature and S is the entropy. One can rewrite this equation:

$$G = H - TS, \tag{4.2}$$

where H is the enthalpy. The Gibbs energy is a state function that is minimized when a system reaches an equilibrium at constant pressure and temperature; thus, one can consider the Gibbs energy as a convenient criterion of spontaneity for processes with constant pressure and temperature.

Earlier, we have introduced the entropy (see Eqn. (2.10)) as a physical variable in statistical mechanics and thermodynamics, but one can also define entropy via dS = dq/T, where dq is a heat change. Taking into account that $(\mathrm{dq}/\mathrm{dT})_p = \mathrm{C}_p$, where C_p is the heat capacity at constant pressure, one can write:

$$dS = \frac{C_p}{T} dT. \tag{4.3}$$

Then, one can write the Gibbs energy of a substance as:

$$G = H_{298} + \int_{298}^{T} C_p dT - T\left(S_{298} + \int_{298}^{T} \frac{C_p}{T} dT\right), \tag{4.4}$$

where H_{298} and S_{298} are the enthalpy and the entropy at 298.15 K (and pressure 1 bar), respectively. In practice, the Gibbs energy for pure elements or stoichiometric compounds is usually stored in a database using some polynomial functions, e.g. :

$$G_m = H_m^{298} + a + bT + cT\ln T + \sum_{2}^{n} d_n T^n, \tag{4.5}$$

where the left-hand-side is defined as the molar Gibbs energy relative to a standard element reference state. Usually, the Gibbs energy of a pure phase is called G^o. The symbol m indicating that one deals with molar quantities is usually omitted. For the remainder of this thesis, we will always refer to the molar Gibbs energy, except where explicitly noted otherwise.

4.1.2 Multicomponent system

For a multicomponent ideal mixture one can write the total Gibbs energy function of the system as follows:

$$G^{ideal}(x) = \sum_i x_i G_i^o + RT \sum_i x_i \ln x_i, \tag{4.6}$$

where x$_i$ is a fraction of component i, G_i^o is the Gibbs energy of the phase containing the pure component i (see section above 4.1.1) and the term $RT\sum_i x_i \ln x_i$ is the ideal Gibbs energy of mixing, G_{mix}^{ideal}. However, there is always some interaction between the components. Thus, one needs to introduce the so-called excess Gibbs energy of mixing, which is defined as a difference between the real and the ideal Gibbs energy (see Eqn. (4.6)): $G_{mix}^{ex} = G^{real} - G^{ideal}$. The simplest way to describe the excess Gibbs energy and to take such interactions into account is via the regular solution model. In the case of a two-component system, one can write the excess Gibbs energy of mixing as follows:

$$G_{mix}^{ex} = x_A x_B \Omega, \tag{4.7}$$

where Ω is the regular solution interaction energy parameter which is assumed to be independent of temperature. If Ω is linearly dependent on temperature, we have a quasi-regular solution model. Positive values of Ω are equivalent to repulsive interactions, and negative values of Ω are associated with attractive interactions, respectively. The regular solution model is the simplest of the non-ideal models and basically assumes that the interactions between the components are independent of composition. However, it has been realized for a long time that the assumption of composition-independent interactions is too simplistic. This has led to the development of the sub-regular solution model, where interaction energies are considered to vary linearly with composition:

$$G_{mix}^{ex} = x_A x_B (g_0 + g_1 x_B). \tag{4.8}$$

Taking this process further, more complex composition dependences of the interaction parameters can be considered. One of the most common methods is based on the Redlich-Kister (118) approximation:

$$G_{mix}^{ex} = x_A x_B \sum_v g_v (x_A - x_B)^v, \tag{4.9}$$

where the parameters g_i can be temperature dependent. However, for phases such as interstitial solutions, ordered intermetallics, ceramic compounds, slags, ionic liquids and aqueous solutions, simple substitutional models are generally not adequate[2].

For a general multicomponent mixture, the complete expression for the total Gibbs energy will be:

$$\begin{aligned} G(x) = \sum_i x_i G_i^o \quad &+ \quad RT \sum_i x_i \ln x_i + \\ \sum_i \sum_{j>i} x_i x_j \sum_v g_v^{(2)} (x_i - x_j)^v \quad &+ \quad \sum_i \sum_{j>i} \sum_{k>j} x_i x_j x_k \sum_v g_v^{(3)} x_v + \ldots, \end{aligned} \tag{4.10}$$

where $g_v^{(i)}$ are the interaction parameters. Equation (4.10) includes not only the binary interaction parameters, but also one of the simplest ternary interaction parameters, which have been considered in the present thesis for the quasi-ternary semiconductor systems

---

[2] In those cases the models used most often are sublattice models (see subsequent section) and associated solution models (see (2)).

(see Chapter 7). When dealing with the Gibbs energy of mixing, it is often useful to define the Gibbs energy of formation:

$$\Delta_f G = G_{total} - \sum_i x_i G_i^o = RT \sum_i x_i \ln x_i + \sum_i \sum_{j>i} x_i x_j \sum_v g_v^{(2)} (x_i - x_j)^v + \ldots . \tag{4.11}$$

4.1.3 Sublattice model

Earlier we have shown how one can approximate the Gibbs energy functions to calculate the phase equilibrium using simple substitutional methods. But quite often such models are not satisfactory and one needs to use special approaches to get satisfactory results. One of the most useful models is the sublattice model, which is widely used to describe intermetallics, ceramic compounds or other similar systems.

A sublattice phase can be envisaged as being composed of interlocking sublattices for the atomic positions, on which the various components can mix. The model is phenomenological in nature and does not define any particular crystal structure within its general mathematical formulation. Thus, one needs to define so-called site fractions y_i^s and mole fractions x_i. Site fractions are defined via the equations:

$$y_i^s = \frac{n_i^s}{n_{Va}^s + \sum_i n_i^s}, \tag{4.12}$$

where n_{Va}^s is the number of vacancies and, n_i^s is the number of atoms of component i on sublattice s. Mole fractions x_i are related to site fractions by the following equation:

$$x_i = \frac{\sum_s N^s y_i^s}{\sum_s N^s (1 - y_{Va}^s)}, \tag{4.13}$$

where N^s is total number of sites on the sublattices.

The ideal entropy of mixing is due to the many different configurations possible when the components randomly mix on each of the sublattices. The number of permutations which are possible, assuming ideal interchanges within each sublattice, is given by the following formula:

$$W_p = \prod_s \frac{N^s!}{\prod_i n_i^s!}, \tag{4.14}$$

and the molar Gibbs ideal mixing energy is:

$$G_{mix}^{ideal} = -TS_{mix}^{ideal} = k_B T \sum_s N^s \sum_i y_i^s \ln y_i^s. \tag{4.15}$$

Next, one defines the "reference" and "excess" Gibbs energies. The Gibbs energy reference state can be defined by the "end members" generated when only the pure components exist on the sublattice. The excess Gibbs energy can be defined as the difference between the real energy and the ideal Gibbs energy, and it is due to the interactions between different types of atoms within each sublattice. For the two-sublattice system (A,B)(C,D) we can write the reference Gibbs energy:

$$G_m^{ref} = y_A y_C G^o_{AC} + y_B y_C G^o_{BC} + y_A y_D G^o_{AD} + y_B y_D G^o_{BD}, \tag{4.16}$$

where G^o_{XY} are the Gibbs energies of the pure phases. In such an alloy (A,B)(C,D), A-C, A-D, B-C and B-D interactions are included in the Gibbs energies of the pure compounds. Mixing on the sublattice occurs in response to the A-B and C-D interactions, and the simplest form of the interaction can again be modeled in a regular solution format:

$$G^{xs}_{mis} = y^1_A y^1_B L^o_{A,B:*} + y^1_C y^1_D L^o_{*:C,D}, \tag{4.17}$$

where $L^o_{A,B:*}$ and $L^o_{*:C,D}$ denote regular solution parameters for mixing on the sublattice irrespective of site occupation of the other sublattice. As before (see Eqn. (4.8)) we introduce a sub-regular model as a part of the Redlich-Kister polynomial, and we can write the analogous sublattice sub-regular model as follows:

$$\begin{aligned} G^{xs}_{mis} = \quad & y^1_A y^1_B y^2_C L^o_{A,B:C} + y^1_A y^1_B y^2_D L^o_{A,B:D} + \\ & y^1_C y^1_D y^2_A L^o_{A:C,D} + y^1_C y^1_D y^2_D L^o_{B:C,D}. \end{aligned} \tag{4.18}$$

As a next step, we can introduce some site fraction dependence, etc. In general, we can make our models as complicated as necessary to obtain the appropriate results for the current tasks.

Up to now, we have considered a few of the most useful methods (models) which allow one to describe the thermodynamic properties of a system and to write the total Gibbs energy of a system. In the next section, a brief introduction to phase diagram construction will be given.

4.2 Construction of phase diagrams: Convex hull method

Nowadays, in most cases the methods of phase diagram construction do not differ from the separate calculations of the phase equilibrium, since each point of the phase diagram is calculated without taking into account other fields of the phase diagram. For example, one of the most commonly used methods of the phase equilibrium calculation, the method of Gibbs energy minimization, solves the task for each point of the p-T-x phase diagrams completely. In the case of a K-component system with n phases, one can write the Gibbs energy minimization problem as follows:

$$\begin{aligned}
&\min_{(f,x)} \left\{ G = \sum_{i=1}^{n} f^{(i)} G^{(i)}(x^{(i)}) \right\} \\
&\sum_{i=1}^{n} f^{(i)} x^{(i)} = f, \\
&\sum_{k=1}^{K} x_k^i = 1, i = 1, ..., n \\
&f^{(i)} \geq 0, x_k^i \geq 0.
\end{aligned} \tag{4.19}$$

Here, $f^{(i)}$ is the number of moles of the phase i; $x^{(i)} = (x_k^i)_{k=1,...,K}$ is a vector of mole fractions of the kth component in the phase i and $G^{(i)}$ is the corresponding molar Gibbs energy. Let us also assume, that f_k is the total amount of the kth component in the system, f_k^i is the amount of the kth component in the ith phase (by our assumption $\sum_{k=1}^{K} f_k^i = f^{(i)}$). To reconstruct the whole phase diagram one needs to calculate all possible equilibria for the whole range of the values (p,T,x). As a next (non-trivial) step, one deletes all unnecessary curves, which describe the metastable equilibria. Even using modern computers, such methods are laborious and difficult to implement.

Recently, in the literature a new approach to phase diagram construction has been proposed (52). This method is based on the convex hull construction of the initial thermodynamic data. The system will exhibit only one phase, if the initial surface is equal to the convex hull. If the Gibbs energies are different on the initial surfaces and on the convex hull, then the system will exhibit several phases belonging to the respective border of the heterogeneous fields.

This method allows one to combine the advantages of analytical and graphical methods of the phase diagram analysis. To use this method, one should write the Gibbs energy functions of all possible phases in the system in the terms of convex mathematical analysis. This approach allows one to calculate an uniform phase diagram in the whole range of the thermodynamic variables (p,T,x). Also one should mention, that here one does not need to explicitly minimize the Gibbs energy or solve the system of nonlinear equations, thus making the Convex-hull method easier to visualise and implement.

4.2.1 Convex hull algorithm

The main algorithm of phase diagram construction via the Convex hull method is most easily presented using an example. In the Fig. 4.1, the Gibbs energy surface of the KBr-NaBr system is depicted.

The typical double minimum shape of the function indicates the presence of a miscibility gap in the system. To calculate the phase diagram one needs to find the boundary points which are responsible for the equilibrium compositions.

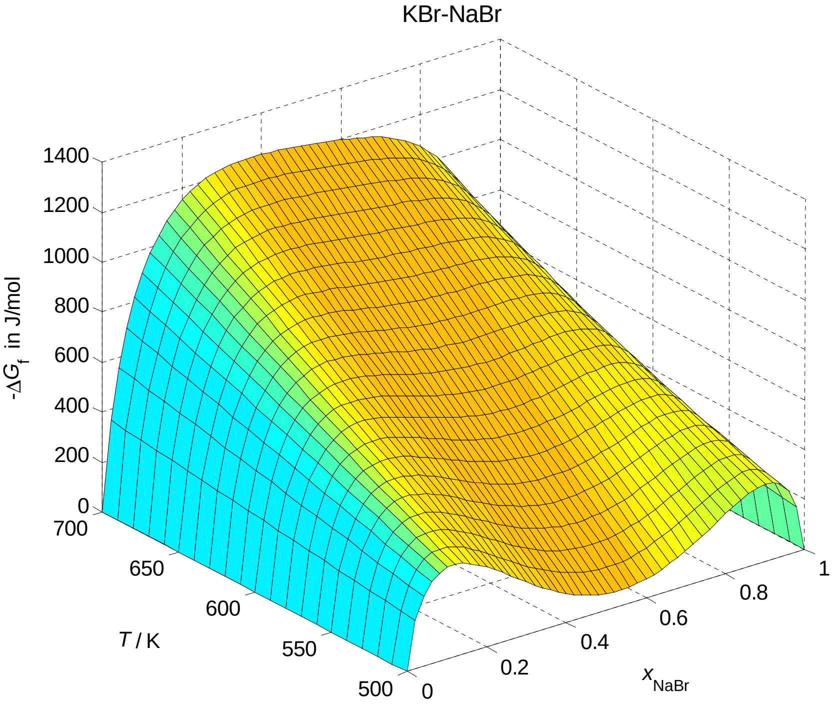

Figure 4.1: The Gibbs energy surface for the system KBr-NaBr, calculated using HF-data.

Next, one constructs the convex hull, in the following example with a step size of 10 degrees. The projection of the boundary points of the energy function and convex hull crossing on the T-x plane gives us the miscibility gap (see Fig. 4.2).

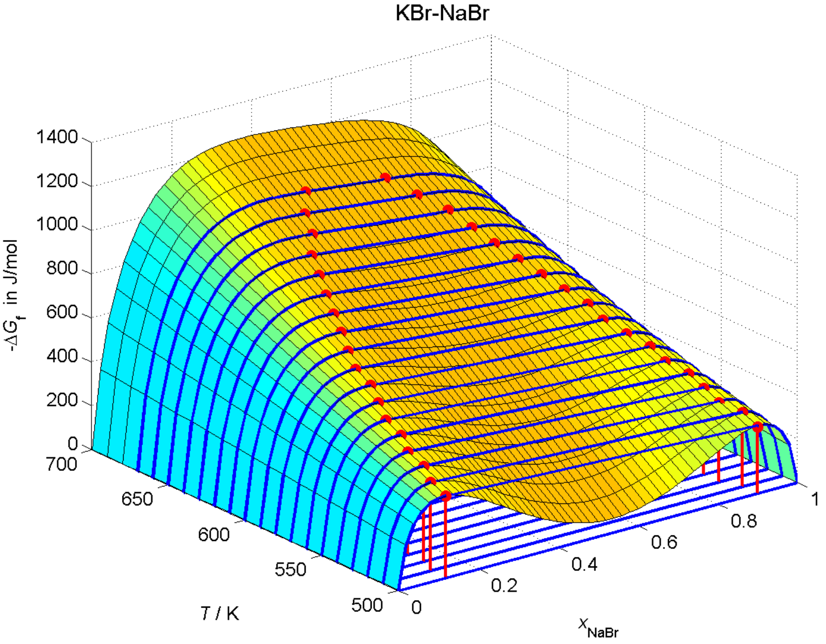

Figure 4.2: The Gibbs energy surface and convex hull (blue lines). The red points correspond to the boundary points of the energy function and convex hull crossing.

Part III

Methods

5 Method

5.1 General approach

Starting point for our method is the energy/enthalpy landscape of a chemical system, which is the hypersurface of the potential energy/enthalpy over the space of atom configurations in the system (41). Quite generally, the modifications in the system that should be capable of existence correspond to locally ergodic regions on the landscape of the system. At very low temperatures, this implies that all atom configurations that correspond to local minima of the landscape are possible structure candidates. Finding these minima requires the use of a global optimization method, where we permit free variation of the atom positions, cell parameters and ionic charges, during the global landscape exploration. Since these explorations require many millions of energy evaluations, we perform the global search using some robust classical potential, and subsequently locally optimize the candidates employing various ab initio methods for the energy calculation.

However, at elevated temperatures, the locally ergodic regions are not necessarily localized around a single local minimum, but may contain many such local minima (119)[1]. This is clearly the case in crystalline solid solutions, where each atom configuration (microstate) j that contributes to the solid solution macrostate belongs to a different local minimum m_i of the potential energy. However, at the temperature at which the solid solution is formed, all these minima m_i are in equilibrium, and thus the basins around them $B(m_i)$ form a single large locally ergodic region $\mathscr{R} = \bigcup_i B(m_i)$, whose local free energy can be computed as

$$F(\mathscr{R}) = -k_B T \ln Z(\mathscr{R}); Z(\mathscr{R}) = \sum_i \exp(-F(m_i)/k_B T), \tag{5.1}$$

where $F(m_i) = -k_B T \ln[\sum_{j \in B(m_i)} \exp(-E_j/k_B T)]$ is the local free energy associated with the basin around a single local minimum $B(m_i)$. One necessary condition for the existence of such a locally ergodic region is that the energies of these local minima are approximately equal. Else, if the energies differ by more than $k_B T$, the set of minima will split into several pieces, which are occupied with greatly different probability. Furthermore, we note that one usually only speaks of a solid solution, if an average periodic structure exists over which some or all of the various atom types are randomly distributed. Else, we deal with a structurally disordered amorphous compound, e.g. a metallic or covalent glass[2].

---

[1] In principle, such regions can be identified using swarms of extremely long Monte Carlo simulations (120). However, for certain systems such as solid solutions or compounds containing complex ions, alternative approaches are feasible (119) as described here for the case of solid solution-like phases.

Thus, the signature for the existence of a solid solution is the existence of a structurally related family of local minima, which all possess nearly the same energy. We therefore proceed as follows in our search for possible solid solution-like phases: In a first step, we employ the structure comparison algorithm CMPZ (122) (CMPZ is an acronym for CoMPare Zelle = compare cell) in order to check, whether two local minimum configurations found during the global landscape exploration at a given composition exhibit the same structure if we do not distinguish between those atom types which might be randomly distributed on the same sub-lattice in a solid solution structure[3]. If such a set of structurally related minima exists, we next check their energies, both on empirical potential and ab initio level (see below section 5.2). If these energies are similar, we construct supercells of the parent structure of the family and generate all (or a random subset for large supercells) of the possible structures in this family followed by a local optimization on empirical potential and ab initio level (see below section 5.2). If all the minimum energies fall within a narrow energy band, we can compute the local free energy of the solid solution state approximately in the thermodynamic limit by replacing the energy of the solid solution by the average over the minimum energies, and taking for the entropy contribution the appropriate entropy of mixing of an ideal solution at the given composition. Alternatively, one could compute an estimate of the partition function in the thermodynamic limit by explicitly summing the Boltzmann factors $\exp(-F(m_i)/k_BT) \approx \exp(-E(m_i)/k_BT)$ over a sufficiently large number of minimum regions corresponding to solid-solution-like atom configurations m_i. Thus, we could avoid using the entropy of mixing of an ideal solution which is only approximately valid, of course. However, the number of configurations needed to proceed in this fashion is too expensive computationally, since for each configuration (containing $O(10^2)$ atoms) a local minimization on ab initio level would be required.

Of course, if some ordered crystalline compound exhibits a lower free energy than the solid solution, the solid solution-like phase would only be metastable. Here, we ignore the contribution of the vibrational degrees of freedom to the local free energy. However, since the answer to the question, whether at composition x an ordered crystalline phase, a solid solution phase or the separation into two boundary phases with other compositions $x_1 < x < x_2$, constitutes the thermodynamically stable phase, depends on the difference between free energies, dropping the vibrational free energy for all these candidates is likely to cause only a higher order error.

---

[2] In contrast, crystalline solid solutions are often called substitutionally or chemically disordered (121).

[3] Note that, in principle, for each composition the crystalline solid solution phase (if it exists at all) could exhibit a different structure.

5.2 Ab initio calculations and global exploration: technical details

When all structure candidates have been selected, we employ ab initio calculations with the program CRYSTAL2003/06 (117; 123). For each distinct structure candidate, after symmetry identification and idealization using the algorithms SFND (124) (acronym for SymmetrieFiNDer = symmetry finder) and RGS (125) (acronym for RaumGruppenSucher = space group searcher) as implemented in the program KPLOT (126), we refine the structure by varying the cell parameters and the atom positions until a minimum of the energy is found. Here, we use a heuristic algorithm described in detail in Refs. (48; 127), which is based on a nested sequence of line search minimizations. Finally, the energy as function of the volume $E(V)$ is obtained by interpolation of the calculated data points with the standard Murnaghan formula (128).

In the examples shown in Part IV, all calculations were performed on both the Hartree-Fock and DFT (Density Functional Theory) level, since experience has shown (48) that one needs at least two different ab initio methods, in order to gain some feeling for the quantitative validity of the results. For the DFT calculations the B3LYP functional (Becke's three parameter functional (112)), where the exchange-correlation term is a weighted combination of the LDA-, Becke-, Hartree-Fock-, Vosko-Wilk-Nusair- and LYP-exchange/correlation terms, and the LDA-VBH functional were usually employed.

The empirical potential employed during the global search for local minima consisted of a damped Coulomb-term plus a Lennard-Jones-type potential, where the Lennard-Jones parameters $\sigma_{ij} = r_i + r_j$ are given by the sum of the ionic radii of atoms i and j with charge q_i and q_j. As a global optimization algorithm, stochastic simulated annealing (89; 90) runs based on random Monte Carlo walks on the energy landscape with decreasing temperature parameter were used, for each fixed composition with up to 20-30 atoms/simulation cell. Both atom positions (85% of all Monte Carlo steps) and the parameters of the periodically repeated simulation cell (15% of all Monte Carlo steps) were freely varied during the random walks. In the case of the mixed quasi-binary alkali halide systems, the supercells contained up to 64 atoms and were generated by simple multiplication of the original cell on the vector, e.g. (1 1 2); with posterior random changing of atom position into one of the sublattices in order to generate new "structure-family" candidates (see Section 6.3). These candidates were then quenched both on empirical potential and *ab initio* level. For the lanthanum halide systems, the supercells contained up to 96 atoms and were generated by the same procedure. In addition, these newly generated structures were used as input for threshold runs, which served as an additional method besides the standard simulated annealing to find new structure candidates with a large number of formula units (see Section 8.1).

5.3 Computation of the enthalpy of formation

After the energies of the local minima for structure candidates that belong to the solid solution-like phase or to individual ordered crystalline modifications have been obtained, it is possible to calculate the enthalpy of formation of a compound A_xB_{1-x} by the following formula:

$$\Delta_f H(A_xB_{1-x}) = \langle E(A_xB_{1-x})\rangle - xE(A) - (1-x)E(B) + p\Delta V(x), \tag{5.2}$$

where $\langle E(A_xB_{1-x})\rangle$ is the total energy of the solid solution state averaged over all minima belonging to this state, $E(A)$ and $E(B)$ are the energies of the pure compounds A and B, respectively, and x is the fraction of A in the overall composition. Also, one should note, that at standard pressure the contribution of the $p\Delta V(x)$-term is negligible, but it becomes noticeable at elevated pressures (see Section 6.3.4).

Obviously, this procedure yields a finite number of data points for different values of x, and the Redlich-Kister polynomial (118) was used to fit the results:

$$\Delta_f H(x) = x(1-x)\sum_{i=0}^{N} a_i(1-2x)^i, \tag{5.3}$$

where a_i are the fitting parameters. Usually, we have only included the first two terms in the polynomial expansion, since the total number of data points and the spread in energies for given compositions would not justify the use of higher-order polynomials.

Of course, if the compound A_xB_{1-x} is an ordered crystalline compound, only one minimum contributes to the locally ergodic region, and the energy average trivially equals the energy $E(A_xB_{1-x})$. Furthermore, these data points should be treated individually, and it is usually not appropriate to try to fit $\Delta_f H(x)$ with some kind of polynomial function - the energies of such ordered structures do not change smoothly as a function of x, since these structures are usually not simply related to each other[4].

5.4 Construction of the phase diagram

As mentioned above, the Gibbs energy of formation with respect to the pure compounds ($x = 0$ and $x = 1$) is then calculated by adding the standard entropy of mixing $S_{mix}(x) =$

---

[4] We would also expect a discontinuity in $\Delta_f H(x)$ to occur, if the family of solid solution-like structures changed from e.g. a NaCl- to a CsCl-superstructure at some value of x.

$-R[x\ln(x) + (1-x)\ln(1-x)]$[5]:

$$\Delta_f G(x) = RT[x \ln x + (1-x)\ln(1-x)] + x(1-x)\sum_{i=0}^{N} a_i(1-2x)^i, \tag{5.4}$$

where R = 8.31451 (J/(mol*K)) is the universal gas constant. From $\Delta_f G(x)$, the phase diagram can now be obtained by means of the so-called convex hull method described in the Section 4.2 (for more detail see the original reference (52)), since the thermodynamically preferred combination of phases corresponds to linear combinations of appropriately chosen boundary phases with fractions $x_1, x_2, \ldots$ of A that minimize the total Gibbs energy of the system. We note that as long as $\Delta_f H(A_x B_{1-x})$ can be described by a sufficiently low-order Redlich-Kister polynomial, there will never be more than two boundary phases for a given value of x. Furthermore, since $\lim_{x\to 0} \partial\Delta_f G(x)/\partial x = -\infty$ and $\lim_{x\to 1} \partial\Delta_f G(x)/\partial x = +\infty$, these boundary phases will never occur at $x = 0$ or $x = 1$ for non-zero temperature.

---

[5] Of course, if we are dealing with an ordered compound $A_x B_{1-x}$, only one minimum contributes, and the additional entropy term equals zero.

Part IV

Systematic application to selected chemical systems

6 Quasi-binary alkali halogenide systems

6.1 Introduction

As we have mentioned earlier, nowadays, the availability of high quality phase diagrams plays a key-role in materials science and engineering. Thus, one can find on the market several commercial products, e.g. FactSage (129), Thermo-Calc (130), MTDATA (131), PANDAT (132); and many research groups are involved in the business of computing or improving phase diagrams. Recently, many studies of phase diagram and structure calculations started to be supported by *ab initio* calculations with great success, e.g. a new metastable modification of lithium bromide, recently predicted in our group as a possible structure candidate, has been synthesized (133).

In this thesis, a new methodology for the prediction of the low temperature region of phase diagrams is presented. We expect, that our data can be used by experimentalists as a starting point in their work, and can help to remove all, or as many as possible, white spots on the phase diagrams. To validate our methodology discussed in the previous chapter, we were guided by the following considerations: enough thermodynamic data should be available for the systems under investigation, and the systems should be sufficiently simple to allow a systematic study while still allowing for the possibility of reasonably complex phase diagrams. Thus, the first systems we chose were the quasi-binary alkali halide systems, some of which exhibit continuous solutions in the solid phase, while others only possess ordered crystalline phases according to the literature (134). Moreover, we took some examples where there is a lack of thermodynamic data for the solid phase, especially at low temperatures, since here the theoretical calculations could not only validate the phase diagrams but also yield quantitative improvements. In particular, we analyzed the following systems: NaX-LiX, NaX-KX, KX-RbX (where X = Cl or Br), MBr-MI (where M = Li, Na, K, Rb or Cs) and MBr-MCl (where M = Li, Na or K), all of which should exhibit a miscibility gap, and CsX-LiX (where X = F, Cl, Br or I) and LiX-RbX (where X = Cl, Br), where crystalline compounds are expected.

6.2 General remarks

Our general approach to the determination of structure candidates has been given in detail in the Part III. Specifically, the atoms in the quasi-binary halides were modeled as spherical ions that interact via a simple empirical two-body potential, $V_{ij}(r_{ij})$, consisting of a Coulomb- and a Lennard-Jones-term that depend only on the atom-atom distance r_{ij}, in order to allow fast calculations of the energy of a given configuration. The Lennard-Jones parameters $\sigma_{ij} = r_s(r_i + r_j)$ are given by the sum of the ionic radii of atoms i and j with charges q_i adn q_j multiplied by a scaling factor r_s. The ionic radii are presented in the Appendix (see the Table A.1).

The *ab initio* runs were performed on both Hartree-Fock (HF) and density functional theory (DFT) level; the basis sets were optimized versions (135) of data sets available in the literature (136) (see Appendix, Tables A.2, A.3 and A.4).

6.3 Phase diagrams with miscibility gaps

6.3.1 NaCl-LiCl, NaBr-LiBr and NaCl-KCl

Introduction

The NaCl-LiCl, NaBr-LiBr and NaCl-KCl systems have been studied in detail experimentally in both the liquid/solid (137; 138; 139) and the low-temperature regions, including the determination of their miscibility gaps (140; 141; 142; 143; 144). Thus, we decided to use them as test systems for our new methodology.

Results and Discussion

For each chemical system, several hundred global optimization runs were performed for a number of different compositions each, at a pressure of 0 Pa. In the case of the NaCl-LiCl system, we performed calculations for 9 different compositions (1:9, 1:3, 1:2, 2:3, 1:1, 3:2, 2:1, 3:1, 9:1) besides the binary systems, and for the other systems, we considered 5 (1:3, 1:2, 1:1, 2:1, 3:1) compositions. The resulting structure candidates for each system were analyzed with respect to their symmetries.

For a number of supercells containing up to 64 atoms, structure candidates with rocksalt lattice super-structure were generated by permutation of the cation positions followed by two local optimization runs: first with the empirical potential, and subsequently on ab initio level. In Fig. 6.1, we present as a representative example the resulting $E(V)$ curves in the NaCl-LiCl system for 11 selected candidates with composition NaCl:LiCl = 1:1, all belonging to the solid-solution-like phase in the rock salt structure type. Each atom configuration represents one of the many possible random arrangements of Na and Li over the cation positions in the rock salt structure type. One clearly sees that their energies are very similar, with the spread in energy corresponding to a temperature of about 30 K.

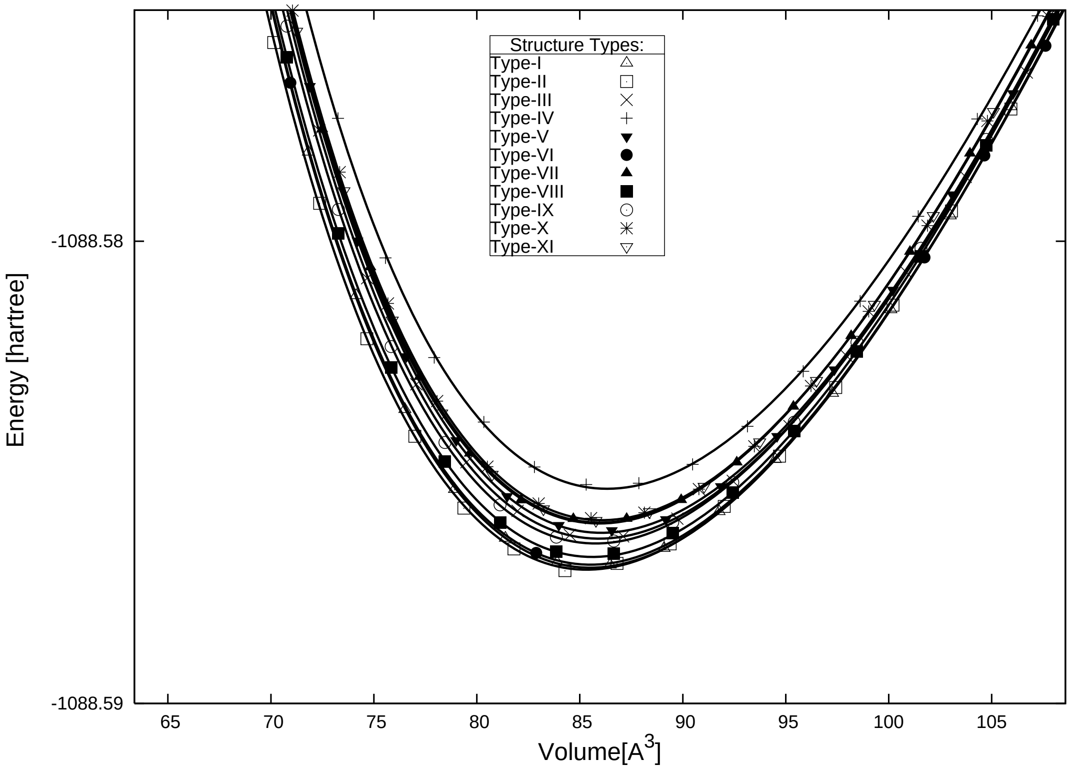

Figure 6.1: $E(V)$ curves for 11 structure candidates belonging to the solid solution state (rocksalt superstructure) of the NaCl-LiCl system with composition 1:1, calculated via the Hartree-Fock method using an all-electron basis set. Each of these structures is a representative of the set of atom configurations that are generated by randomly arranging the Na and Li atoms on the cation sublattice of the rock salt structure type. Note that the energies of these structures are very similar, with a spread in energy corresponding to a temperature of about 30 K.

In the next step, the enthalpies of formation of each compound were obtained according to equation (5.2). Fitted parameters according to equation (5.3) for all systems are listed in Table 6.1.

The data above allows us to calculate the Gibbs energy of the solid phase and to predict the location of the miscibility gap. The critical parameters are listed in Table 6.2. In

Table 6.1: The parameters of the enthalpy of formation for the NaCl-LiCl, NaBr-LiBr and NaCl-KCl systems obtained in the present work (in Joule/mol).

System	HF		DFT-B3LYP	
	a_0	a_1	a_0	a_1
NaCl-LiCl	8267.1	-1841.7	8362.7	-650.5
NaBr-LiBr	7564.9	-580	7892.2	-693.2
NaCl-KCl	15059	2561	12667	2817

Figs. 6.2 - 6.4 one can see the predicted binodal curves (both for HF- and DFT-based calculations), the experimental data and a plot of the miscibility gaps (134) based on the experimental thermodynamic data.

Table 6.2: The critical parameters for the NaCl-LiCl, NaBr-LiBr and NaCl-KCl systems obtained in the present work. T_c is the critical temperature of the decomposition in K, and x_c is the concentration of the second compound. T_c^{lit} and x_c^{lit} are values suggested in the literature.

System	*Method*	T_c	x_c	T_c^{lit}	x_c^{lit}	Reference
NaCl-LiCl	*HF*	544	0.63	$544, 587$	$0.58, 0.65$	(141), (140)
	DFT	509	0.56			
NaBr-LiBr	*HF*	460	0.55	519^*	0.51	(134)
	DFT	483	0.56			
NaCl-KCl	*HF*	959	0.39	771	0.47	(144)
	DFT	833	0.37			

* based on fitting the experimental data (142)

An important condition for the presence of a solid-solution phase is the existence of a family of structurally related minima, which exhibit the same superstructure. Furthermore, the energies of these minima must be sufficiently close such that they exhibit similar probabilities of finding the system in these basins in the thermodynamic limit. As one can see (Fig. 6.1), the resulting $E(V)$ curves are closely the same, with the spread in energies per atom $\delta(E) \approx 3 \times 10^{-3}$ eV $<< k_B T_c \approx 5 \times 10^{-2}$ eV.

Thus, we can assume that the systems will exhibit a solid solution-like phase where the cations are randomly distributed over the cation sublattice of the rocksalt structure. One should mention that the same behavior was observed regardless of whether the Hartree-Fock or the DFT method was used. In the case of the NaCl-LiCl system, in the beginning of our study, we investigated 9 different compositions besides the binary compounds. When analyzing the data and computing the critical parameters, we noted that already the five compositions (3:1, 2:1, 1:1, 1:2, 1:3) yielded essentially the same values for the parameters in the Redlich-Kister polynomial and the critical parameters as we had deduced with using all nine compositions. Since the computational effort required for the local optimizations of the supercells on ab initio level is very high, we decided to include only five compositions in the final analysis of the other two systems once it had become clear that a solid solution-like phase was present.

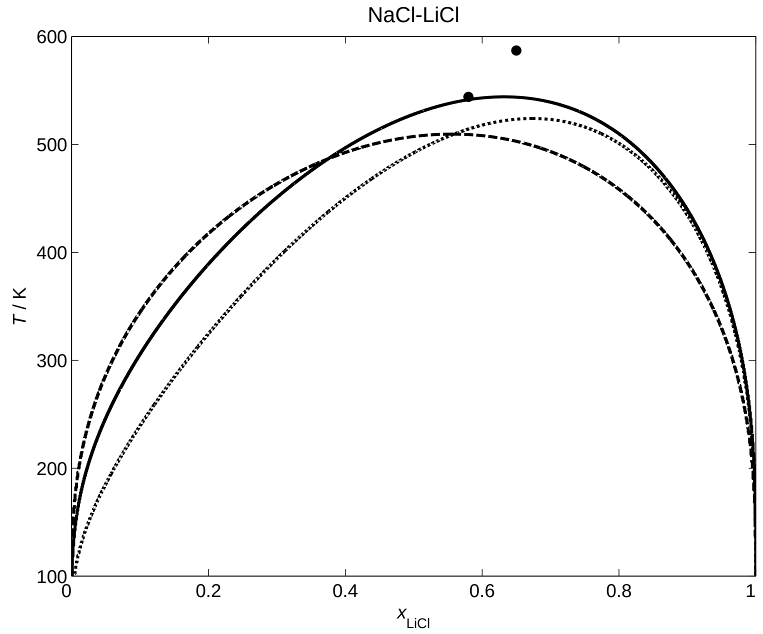

Figure 6.2: The miscibility gaps in the NaCl-LiCl system. Solid curve - based on HF-calculations, dashed curve - based on DFT-calculations, dotted curve - fit to experimental data (134), points - experimental data from (140; 141).

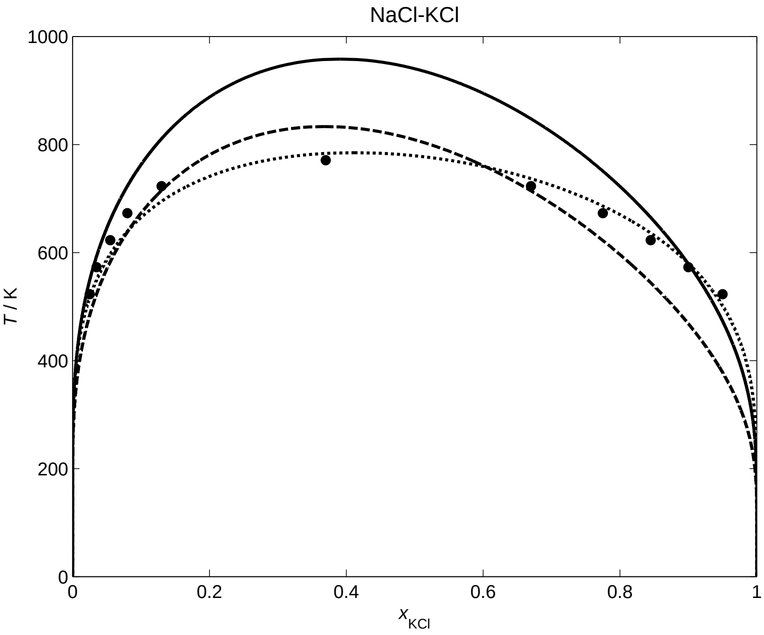

Figure 6.3: The miscibility gaps in the NaCl-KCl system. Solid curve - based on HF-calculations, dashed curve - based on DFT-calculations, dotted curve - fit to experimental data (134), points - experimental data from (144).

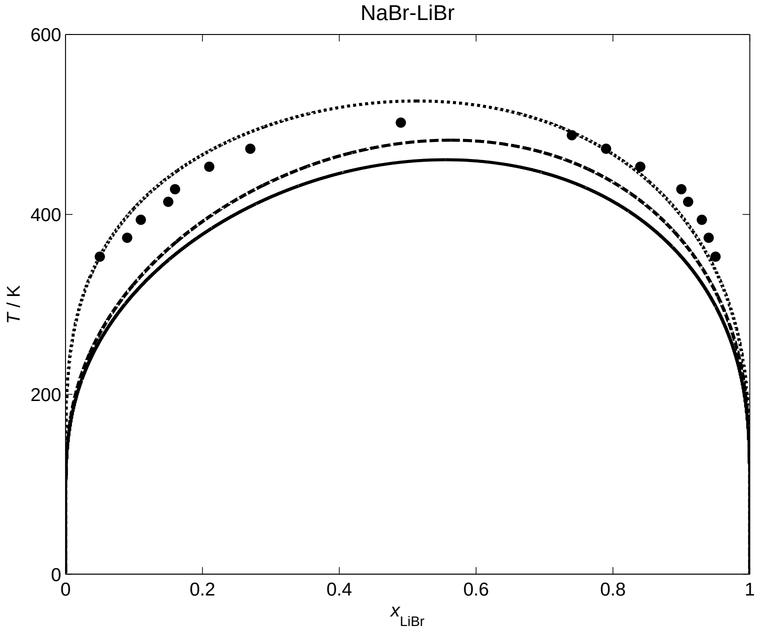

Figure 6.4: The miscibility gaps in the NaBr-LiBr system. Solid curve - based on HF-calculations, dashed curve - based on DFT-calculations, dotted curve - fit to experimental data (134), points - experimental data from (142).

As is well known, every solid solution becomes unstable as the temperature decreases: ordering sets in, and, finally, a separation into its pure components takes place. Hence, the existence of the miscibility gaps in all these systems was expected once the existence of a solid solution-like phase had been established. The data obtained for the enthalpy of formation at ≈ 0 K allowed us to calculate the Gibbs energy of formation using equation (5.4) and to construct parts of the phase diagrams at low temperatures. In Fig. 6.2, one can see the good agreement for the NaCl-LiCl system with the experimental data. In the case of the NaCl-KCl and the NaBr-LiBr systems, we also correctly deduce the existence of the miscibility gaps without input from experiment, but the quantitative agreement with the experimental data is not as high as in case of the NaCl-LiCl system.

6.3.2 KBr-NaBr, KCl-RbCl and KBr-RbBr

Introduction

Next we would like to present the investigations for the KBr-NaBr, KCl-RbCl and KBr-RbBr systems. The first one had been experimentally studied in detail both in the liquid/solid and low-temperature regions, including the miscibility gap, thus the KBr-NaBr system could serve as a test system. In contrast KCl-RbCl and KBr-RbBr have not yet been properly investigated experimentally, especially in the low-temperature region. Thus, systems containing rubidium were of particular interest.

Results and Discussion

As before, for each chemical system, several hundred global optimization runs were performed for a number of different compositions each, at a pressure of 0 Pa. We performed calculations for 7 different compositions (4:1, 3:1, 2:1, 1:1, 1:2, 1:3, 1:4) besides the limiting binary phases. In all three cases the minima with the lowest energies belonged to the rocksalt structure type. Thus, we generated a number of supercells containing up to 64 atoms, with rocksalt lattice super-structure by systematic permutation of the cation positions followed by two local optimization runs: first with the empirical potential, and subsequently on the *ab initio* level. In the next step, the enthalpies of formation of each compound were obtained according to equation (5.2). Fitted parameters according to equation (5.3) for all these systems are listed in Table 6.3.

Table 6.3: The parameters of the enthalpy of formation (according to equation (5.2)) for the rocksalt - type solid solution phases in the KBr-NaBr, KCl-RbCl and KBr-RbBr systems obtained in the present work (in Joule/mol).

System	HF		DFT-B3LYP	
	a_0	a_1	a_0	a_1
KBr-NaBr	11253	-419	10276	-380
KCl-RbCl	3146.8	374.7	3295.4	35.1
KBr-RbBr	2017.7	58.2	2735.3	797.5

From these data we calculated the Gibbs energy of the solid phase and predicted the location of the miscibility gap. The critical parameters are listed in Table 6.4.

Table 6.4: The critical parameters for the rocksalt - type solid solution phases in the KBr-NaBr, KCl-RbCl and KBr-RbBr systems obtained in the present work. T_c is the critical temperature of the decomposition in K, and x_c is the concentration of the second compound. T_c^{lit} and x_c^{lit} are values suggested in the literature (134).

System	*Method*	T_c	x_c	T_c^{lit}	x_c^{lit}
KBr-NaBr	*HF*	679	0.53	668*	0.5*
	DFT	620	0.53		
KBr-RbBr	*HF*	121	0.48	120	0.5
	DFT	189	0.345		
KCl-RbCl	*HF*	195	0.42	90	0.5
	DFT	198	0.49		

* values based on fitting the experimental data (143)

In Figs. 6.5 - 6.7 one can see the predicted binodal curves (for both HF- and DFT-based calculations), and the experimental data that are available for the KBr-NaBr system. In

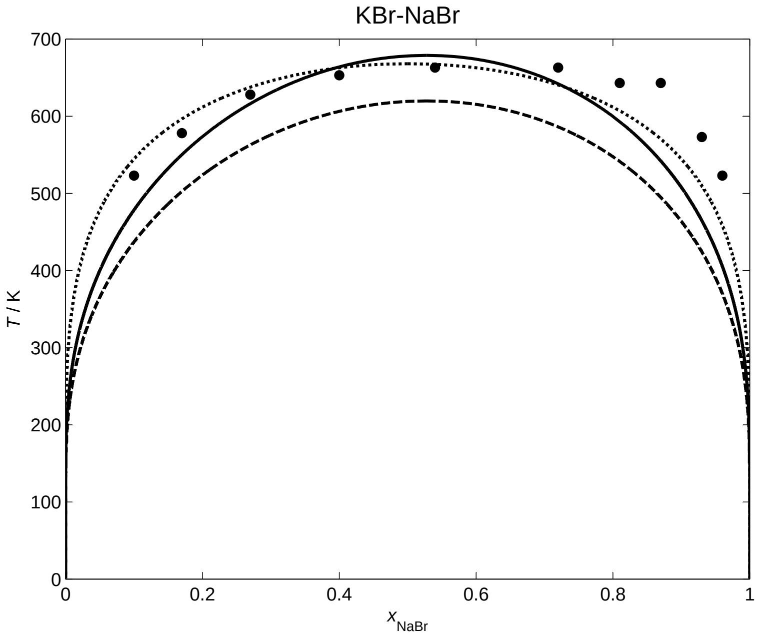

Figure 6.5: The miscibility gaps in the KBr-NaBr system. Solid line - based on Hartree-Fock-calculations, dashed curve - based on DFT-B3LYP-calculations, dotted line - fit to experimental high- and low-temperature data (134), points - experimental data from (143).

the case of the KCl-RbCl and KBr-RbBr systems, the miscibility gaps based on the extrapolation from high-temperature data (134) are presented.

Earlier, we noted that one important condition for the presence of a solid-solution phase is the existence of a family of structurally related minima, which exhibit the same superstructure (see Section 6.3.1). Furthermore, the energies of these minima must be sufficiently close such that there exist similar probabilities of finding the system in these basins in the thermodynamic limit. For the KBr-NaBr, KCl-RbCl and KBr-RbBr systems, we find that the resulting $E(V)$ curves belonging to a family of minima (rocksalt structure family) are closely the same, with the spread in energies per atom $\delta(E) \approx 5 \times 10^{-4}$ eV $<< k_B T_c$ $\approx 2 - 6 \times 10^{-2}$ eV. We can assume that these systems will exhibit a solid solution-like phase where the cations are randomly distributed over the cation sublattice of the rocksalt structure. One should mention that the same behavior was observed regardless of whether the energy was calculated on Hartree-Fock or DFT level.

In Fig. 6.5, one can see the good qualitative and quantitative agreement of the miscibility gap prediction (both for HF and DFT-B3LYP based calculations) with the experimental data for the KBr-NaBr system. Figs. 6.6 and 6.7 show the corresponding results for the KCl-RbCl and the KBr-RbBr systems. In both cases, we predict the existence of miscibility gaps. These results agree qualitatively with the extrapolations from high-temperature experimental data for these two systems. However, we feel that the numerical values of the extrapolated critical temperatures and the shape of the gap are not very reliable, and we suggest that our calculated values are more appropriate. In particular, this

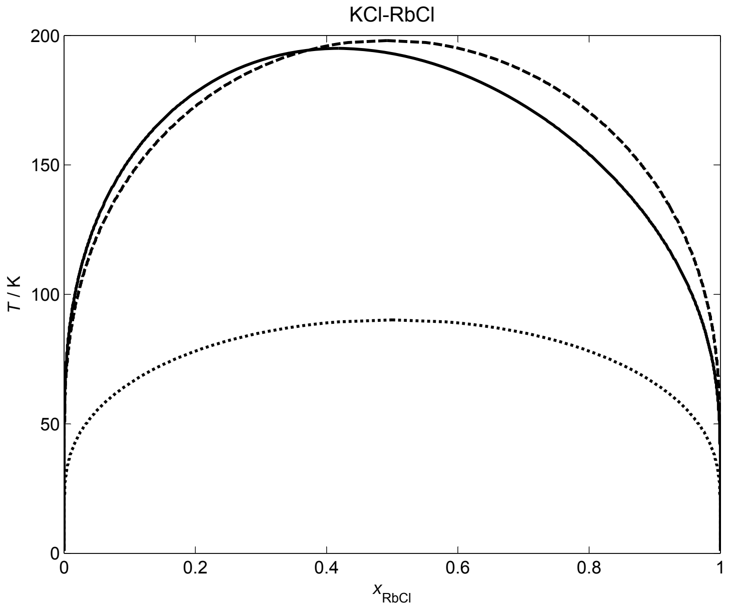

Figure 6.6: The miscibility gaps in the KCl-RbCl system. Solid line - based on Hartree-Fock-calculations, dashed curve - based on DFT-B3LYP-calculations, dotted line - extrapolated from high-temperature experimental data (134).

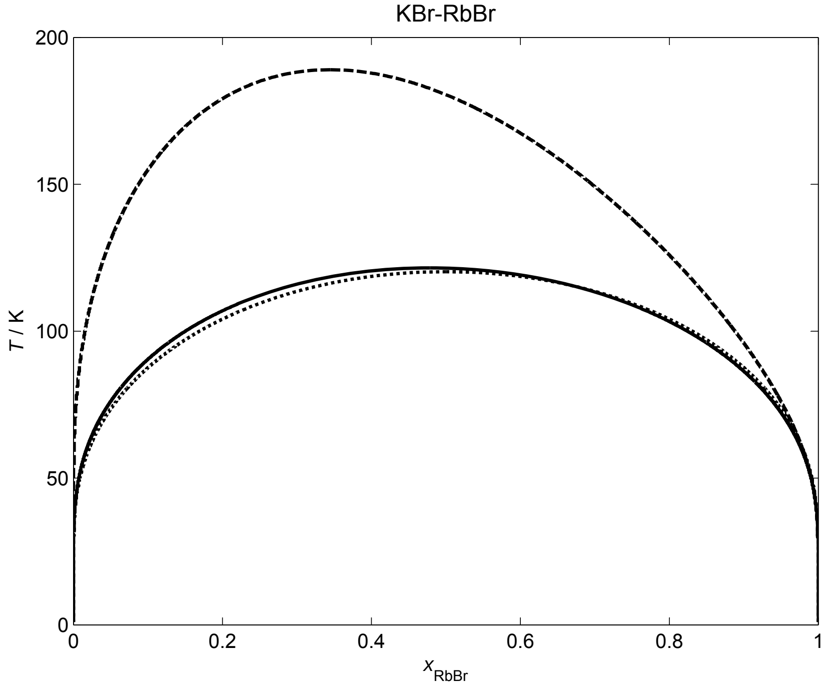

Figure 6.7: The miscibility gaps in the KBr-RbBr system. Solid line - based on Hartree-Fock-calculations, dashed curve - based on DFT-B3LYP-calculations, dotted line - extrapolated from high-temperature experimental data (134).

should hold for the KCl-RbCl system, since the HF and DFT calculations give very similar results (see Fig. 6.6 and Table 6.4). In the case of the KBr-RbBr system, we expect that the true location of the miscibility gap will be somewhere between the curves calculated via HF and DFT, and we strongly suspect that the extrapolation from the experimental high-temperature data underestimates the size of the gap. One the other hand, a possible source of error in the exact location of the miscibility gaps is the contribution of phonons to the free energy of formation. However, our earlier studies (145) suggest that the phonon contributions of the ternary structures and the binary compounds cancel to first order, and thus will not greatly influence the location of the miscibility gap (see Critical discussions part 6.5).

6.3.3 The MBr-MI systems, where M = Li, Na, K, Rb or Cs

Introduction

In the previous sections 6.3.1 and 6.3.2, we dealt with systems which have two types of cations and only one type of anion. In the present section we consider systems with two different anions and only one type of cation. As examples, we investigated the alkali metal bromide-iodide systems with composition MBr_xI_{1-x} ($0 \leq x \leq 1$; where M = Li, Na, K, Rb or Cs). Several of these systems constitute materials of practical interest; e.g. chemical sensors based on the solid solution of KBr and KI are employed for ozone measurements in the stratosphere (146).

Results and Discussion

For each chemical system, several hundred global optimization runs were performed for a number of different compositions each, at a pressure of 0 Pa. We performed calculations for 5 different compositions (1:3, 1:2, 1:1, 2:1, 3:1) besides the limiting binary phases for each system. Our previous studies (see Sections 6.3.1 and 6.3.2) show that nine, seven or five different compositions give essentially the same values for the parameters in the Redlich-Kister polynomial and the critical parameters. Thus, since the computational effort required for the local optimizations of the supercells on *ab initio* level is very high, we decided to include only five compositions in the analysis, once it had become clear that a solid solution-like phase was going to be the thermodynamically stable one.

The resulting structure candidates were analyzed with respect to their symmetries. In all systems, we found that the minima with the lowest energies belonged to the rocksalt structure type constituting a structural family likely to result in a solid solution-like phase. Next, supercells, containing up to 64 atoms, were generated and locally optimized on *ab initio* level. Subsequently, the enthalpies of formation of each compound were obtained according to equation (5.2). Fitted parameters according to equation (5.2) for all systems are listed in Table 6.5.

Table 6.5: The parameters of the enthalpy of formation for the rocksalt-type solid solution phases in the MBr-MI systems where (M = Li, Na, K, Rb or Cs) obtained in the present work (in Joule/mol).

System	HF		DFT-B3LYP		DFT-LDA-VBH	
	a_0	a_1	a_0	a_1	a_0	a_1
LiBr-LiI	6717.3	955.7	5757.7	986.4	-	-
NaBr-NaI	5747.5	873.4	4860.5	660.6	-	-
KBr-KI	4975.6	666.8	5136.8	79.9	-	-
RbBr-RbI	4427.8	722.3	4309.7	625.7	4324.7	726.8
CsBr-CsI	4563.5	1016.2	4417.1	1024.2		

From these data we calculated the Gibbs energy of the solid phase and predicted the location of the miscibility gap. The critical parameters are listed in Table 6.6.

Table 6.6: The critical parameters for the rocksalt-type solid solution phases in the MBr-MI systems where (M = Li, Na, K, Rb or Cs) obtained in the present work. T_c is the critical temperature of the decomposition in K, and x_c is the concentration of the second compound. T_c^{lit} and x_c^{lit} are values suggested in the literature (134).

System	$Method$	T_c	x_c	T_c^{lit}	x_c^{lit}
LiBr-LiI	HF	421	0.40	481	0.5
	$B3LYP$	366	0.39		
NaBr-NaI	HF	362	0.4	370	0.4
	$B3LYP$	303	0.4		
KBr-KI	HF	310	0.4	364	0.5
	$B3LYP$	309	0.49		
RbBr-RbI	HF	281	0.4	395	0.33
	$B3LYP$	270	0.4		
	$LDA-VBH$	275	0.39		
CsBr-CsI	HF	300	0.37	391	0.5
	$B3LYP$	292	0.36		
	$LDA-VBH$	368	0.4		

In Figs. 6.8 - 6.13 one can see the predicted binodal curves (both for HF- and DFT-based calculations), the experimental data and a plot of the miscibility gaps extrapolated from the experimental thermodynamic data(134).

Earlier in Section 6.3.1, we noted that one important condition for the presence of a solid solution phase is the existence of a family of structurally related minima, which exhibit the same superstructure. Furthermore, the energies of these minima must be sufficiently close such that they exhibit similar probabilities of finding the system in these basins in

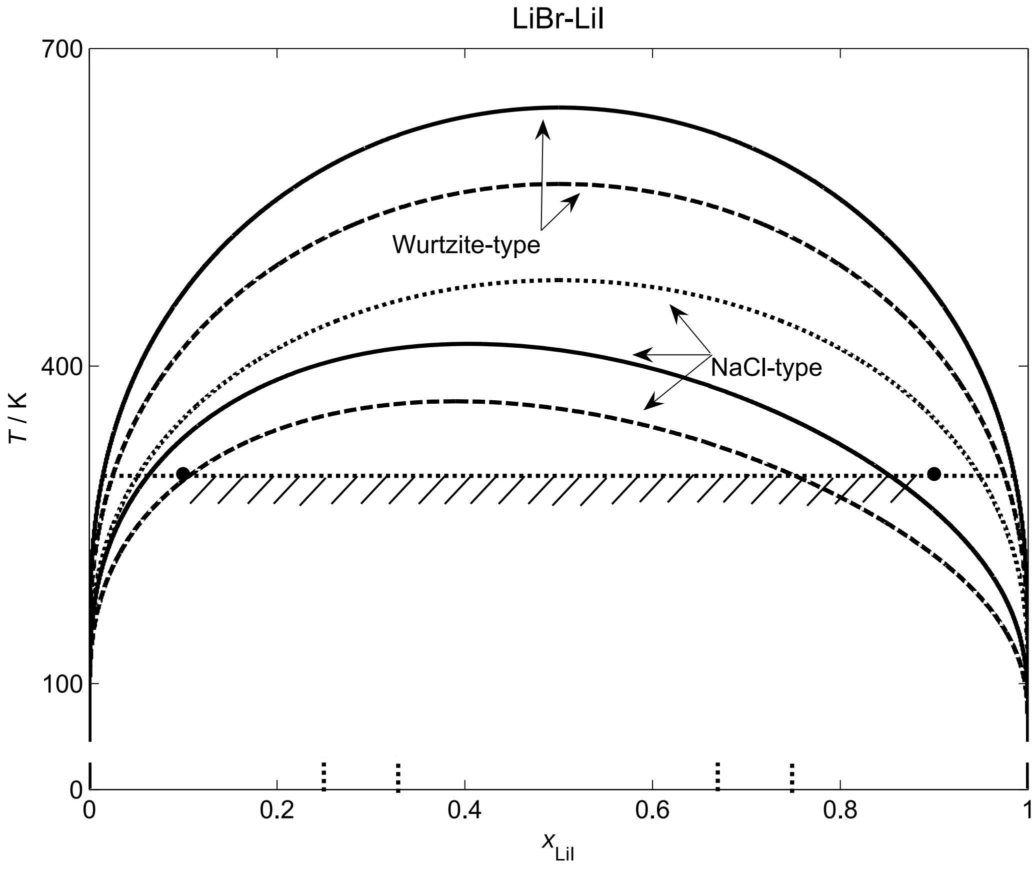

Figure 6.8: The miscibility gaps in the LiBr-LiI system. Solid curve - based on HF-calculations, dashed curve - based on DFT-B3LYP-calculations; dotted miscibility curve - has been extrapolated from experimental high-temperature data (134). Bullet point on the left (T = 298 K, x_{LiI} = 0.1): experimental data by (147; 148) (rocksalt-type); bullet point on the right (T = 298 K, x_{LiI} = 0.9): experimental data by (148) (rocksalt-type). In the region below the horizontal dotted line, a metastable solid solution based on the wurtzite structure type has been observed (148). Locations of the metastable ordered crystalline modifications are indicated by dotted lines.

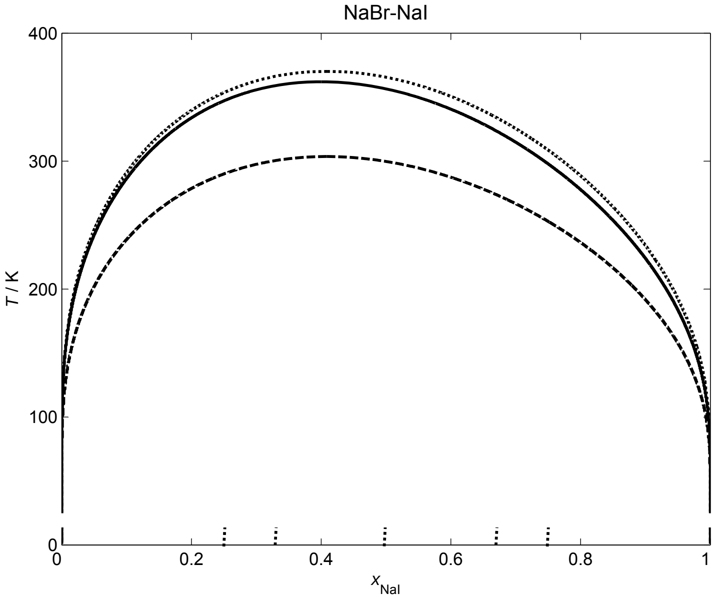

Figure 6.9: The miscibility gap in the NaBr-NaI system. Solid curve - based on HF-calculations, dashed curve - based on DFT-B3LYP-calculations, dotted curve - estimated from experimental data (134). Locations of the metastable ordered crystalline modifications are indicated by dotted lines.

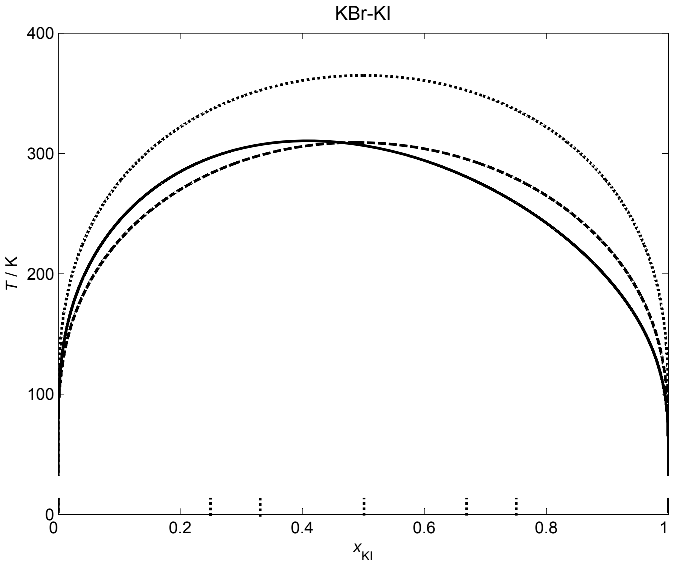

Figure 6.10: The miscibility gap in the KBr-KI system. Solid curve - based on HF-calculations, dashed curve - based on DFT-B3LYP-calculations, dotted curve - estimated from experimental data (134). Locations of the metastable ordered crystalline modifications are indicated by dotted lines.

the thermodynamic limit. For all systems in this section, we find that the resulting $E(V)$ curves belonging to a family of minima are closely the same, with the spread in energies per atom $\delta(E) \approx 5\times10^{-3}$ eV $<< k_B T_c \approx 3\times10^{-2}$ eV. We thus can assume that the systems will exhibit a solid solution-like phase where the anions are randomly distributed over the anion sublattice of the rocksalt structure. One should mention that the same behavior was observed regardless of whether the energy was calculated on Hartree-Fock or DFT basis. This allows us to calculate the miscibility gaps in all systems investigated. Figs. 6.8 - 6.13 show our data together with the miscibility gaps based on the optimization of the experimental thermodynamic data available. Of course, in every system investigated a number of structure candidates exhibiting ordered crystalline structures that do not appear to belong to one of the major structure families (rocksalt, CsCl, wurtzite) have also been observed. These candidates are all metastable with respect to the structures belonging to the rocksalt family.

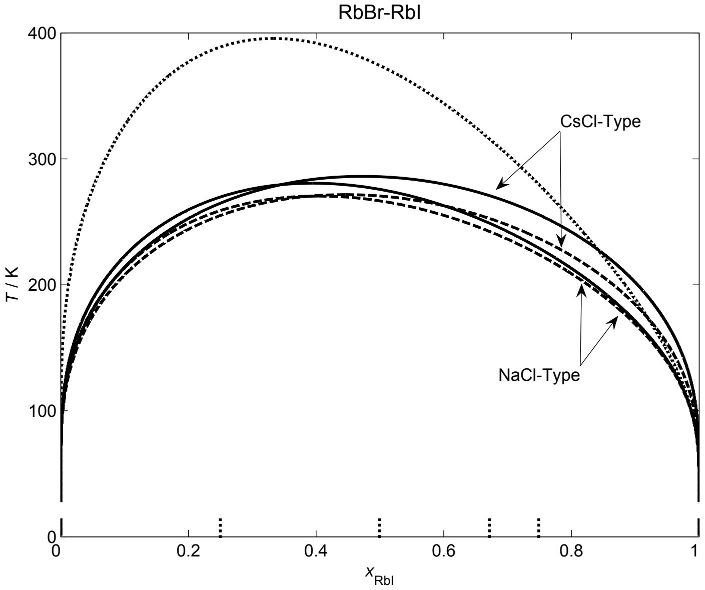

Figure 6.11: The miscibility gaps in the RbBr-RbI system (stable rocksalt- and metastable CsCl-type). Solid curve - based on HF-calculations, dashed curve - based on DFT-B3LYP-calculations, dotted curve - extrapolated from experimental high-temperature data (134) (rocksalt-type solid solution). Locations of the metastable ordered crystalline modifications are indicated by dotted lines.

The stability of the solid solution of the RbBr-RbI systems has been discussed in many publications (149; 150; 151; 152; 153). On the one hand many authors proposed critical parameters above room temperature: e.g. Hovi (149) suggested that the solid solution would be stable above 433 K, and Ahtee and Koski (150) gave 346 K as the critical temperature. On the other hand, Ahtee and Koski (150), Thomas and Wood (151), and Ahtee (152) were able to record X-ray powder patterns of a single solid solution-like phase at room temperature in a dry atmosphere. From this and additional experiments Swamy and co-workers (153) concluded that the solid solution in the RbBr-RbI system should be stable already at room temperature. In this context our prediction ($T_c \approx$ 280-290 K) us-

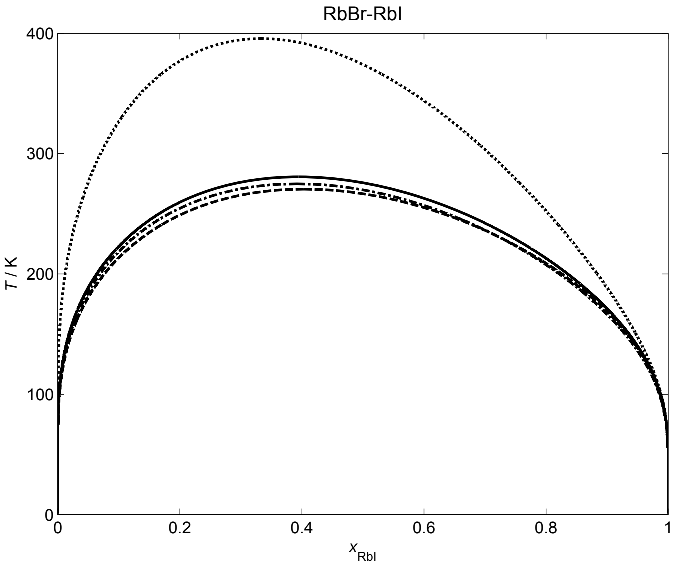

Figure 6.12: The miscibility gap for the stable solid solution phase (rocksalt-type) in the RbBr-RbI system. Solid curve - based on HF-calculations, dashed curve - based on DFT-B3LYP-calculations, dotted-dashed curve - based on DFT-LDA-VBH-calculations, dotted curve - extrapolated from experimental high-temperature data (134).

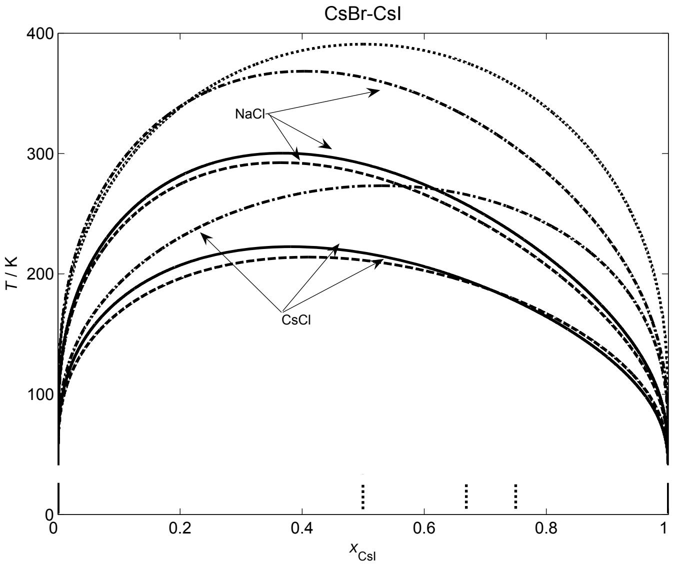

Figure 6.13: The miscibility gaps in the CsBr-CsI system (stable rocksalt- and metastable CsCl-type). Solid curve - based on HF-calculations, dashed curve - based on DFT-B3LYP-calculations, dotted-dashed curve - based on DFT-LDA-VBH-calculations, dotted curve - extrapolated from experimental high-temperature data (134) (rocksalt-type solid solution). Locations of the metastable ordered crystalline modifications are indicated by dotted lines.

ing three quite different *ab initio* methods is noticeably closer to the experimental results than the one suggested by Pelton (134) based on extrapolation from high-temperature data. In the case of the CsBr-CsI system, the few experimental data available (152; 154) only confirm that at room temperature a solid solution phase is present for x close to 0 and 1, which agrees both with our calculations and the miscibility curve suggested by Pelton (134) based on extrapolation from high-temperature data. No other experimental information concerning the location of the miscibility gap or some upper bound of the critical temperatures is available. Taking the uncertainty both in the calculations and thermodynamic extrapolations into account, we suggest that the miscibility gap is most likely located somewhere between the HF- / B3LYP-results and the two curves calculated with the LDA-VBH functional and extrapolated from high-temperature data, respectively.

One should mention, that in both RbBr-RbI and CsBr-CsI, we observed that the low-energy structure candidates of all compositions belonged to two main families exhibiting the rocksalt and CsCl-structure type, respectively, for the anion-cation arrangement. The small difference in energies among the structure candidates belonging to the metastable CsCl family allowed us to conclude, that if the system could not reach the thermodynamically stable rocksalt-like phase we would nevertheless observe solid solution-like behavior in the CsCl-structure type, and we have calculated the miscibility gap for this metastable solid solution. In the Rb-system, HF-, DFT-B3LYP- and LDA-VBH-calculations yielded essentially the same critical parameters and miscibility gaps for the metastable solid solution-like phase (see Tables 6.7 and 6.8), while in the case of cesium, the values computed with the LDA-VBH-functional are larger then the ones for HF and B3LYP. The resulting curves are also presented in figures 6.11 - 6.13. One can see that in the case of the RbBr-RbI system (Figs. 6.11, 6.12) the miscibility gaps for the stable and metastable solid solution, based on the data obtained by all *ab initio* methods, are very close. In contrast, in the case of the CsBr-CsI system, the metastable miscibility curve lies noticeably below the stable one (see Fig. 6.13).

Table 6.7: The parameters of the enthalpy of formation for the metastable wurtzite (LiBr-LiI system) and CsCl (in RbBr-RbI and CsBr-CsI systems) type solid solution phases obtained in the present work (in Joule/mol).

System	HF		DFT-B3LYP	
	a_0	a_1	a_0	a_1
LiBr-LiI	10711	0	9513.5	0
RbBr-RbI	4744.4	171.7	4462.2	333.6
CsBr-CsI	3455	656.9	3430.5	456.6

According to the literature a solid solution is observed in the LiBr-LiI system, which exhibits the metastable wurtzite structure-type (148) up to room temperature. During our global exploration of the enthalpy landscape we only find the thermodynamically stable rocksalt structure type; the metastable wurtzite type is only detected on the landscape of the binary LiI - compound. This indicates that the corresponding local minima on the empirical energy landscape are at rather high energies and are quite shallow. Nevertheless, we have computed not only the miscibility gap for the thermodynamically stable rocksalt

Table 6.8: The critical parameters for the metastable wurtzite (LiBr-LiI system) and CsCl (in RbBr-RbI and CsBr-CsI systems) type solid solution phases obtained in the present work. T_c is the critical temperature of the decomposition in K, and x_c is the concentration of the second compound.

System	$Method$	T_c	x_c
LiBr-LiI	HF	644	0.5
	$B3LYP$	572	0.5
RbBr-RbI	HF	286	0.47
	$B3LYP$	272	0.45
CsBr-CsI	HF	222	0.38
	$B3LYP$	214	0.4
	$LDA-VBH$	273	0.53

solid solution, but also the miscibility gap for the metastable wurtzite solid solution (see Tables 6.7 and 6.8), since in the binary lithium halides the energies of the wurtzite structure are quite close to those of the rocksalt modification on *ab initio* level (135; 155). Both gaps are plotted in Fig. 6.8, and we note that the one associated with the wurtzite-type extends to higher temperature than the stable one belonging to the rocksalt-type. As we mentioned above, a solid solution of the metastable wurtzite structure-type has been observed (148) up to room temperature (see horizontal dotted line in Fig. 6.8), but over a period of several weeks at room temperature it transforms into a mixture of two more stable rocksalt-type solid solution phases with different compositions exhibiting between 90% - 100% of LiI and LiBr, respectively. From our calculations, we can conclude, that the wurtzite solid solution is actually metastable both with respect to the rocksalt solid solution and with respect to the separation into a mixture of two solid solution phases containing over 90% LiI and LiBr, respectively, in the (metastable) wurtzite type (see Fig. 6.8).

Also, one should mention, that for the LiBr-LiI system most experimental thermodynamic information is still lacking; only the liquid-solid minimum has been measured so far. Thus, the prediction of the miscibility gap for a rocksalt-type solid solution phase by Pelton (134) appears to be quite speculative; from our data, we conclude that the critical parameters should lie between 420 and 366 K. In this connection, the observation by Gupta and co-workers (147), that the solubility of LiI in LiBr (in the rocksalt type solid solution) at room temperature is about 10 mole % LiI, is in quite satisfactory agreement with our calculations; analogous results and an additional data point at 90 mole % LiI at room temperature have been obtained in Ref. (148) (see Fig. 6.8).

6.3.4 The MBr-MCl systems, where M = Li, Na or K

Introduction

In the present section we consider another family of systems with two different anions and only one type of cation. We investigated the alkali metal bromide-chloride systems with composition MBr_xCl_{1-x} ($0 \leq x \leq 1$; where M = Li, Na, K). We can confirm the general observation in the literature (134) that the phase diagrams of these three alkali bromide-chloride systems show solid solution behaviour, and we compute the miscibility gaps at low temperatures. This information about the systems' stability and critical parameters of decomposition should be useful for experimentalists who study the crystal growth and the chemical and physical properties of these systems (156; 157; 158; 159).

Results and Discussion

For each chemical system, several hundred global optimization runs were performed for a number of different compositions each, at a pressure of 0 Pa. We performed calculations for 5 different compositions (3:1, 2:1, 1:1, 1:2, 1:3) besides the limiting binary phases. For each composition we found for the set of structure candidates with the lowest energies, that the energy differences between the candidates were very small. These candidates belonged to the same structure family, indicating a solid-solution behaviour for all three systems. After confirming this assumption by generating additional structures belonging to this family, the enthalpy of formation for each composition x were obtained according to equation (5.2).

The parameters for a fit of $\Delta_f H(x)$ with a Redlich-Kister polynomial for all of the systems are listed in Table 6.9.

Table 6.9: The Redlich-Kister polynomial fitting parameters of the enthalpy of formation (according to equation 5.2) for the rocksalt-type solid solution phases in the MBr-MCl systems (M = Li, Na or K) at standard pressure obtained in the present work (in Joule/mol).

System	HF		DFT-B3LYP	
	a_0	a_1	a_0	a_1
LiBr-LiCl	5938.1	-1474.8	5769.8	-1632.7
NaBr-NaCl	4802.3	16.7	4207.6	90.1
KBr-KCl	3956.53	-378.86	3317.0	245.5

From this data we calculated Gibbs energies of the solid phase and predicted the location of the miscibility gaps. The critical parameters are listed in Table 6.10.

Table 6.10: The critical parameters for the LiBr-LiCl, NaBr-NaCl and KBr-KCl systems at standard pressure obtained in the present work. T_c is the critical temperature of the decomposition in K, and x_c is the concentration of the second compound. T_c^{lit} and x_c^{lit} are values suggested in the literature (134).

System	$Method$	T_c	x_c	T_c^{lit}	x_c^{lit}
LiBr-LiCl	HF	398	0.64	301	0.5
	$DFT-B3LYP$	396	0.65		
NaBr-NaCl	HF	289	0.5	289	0.5
	$DFT-B3LYP$	253	0.48		
KBr-KCl	HF	242	0.57	210	0.5
	$DFT-B3LYP$	202	0.45		

In Figures 6.14 - 6.16 one can see the predicted binodal curves (both for HF- and DFT-B3LYP-based calculations) and a plot of the miscibility gaps extrapolated from high-temperature data (134).

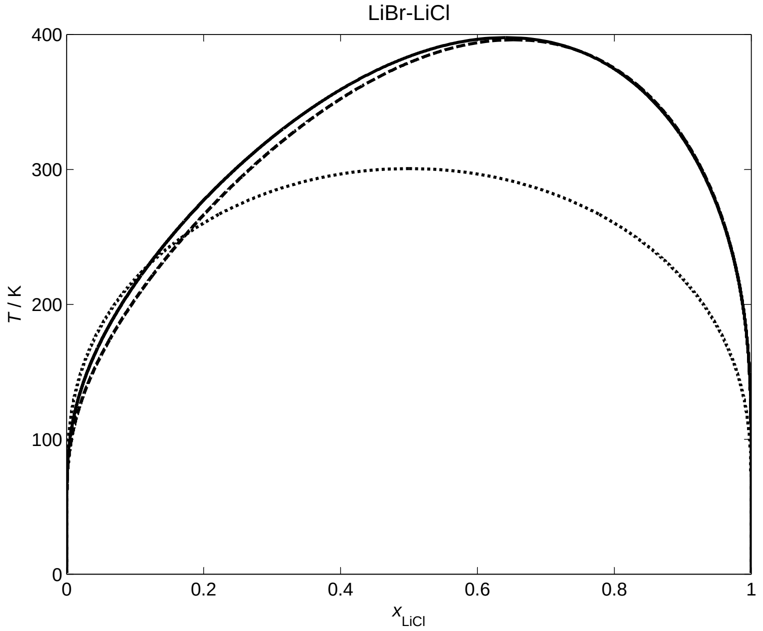

Figure 6.14: The miscibility gap in the LiBr-LiCl system. Solid curve - based on HF-calculations, dashed curve - based on DFT-B3LYP-calculations, dotted curve - estimated from experimental data (134).

We found that for all systems under investigation (LiBr-LiCl, NaBr-NaCl and KBr-KCl) the system should exhibit a solid solution-like phase regardless of whether the energy was calculated on a HF or DFT basis. As one can see from figures 6.15 - 6.16 and table 6.10, the critical parameters of decomposition predicted in the present work and those based on the optimization of the available experimental thermodynamic data (134) are in good agreement. In the case of the LiBr-LiCl system, one can see that our prediction (both HF and DFT results) and the high-temperature extrapolation are quite different. We

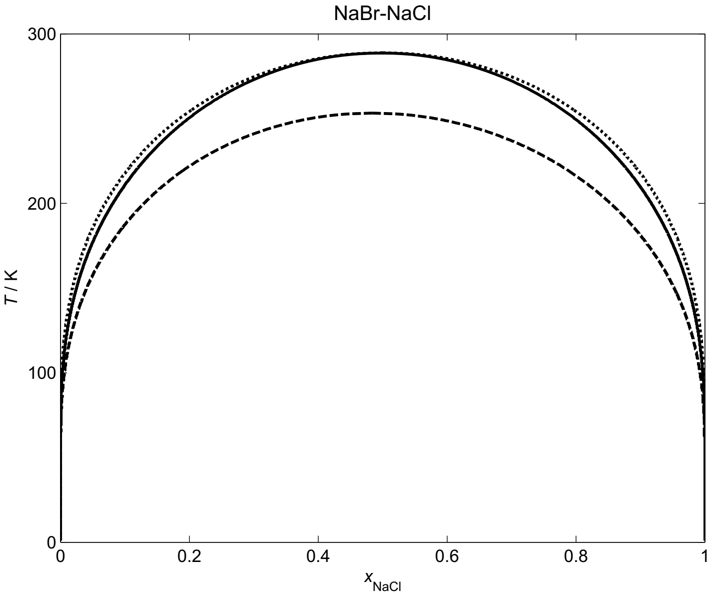

Figure 6.15: The miscibility gap in the NaBr-NaCl system. Solid curve - based on HF-calculations, dashed curve - based on DFT-B3LYP-calculations, dotted curve - estimated from experimental data (134).

note that this extrapolation cannot be expected to be very reliable, since no solidus data or thermodynamic properties for the solid phase are available in the literature, and the authors in Ref. (134) employed an essentially arbitrary parameter in the regular solution model (the interaction parameter is just set equal to 5000 Joule/mol based on experience with other systems!). Thus, we suggest, that our prediction is more reasonable than the extrapolation based on the literature data, in particular, since the HF and DFT calculations yielded practically the same results (see Figure 6.14 and Table 6.10). Our predictions are also corroborated by the results based on empirical relations for the thermodynamic excess behaviour for alkali halide systems (160). The authors suggested the following critical temperatures: 373K, 286K and 214K for Li-, Na- or K- bromide-chloride, respectively, which compare well with our values (c.f. Table 6.10).

One should mention that for all systems we observed that the rocksalt structure-type family was the thermodynamically stable one. But in the case of the KBr-KCl system, a metastable CsCl-structure family is also present. We calculated a transition pressure between the two different types of structure families for all compositions x individually, and we found that for the binaries and all five ternary compositions investigated the transition pressure is about 4.15 - 4.65 GPa (based both on HF and DFT-B3LYP calculations). Thus, we estimate that there should be a phase transition from a rocksalt-type solid solution to a CsCl-type solid solution somewhere between 4 and 5 GPa. Since both HF and DFT-B3LYP are known to overestimate the transition pressure in the alkali halides (135), our calculations are in satisfactory agreement with the experimental value of about 2 GPa for the binary compounds KCl and KBr (161). We also predict the shape of the miscibility gap for the CsCl-structure type at 5.0 GPa, where this structure family is

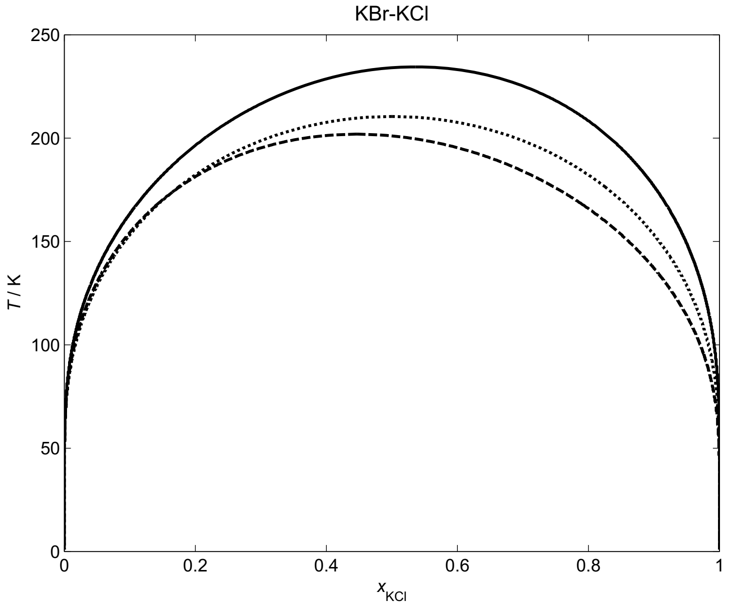

Figure 6.16: The miscibility gap in the KBr-KCl system. Solid curve - based on HF-calculations, dashed curve - based on DFT-B3LYP-calculations, dotted curve - estimated from experimental data (134).

stable against the rocksalt-structure type (c.f. Fig. 6.17). In addition, we calculated the P-T-x phase diagram for the rocksalt structure-type up to 4 GPa, shown in Fig. 6.18 (see also Table 6.11). We notice that the critical temperature decreases by about 25 degrees with increasing pressure.

Table 6.11: The critical parameters for the KBr-KCl solid solution, from standard pressure up to 5 GPa, and the Redlich-Kister polynomial fitting parameters (a_1, a_0) of the enthalpy of formation (according to equation 5.2) based on the HF data obtained in the present work. T_c is the critical temperature of the decomposition in K, x_c is the concentration of the second compound, and ”Type” indicates the structure family stable at the given pressure (in GPa).

Pressure	Type	T_c	x_c	a_1	a_0
0	NaCl	242	0.57	3956.53	-378.86
1	NaCl	231	0.59	3717.59	-479.22
2	NaCl	224	0.6	3531.82	-579.05
3	NaCl	218	0.62	3369.22	-678.83
4	NaCl	214	0.64	3219.45	-778.65
5	CsCl	256	0.65	3760.33	-1020.28

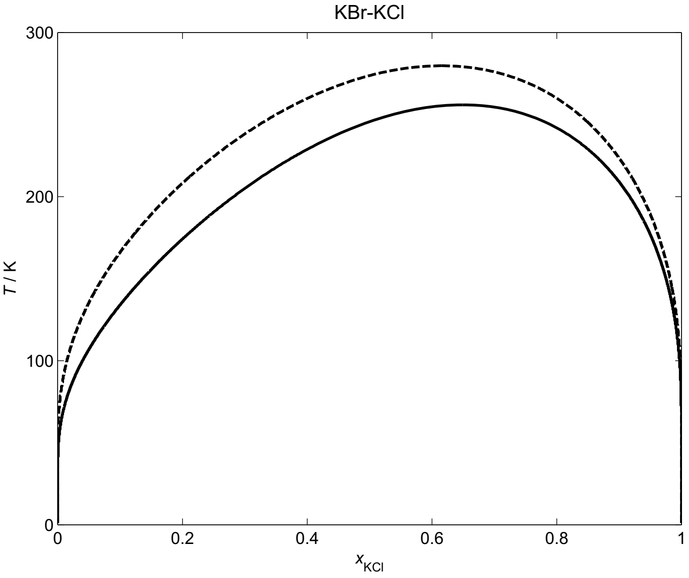

Figure 6.17: The miscibility gap in the KBr-KCl system for the "CsCl" modification at 5 GPa. Solid curve - based on HF-calculations, dashed curve - based on DFT-B3LYP-calculations.

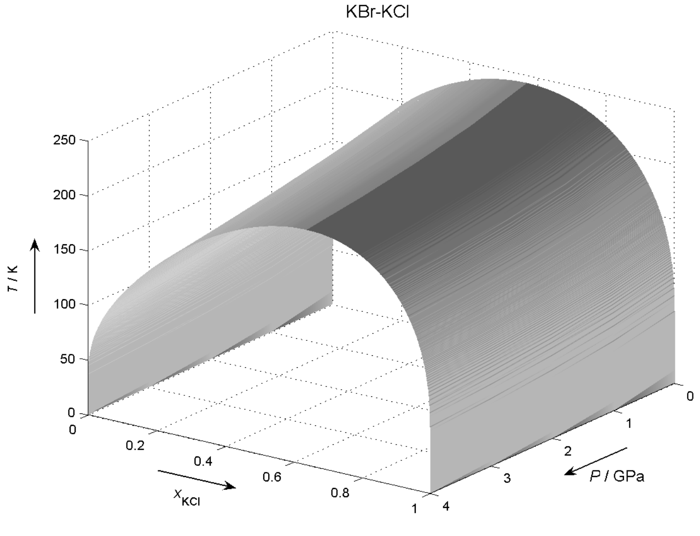

Figure 6.18: The P-T-x low temperature phase diagram in the KBr-KCl system for the "rocksalt" modification for pressures between 0 and 4 GPa.

6.4 Phase diagrams with ordered crystalline phases

6.4.1 Introduction

Earlier (see Section 6.3: Phase diagrams with miscibility gaps), we have shown the ability of our methodology in the case of the exploration of alkali halide systems exhibiting continuous solutions in the solid phase, and predicted the miscibility gap at low temperature as a result of the decomposition of such solid solutions. But alkali halide systems exhibit not only a solid solution behaviour but one can also observe ordered crystalline phases (134). Thus, we have investigated two families of systems where we found ordered crystalline phases and in which solid solutions phase would only be metastable: CsX-LiX (X = F, Cl, Br or I) and LiX-RbX (X = Cl, Br). Besides the already known phases (162; 163; 164; 165; 166), we find a number of additional ordered phases that should be capable of existence but which have not yet been observed experimentally.

6.4.2 The CsX-LiX systems, where X = F, Cl, Br, I

Results and Discussion

For each chemical system, several hundred global optimization runs were performed for a number of different compositions each, at a pressure of 0 Pa. We performed calculations for 7 different compositions (3:1, 2:1, 3:2, 1:1, 2:3, 1:2, 1:3) in addition to the limiting binary phases. For each composition we found a list of structure candidates and calculated the $E(V)$-curves for all these candidates at an *ab initio* level. For given composition, the energy differences between the candidates with the lowest energies were at least equal and in most cases considerably larger than the thermal energy at room temperature. In addition, their cation-anion arrangements were different, and thus these candidates could not be considered as members of one “structure family”. Furthermore, when comparing different compositions the candidates with the lowest energies also did not exhibit the same cation-anion superstructure either. Thus, we suggest that in these systems no solid solutions are present as thermodynamically stable phases over the full range of compositions and instead the low-temperature part of the phase diagram exhibits ordered crystalline phases. Of course, standard statistical mechanical considerations of the formation of defects show that there must be some limited solubility of the minority cation in the host matrix of the halogenide of the majority cation for x very close to 0 or 1, which might be interpreted as the existence of metastable solid solutions with extremely high critical temperatures $T_{crit} \gg T_{melt}$. In the next step, the enthalpies of formation of each compound were obtained according to equation (5.2). Also, one should note that in the current calculations the contribution of the pV-term is negligible since all runs were done at standard pressure.

The calculations of the enthalpies of formation according to equation (5.2) showed that some of these intermediate phases are stable against decomposition into the boundary compounds at 0 K. Tables 6.12 - 6.13 show, for each composition, the structural data for the most stable among these structure candidates[1]. Regarding the structures of these compounds, we predominantly find Li and Cs in four (or five)-fold and eight (or seven)-fold coordination by the halogen atoms, respectively. Furthermore, the structures usually do not exhibit any strong tendency towards the formation of layers containing only Li or Cs, respectively.

Table 6.12: Structure parameters, bulk moduli and enthalpies of formation (kJ/mol) with respect to the binary compounds CsF and LiF at 0 K for the structure candidates with the lowest energy for each composition for the CsF-LiF system after local optimization on Hartree-Fock and DFT-B3LYP (in brackets) level. Structure data, volume V_{min} and bulk moduli are only given for the HF-calculations.

Space group (no.)	Lattice constants	Atom (Multip., Wyckoff lett.),				V_{min}[Å^3]	$\Delta_f H$
Crystal system,	a, b, c [Å];	Relative coordinates				Bulk modulus	HF
Type	α, β, γ [∘]	atom	x	y	z	[GPa]	(DFT)
$C2/m$ (12)	$a = 14.29$	Cs1(4i)	0.56380	0	0.23608	764.025	-2.6
monoclinic	$b = 6.12$	Cs2(4i)	0.86573	0	0.09572	25.437	(-3.5)
$Cs_3LiF_4 - Type1$	$c = 9.04$	Cs3(4i)	0.30816	0	0.34670		
	$\alpha = \gamma = 90$	Li1(4i)	0.91279	0	0.54995		
	$\beta = 105.05$	F1(4i)	0.78282	0	0.38188		
		F2(4h)	0	0.75201	1/2		
		F3(4i)	0.64529	0	0.95799		
		F4(4i)	0.08672	0	0.22032		
$Cmc2_1$ (36)	$a = 3.94$	Cs1(4a)	0	0.41489	0.60342	545.904	-2.3
orthorhombic	$b = 22.05$	Cs2(4a)	0	0.79996	0.10317	25.755	(-2.7)
$Cs_2LiF_3 - Type1$	$c = 6.28$	Li1(4a)	0	0.95685	0.10335		
	$\alpha = \beta = \gamma = 90$	F1(4a)	0	0	0.35323		
		F2(4a)	0	0.58933	0.60332		
		F3(4a)	0	0.19734	0.10311		
$Fmm2$ (42)	$a = 22.68$	Cs1(8d)	0.13616	0	0.45358	856.295	-1.9
orthorhombic	$b = 6.14$	Cs2(4a)	0	0	0.95080	27.747	(-2.1)
$Cs_3Li_2F_5 - Type1$	$c = 6.14$	Li1(8d)	0.21956	0	0.92418		
	$\alpha = \beta = \gamma = 90$	F1(4a)	0	0	0.45042		
		F2(8b)	1/4	1/4	0.27924		
		F3(8d)	0.13826	0	0.95597		
$C2/c$ (15)	$a = 6.15$	Cs1(8f)	0.25280	0.40890	1/4	613.487	-5.1
monoclinic	$b = 11.91$	Li2(8f)	1/4	0.20900	0.36200	30.324	(-5.2)
$CsLiF_2 - Type1$	$c = 8.37$	F3(8f)	0.24400	0.35700	0.42300		
	$\alpha = \gamma = 90$	F4(4e)	0	0.15100	1/4		
	$\beta = 90.81$	F5(4e)	0	0.66300	1/4		
$Amm2$ (38)	$a = 4.14$	Cs1(2b)	1/2	0	0.61836	347.957	7.3
orthorhombic	$b = 4.23$	Cs2(2a)	0	0	0.26769	33.686	(8.8)
$Cs_2Li_3F_5 - Type1$	$c = 19.86$	Li1(2b)	1/2	0	0.87685		
	$\alpha = \beta = \gamma = 90$	Li2(2a)	0	0	0.42380		
		Li3(2a)	0	0	0.01384		
		F1(2b)	1/2	0	0.39120		
		F2(2a)	0	0	0.51228		
		F3(2a)	0	0	0.91576		
		F4(2b)	1/2	0	0.78132		
		F5(2a)	0	0	0.10817		
$I4/mmm$ (139)	$a = 4.15$	Cs1(2a)	0	0	0	171.971	5.4
tetragonal	$c = 10.00$	Li1(4e)	0	0	0.68799	42.313	(5.0)
$CsLi_2F_3 - Type1$	$\alpha = \beta = \gamma = 90$	F1(4d)	0	1/2	1/4		
		F2(2b)	0	0	1/2		
$C2/m$ (12)	$a = 9.95$	Cs1(4i)	0.67593	0	0.27488	417.024	10.8
monoclinic	$b = 5.76$	Li1(4i)	0.99701	0	0.30153	45.300	(9.2)
$CsLi_3F_4 - Type1$	$c = 7.65$	Li2(4i)	0.59339	0	0.67741		
	$\alpha = \gamma = 90$	Li3(4i)	0.77932	0	0.95005		
	$\beta = 108.01$	F1(8j)	0.88520	0.74519	0.12156		
		F2(4h)	0	0.75625	1/2		
		F3(4i)	0.79914	0	0.69358		

---

[1] For some compositions, no candidate was found which was stable with respect to the boundary compounds.

Table 6.13: Structure parameters, bulk moduli and enthalpies of formation (kJ/mol) with respect to the binary compounds CsCl and LiCl at 0 K for the structure candidates with the lowest energy for each composition for the CsCl-LiCl system after local optimization on Hartree-Fock and DFT-B3LYP (in brackets) level. Structure data, volume V_{min} and bulk moduli are only given for the HF-calculations.

Space group (no.)	Lattice constants	Atom (Multip., Wyckoff lett.), Relative coordinates				V_{min}[Å^3]	$\Delta_f H$
Crystal system,	a, b, c [Å];					Bulk modulus	HF
Type	α, β, γ [○]	atom	x	y	z	[GPa]	(DFT)
$Amm2$ (38)	$a = 10.80$	Cs1(2a)	0	0	0.10578	646.334	3.1
$orthorhombic$	$b = 4.53$	Cs2(4c)	0.26433	0	0.32056	12.695	(3.1)
$Cs_3LiCl_4 - Type1$	$c = 13.21$	Li1(2b)	1/2	0	0.54595		
	$\alpha = \beta = \gamma = 90$	Cl1(4c)	0.73241	0	0.59817		
		Cl2(2b)	1/2	0	0.92747		
		Cl3(2a)	0	0	0.83026		
$Cmcm$ (63)	$a = 4.47$	Cs1(4c)	0	0.00168	1/4	879.737	-2.0
$orthorhombic$	$b = 24.62$	Cs2(4c)	0	0.82195	1/4	13.646	(-1.8)
$Cs_2LiCl_3 - Type1$	$c = 8.00$	Li1(4c)	0	0.64753	1/4		
	$\alpha = \beta = \gamma = 90$	Cl1(8f)	0	0.58853	0.00437		
		Cl2(4c)	0	0.20164	1/4		
Cm (8)	$a = 7.41$	Cs1(4b)	0.24837	0.11452	0.74037	670.247	0.8
$monoclinic$	$b = 25.25$	Cs2(2a)	0.25461	0	0.24875	15.580	(0.8)
$Cs_3Li_2Cl_5 - Type1$	$c = 5.94$	Li1(4b)	0.73805	0.21766	0.70072		
	$\alpha = \gamma = 90$	Cl1(2a)	0.77655	0	0.28555		
	$\beta = 142.91$	Cl2(4b)	0.78197	0.11581	0.79092		
		Cl3(4b)	0.74565	0.77129	0.26554		
$P4/nmm$ (129)	$a = 5.13$	Cs1(2c)	1/4	1/4	0.69570	260.340	-2.6
$tetragonal$	$c = 9.90$	Li1(2c)	1/4	1/4	0.08850	15.430	(-2.7)
$CsLiCl_2 - Type1$	$\alpha = \beta = \gamma = 90$	Cl1(2a)	3/4	1/4	0		
		Cl2(2c)	1/4	1/4	0.3318		
$Imm2$ (44)	$a = 23.50$	Cs1(4c)	0.11470	0	0.01373	612.829	2.7
$orthorhombic$	$b = 4.77$	Li1(2b)	0	1/2	0.50756	16.638	(1.4)
$Cs_2Li_3Cl_5 - Type1$	$c = 5.47$	Li2(4c)	0.28002	0	0.01149		
	$\alpha = \beta = \gamma = 90$	Cl1(4c)	0.73339	0	0.48708		
		Cl2(4c)	0.38875	0	0.99245		
		Cl3(2b)	0	1/2	0.99056		
$Immm$ (71)	$a = 5.58$	Cs1(2c)	1/2	1/2	0	333.587	-1.7
$orthorhombic$	$b = 4.65$	Li1(4i)	0	0	0.80940	17.955	(-1.6)
$CsLi_2Cl_3 - Type1$	$c = 12.85$	Cl1(2a)	0	0	0		
	$\alpha = \beta = \gamma = 90$	Cl2(4j)	1/2	0	0.76555		
$Cmcm$ (63)	$a = 5.18$	Cs1(4c)	0	0.65137	1/4	785.994	4.0
$orthorhombic$	$b = 29.25$	Li1(4c)	0	0.76770	1/4	22.802	(3.8)
$CsLi_3Cl_4 - Type1$	$c = 5.19$	Li2(4c)	0	0.53759	1/4		
	$\alpha = \beta = \gamma = 90$	Li3(4c)	0	0.94167	1/4		
		Cl1(4c)	0	0.04823	1/4		
		Cl2(4c)	0	0.24874	1/4		
		Cl3(4c)	0	0.85326	1/4		
		Cl4(4c)	0	0.44980	1/4		

Table 6.14: Structure parameters, bulk moduli and enthalpies of formation (kJ/mol) with respect to the binary compounds CsBr and LiBr at 0 K for the structure candidates with the lowest energy for each composition for the CsBr-LiBr system after local optimization on Hartree-Fock and DFT-B3LYP (in brackets) level. Structure data, volume V_{min} and bulk moduli are only given for the HF-calculations.

Space group (no.)	Lattice constants	Atom (Multip., Wyckoff lett.), Relative coordinates				V_{min}[Å^3]	$\Delta_f H$
Crystal system,	a, b, c [Å];					Bulk modulus	HF
Type	α, β, γ [○]	atom	x	y	z	[GPa]	(DFT)
$C222_1$ (20)	$a = 12.60$	Cs1(4b)	0	0.27911	1/4	1592.498	0.03
$orthorhombic$	$b = 14.25$	Cs2(8c)	0.27699	0.92745	0.76645	9.053	(-0.1)
$Cs_3LiBr_4 - Type1$	$c = 8.87$	Li1(4b)	0	0.89407	1/4		
	$\alpha = \beta = \gamma = 90$	Br1(8c)	0.18067	0.18213	0.85394		
		Br2(4a)	0.51006	0	0		
		Br3(4a)	0.94916	0	0		
$C2/m$ (12)	$a = 25.88$	Cs1(4i)	0.99739	0	1/4	1054.473	-2.6
$monoclinic$	$b = 4.76$	Cs2(4i)	0.82304	0	0.74565	10.415	(-2.7)
$Cs_2LiBr_3 - Type1$	$c = 8.56$	Li1(4i)	0.64893	0	0.75211		
	$\alpha = \gamma = 90$	Br1(4i)	0.58749	0	0.50213		
	$\beta = 91.32$	Br2(4i)	0.79626	0	0.25072		
		Br3(4i)	0.58871	0	0.99837		
Cm (8)	$a = 7.95$	Cs1(4b)	0.23002	0.38777	0.25725	814.084	0.6
$monoclinic$	$b = 26.97$	Cs2(2a)	0.81976	0	0.85226	11.493	(0.3)
$Cs_3Li_2Br_5 - Type1$	$c = 6.44$	Li1(4b)	0.21395	0.21734	0.20952		
	$\alpha = \gamma = 90$	Br1(2a)	0.27346	0	0.81868		
	$\beta = 143.85$	Br2(4b)	0.22743	0.22496	0.78267		

continued on next page

continued from previous page

Space group (no.)	Lattice constants	Atom (Multip., Wyckoff lett.),				V_{min}[Å^3]	$\Delta_f H$
Crystal system,	a, b, c [Å];	Relative coordinates				Bulk modulus	HF
Type	α, β, γ [∘]	atom	x	y	z	[GPa]	(DFT)
		Br3(4b)	0.80567	0.61492	0.34862		
$P4/nmm$ (129)	$a = 5.50$	Cs1(2c)	1/4	1/4	0.69600	318.370	-3.1
tetragonal	$c = 10.52$	Li1(2c)	1/4	1/4	0.08800	11.665	(-3.2)
$CsLiBr_2 - Type1$	$\alpha = \beta = \gamma = 90$	Br1(2a)	3/4	1/4	0		
		Br2(2c)	1/2	1/2	0.33200		
$C2/m$ (12)	$a = 16.00$	Cs1(4i)	0.81078	0	0.26212	750.520	-1.4
monoclinic	$b = 4.60$	Li1(2a)	0	0	0	12.064	(-1.6)
$Cs_2Li_3Br_5 - Type1$	$c = 11.08$	Li2(4i)	0.55607	0	0.30989		
	$\alpha = \gamma = 90$	Br1(4i)	0.40574	0	0.07214		
	$\beta = 113.09$	Br2(4i)	0.86980	0	0.70521		
		Br3(2d)	0	1/2	1/2		
$Immm$ (71)	$a = 4.71$	Cs1(2b)	0	1/2	1/2	413.313	-1.9
orthorhombic	$b = 6.04$	Li1(4j)	1/2	0	0.31000	13.507	(-2.1)
$CsLi_2Br_3 - Type1$	$c = 14.53$	Br1(4i)	0	0	0.21681		
	$\alpha = \beta = \gamma = 90$	Br2(2d)	1/2	0	1/2		
$Pmc2_1$ (26)	$a = 5.65$	Cs1(2b)	1/2	0.53888	0.34551	529.484	4.9
orthorhombic	$b = 11.01$	Li1(2b)	1/2	0.02940	0.71405	15.118	(4.4)
$CsLi_3Br_4 - Type1$	$c = 8.52$	Li2(2a)	0	0.78211	0.90724		
	$\alpha = \beta = \gamma = 90$	Li3(2a)	0	0.16663	0.00083		
		Br1(2a)	0	0.00425	0.74631		
		Br2(2a)	0	0.60601	0.65551		
		Br3(2b)	1/2	0.83947	0.49824		
		Br4(2b)	1/2	0.77198	0.00324		

Table 6.15: Structure parameters, bulk moduli and enthalpies of formation (kJ/mol) with respect to the binary compounds CsI and LiI at 0 K for the structure candidates with the lowest energy for each composition for the CsI-LiI system after local optimization on Hartree-Fock and DFT-B3LYP (in brackets) level. Structure data, volume V_{min} and bulk moduli are only given for the HF-calculations.

Space group (no.)	Lattice constants	Atom (Multip., Wyckoff lett.),				V_{min}[Å^3]	$\Delta_f H$
Crystal system,	a, b, c [Å];	Relative coordinates				Bulk modulus	HF
Type	α, β, γ [∘]	atom	x	y	z	[GPa]	(DFT)
$P2_1/m$ (11)	$a = 17.27$	Cs1(2e)	0.44897	1/4	0.70436	975.698	-0.6
monoclinic	$b = 9.83$	Cs2(2e)	0.73453	1/4	0.37799	7.158	(-0.6)
$Cs_3LiI_4 - Type1$	$c = 5.76$	Cs3(2c)	0	0	1/2		
	$\alpha = \gamma = 90$	Li1(2e)	0.25026	1/4	0.11581		
	$\beta = 93.63$	I1(4f)	0.63613	0.00019	0.83294		
		I2(2e)	0.18474	1/4	0.58631		
		I3(2e)	0.90995	1/4	0.95851		
$Cmc2_1$ (36)	$a = 5.05$	Cs1(4a)	0	0.32488	0.50760	1309.730	-3.1
orthorhombic	$b = 27.65$	Cs2(4a)	0	0.49672	0.01356	7.902	(-3.0)
$Cs_2LiI_3 - Type1$	$c = 9.37$	Li1(4a)	0	0.15031	0.51697		
	$\alpha = \beta = \gamma = 90$	I1(4a)	0	0.91406	0.26420		
		I2(4a)	0	0.29250	0.02942		
		I3(4a)	0	0.91130	0.76478		
$C2/m$ (12)	$a = 30.72$	Cs1(4i)	0.94142	0	0.34962	2103.913	-1.8
monoclinic	$b = 5.19$	Cs2(4i)	0.74436	0	0.73188	8.340	(-1.6)
$Cs_3Li_2I_5 - Type1$	$c = 13.44$	Cs3(4i)	0.94853	0	0.85296		
	$\alpha = \gamma = 90$	Li1(4i)	0.65445	0	0.97130		
	$\beta = 100.93$	Li2(4i)	0.34896	0	0.58272		
		I1(4i)	0.55205	0	0.40296		
		I2(4i)	0.81303	0	0.10596		
		I3(4i)	0.44586	0	0.10789		
		I4(4i)	0.65761	0	0.19669		
		I5(4i)	0.81547	0	0.47879		
$Cmc2_1$ (36)	$a = 4.96$	Cs1(4a)	0	0.34484	0.48582	1561.668	-1.7
orthorhombic	$b = 22.38$	Cs2(4a)	0	0.50971	0.26219	8.781	(-1.6)
$CsLiI_2 - Type1$	$c = 14.06$	Li1(4a)	0	0.86954	0.04859		
	$\alpha = \beta = \gamma = 90$	Li2(4a)	0	0.27872	0.78453		
		I1(4a)	0	0.30871	0.98012		
		I2(4a)	0	0.14886	0.75584		
		I3(4a)	0	0.99680	0.00774		
		I4(4a)	0	0.83866	0.71686		
$C2/m$ (12)	$a = 17.78$	Cs1(4i)	0.30986	0	0.76639	946.110	-2.9
monoclinic	$b = 5.04$	Li1(2d)	0	1/2	1/2	9.114	(-2.8)
$Cs_2Li_3I_5 - Type1$	$c = 11.72$	Li2(4i)	0.05212	0	0.80234		
	$\alpha = \gamma = 90$	I1(2a)	0	0	0		
	$\beta = 115.73$	I2(4i)	0.09746	0	0.43083		
		I3(4i)	0.63309	0	0.79485		
$P-4m2$ (115)	$a = 4.88$	Cs1(1c)	1/2	1/2	1/2	268.434	-2.3
tetragonal	$c = 11.29$	Li1(2g)	0	1/2	0.86800	9.506	(-2.5)
$CsLi_2I_3 - Type1$	$\alpha = \beta = \gamma = 90$	I1(1b)	1/2	1/2	0		
		I2(2e)	0	0	0.71613		
Pm (6)	$a = 11.30$	Cs1(1b)	0.11957	1/2	0.15907	701.629	-2.6
monoclinic	$b = 4.94$	Cs2(1b)	0.55730	1/2	0.29812	9.737	(-2.6)

continued on next page

continued from previous page

Space group (no.)	Lattice constants	Atom (Multip., Wyckoff lett.),				V$_{min}$[Å^3]	$\Delta_f H$
Crystal system,	a, b, c [Å];	Relative coordinates				Bulk modulus	HF
Type	α, β, γ [$\circ$]	atom	x	y	z	[GPa]	(DFT)
$CsLi_3I_4 - Type1$	c = 12.60	Li1(1b)	0.07648	1/2	0.78160		
	$\alpha = \gamma = 90$	Li2(1b)	0.44888	1/2	0.92827		
	$\beta = 86.57$	Li3(1a)	0.36605	0	0.60942		
		Li4(1a)	0.01004	0	0.48414		
		Li5(1b)	0.70600	1/2	0.65805		
		Li6(1a)	0.79574	0	0.98332		
		I1(1a)	0.40552	0	0.05658		
		I2(1b)	0.32685	1/2	0.72986		
		I3(1b)	0.95302	1/2	0.58347		
		I4(1b)	0.69994	1/2	0.88971		
		I5(1a)	0.03584	0	0.89524		
		I6(1a)	0.24843	0	0.40667		
		I7(1a)	0.83321	0	0.21124		
		I8(1a)	0.61707	0	0.56348		

As mentioned above, the lithium cesium halides do not exhibit solid-solution behavior. For each composition in these systems, the observed structure candidates with the lowest free energy correspond to ordered crystalline phases, which are at least metastable. It is known from experiment, that there exist several crystalline modifications in the four systems: $CsLiF_2$ (162), $CsLiCl_2$ (163; 164), Cs_2LiCl_3 (164), $CsLiBr_2$ (165) and $Cs_2Li_3I_5$ (167). According to our calculations these phases have a negative enthalpy of formation and, thus, should be stable with respect to decomposition into the binary compounds. In addition, we predict the existence of several new phases stable with respect to the binary compounds. These occur in the CsF-LiF system for the compositions 3:1, 2:1 and 3:2, in the case of the CsCl-LiCl system for the composition 1:2, in the CsBr-LiBr system for the compositions 2:1, 2:3 and 1:2, and in the CsI-LiI system for all compositions investigated (see Tables 6.12 - 6.15). Some of the new predicted phases appear to be thermodynamically stable with respect to decomposition into neighboring phases (see Figs. 1 - 4) and are probably accessible to synthesis. We also note that no information about the structure of the experimentally observed compound Cs_2LiCl_3 appears to be available in the literature (164). Since the structure candidate that we have found for the composition Cs_2LiCl_3 (see Table 6.13) is stable with respect to a decomposition into two neighboring phases, we suggest it is a strong candidate to be the compound that has been found in experiment.

In Figs. 6.19 - 6.22, we have indicated the experimentally known phases by a thin solid line, the - according to the calculations - predicted stable phases with a fat solid line, while those among the predicted metastable phases that nevertheless are stable with respect to the binary compounds are represented by a dashed line. Finally, the phases that are metastable with respect to the binary compounds are indicated by dotted lines. Furthermore, below the actual phase diagrams, we show the enthalpies of formation with respect to the binary compounds at 0 K, in order to give some insight into the thermodynamic stability of the various phases.

One should mention, that we cannot exclude the possibility that structure families might exist that exhibit a rather complicated superstructure consisting of complex arrangements of e.g. $CsCl_8$-cubes and $LiCl_4$-tetrahedra or $LiCl_6$-octahedra, where the members of the families have very similar (relatively low) energies. Such a hypothetical structure family might then possess a high enough configurational entropy to compete with the crystalline low energy structures at elevated temperatures. Multi-polyhedra configurations belonging to such structure families actually show marked similarities to structural glasses, where

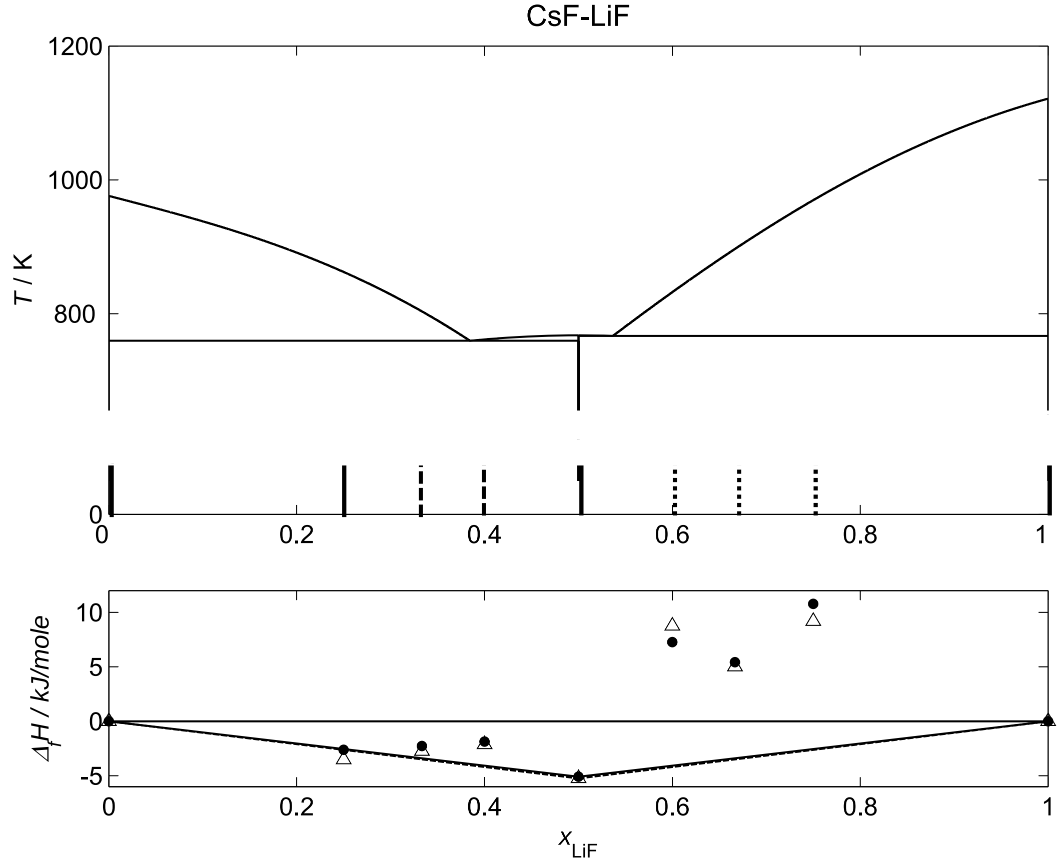

Figure 6.19: Top: The phase diagram of the CsF-LiF system. Thin solid line - experimentally known high-temperature part of the phase diagram, bold solid line - predicted stable phases, dashed line - predicted metastable phases which are stable with respect to the binary compounds CsF and LiF, dotted line - predicted phases that are metastable with respect to the binary compounds. Bottom: Enthalpies of formation at 0 K with respect to the binary compounds for the crystalline modifications with the lowest energy for each concentration investigated. Bullets - Hartree-Fock-calculations, triangles - DFT-B3LYP-calculations.

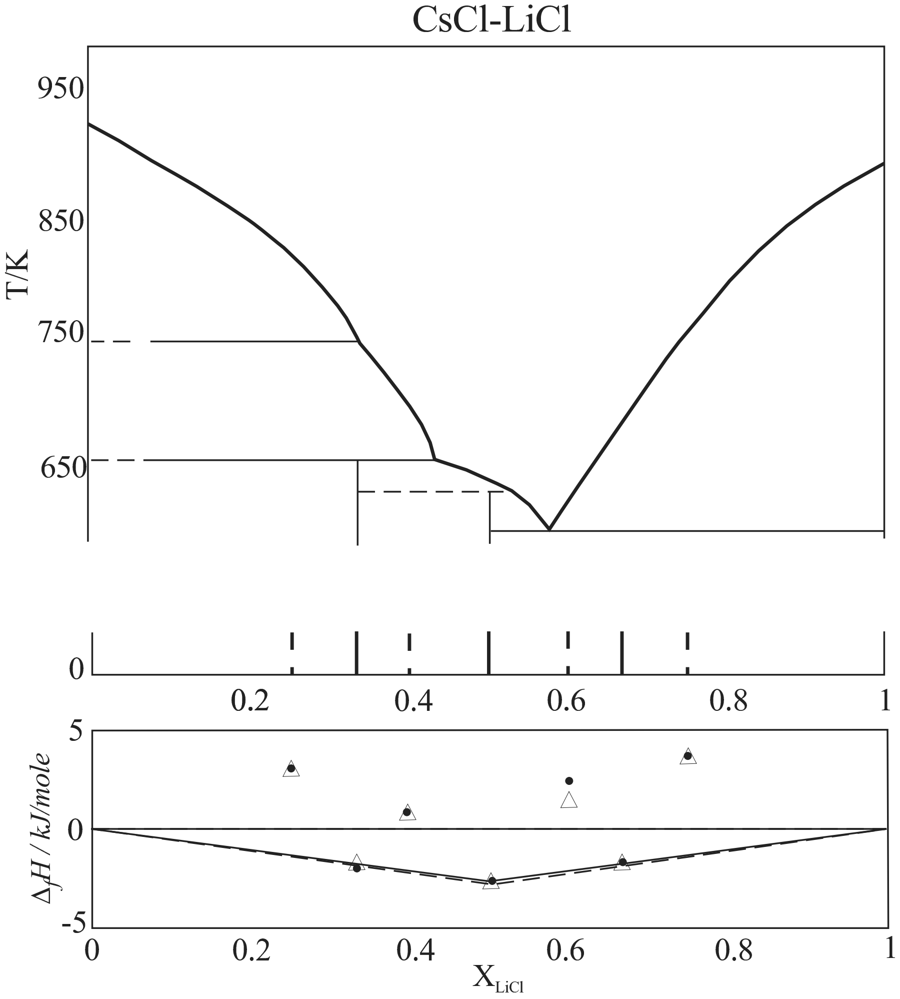

Figure 6.20: Top: The phase diagram of the CsCl-LiCl system. Thin solid line - experimentally known high-temperature part of the phase diagram, bold solid line - predicted stable phases, dashed line - predicted metastable phases which are stable with respect to the binary compounds CsCl and LiCl, dotted line - predicted phases that are metastable with respect to the binary compounds. Bottom: Enthalpies of formation at 0 K with respect to the binary compounds for the crystalline modifications with the lowest energy for each concentration investigated. Bullets - Hartree-Fock-calculations, triangles - DFT-B3LYP-calculations.

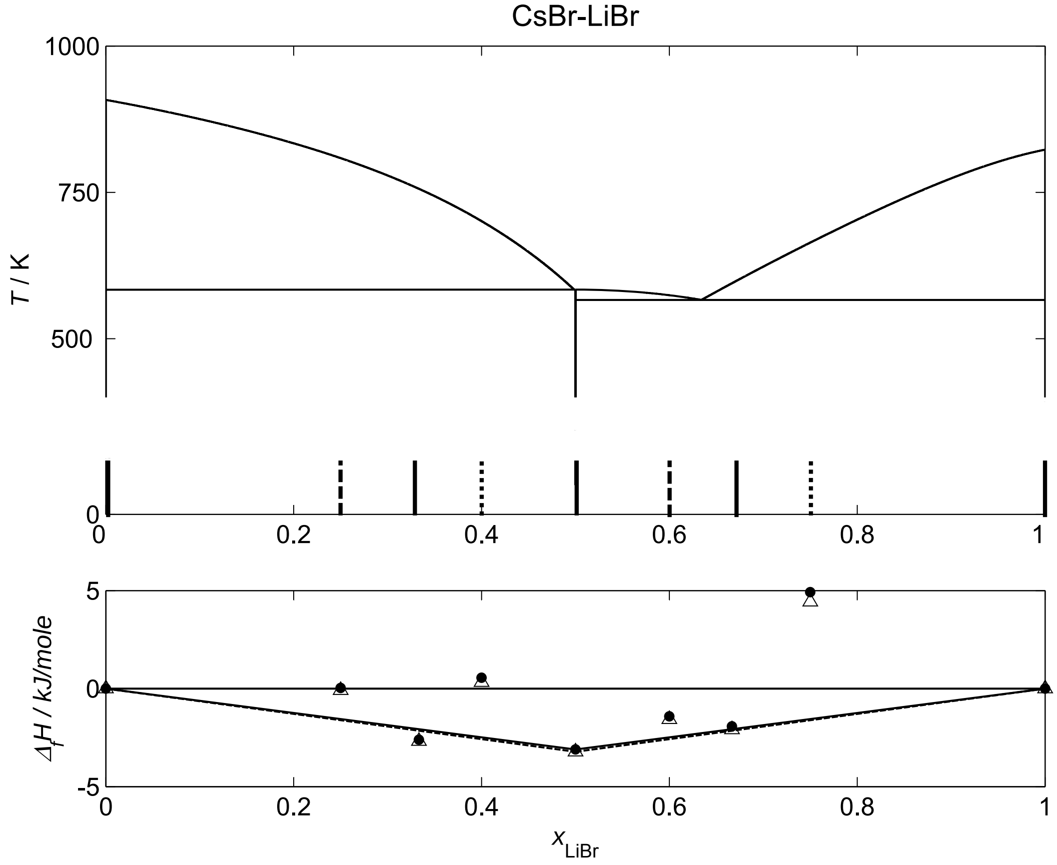

Figure 6.21: Top: The phase diagram of the CsBr-LiBr system. Thin solid line - experimentally known high-temperature part of the phase diagram, bold solid line - predicted stable phases, dashed line - predicted metastable phases which are stable with respect to the binary compounds CsBr and LiBr, dotted line - predicted phases that are metastable with respect to the binary compounds. Bottom: Enthalpies of formation at 0 K with respect to the binary compounds for the crystalline modifications with the lowest energy for each concentration investigated. Bullets - Hartree-Fock-calculations, triangles - DFT-B3LYP-calculations.

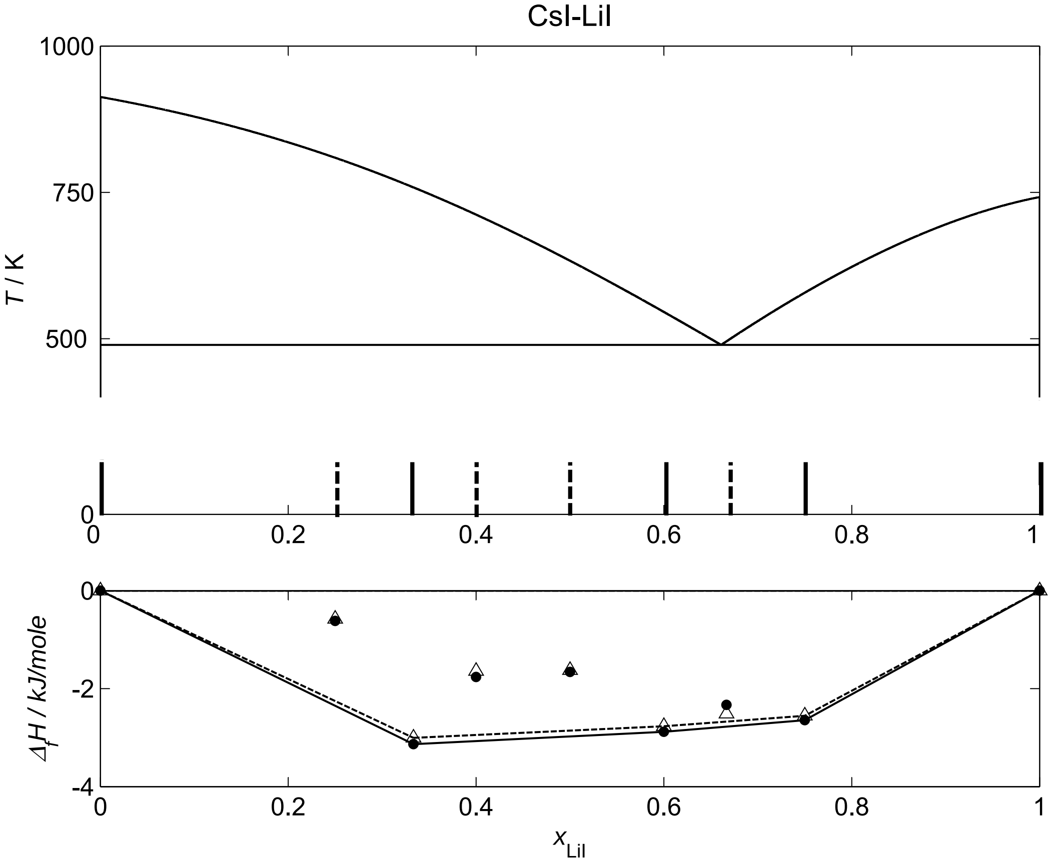

Figure 6.22: Top: The phase diagram of the CsI-LiI system. Thin solid line - experimentally known high-temperature part of the phase diagram, bold solid line - predicted stable phases, dashed line - predicted metastable phases which are stable with respect to the binary compounds CsI and LiI, dotted line - predicted phases that are metastable with respect to the binary compounds. Bottom: Enthalpies of formation at 0 K with respect to the binary compounds for the crystalline modifications with the lowest energy for each concentration investigated. Bullets - Hartree-Fock-calculations, triangles - DFT-B3LYP-calculations.

random networks of coordination polyhedra with a high configurational entropy are often found to be good models of the structure of the glass.

In Figs. 6.23 and 6.24, we have shown two examples of predicted structure candidates for the $CsLi_2Cl_3$ and Cs_2LiCl_3 compounds.

In case of the $CsLi_2Cl_3$ structure candidate, there is one independent position of a Li atom and one of a Cs atom. The Li atoms are coordinated by 5 atoms of Cl (in a distorted tetragonal pyramid arrangement; the same arrangement is observed in the experimentally known structure $CsLiCl_2$). Each polyhedron is sharing an edge with the neighboring Li- and Cs-centered polyhedra. The Cs atoms are coordinated by 8 atoms of Cl (in a slightly distorted cubic arrangement), and each polyhedron is sharing a face with other Cs-centered polyhedra.

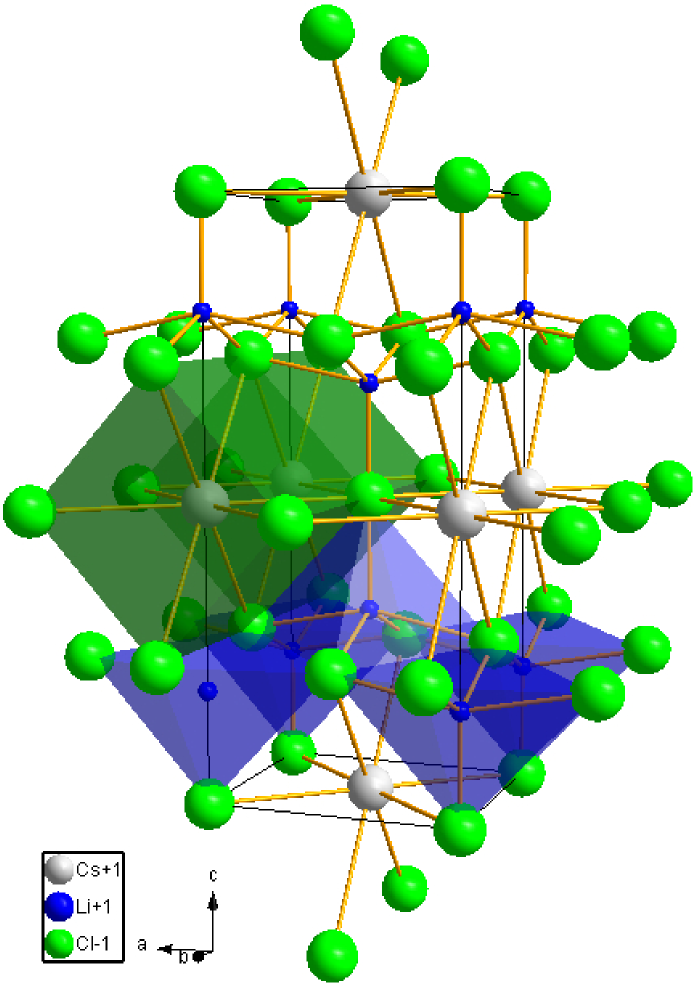

Figure 6.23: The $CsLi_2Cl_3$ structure candidate. The cell parameters and atom positions are listed in Table 6.13.

In the case of the Cs_2LiCl_3 structure candidate, there are two crystallographically independent positions of Cs atoms and one for the Li atom. The Li atoms are coordinated by 4 (tetrahedrally arranged) atoms, where each polyhedron is sharing a vertex with another tetrahedron and an edge with Cs-centered polyhedra. The Cs atoms are coordinated by 8 atoms of Cl. There are two types of arrangements: a slightly distorted cubic arrangement and a bi-capped trigonal prism. The Cs-centered polyhedra are connected with each other via faces containing three (in the case of bi-capped trigonal prisms) or four (in the case of distorted cube) Cl atoms and edges (when connecting two bi-capped trigonal prisms with each other). The Li-Cl (≈ 2.4 - 2.8 Å) and Cs-Cl (≈ 3.6 - 4.0 Å) distances in both structures are close to the experimental ones observed in LiCl (2.56 Å), CsCl (3.56 Å) and $CsLiCl_2$ (Li-Cl ≈ 2.3 - 2.6 Å; Cs-Cl ≈ 3.4 - 3.8 Å). Of course, there is some disagreement, since usually the calculated cell parameters differ from experimental ones.

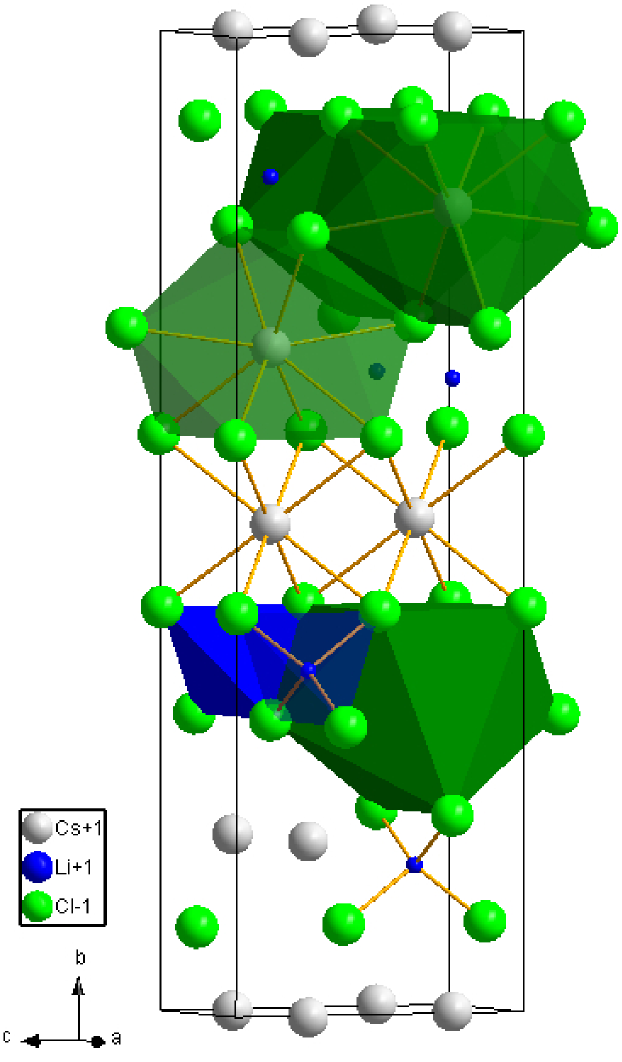

Figure 6.24: The Cs_2LiCl_3 structure candidate.The cell parameters and atom positions are listed in Table 6.13.

Table 6.16: Cell parameters of the experimentally known phases available in the literature (39) and obtained in the present work.

Space group (no.)	ICSD data	HF data	DFT-B3LYP data
	Lattice constants a, b, c [Å]; α, β, γ [$\circ$]		
$CsLiF_2$ (162)	a = 6.01	6.15	6.13
monoclinic	b = 11.64	11.91	11.87
$P2/c$ (15)	c = 8.18	8.37	8.34
	$\alpha = \gamma = 90$	90	90
	$\beta = 90.81$	90.81	90.81
$CsLiCl_2$ (163)	a = 4.92	5.13	5.05
tetragonal	c = 9.50	9.90	9.74
$P4/nmm$ (129)	$\alpha = \beta = \gamma = 90$	90	90
$CsLiBr_2$ (165)	a = 5.19	5.50	5.38
tetragonal	c = 9.92	10.52	10.29
$P4/nmm$ (129)	$\alpha = \beta = \gamma = 90$	90	90
$Cs_2Li_3I_5$ (167)	a = 16.67	17.78	17.31
monoclinic	b = 4.72	5.04	4.90
$C2/m$ (12)	c = 10.99	11.72	11.41
	$\alpha = \gamma = 90$	90	90
	$\beta = 115.73$	115.73	115.73

6.4.3 The LiX-RbX systems, where X = Cl or Br

Results and Discussion

For each chemical system, several hundred global optimization runs were performed for a number of different compositions each, at a pressure of 0 Pa. We performed calculations for 7 different compositions (3:1, 2:1, 3:2, 1:1, 2:3, 1:2 and 1:3) besides the limiting binary phases. For each composition of the LiCl-RbCl and LiBr-RbBr systems we found a list of structure candidates, where the energy differences between the candidates with the lowest energies were quite large. Furthermore, their cation-anion arrangements were different, and thus they could not be considered as members of one "structure family". Thus, we propose that in these systems no solid solutions are present as thermodynamically stable phases, and instead the low-temperature part of the phase diagram exhibits ordered crystalline phases. The calculations of the enthalpies of formation according the equation (5.2) showed that some of these phases are stable against decomposition into the boundary compounds at 0 K. The structural data for the most stable structure candidate for each composition investigated are listed in Tables 6.17 and 6.18. Additional candidates that are stable with respect to the binary compounds in each system are given in Tables A.5 and A.6 in the appendix.

Earlier in Section 6.3.1, we noted that one important condition for the presence of a solid-solution phase is the existence of a family of structurally related minima, which exhibit the same superstructure. Furthermore, the energies of these minima must be sufficiently close such that there exist similar probabilities of finding the system in these basins in the thermodynamic limit. For the LiCl-RbCl and LiBr-RbBr systems we found that the difference in energies per atom of the modifications with the lowest energies are comparable to or larger than room temperature (T_R), e.g. for the composition Li_2RbCl_3 $\Delta(E) \approx 7 \times 10^{-2}$ eV $> k_B T_R \approx 3 \times 10^{-2}$ eV. Thus, we should consider all structures individually as possible candidates for ordered stable or metastable phases at low-temperatures $T << T_R$.

For each composition in these systems, the observed structure candidates with the lowest energy correspond to ordered crystalline phases, which are at least metastable. It is known from experiment, that there are crystalline modifications in both these systems with compositions $LiRbCl_2$ (163) and $LiRbBr_2$ (165). According to our calculations these phases have a negative enthalpy of formation and, thus, should be stable with respect to decomposition into the binary compounds ($x = 0{,}1$). In addition we predict the existence of several new phases stable with respect to the binary compounds: in the case of the LiCl-RbCl system for compositions 2:1, 2:3, 1:2 and 1:3, and in the case of the LiBr-RbBr system for compositions: 2:1, 3:2, 2:3, 1:2 and 1:3. The list of structure candidates are presented in Tables 6.17 and 6.18. In addition, many metastable modifications were identified. These are listed in the appendix material in Ref. (168).

In Figs. 6.25 and 6.26, we have indicated the experimentally known phases by a thin

Table 6.17: Structure parameters, bulk moduli and enthalpies of formation per mole with respect to the binary compounds LiCl and RbCl at 0 K for the structure candidates with the lowest energy for each composition for the LiCl-RbCl system, after local optimization on Hartree-Fock and DFT-B3LYP (in brackets) level. Structure data, volume V_{min} and bulk moduli are only given for the HF-calculations.

Space group (no.)	Lattice constants	Atom (Multip., Wyckoff lett.),				V_{min}[Å^3]	$\Delta_f H$[kJ]
Crystal system,	a, b, c [Å];	Relative coordinates				Bulk modulus	HF
Type	α, β, γ [o]	atom	x	y	z	[GPa]	(DFT)
$P2_1/m$ (11)	$a = 9.51522$	Li1(2e)	0.59058	1/4	0.13413	429.194	1.2249
monoclinic	$b = 5.07925$	Li2(2e)	0.39632	1/4	0.58343	18.343	(0.9682)
$Li_3RbCl_4 - Type1$	$c = 8.90732$	Li3(2e)	0.87396	1/4	0.41927		
	$\alpha = \gamma = 90$	Rb4(2e)	0.20644	1/4	0.11577		
	$\beta = 94.45120$	Cl5(2e)	0.13860	1/4	0.48117		
		Cl6(2e)	0.60258	1/4	0.41883		
		Cl7(2e)	0.49996	1/4	0.85831		
		Cl8(2e)	0.85540	1/4	0.12523		
$Immm$ (71)	$a = 13.13455$	Li1(4f)	0.69013	1/2	0	311.692	-2.5411
orthorhombic	$b = 4.35029$	Rb2(2d)	1/2	0	1/2	19.186	(-1.6328)
$Li_2RbCl_3 - Type1$	$c = 5.45497$	Cl3(4e)	0.78681	0	0		
	$\alpha = \beta = \gamma = 90$	Cl4(2c)	1/2	1/2	0		
$Amm2$ (38)	$a = 3.99163$	Li1(4d)	0	0.83182	0.07617	585.760	1.6089
orthorhombic	$b = 19.17252$	Li2(2a)	0	0	0.18580	16.990	(1.5257)
$Li_3Rb_2Cl_5 - Type1$	$c = 7.65403$	Rb3(4e)	1/2	0.85940	0.55693		
	$\alpha = \beta = \gamma = 90$	Cl4(4e)	1/2	0.90739	0.12684		
		Cl5(2a)	0	0	0.52282		
		Cl6(4d)	0	0.75682	0.81396		
$Cmcm$ (63)	$a = 4.29553$	Rb1(4c)	0	0.63118	1/4	485.192	-5.0440
orthorhombic	$b = 15.00627$	Li2(4c)	0	0.89962	1/4	16.965	(-4.8584)
$LiRbCl_2 - Type1$	$c = 7.50574$	Cl3(4a)	0	0	0		
	$\alpha = \beta = \gamma = 90$	Cl4(4c)	0	0.31314	1/4		
Cm (8)	$a = 7.08129$	Li1(4b)	0.54266	0.21756	0.24065	603.145	-1.7013
monoclinic	$b = 24.71031$	Rb2(2a)	0.51382	0	0.69676	16.449	(-1.8029)
$Li_2Rb_3Cl_5 - Type1$	$c = 4.27891$	Rb3(4b)	0.01685	0.12080	0.21317		
	$\alpha = \gamma = 90$	Cl4(4b)	0.97455	0.76745	0.67202		
	$\beta = 126.33570$	Cl5(4b)	0.50790	0.88064	0.20180		
		Cl6(2a)	0.01185	0	0.69406		
$C2/m$ (12)	$a = 23.33451$	Li1(4i)	0.65195	0	0.25448	779.336	-2.4789
monoclinic	$b = 4.20317$	Rb2(4i)	0.99634	0	0.75022	15.585	(-2.6331)
$LiRb_2Cl_3 - Type1$	$c = 7.95992$	Rb3(4i)	0.17432	0	0.76673		
	$\alpha = \gamma = 90$	Cl4(4i)	0.41413	0	0.99690		
	$\beta = 93.38770$	Cl5(4i)	0.20921	0	0.24167		
		Cl6(4i)	0.58990	0	0.49796		
Pm (6)	$a = 6.96388$	Li1(1b)	0.47661	1/2	0.25295	311.710	-2.7796
monoclinic	$b = 9.45272$	Rb2(1a)	0.55969	0	0.56566	12.654	(-2.7458)
$LiRb_3Cl_4 - Type1$	$c = 4.74932$	Rb3(2c)	0.05905	0.25777	0.00624		
	$\alpha = \gamma = 90$	Cl4(1b)	0.16407	1/2	0.49155		
	$\beta = 85.58797$	Cl5(2c)	0.56794	0.72892	0.07805		
		Cl6(1a)	0.06069	0	0.51301		

solid line, the - according to the calculations - predicted stable phases with a fat solid line, while the predicted metastable phases - which nevertheless are stable with respect to the binary compounds - are represented by a dashed line. Finally, the phases that are metastable with respect to the binary compounds are indicated by dotted lines (see Tables 6.17 and 6.18). Furthermore, below the actual phase diagrams, we show the enthalpies of formation with respect to the binary compounds at 0 K, in order to give some insight into the thermodynamic stability of the various phases.

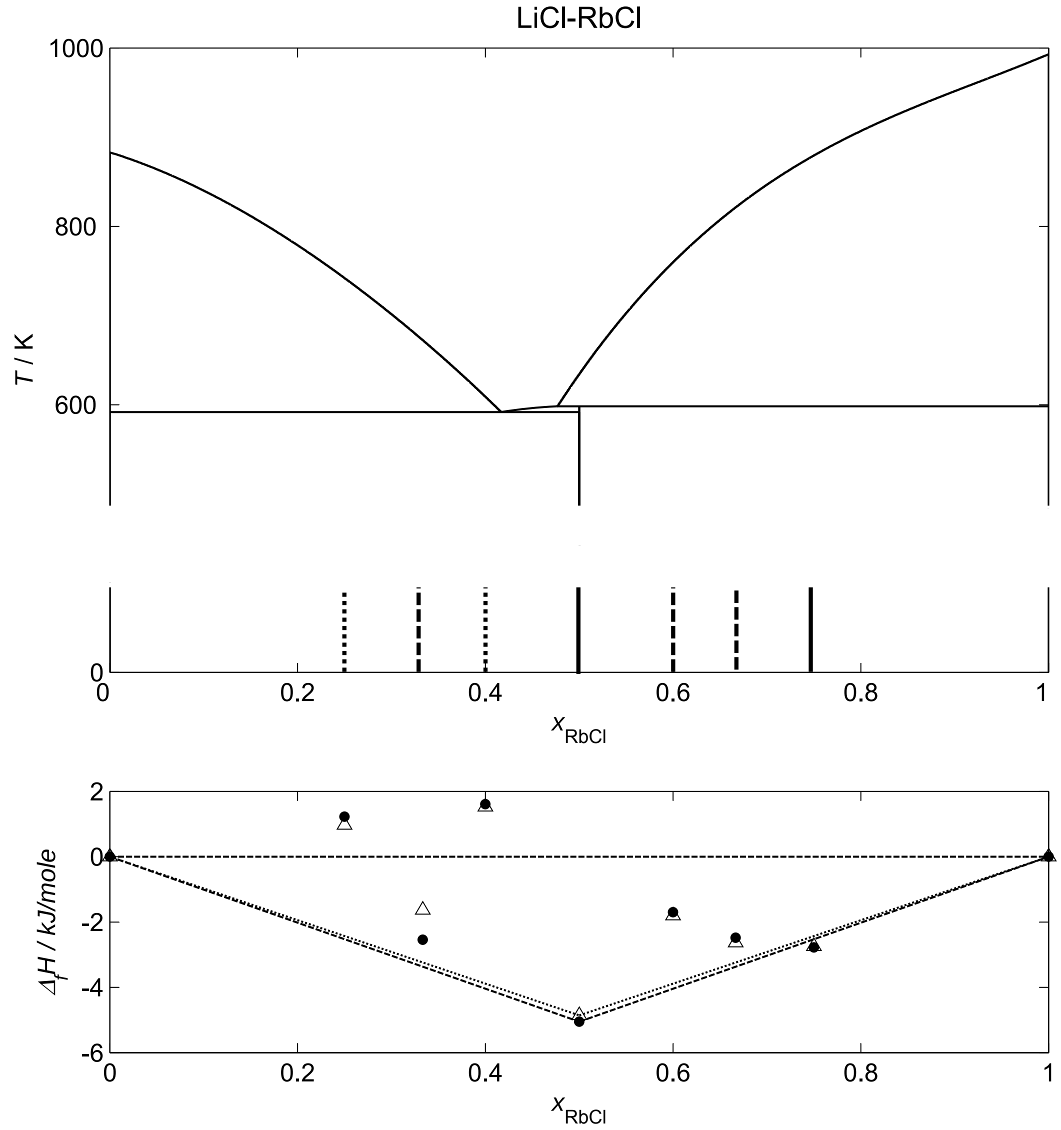

Figure 6.25: Top: The phase diagram of the LiCl-RbCl system. Thin solid line - experimentally known high-temperature part of the phase diagram, bold solid line - predicted stable phases, dashed line - predicted metastable phases which are stable with respect to the binary compounds LiCl and RbCl, dotted line - predicted phases that are metastable with respect to the binary compounds. Bottom: Enthalpies of formation at 0 K with respect to the binary compounds for the crystalline modifications with the lowest energy for each concentration investigated. Bullets - Hartree-Fock-calculations, triangles - DFT-B3LYP-calculations.

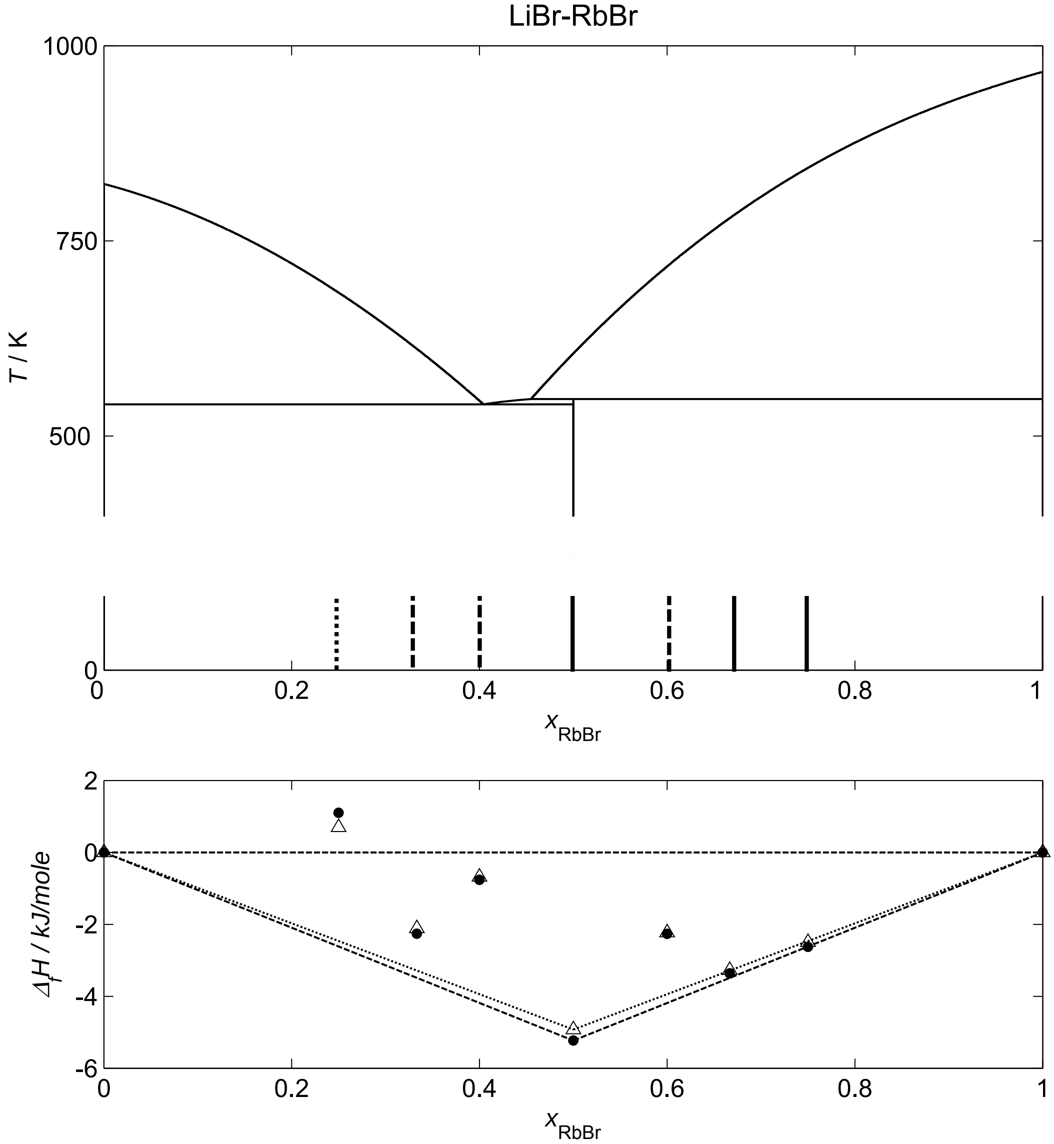

Figure 6.26: Top: The phase diagram of the LiBr-RbBr system. Thin solid line - experimentally known high-temperature part of the phase diagram, bold solid line - predicted stable phases, dashed line - predicted metastable phases which are stable with respect to the binary compounds LiBr and RbBr, dotted line - predicted phases that are metastable with respect to the binary compounds. Bottom: Enthalpies of formation at 0 K with respect to the binary compounds for the crystalline modifications with the lowest energy for each concentration investigated. Bullets - Hartree-Fock-calculations, triangles - DFT-B3LYP-calculations.

Table 6.18: Structure parameters, bulk moduli and enthalpies of formation per mole with respect to the binary compounds LiBr and RbBr at 0 K for the structure candidates with the lowest energy for each composition for the LiBr-RbBr system, after local optimization on Hartree-Fock and DFT-B3LYP (in brackets) level. Structure data, volume V$_{min}$ and bulk moduli are only given for the HF-calculations.

Space group (no.) Crystal system, Type	Lattice constants a, b, c [Å]; α, β, γ [$\circ$]	Atom (Multip., Wyckoff lett.), Relative coordinates				V$_{min}$[Å^3] Bulk modulus [GPa]	$\Delta_f H$[kJ] HF (DFT)
		atom	x	y	z		
Pc (7)	$a = 7.93088$	Li1(2a)	0.78287	0.40328	0.80755	533.905	1.1013
monoclinic	$b = 8.56512$	Li2(2a)	0.33119	0.59837	0.59089	15.185	(0.6955)
$Li_3RbBr_4 - Type1$	$c = 7.87443$	Li3(2a)	0.54509	0.91577	0.00060		
	$\alpha = \gamma = 90$	Rb4(2a)	0.05132	0.17383	0.49939		
	$\beta = 93.49810$	Br5(2a)	0.32895	0.90267	0.68506		
		Br6(2a)	0.76693	0.90970	0.32960		
		Br7(2a)	0.59620	0.41172	0.50225		
		Br8(2a)	0.11738	0.45936	0.81027		
$P-4m2$ (115)	$a = 4.33938$	Li1(2g)	0	1/2	0.85769	197.062	-2.2618
tetragonal	$c = 10.46516$	Rb2(1c)	1/2	1/2	1/2	13.802	(-2.1142)
$Li_2RbBr_3 - Type1$	$\alpha = \beta = \gamma = 90$	Br3(1b)	1/2	1/2	0		
		Br4(2e)	0	0	0.29574		
$Amm2$ (38)	$a = 4.30296$	Li1(4e)	1/2	0.17428	0.62611	723.781	-0.7619
orthorhombic	$b = 20.40089$	Li2(2b)	1/2	0	0.52903	12.353	(-0.6828)
$Li_3Rb_2Br_5 - Type1$	$c = 8.24501$	Rb3(4d)	0	0.86360	0.12974		
	$\alpha = \beta = \gamma = 90$	Br4(4d)	0	0.09750	0.61344		
		Br5(2b)	1/2	0	0.21754		
		Br6(4e)	1/2	0.24722	0.87965		
$Cmcm$ (63)	$a = 4.60474$	Rb1(4c)	0	0.62710	1/4	593.407	-5.2284
orthorhombic	$b = 15.94588$	Li2(4c)	0	0.10290	3/4	12.355	(-4.9250)
$LiRbBr_2 - Type1$	$c = 8.08163$	Br3(4a)	0	0	0		
	$\alpha = \beta = \gamma = 90$	Br4(4c)	0	0.30380	1/4		
Cm (8)	$a = 7.70886$	Li1(4b)	0.26688	0.21643	0.80306	739.558	-2.2655
monoclinic	$b = 25.89668$	Rb2(4b)	0.76693	0.11872	0.77433	12.324	(-2.2291)
$Li_2Rb_3Br_5 - Type1$	$c = 6.33344$	Rb3(2a)	0.76016	0	0.26158		
	$\alpha = \gamma = 90$	Br4(4b)	0.25952	0.11657	0.75047		
	$\beta = 144.20250$	Br5(2a)	0.26419	0	0.26037		
		Br6(4b)	0.26832	0.23110	0.21937		
$Cmc2_1$ (36)	$a = 4.54239$	Li1(4a)	0	0.65247	0.23729	939.702	-3.3615
orthorhombic	$b = 24.68284$	Rb2(4a)	0	0.00407	0.24164	11.641	(-3.2746)
$LiRb_2Br_3 - Type1$	$c = 8.38169$	Rb3(4a)	0	0.17392	0.74734		
	$\alpha = \beta = \gamma = 90$	Br4(4a)	0	0.41451	0.48936		
		Br5(4a)	0	0.78945	0.72392		
		Br6(4a)	0	0.41103	0.99086		
$P2_1$ (4)	$a = 7.18889$	Li1(2a)	0.58003	0.42659	0.57805	739.104	-2.9998
monoclinic	$b = 7.22087$	Rb1(2a)	0.50155	0.34596	0.13319		(-2.8445)
$LiRb_3Br_4 - Type1$	$c = 14.23860$	Rb2(2a)	0.99262	0.35216	0.87258		
	$\alpha = \gamma = 90$	Rb3(2a)	0.99313	0.86164	0.62437		
	$\beta = 90.44890$	Br1(2a)	0.08085	0.85849	0.37817		
		Br2(2a)	0.49115	0.34581	0.87108		
		Br3(2a)	0.00127	0.35206	0.12774		
		Br4(2a)	0.50413	0.27611	0.41273		

6.5 Critical discussion

In the current Chapter we have presented results obtained for the quasi-binary alkali halide systems via the new strategy suggested in this thesis. When comparing our approach with those suggested in the literature (12; 14), the most important difference is our global landscape exploration combining, in a systematic fashion, a global search for locally ergodic regions at low temperatures with the identification of regions which correspond to ordered crystalline phases or larger ergodic regions stable at elevated temperatures, which correspond to solid solution-like phases of the system comprising families of many structurally related minima. This approach allows us to predict the existence / non-existence of a miscibility gap or ordered crystalline phases in an unexplored chemical system without any recourse to experimental information or chemical intuition. In contrast, the studies found in the literature always assume that both the superstructure of the solid solution/alloy type compound and the sublattice on which the chemical substitution takes place, are known beforehand, e.g. from chemical intuition or based on experimental information. The authors then typically employ Ising type models, e.g. within the quasi-chemical approximation, to compute the free energy of mixing, while we endeavour to directly estimate the partition function of the alloy phase.

In this context, we note that the specific methodology presented in this thesis, i.e., the analysis of structurally related families of minimum configurations, can also be applied to chemical systems, where phase transitions occur due to the freezing / unfreezing of e.g. rotational degrees of freedom of complex ions or molecules (119; 169). Of course, in that type of problem, the configurational entropy contribution will be quite different from the cases presented in this work. On the other hand, phase transitions that are not associated with a structural change of the system would require different concepts within an energy landscape approach than the ones discussed in this work[2].

Concerning the accuracy of the *ab initio* calculations, there appears to be a satisfactory general agreement between the results of the HF and DFT calculations. As one would expect, essentially all cell parameters calculated with HF are somewhat larger than the experimental ones, if available, and cells computed with DFT are closer to experiment, respectively (e.g. see Table 6.16).

The main problems associated with the *ab initio* calculations appeared when we dealt with the rubidium and cesium compounds. Here, the limitations of the *ab initio* calculations are expected to be particularly noticeable, since here relativistic effects play a role. Typically, one uses pseudopotentials - in particular effective core potentials (ECP) (172; 173) -, in order to simulate chemically inactive atomic cores and to mimic relativistic effects for heavy-atom compounds. As we have noticed earlier (48), one needs to pay great attention to the type of basis set employed and one might have to perform an additional basis set optimization. Thus, we have employed a specially optimized basis set from the literature (135) which uses such an effective core potential. The starting basis set (135) was a Stuttgart-Dresden ECP28MBW quasirelativistic pseudopotential with a core charge of nine and equal number of the valence electrons (174). The authors (135) optimized the most diffuse s functions and the most diffuse p function, and in order to allow the polarization of the $5s5p$ shell, the authors added a single d function.

---

[2] For an example of an energy landscape analysis of magnetic systems see e.g. work by Sibani and co-workers (170; 171).

Furthermore, we have repeated our calculations for a number of systems, where miscibility gaps were predicted, with another density functional, LDA-VBH, which is very different from the B3LYP-functional. In the case of the rubidium compounds (see Fig. 6.12), we find that the three computed miscibility gaps are very similar - both for the stable (rocksalt-type) and the metastable (CsCl-type) solid solution phase. For the cesium compounds (see Fig. 6.13), the critical temperatures computed with LDA-VBH for the stable (rocksalt-type) and metastable (CsCl-type) solid solutions are larger than the ones found for the HF- and B3LYP-calculations, but they still lie within the general error bars we estimate for our predictions. The inherent limitations of the quantum mechanical computations - e.g. choice of functionals for DFT-calculations, choice of basis sets and pseudopotentials -, the (according to our estimates usually quite reasonable) assumption that the phonon contributions to the excess enthalpy are negligible, together with the finite size of the supercells we can deal with, lead to error bars in the calculated critical temperatures of probably up to 10%.

In this context, we note that using two or more different *ab initio* methods gives us confidence that our computed critical parameters are quite satisfactory. In particular, one should note that in the low-temperature region of the phase diagrams it is also often very difficult to establish the thermodynamic stability or metastability of the observed phase from experiment. Taking this into consideration, we would conclude that the obtained results are quite trustworthy for most systems.

Also one should mention, that performing the local optimizations of the various structures on *ab initio* level is very expensive computationally. Thus, we have also computed the binodal curves and miscibility gaps using only the simple empirical potential for three test systems: NaCl-LiCl, NaBr-LiBr and NaCl-KCl. While the qualitative result is similar to the one obtained on *ab initio* level, the quantitative agreement with experiment is much better for the *ab initio* calculations. For instance, the critical temperatures using the empirical potential are twice as large as the ones based on the *ab initio* calculations. Thus, it is essential to perform the local optimization runs on the *ab initio* level to get the satisfactory results. As an alternative, one could attempt to construct highly-refined empirical potentials. However, even if good approximate energy functions can be constructed at all, the effort of deriving trustworthy quantitatively accurate and globally valid robust potentials is usually very large. Furthermore, typically experimental input for fitting the parameters is required, which would contradict the a priori approach pursued in this work.

We note, that the individual solid solution-structure candidates typically exhibit space groups with few symmetries. In such cases, the minimization of the energy on the *ab initio* level is difficult, since there are very many degrees of freedom. Furthermore, additional refinements of the (already optimized) basis sets for the compounds might result in some further degree of improvement. Since small errors in the total energies can be magnified when computing the phase diagrams, such minor changes might be of relevance. We had already mentioned above that the enthalpies of formation of the compounds were obtained for 0 K; for a more correct description of the Gibbs energy we need to know the temperature dependence of the excess Gibbs energy, of course.

One possible improvement would be replacing the self-consistent combination of the average of the minimum energies and the entropy of mixing of an ideal solution in the free energy calculation, by a direct computation of the free energy via a sum over Boltzmann factors belonging to several thousand large ($O(10^2)$ atoms/simulation cell) locally optimized atom configurations which in their totality represent the solid solution-like state. However, such an approach is still very expensive computationally.

Another step would be to include the phonon contribution to the free energy, but, again, the computational effort required is extremely large. In order to gain at least some rough estimate of the importance of this contribution, we have computed the phonon contribution to the free energy of formation on empirical potential level. We find that e.g. for the NaCl-LiCl system this contribution is less than 1%, while the relative contribution of the phonons is somewhat larger in the e.g. NaBr-LiBr and NaCl-KCl systems. A closer analysis of the phonon data suggests that the importance of the phonon term might correlate with deviations of the solid solution-like state from Vegard's law, which states that the cell parameters (and thus the cell volume) of an alloy are a linear combination of the parameters of the end phases a_1 and a_2 as function of composition x, $a(x) = xa_1 + (1-x)a_2$. As a consequence, this implies that one should use as large supercells as possible for the computation of the phonon contribution, in order to avoid finite size effects that can make themselves felt as spurious deviations from Vegard's law. Quite generally, the results support our expectation that the vibrational contributions to the (excess) heat capacity of the solid solution should not vary very much as function of composition even at moderately high temperatures.

Thus, we expect that our computed data are sufficiently accurate to correctly predict the existence/nonexistence of the miscibility gap and its location. Quite generally, we estimate from the spread in energies over the minima belonging to the solid solution-state that the intrinsic error in the calculations of the critical parameters T_c and x_c should not exceed 10% and ±0.05 mole fractions, respectively. We also note that part of the discrepancy between theory and experiment might be due to difficulties in performing the actual experiments. After all, our calculations refer to the ideal crystals in the pure system without impurities or defects. In contrast, the experimentalist deals with the real crystals, i.e. crystals containing defects and foreign atoms. Thus, both qualitative and quantitative agreement of our calculations with the experimental results if available is quite satisfactory.

Concerning the CsX-LiX and LiX-RbX systems, for a given halide system, the enthalpies of formation for the different stable structure candidates listed in Tables 6.12 - 6.15 and Tables 6.17 and 6.18 are rather similar. Considering the limited accuracy of the *ab inito* calculations, it is difficult to draw any firm conclusion about whether a phase at a particular composition x is thermodynamically stable or only metastable with respect to a decomposition into two neighboring phases i and j with compositions $x_i < x < x_j$. When referring to the stability of the phases, we consider both the stability against the binary compounds ($x = 0{,}1$) and the overall stability against combinations of neighboring phases.

In principle, general statistical mechanical considerations show that there must be some, though probably very small, degree of solubility of the minority cation in the structure of the halide of the majority cation. Apart from trying to compute at an *ab initio* level the defect energy associated with introducing e.g. a Li-atom at the position of a Cs-atom, one could try to estimate the thermodynamically allowed amount of solubility by computing the hypothetical miscibility gap of a CsX/LiX or LiX/RbX solid solution in the structure type of the binary compounds CsX or RbX and LiX, the CsCl- and the rocksalt-type, respectively. This feature of defect formation / boundary solubility would be most noticeable at high temperatures close to the melting point. We have computed these hypothetical miscibility gaps for the CsCl/LiCl system, and we find that even for temperatures in the range of the melting temperatures of LiCl and CsCl the degree of solubility of the minority cation in the structure of the binary halide of the majority cation is considerably below one percent. Since the high-temperature region of the phase diagram is not the focus of this thesis, we do not attempt to show the curves delimiting the regions of the phase diagrams exhibiting boundary solubility in the figures.

Usually, predicted phases remain stable at non-zero (low) temperatures, but at elevated temperatures phonon contributions might lead to a shift in the relative Gibbs energies. Again, we have not calculated these vibrational terms; our experience has shown that they are rather similar at low temperatures, and thus are only expected to be of importance at high temperatures. An indication that this also holds true for the CsX-LiX and LiX-RbX systems is the similarity of the bulk moduli for all candidates with a given composition, and the systematic trend in the bulk moduli as function of composition. Since the newly proposed structure candidates are not observed in the solidus-liquidus region of the phase diagrams, they are expected to decompose at temperatures below the known eutectic and / or peritectic temperatures in the two families of systems. However, our calculations cannot determine these decomposition temperatures; the length of the lines in the phase diagrams on each figure is no indication of the temperature of decomposition. Note that these considerations do not allow any statements about whether a particular metastable phase could exist or whether a particular phase is easy to access, since these issues are dominated by the kinetic stability of the phases and the kinetic pathways on the energy landscape at the low temperatures involved.

We note that we cannot exclude the possibility that there might be some additional relevant structure candidates our global explorations have failed to identify so far, since in particular for complicated compositions stable modifications might exist, which exhibit more atoms in the primitive unit cell than can be employed during the global optimization due to limits in computer time.

6.6 Conclusion

To summarize the results of the quasi-binary alkali halide systems, we have used these system primarily to test a new general methodology that allows us to determine whether a crystalline solid solution-like phase or ordered crystalline phases will occur in the low-temperature part of the phase diagram of a chemical system, and to obtain the critical parameters of the miscibility gap, without any experimental data or *a priori* knowledge about the phase diagram of the system under investigation.

We have determined the critical parameters of the miscibility gap in the NaCl-LiCl, NaBr-LiBr, NaCl-KCl and KBr-NaBr systems, which are satisfactorily close to the experimental data. Also, we predict the miscibility gap locations in KCl-RbCl and KBr-RbBr systems for which no low-temperature experimental data exist.

Furthermore, we have shown that our approach to the *ab initio* prediction of low-temperature phase diagrams including solid solution phases can be used not only for systems with two different cations, but also those that contain two types of anions. We find good quantitative agreement with experimental data for the MBr-MI systems, where M = Li, Na, K, Rb or Cs, and we suggest improved critical parameters for the LiBr-LiI, KBr-KI and RbBr-RbI systems.

We have found good qualitative and quantitative agreement with the miscibility gaps based on optimization of the available thermodynamic data for the NaBr-NaCl and KBr-KCl systems, and we have predicted the location of the miscibility gap for the LiBr-LiCl system, for which there is no experimental data available. Finally, we have shown that our general approach can be successfully applied not only to the prediction of the low-temperature part of T-x phase diagrams at standard pressure, but also to the prediction of the low-temperature part of P-T-x phase diagrams, which exhibit miscibility gaps.

We have shown that our approach to the study of the low-temperature region of phase diagrams of multinary systems yields results that are in good agreement with the data available for the lithium cesium and lithium rubidium halides. In addition, our investigations point to a multitude of yet to be synthesized stable and metastable phases in these quasi-binary systems. We confirmed the existence of the experimentally known phases in all the systems under investigation. In addition, our investigations point to a multitude of not-yet synthesized stable and metastable phases.

In the following two chapters, we are going to apply our new method to two classes of systems, where no experimental information regarding the low temperature phase diagrams is available: quasi-binary and quasi-ternary arsenide and antimonide based semiconductors (Chapter 7) and quasi-binary lanthanum halides (Chapter 8).

7 Quasi-binary and quasi-ternary semiconductors in A^{III}B^{V} systems (A = Al, Ga or In; B = As or Sb)

7.1 Introduction

The A^{III}B^{V} semiconductor compounds have received much attention over the past decades because of their important applications in materials science and engineering. Up to now, a number of studies have been reported on the liquid-solid phase equilibria in the systems MX-M'X where M,M' - Al, Ga or In and X - As or Sb (175; 176; 177; 178; 179; 180; 181; 182; 183; 184; 185), since such information plays a key role in the growth of alloy semiconductor crystals by liquid phase epitaxy. However, the low-temperature parts of the phase diagrams exhibit a lack of thermodynamic data, especially for the quasi-ternary systems. Nevertheless, such information is no less important than the one about the high temperature parts of the phase diagrams, since the knowledge of the location of the miscibility gap gives us information at what conditions the final products can be used without a crash as a result of a decomposition of the solid solution at low (room) temperatures.

However, direct experiments at low temperatures are quite difficult; it is even often nearly impossible to access the thermodynamic equilibrium due to the low speed of solid state reactions. Thus, computational methods based on the optimization of the direct experimental thermodynamic data (Calpad approach) or theoretical studies are needed to supplement the experiments in deriving the phase diagrams. There are many studies available which describe the liquidus-solidus equilibria and the extrapolated miscibility gaps for the MX-M'X systems where M,M' = Al, Ga or In and X = As or Sb (186; 187; 188; 189; 190; 191; 192; 193; 194). But nevertheless, the critical parameters are not satisfactory and sometimes the proposed values are spread over a range of hundreds of degrees.

In this section, we apply the new strategy suggested in this thesis (see Part III) to these quasi-binary semiconductor alloys, and where there is a lack of experimental thermodynamic data at low temperatures, we predict the low-temperature part of their phase diagrams. Moreover, we calculate the quasi-ternary phase diagrams at low-temperature using not only information about the quasi-binary compounds but also additional simulation data for the quasi-ternary systems.

7.2 General remarks

Our general approach to the determination of structure candidates has been given in detail in the Part III. The systems were modeled as spherical ions that interact via a simple empirical two-body potential, $V_{ij}(r_{ij})$, consisting of a Coulomb- and a Lennard-Jones-term that depend only on the atom-atom distance r_{ij}, in order to allow fast calculations of the energy of a given configuration. The Lennard-Jones parameters $\sigma_{ij} = r_s(r_i + r_j)$ are given by the sum of the ionic radii of atoms i and j with charges q_i and q_j multiplied by a scaling factor r_s. The ionic radii are presented in the Appendix (see the Table B.1).

The *ab initio* runs were performed on both Hartree-Fock (HF) and density functional theory (DFT) level; the basis sets used were taken from the CRYSTAL web page (136).

7.3 Results and Discussion

For each chemical system, several hundred global optimization runs were performed for a number of different compositions each, at a pressure of 0 Pa. We performed calculations for 5 different compositions (MX:M'X = 3:1, 2:1, 1:1, 1:2, 1:3) besides the limiting binary phases for all six MX-M'X systems (M,M' = Al, Ga or In; X = As or Sb); and for 10 different compositions (AlX:GaX:InX = 1:1:1, 1:1:2, 1:2:1, 2:1:1, 1:2:2, 2:1:2, 2:2:1, 1:1:3, 1:3:1, 3:1:1) for both quasi-ternary systems. For each composition, we found for the set of structure candidates with the lowest energies, that the energy differences between the candidates were very small. These candidates belonged to the same structure family (sphalerite with M and M' located on the Zn-positions in ZnS), indicating a solid-solution behaviour for all quasi-binary and quasi-ternary systems. As a next step, we calculated the enthalpy of formation for each composition according to Eqn. (5.2). The parameters for the fit of Δ_fH(x) with a Redlich-Kister polynomial for all of the quasi-binary systems are listed in Table 7.1.

Table 7.1: The Redlich-Kister polynomial fitting parameters of the enthalpy of formation (according to equation 5.2) for solid solution phases in the MX-M'X systems (M,M' = Al, Ga or Sb; X = As or Sb) at standard pressure obtained in the present work (in Joule/mol).

System	HF		DFT-B3LYP	
	a_0	a_1	a_0	a_1
AlAs-GaAs	4436.5	-120.4	4343.1	-229.2
AlAs-InAs	7777.4	122.8	8198.6	-285.3
GaAs-InAs	5727.7	-331.8	5184.4	-690.9
AlSb-GaSb	1595	368.1	2848.6	-33.7
AlSb-InSb	5268.1	309.9	5430.8	-51.5
GaSb-InSb	4355.3	375.6	4390	187.1

From this data we calculated Gibbs energies of the solid phase and predicted the location of the miscibility gaps. The critical parameters are listed in Table 7.2.

Table 7.2: The critical parameters for the MX-M'X systems (M,M' = Al, Ga or Sb; X = As or Sb) systems at standard pressure obtained in the present work. T_c is the critical temperature of the decomposition in K, and x_c is the concentration of the second compound. The literature data (x_c^{lit} and T_c^{lit}) are based on extrapolation from the liquidus-solidus region.

System	HF		DFT-B3LYP		Literature data		
	x_c	T_c	x_c	T_c	x_c^{lit}	T_c^{lit}	Ref.
AlAs-GaAs	0.53	267	0.54	263	0.5	131	(186)
AlAs-InAs	0.49	468	0.52	494	0.5	553, 629	(180; 195)
GaAs-InAs	0.54	347	0.59	323	0.5	816, 505	(196; 197)
AlSb-GaSb	0.37	105	0.5	171	0.5	207	(188)
AlSb-InSb	0.46	319	0.5	327	0.5	217, 180	(183; 189)
GaSb-InSb	0.44	266	0.47	265	0.5	466	(190)

As a next step, we calculated the enthalpy of formation for the quasi-ternary systems for each composition xb and xc by the following formula:

$$\begin{aligned}&\Delta_f H(Al_{1-xb-xc}Ga_{xb}In_{xc}X) = E(Al_{1-xb-xc}Ga_{xb}In_{xc}X) - \\ &(1-xb-xc)E(AlX) - xbE(GaX) - xcE(InX), \qquad (7.1)\end{aligned}$$

where E(Al$_{1-xb-xc}$Ga$_{xb}$In$_{xc}$X) is the energy of the structure candidate, E(AlX), E(GaX) and E(InX) are the energies of the boundary compounds AlX, GaX and InX, respectively; xb is the fraction of GaX, and xc is the fraction of InX in the overall composition (X = As or Sb). In Figures 7.1 and 7.2 one can see the predicted binodal curves (both for HF- and DFT-B3LYP-based calculations) and plots of the miscibility gaps based on extrapolation of high-temperature data from the literature for two of the quasi-binary systems (AlAs-GaAs-InAs and AlSb-GaSb-InSb).

The parameters for a fit of the excess Gibbs energy for both quasi-ternary systems are listed in Table 7.3. From this data we calculated the Gibbs energies of the solid phase using the Redlich-Kister model and predicted the location of the miscibility gaps according to the following formula:

$$\begin{aligned}\Delta G^{sol} &= \Delta_f H_{AlX-InX} + \Delta_f H_{AlX-GaX} \\ &+\Delta_f H_{GaX-InX} - TS_{id} + x_{AlX}x_{GaX}x_{InX}\sum_{i=1}^{3} x_i L_i, \qquad (7.2)\end{aligned}$$

where $\Delta_f H_{MX-M'X}$ is the enthalpy of formation of the quasi-binary system (M,M' = Al, Ga, or In; X = As or Sb), obtained earlier in the present work (according Eqn. (5.2)); L$_i$ = fitting parameters (see Table 7.3); S_{id} = ideal entropy of mixing. In Figures 7.3 and 7.4 one can see the isothermal projections of the predicted binodal curves (for HF-based calculations) for both quasi-ternary systems.

Table 7.3: The fitting parameters of the enthalpy of formation (according to equation (7.2)) for solid solution phases in the AlX-GaX-InX systems (X = As or Sb) at standard pressure obtained in the present work (in Joule/mol).

System	HF			DFT-B3LYP		
	L_1	L_2	L_3	L_1	L_2	L_3
AlAs-GaAs-InAs	11991	-282	4648	16105	9927	-2842
AlSb-GaSb-InSb	14289	-6698	26338	11467	-3096	15701

As we have already mentioned in the section 7.1, the pseudobinary semiconductor systems $A^{III}B^{V}$ have been well studied, using both experimental and theoretical methods, especially the high temperature parts of the phase diagram. But there are no direct experimental results which yield the miscibility gaps in those systems. Nevertheless, standard thermodynamic methods can be used to estimate the location of the miscibility gap from the available liquidus-solidus data. The authors in Ref. (186) applied the regular solution model to describe the thermodynamic properties of the solid phase in the system AlAs-GaAs. The same model was used to describe the solidus curve in the system AlAs-InAs (187). The GaAs-InAs system has attracted much more attention from scientists, but there is no final conclusion about the critical parameters so far: the suggested critical temperatures lie between 505K (197) and 875K (198). In one of the last studies devoted to the optimization of the thermodynamic properties in this system, the authors suggested 816K as a temperature of solid solution decomposition (196). The authors in Refs. (188; 189) also apply the regular solution model to describe the solid phase in the pseudobinary AlSb-GaSb and AlSb-InSb systems. Y. Jianrong and A. Watson (190) improved the regular solution model by adding temperature dependent variables to describe the GaSb-InSb system. In all of these studies, the prediction of the miscibility gaps was based on the low temperature extrapolation of the thermodynamic functions that had been obtained at temperatures close to the liquid-solid equilibrium. Usually, such extrapolations are not very satisfactory, especially when heat capacities are not taken into account. On the other hand, when one performs extrapolations from (theoretically calculated) zero temperature data, contributions of the heat capacities to the Gibbs energy can often be neglected.

In the present work we found that for all systems under investigation the phase diagram should exhibit a solid solution-like phase regardless of whether the energy was calculated on a HF or DFT basis. Figures 7.1 and 7.2 depict quite good agreement between HF (solid curve) and DFT (dashed curve) studies. Moreover, the same behavior was observed not only for the six pseudobinary systems, but also for both quasi-ternary systems. Thus, we can conclude, that there are no stable ordered compounds, at least at the compositions investigated in the present work, in either of the two ternary systems, and that the low-temperature phase diagrams of both quasi-ternary systems exhibit miscibility gaps.

The additional information about the enthalpies of formation for the ternary compounds derived from the calculated data can improve the predictions of the location of the miscibility gaps in the quasi-ternary systems in comparison with results obtained using only

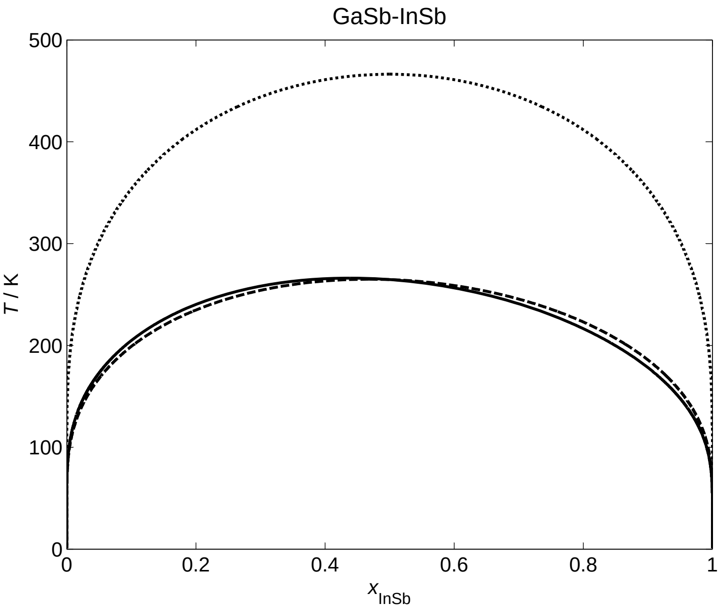

Figure 7.1: The miscibility gap in the GaSb-InSb system. Solid curve based on HF-calculations, dashed curve based on DFT-B3LYP calculations, dotted curve based on the extrapolated data from liquid/solid equilibria (190).

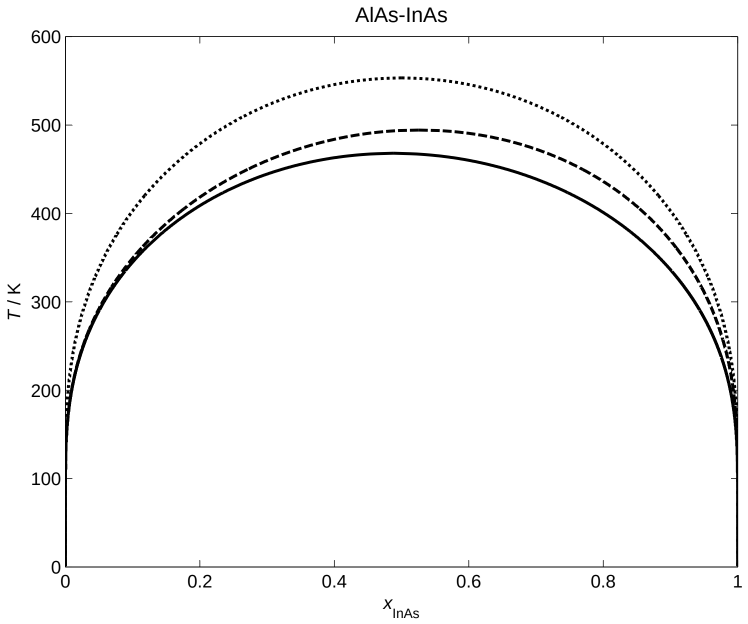

Figure 7.2: The miscibility gap in the AlAs-InAs system. Solid curve based on HF-calculations, dashed curve based on DFT-B3LYP calculations, dotted curve based on the extrapolated data from liquid/solid equilibria (180).

the pseudobinary data (199). E.g. if one constructs a miscibility gap based only on the data about the pseudobinary systems, one will never observe any miscibility gaps higher in temperature than the highest critical temperature of decomposition observed for the three quasi-binary systems. But additional data for the enthalpies of formation of the quasi-ternary compounds obtained in the present work allow us to predict the full miscibility gaps in both quasi-ternary systems under investigation even if the gap extends to temperatures higher than the critical temperatures of decomposition for the quasi-binary systems.

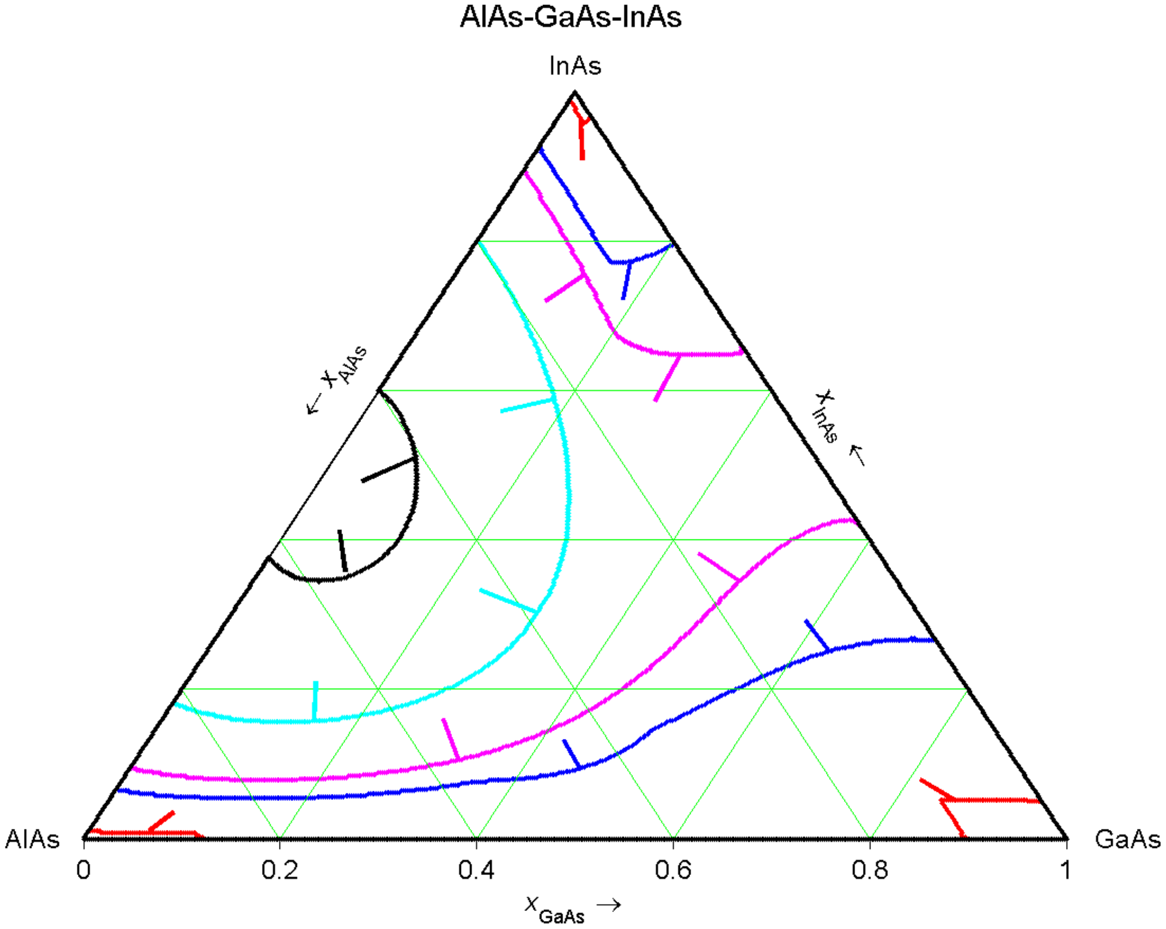

Figure 7.3: The 5 isothermal projections of the phase diagram for the AlAs-GaAs-InAs system at [200 310 340 400 460] K, based on the HF-calculations. Red curve - 200 K, blue curve - 310 K, magenta curve - 340, cyan curve - 400 K and black curve - 460 K.

Figures 7.3 and 7.4 depict the isothermal sections of the phase diagram for the AlAs-GaAs-InAs and AlSb-GaSb-InSb systems at five different temperatures, chosen usually a little bit lower and higher[1] than the critical temperatures of decomposition for the quasi-binary systems, based on the HF-data. The thin lines indicate the area of miscibility gaps.

---

[1] For the AlSb-GaSb-InSb the last three miscibility curves lie much higher than the highest critical temperature of the quasi-binary systems.

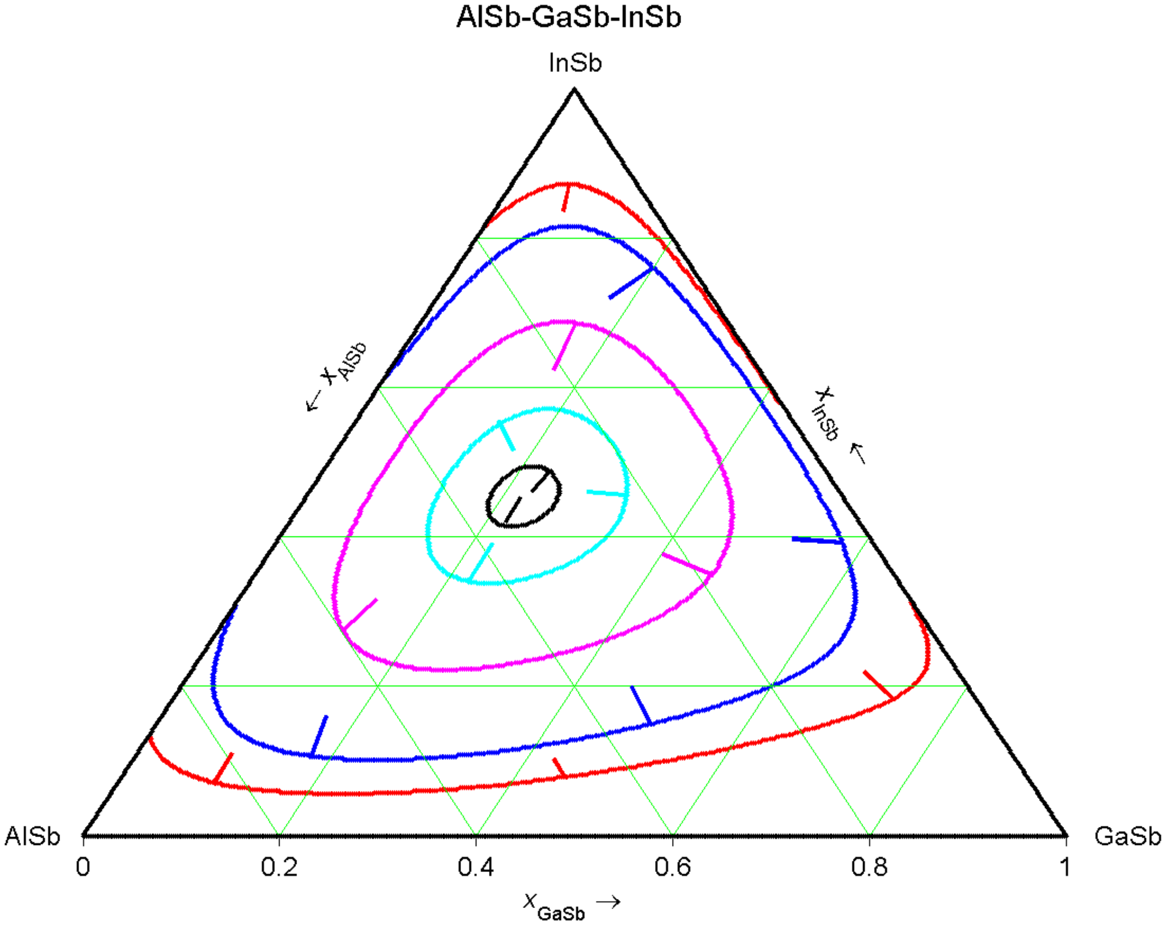

Figure 7.4: The 5 isothermal projections of the phase diagram for the AlSb-GaSb-InSb system at [260 310 400 450 472] K, based on the HF-calculations. Red curve - 260 K, blue curve - 310 K, magenta curve - 400, cyan curve - 450 K and black curve - 465 K.

Here, one should point out the qualitative difference in the observed miscibility gaps of the two quasi-ternary systems. In the case of the AlAs-GaAs-InAs system we do not observe a miscibility gap at temperatures above the highest critical temperature of decomposition for the binaries. One should mention, that the same behaviour was observed for both HF and DFT-B3LYP methods. Those results are in qualitative agreement with data from (200). In contrast, for the AlSb-GaSb-InSb system, a gap exists up to 467 K and 381 K for HF and DFT-B3LYP data, respectively. To explain that fact, one should refer to the predicted enthalpies of formation and the final fitting parameters (or ”interaction” parameters) for the excess Gibbs energies for both quasi-binary and quasi-ternary systems (see Tables 7.1 and 7.3). In general, the binary data for the arsenide systems are bigger than for the antimonide systems. In contrast, the final fitting parameters for the excess Gibbs energies for quasi-ternary systems are bigger for the antimonide systems than for the arsenide systems. This results in different shapes of the miscibility gaps for the quasi-ternary systems.

As an example, figure 7.5 depicts the isothermal section of the phase diagram for the AlAs-GaAs-InAs system at 320 K, with the phase diagrams of the three quasi-binary systems on the corresponding sides. The dotted lines show the projections of the binaries onto the quasi-ternary phase diagram.

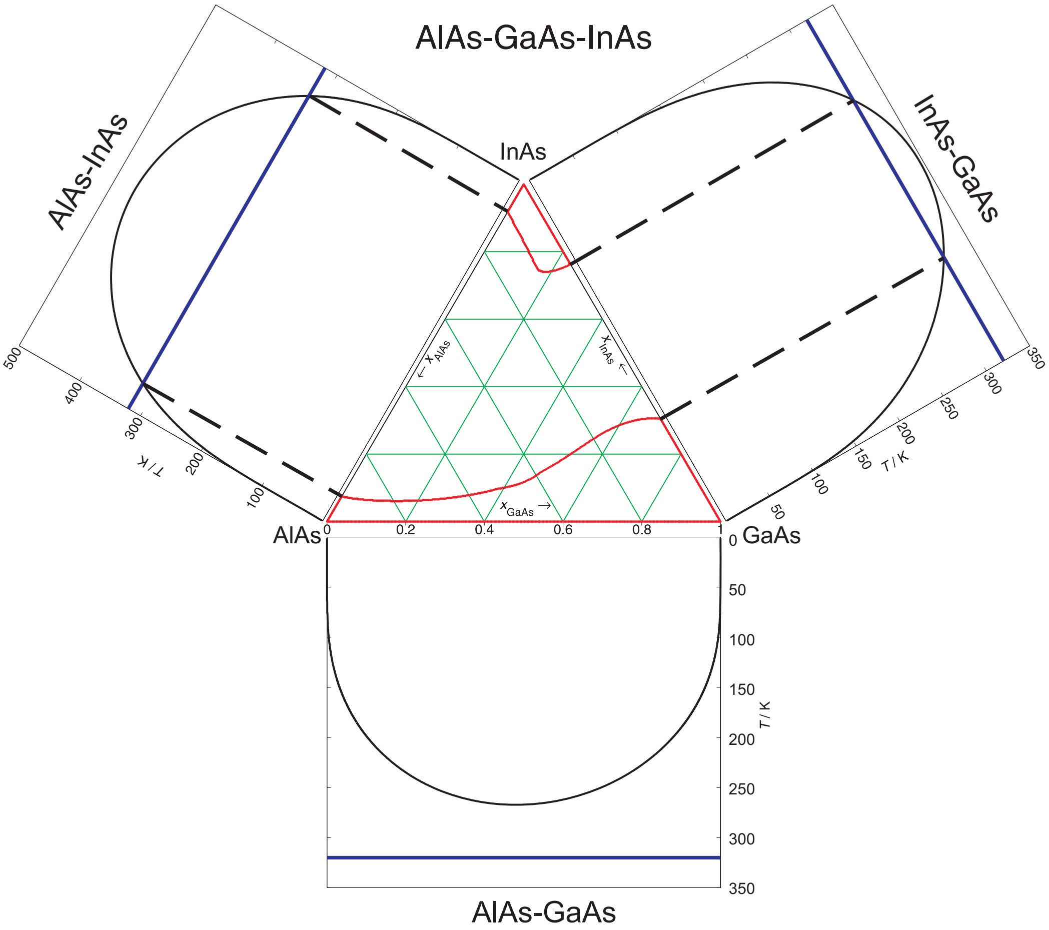

Figure 7.5: Isothermal section of the phase diagram for the AlAs-GaAs-InAs system at 320 K. Blue lines indicate a temperature of 320 K, red curves are the border of the miscibility gap in the quasi-ternary system at 320 K, black curves are the full miscibility gaps in the quasi-binary systems.

7.4 Conclusion

To summarize, we have shown that our approach can be successfully applied to the investigation of the quasi-binary and quasi-ternary semiconductor systems $A^{III}B^{V}$. For the first time, the miscibility gaps for the quasi-ternary systems were calculated based not only on the data of the quasi-binary systems, but also including additional information about enthalpies of formation of the quasi-ternary compounds. Previous results for the alkali-halide systems (see Chapter 6) allow us to expect that the predicted data are quite close to reality.

8 Quasi-binary lanthanum halogenide systems

8.1 Introduction

In this section, we present an investigation of the quasi-binary lanthanum halogenide systems LaX_3-LaY_3 (where X,Y = F, Cl, Br or I). There are no data available in the literature about any compounds in those systems, besides the binary compounds LaX_3 (201), and only one synthesis of a mixed halide of a rare-earth element, $TbFCl_2$, has been reported (202). But such mixed halide compounds might be quite interesting for technological applications: the binary compounds are widely used, e.g. $LaCl_3$ and $LaBr_3$ doped by Ce are employed as scintillator materials (203; 204), and the layered lanthanum carbide halides exhibit superconducting properties (205). Thus, the investigation of the phase diagrams of the quasi-binary lanthanum halides, including the prediction of new structure candidates, should prove to be quite valuable, both for basic research in chemistry and for applications in materials science.

8.2 General remarks

Our general approach to the determination of structure candidates has been given in detail in the Part III. The systems were modeled as spherical ions that interact via a simple empirical two-body potential, $V_{ij}(r_{ij})$, consisting of a Coulomb- and a Lennard-Jones-term that depend only on the atom-atom distance r_{ij}, in order to allow fast calculations of the energy of a given configuration. The Lennard-Jones parameters $\sigma_{ij} = r_s(r_i + r_j)$ are given by the sum of the ionic radii of atoms i and j with charges q_i adn q_j multiplied by a scaling factor r_s. The ionic radii were presented in Appendix, see the Table A.1.

The *ab initio* runs were performed on both Hartree-Fock (HF) and density functional theory (DFT) level; the basis sets were optimized versions (135) of data sets available in the literature (136) in case of the halogenides (see Appendix Table C.2); for lanthanum we used the data available on the web page of Mike Towler (206).

8.3 Results and Discussion

8.3.1 Binary halides LaX_3 (X = F, Cl, Br or I)

As a preliminary for our study we performed a global exploration of the energy landscape of the pure binary lanthanum halides at a pressure of 0 Pa. We noticed that the *ab initio* calculations based on the Hartree-Fock and DFT-B3LYP basis for the pure lanthanum halides give an incorrect ranking of the candidates by energy: the new predicted modifications, obtained during the global search, appear to be more stable than the experimental ones. Thus, we decided to repeat the *ab initio* calculations with an additional functional: DFT-LDA-VBH. In this case, the "right" results for the binary compounds (at least as far as the ranking by energy was concerned) were obtained. As a consequence, we used all three methods for the investigation of the mixed compounds, in order to get a better estimate of the validity of our results.

8.3.2 Quasi-binary halides LaX_3-LaY_3 (X,Y = F, Cl, Br, I)

As a preliminary step of the investigation, for each chemical system LaX_3-LaY_3, several hundred global optimization runs were performed for a number of different compositions each, at a pressure of 0 Pa. We performed calculations for 5 different compositions (X:Y = 3:1, 2:1, 1:1, 1:2, 1:3) in addition to the limiting binary phases. For each composition we found a list of structure candidates and calculated the $E(V)$-curves for all these candidates at an *ab initio* level. For given composition, the energy differences between the candidates with the lowest energies were at least equal, and in most cases considerably larger, than the thermal energy at room temperature. In addition, their cation-anion arrangements were different, and thus these candidates could not be considered as members of one "structure family", which would have indicated the possible presence of a solid solution-like phase. Furthermore, when comparing different compositions the candidates with the lowest energies did not exhibit the same cation-anion superstructure either. Thus, we deduced that in these systems no solid solutions are present as thermodynamically stable phases over the full range of compositions, and instead the low-temperature part of the phase diagram exhibits ordered crystalline phases. In the next step, the enthalpies of formation of each compound were obtained according to equation (5.2).

The calculations of the enthalpies of formation according to equation (5.2) showed that some of these intermediate phases are stable against decomposition into the boundary compounds at 0 K. Tables 8.1 - 8.6 show, for each composition, the structural data for the most stable among these structure candidates.

As we mentioned earlier, there are no experimental data available for compounds in the quasi-binary lanthanum halide systems. At first sight, one might expect a solid-solution behaviour for the $LaBr_3$-$LaCl_3$ system, since pure $LaBr_3$ and $LaCl_3$ crystallize in the same structure type (UCl_3-Type) (201). Similarly, for the other five systems, the different structure types of the binary endphases suggest that ordered crystalline phases, stable or metastable, will be more likely to exist at low temperatures than a solid solution phase. But, we found that in all six systems for all compositions investigated the observed structure candidates with the lowest free energy corresponded to ordered crystalline phases, which are at least metastable, and that no solid solution-like phases were present. One should mention that the same behaviour was observed regardless of whether the energy was calculated on HF or DFT basis. This apparent predisposition of the mixed rare earth halides to form crystalline ordered phases is supported by the fact that the only related compound synthesized so far - $TbFCl_2$, by the group of Th. Schleid (202), - is also an ordered crystalline modification.

LaF_3-$LaCl_3$ system

Since we found that all systems under investigation exhibit ordered crystalline phases at least at low temperatures, we decide to focus on one of the systems and perform more detailed investigations. For this purpose, we chose the LaF_3-$LaCl_3$ system. We added six additional compositions (F:Cl = 5:1, 4:1, 3:2, 2:3, 1:4 and 1:5). As a first step, we performed several hundred global optimization runs, then for all structure candidates found local *ab initio* minimizations were performed. Afterwards, for the candidates with the lowest energy, according to the *ab initio* studies, we generated super cells to get new candidates with a higher number of formula units[1], these new structures were quenched and served as starting points for further global searches via the threshold algorithm. Finally, all new structure candidates were analyzed at the *ab initio* level. This procedure allowed us to obtain structure candidates with Z (number of formulas units) equal 3, 4, 6 and 8 for compositions with 16 or 20 atoms per formula unit; the standard random walk based on simulated annealing usually takes too long to find deep lying minima for such large systems.

Figure 8.1 depicts the information about the low-temperature region of the phase diagram of the LaF_3-$LaCl_3$ system derived from the landscape exploration and *ab initio* energy minima studies. The top part of a figure indicates by a solid line, at which composition new possible stable compounds are expected, together with the experimentally known binaries; metastable compounds correspond to dashed lines[2]. The bottom part of the figures shows the convex hulls for the quasi-binary lanthanum halide system at T = 0 K, obtained in the present work. The solid black curves correspond to the HF calculations, the red lines to the DFT-B3LYP data, and finally the blue curves to the DFT-LDA-VBH results, respectively. The circles and squares correspond to the two structure candidates with the lowest energy for a given composition. Here, colors have the same meaning as for the solid curves. If the ranking of these candidates by energy is not the same for all three *ab initio* methods, we depict by circles those, for which the HF calculations yield the lowest energy while the squares correspond to the structure candidates which have

---

[1] Usually, we double or triple the cell in one direction.

[2] Our calculations cannot determine the decomposition temperatures of predicted phases; thus, the length of the lines in the phase diagrams are no indication of the temperature of decomposition.

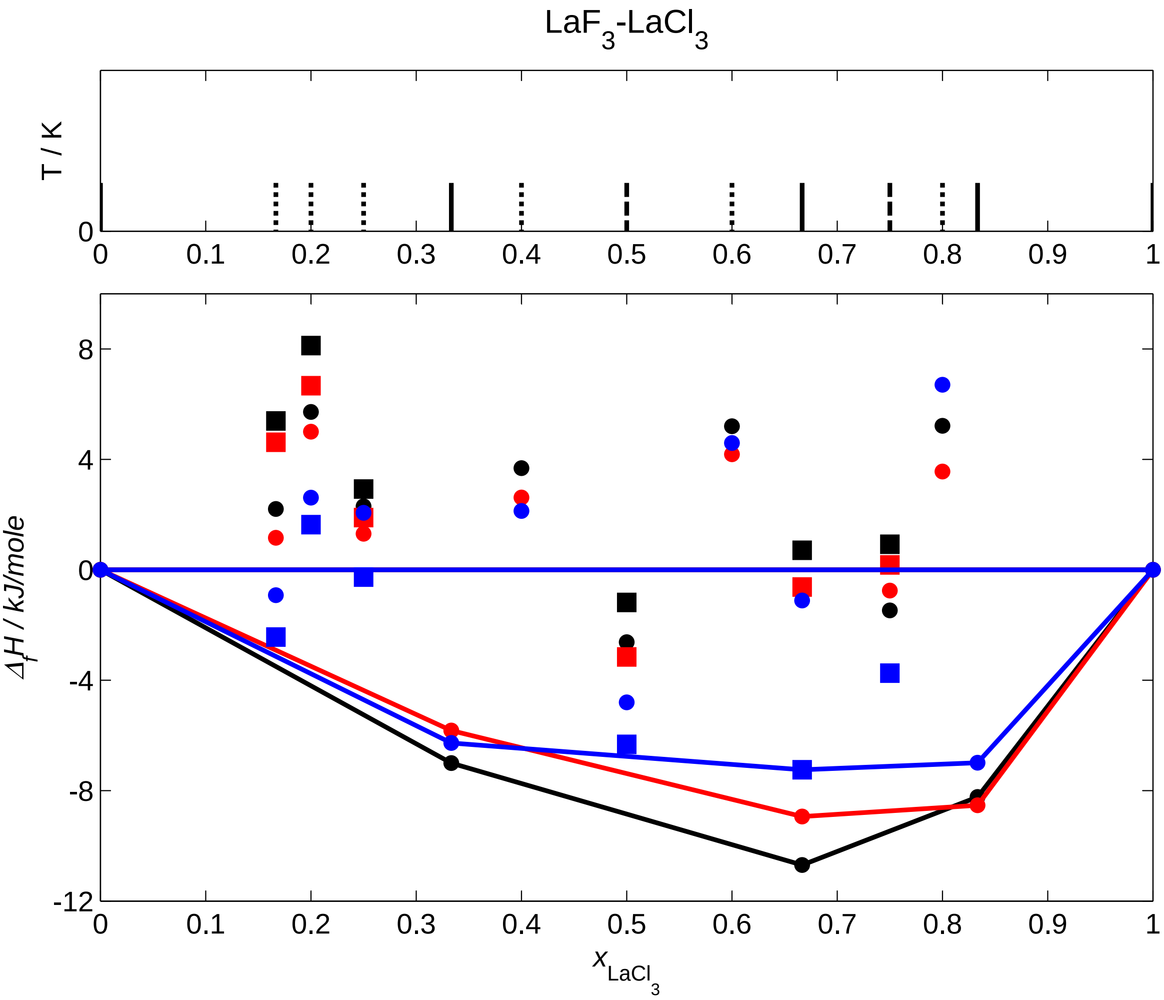

Figure 8.1: Top: Low-temperature phase diagram for the LaF_3-$LaCl_3$ system: solid lines dashed and dotted lines indicate stable metastable and unstable phases, respectively. Bottom: The ground state convex hull for the LaF_3-$LaCl_3$ system; the enthalpies of formation at 0 K are given with respect to the binary compounds. The black curve corresponds to the Hartree-Fock calculations, the red curve to the DFT-B3LYP calculations, the blue curve to the DFT-LDA-VBH calculations. The circles and squares correspond to the structure candidates with the lowest energy according to the HF data and DFT-LDA-VBH data, respectively. Composition 5:1: circles $\widehat{=}$ La_2F_5Cl-Type83, squares $\widehat{=}$ La_2F_5Cl-Type77; 4:1: circles $\widehat{=}$ $La_5F_{12}Cl_3$-Type6, squares $\widehat{=}$ $La_5F_{12}Cl_3$-Type35; 3:1: circles $\widehat{=}$ $La_4F_9Cl_3$-Type14, squares $\widehat{=}$ $La_4F_9Cl_3$-Type10; 2:1: circles $\widehat{=}$ LaF_2Cl-Type16; 3:2: circles $\widehat{=}$ $La_5F_9Cl_6$-Type25; 1:1: circles $\widehat{=}$ $La_2F_3Cl_3$-Type37, squares $\widehat{=}$ $La_2F_3Cl_3$-Type24; 2:3: circles $\widehat{=}$ $\widehat{=}$ $La_5F_6Cl_9$-Type13; 1:2: circles $\widehat{=}$ $LaFCl_2$-Type19, squares $\widehat{=}$ $LaFCl_2$-Type91; 1:3: circles $\widehat{=}$ $La_4F_3Cl_9$-Type4, squares $\widehat{=}$ $La_4F_3Cl_9$-Type3; 1:4: circles $\widehat{=}$ $La_5F_3Cl_{12}$-Type1; 1:5: circles $\widehat{=}$ La_2FCl_5-Type33 (see Table 8.1 for more detail).

the lowest energy when using the DFT-LDA-VBH method.

All modifications present as corners on the convex hull for the three *ab initio* methods can be considered as serious candidates for thermodynamically stable phases at least at 0 K, being stable with respect to the binary compounds and neighboring phases. Thus, in the case of the LaF_3-$LaCl_3$ system promising structure candidates exist for compositions: 2:1, 1:2 and 1:5. We note, that only for one additional composition, La_2FCl_5, we found a new compound that can be considered as a possible thermodynamically stable candidate beyond the ones found for simpler compositions. Structural data is presented in Table 8.1.

Table 8.1: Structure parameters, bulk moduli, minimum energies (in hartree / formula unit) at 0 K for ordered crystalline structure candidates for the LaF_3-$LaCl_3$ system after local optimization on DFT-LDA-VBH level.

Space group (no.)	Lattice constants	Atom (Multip., Wyckoff lett.),				V_{min}[Å^3]	E_{min}
Crystal system,	a, b, c [Å];	Relative coordinates				Bulk modulus	
Type	α, β, γ $[\circ]$	atom	x	y	z	[GPa]	
$P2_1/m$ (11)	$a = 4.14812$	La1(2e)	0.77286	1/4	0.82277	232.501	-17393.5926
monoclinic	$b = 5.32316$	La2(2e)	0.74002	1/4	0.41586	122.152	
$La_2F_5Cl - Type - 77$	$c = 10.52940$	F1(4f)	0.72065	0.99172	0.22066		
	$\alpha = \gamma = 90$	F2(2e)	0.26841	1/4	0.56377		
	$\beta = 90.0303$	F3(4f)	0.76897	0.50072	0.62780		
		Cl1(2e)	0.24269	1/4	0.04264		
$C2/m$ (12)	$a = 17.08088$	La1(4i)	0.39853	0	0.60153	486.354	-17393.5882
monoclinic	$b = 4.10101$	La2(4i)	0.87367	0	0.08712	114.620	
$La_2F_5Cl - Type - 83$	$c = 7.60237$	F1(4i)	0.02781	0	0.23003		
	$\alpha = \gamma = 90$	F2(4i)	0.70758	0	0.96616		
	$\beta = 114.0378$	F3(4i)	0.55439	0	0.68177		
		F4(4i)	0.12441	0	0.59137		
		F5(4i)	0.58369	0	0.06039		
		Cl1(4i)	0.78420	0	0.68223		
Cm (8)	$a = 21.18163$	La1(2a)	0.13661	0	0.97681	639.700	-43663.7377
monoclinic	$b = 4.20016$	La2(2a)	0.67493	0	0.47618	106.452	
$La_5F_{12}Cl_3 - Type - 6$	$c = 7.21497$	La3(2a)	0.34386	0	0.39435		
	$\alpha = \gamma = 90$	La4(2a)	0.00921	0	0.40695		
	$\beta = 94.7342$	La5(2a)	0.86321	0	0.88496		
		F1(2a)	0.10459	0	0.64698		
		F2(2a)	0.65029	0	0.80489		
		F3(2a)	0.45386	0	0.35173		
		F4(2a)	0.38078	0	0.72268		
		F5(2a)	0.22968	0	0.39715		
		F6(2a)	0.80049	0	0.53963		
		F7(2a)	0.56319	0	0.47727		
		F8(2a)	0.11698	0	0.31060		
		F9(2a)	0.88672	0	0.25517		
		F10(2a)	0.61312	0	0.13347		
		F11(2a)	0.35891	0	0.06383		
		F12(2a)	0.92222	0	0.59710		
		Cl1(2a)	0	0	0		
		Cl2(2a)	0.74989	0	0.13745		
		Cl3(2a)	0.24990	0	0.78255		
Pm (6)	$a = 7.43523$	La1(1a)	0.92828	0	0.48308	305.598	-43663.7458
monoclinic	$b = 4.06103$	La2(1b)	0.44937	1/2	0.52503	112.896	
$La_5F_{12}Cl_3 - Type - 35$	$c = 10.14226$	La3(1a)	0.67158	0	0.84532		
	$\alpha = \gamma = 90$	La4(1a)	0.34004	0	0.17901		
	$\beta = 93.7184$	La5(1b)	0.17306	1/2	0.81973		
		F1(1b)	0.77189	1/2	0.50880		
		F2(1a)	0.27736	0	0.42177		
		F3(1a)	0.32697	0	0.67039		
		F4(1b)	0.12953	1/2	0.57363		
		F5(1a)	0.00124	0	0.71851		
		F6(1b)	0.41846	1/2	0.29149		
		F7(1a)	0.64034	0	0.60885		
		F8(1b)	0.26616	1/2	0.05233		
		F9(1a)	0.62132	0	0.35840		
		F10(1b)	0.83709	1/2	0.79261		
		F11(1a)	0.36723	0	0.91844		
		F12(1b)	0.49477	1/2	0.76656		
		Cl1(1a)	0	0	0		
		Cl2(1b)	0.64136	1/2	0.05236		
		Cl3(1b)	0.02359	1/2	0.28534		
Pm (6)	$a = 10.73235$	La1(1a)	0.74753	0	0.77742	259.582	-35146.7580
monoclinic	$b = 4.09359$	La2(1b)	0.00164	1/2	0.38916	103.567	
$La_4F_9Cl_3 - Type - 10$	$c = 5.91147$	La3(1a)	0.26425	0	0.80712		
	$\alpha = \gamma = 90$	La4(1b)	0.49372	1/2	0.35998		
	$\beta = 91.8243$	F1(1a)	0.61483	0	0.43859		
		F2(1b)	0.86189	1/2	0.70129		
		F3(1a)	0.46372	0	0.06066		
		F4(1b)	0.38504	1/2	0.73242		
		F5(1a)	0.38449	0	0.47157		
		F6(1a)	0.11852	0	0.47313		
		F7(1b)	0.62738	1/2	0.69905		
		F8(1a)	0.88316	0	0.45421		
		F9(1b)	0.14769	1/2	0.71054		
		Cl1(1a)	0	0	0		
		Cl2(1b)	0.74365	1/2	0.15115		
		Cl3(1b)	0.24621	1/2	0.17206		
Pm (6)	$a = 7.44598$	La1(1a)	0.34787	0	0.24935	265.141	-35146.7439
monoclinic	$b = 6.72356$	La2(1a)	0.83240	0	0.48403	100.667	
$La_4F_9Cl_3 - Type - 14$	$c = 5.29627$	La3(1b)	0.08654	1/2	0.72638		
	$\alpha = \gamma = 90$	La4(1b)	0.58808	1/2	0.96542		

continued on next page

continued from previous page

Space group (no.)	Lattice constants	Atom (Multip., Wyckoff lett.),				V_{min}[Å^3]	E_{min}
Crystal system,	a, b, c [Å];	Relative coordinates				Bulk modulus	
Type	α, β, γ [o]	atom	x	y	z	[GPa]	
	$\beta = 90.4758$	F1(2c)	0.62660	0.18849	0.19964		
		F2(2c)	0.12459	0.18690	0.50246		
		F3(2c)	0.31220	0.70131	0.97123		
		F4(1a)	0.52291	0	0.64208		
		F5(2c)	0.80011	0.30983	0.71484		
		Cl1(1a)	0	0	0		
		Cl2(1b)	0.42621	1/2	0.47339		
		Cl3(1b)	0.93297	1/2	0.21727		
Pmmn (59)	$a = 4.12273$	La1(2a)	1/4	1/4	0.31045	139.261	-8876.5953
orthorhombic	$b = 5.42062$	F1(4e)	1/4	0.52533	0.61126	93.940	
$LaF_2Cl - Type - 16$	$c = 6.23154$	Cl1(2b)	1/4	3/4	0.07553		
	$\alpha = \beta = \gamma = 90$						
Cm (8)	$a = 21.50564$	La1(2a)	0	0	0	742.170	-44742.5044
monoclinic	$b = 4.22987$	La2(2a)	0.50630	0	0.43702	89.351	
$La_5F_9Cl_6 - Type - 25$	$c = 8.20564$	La3(2a)	0.16441	0	0.39945		
	$\alpha = \gamma = 90$	La4(2a)	0.25836	0	0.91209		
	$\beta = 96.128$	La5(2a)	0.83475	0	0.32171		
		F1(2a)	0.93524	0	0.22319		
		F2(2a)	0.61289	0	0.39113		
		F3(2a)	0.51150	0	0.14306		
		F4(2a)	0.78853	0	0.03185		
		F5(2a)	0.39321	0	0.34765		
		F6(2a)	0.27869	0	0.21181		
		F7(2a)	0.04938	0	0.28516		
		F8(2a)	0.07785	0	0.57037		
		F9(2a)	0.72408	0	0.34394		
		Cl1(2a)	0.53693	0	0.79502		
		Cl2(2a)	0.93266	0	0.59836		
		Cl3(2a)	0.69458	0	0.71831		
		Cl4(2a)	0.14263	0	0.04778		
		Cl5(2a)	0.39082	0	0.94616		
		Cl6(2a)	0.29323	0	0.57290		
Pm (6)	$a = 12.53339$	La1(1a)	0	0	0	313.649	-18112.7735
monoclinic	$b = 4.19471$	La2(1b)	0.77411	1/2	0.59150	84.577	
$La_2F_3Cl_3 - Type - 37$	$c = 5.99003$	La3(1b)	0.33093	1/2	0.54657		
	$\alpha = \gamma = 90$	La4(1a)	0.54848	0	0.18244		
	$\beta = 95.1479$	F1(1a)	0.88046	0	0.63575		
		F2(1b)	0.44482	1/2	0.23398		
		F3(1b)	0.64350	1/2	0.27002		
		F4(1a)	0.41891	0	0.45386		
		F5(1b)	0.92011	1/2	0.86853		
		F6(1a)	0.67956	0	0.50835		
		Cl1(1a)	0.76389	0	0.02749		
		Cl2(1b)	0.55637	1/2	0.77313		
		Cl3(1b)	0.14424	1/2	0.82926		
		Cl4(1a)	0.18608	0	0.33807		
		Cl5(1a)	0.35287	0	0.89386		
		Cl6(1b)	0.96303	1/2	0.33467		
$Pmc2_1$ (26)	$a = 4.26054$	La1(2a)	0	0.80444	0	301.213	-18112.7769
orthorhombic	$b = 8.71145$	La2(2b)	1/2	0.74358	0.44593	87.864	
$La_2F_3Cl_3 - Type - 24$	$c = 8.11557$	F1(2b)	1/2	0.24190	0.64684		
	$\alpha = \beta = \gamma = 90$	F2(2b)	1/2	0.97714	0.93261		
		F3(2a)	0	0.78535	0.30732		
		Cl1(2a)	0	0.52323	0.53107		
		Cl2(2a)	0	0.09552	0.15098		
		Cl3(2b)	1/2	0.34232	0.29978		
Pm (6)	$a = 10.44620$	La1(1a)	0	0	0	863.373	-45821.2453
monoclinic	$b = 8.38723$	La2(2c)	0.08470	0.74251	0.49631	74.197	
$La_5F_6Cl_9 - Type - 13$	$c = 9.90246$	La3(1a)	0.54578	0	0.35675		
	$\alpha = \gamma = 90$	La4(2c)	0.33433	0.74799	0.01192		
	$\beta = 95.659$	La5(2c)	0.61886	0.74839	0.71622		
		F1(1a)	0.40148	0	0.14017		
		F2(1a)	0.22477	0	0.95748		
		F3(2c)	0.52236	0.74740	0.48239		
		F4(1a)	0.56807	0	0.60005		
		F5(2c)	0.10688	0.74374	0.06167		
		F6(1a)	0.13226	0	0.57520		
		Cl1(1b)	0.51429	1/2	0.90988		
		Cl2(2c)	0.33787	0.74340	0.69118		
		Cl3(1a)	0.80867	0	0.76613		
		Cl4(1a)	0.99514	0	0.28792		
		Cl5(2c)	0.27925	0.78910	0.32156		
		Cl6(2c)	0.04479	0.74224	0.78028		
		Cl7(2c)	0.56255	0.71025	0.20175		
		Cl8(2c)	0.80442	0.76849	0.48664		
		Cl9(2c)	0.81373	0.75307	0.02075		
		La6(1b)	0.99102	1/2	0.98952		
		La7(1b)	0.43187	1/2	0.38970		
		F7(1b)	0.33202	1/2	0.15796		
		F8(1b)	0.22120	1/2	0.93528		
		F9(1b)	0.53933	1/2	0.61905		
		F10(1b)	0.21901	1/2	0.48939		
		Cl10(1a)	0.51724	0	0.89256		

continued on next page

continued from previous page

Space group (no.)	Lattice constants	Atom (Multip., Wyckoff lett.),				V$_{min}$[Å^3]	E$_{min}$
Crystal system,	a, b, c [Å];	Relative coordinates				Bulk modulus	
Type	α, β, γ [○]	atom	x	y	z	[GPa]	
		Cl11(1b)	0.79963	1/2	0.75586		
		Cl12(1b)	0.00612	1/2	0.28586		
Cc (9)	a = 8.80746	La1(4a)	0.99887	0.71953	0.98613	386.066	-9236.1748
$monoclinic$	b = 6.39364	F1(4a)	0.99720	0.49908	0.23451	62.994	
$LaFCl_2 - Type - 19$	c = 7.07211	Cl1(4a)	0.81911	0.06208	0.09718		
	$\alpha = \gamma$ = 90	Cl2(4a)	0.17292	0.93748	0.36245		
	β = 104.2052						
Cm (8)	a = 8.37186	La1(4b)	0	0.13760	0	483.729	-9236.1830
$monoclinic$	b = 13.93511	La2(2a)	0.56584	0	0.06717	80.525	
$LaFCl_2 - Type - 91$	c = 5.14552	F1(2a)	0.85933	0	0.08511		
	$\alpha = \gamma$ = 90	F2(2a)	0.86971	0	0.60273		
	β = 126.3099	F3(2a)	0.19163	0	0.15143		
		Cl1(4b)	0.22580	0.13092	0.70062		
		Cl2(4b)	0.75782	0.19796	0.22085		
		Cl3(4b)	0.54937	0.11500	0.52154		
$P2$ (3)	a = 10.80432	La1(2e)	0.63454	0.01076	0.74249	483.198	-37304.1828
$monoclinic$	b = 5.53356	La2(2e)	0.12909	0.02144	0.77597	47.905	
$La_4F_3Cl_9 - Type - 4$	c = 8.08755	F1(1a)	0	0	0		
	$\alpha = \gamma$ = 90	F2(2e)	0.25559	0.08478	0.01118		
	β = 92.1067	Cl1(2e)	0.12588	0.52148	0.76127		
		Cl2(2e)	0.37601	0.03499	0.63577		
		Cl3(2e)	0.34835	0.51242	0.32933		
		Cl4(2e)	0.11826	0.01213	0.36724		
		Cl5(1c)	1/2	0.78167	0		
Pm (6)	a = 8.71193	La1(1a)	0.16556	0	0.57702	347.707	-37304.3022
$monoclinic$	b = 4.48553	La2(1a)	0.72254	0	0.94415	73.479	
$La_4F_3Cl_9 - Type - 3$	c = 8.89835	La3(1b)	0.65392	1/2	0.44415		
	$\alpha = \gamma$ = 90	La4(1b)	0.12083	1/2	0.07616		
	β = 90.6014	F1(1a)	0	0	0		
		F2(1a)	0.54826	0	0.48943		
		F3(1b)	0.84310	1/2	0.01820		
		Cl1(1b)	0.61689	1/2	0.77158		
		Cl2(1b)	0.34118	1/2	0.51148		
		Cl3(1a)	0.21836	0	0.25187		
		Cl4(1b)	0.07578	1/2	0.76670		
		Cl5(1b)	0.98892	1/2	0.39643		
		Cl6(1a)	0.33158	0	0.87305		
		Cl7(1b)	0.49993	1/2	0.13922		
		Cl8(1a)	0.84281	0	0.63193		
		Cl9(1a)	0.76218	0	0.25195		
Cm (8)	a = 24.94958	La1(2a)	0.50204	0	0.13445	1004.602	-46899.9871
$monoclinic$	b = 4.51642	La2(2a)	0.37696	0	0.61756	61.580	
$La_5F_3Cl_{12} - Type - 1$	c = 8.92048	La3(2a)	0.23205	0	0.10983		
	$\alpha = \gamma$ = 90	La4(2a)	0.72976	0	0.60433		
	β = 91.9502	La5(2a)	0.05324	0	0.77781		
		F1(2a)	0	0	0		
		F2(2a)	0.82804	0	0.61086		
		F3(2a)	0.54515	0	0.89882		
		Cl1(2a)	0.68605	0	0.30171		
		Cl2(2a)	0.80434	0	0.13800		
		Cl3(2a)	0.11639	0	0.05546		
		Cl4(2a)	0.28303	0	0.80138		
		Cl5(2a)	0.02066	0	0.32224		
		Cl6(2a)	0.41170	0	0.32476		
		Cl7(2a)	0.16030	0	0.63945		
		Cl8(2a)	0.41624	0	0.91816		
		Cl9(2a)	0.69668	0	0.91015		
		Cl10(2a)	0.27464	0	0.43412		
		Cl11(2a)	0.94726	0	0.64873		
		Cl12(2a)	0.56025	0	0.58573		
$P2_1/m$ (11)	a = 5.87592	La1(2e)	0.54079	1/4	0.35726	390.241	-18831.9521
$monoclinic$	b = 8.69839	La2(2e)	0.99711	1/4	0.87573	64.722	
$La_2FCl_5 - Type - 33$	c = 7.67138	F1(2e)	0.30769	1/4	0.09100		
	$\alpha = \gamma$ = 90	Cl1(4f)	0.80960	0.05786	0.13948		
	β = 95.5694	Cl2(4f)	0.65724	0.06225	0.67512		
		Cl3(2e)	0.10943	1/4	0.52017		

In Figs. 8.2 and 8.3, we have shown two examples of predicted structure candidates for the LaF_2Cl and $LaFCl_2$ compounds.

In the case of the LaF_2Cl candidate, there is one independent position of La in the unit cell (for more details see Table 8.1). The La atoms are coordinated by 6 F atoms and 4 Cl atoms. There are two ways the polyhedra are connected, via an edge containing two atoms of F or Cl, and via a face (containing two atoms of F and one atom of Cl).

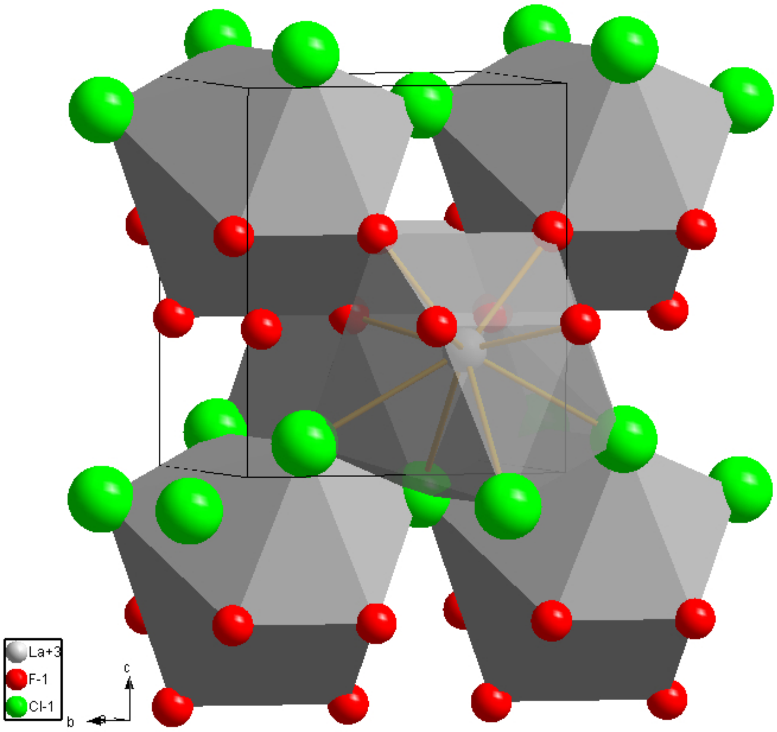

Figure 8.2: The LaF_2Cl-Type16 structure candidate. The cell parameters and atom positions are listed in Table 8.1.

In the case of the $LaFCl_2$ candidate, there are two crystallographically independent positions of La atoms (for more details see Table 8.1). Both La(1) and La(2) are coordinated by 3 F atoms and 6 Cl atoms. The polyhedra around La(1) are connected with each other via Cl- containing edges or F- containing faces. The polyhedra coordinating La(2) are connected with the polyhedra around La(1) via faces containing two atoms of Cl and one atom of F or via a simple Cl vertex. The La-Cl and La-F distances in both structures are in the range of $\approx$ 2.9 - 3.4 Åand $\approx$ 2.3 - 2.5 Å, respectively. They are close to the experimental values observed in crystalline $LaCl_3$ ($\approx$ 2.9 Å) and LaF_3 ($\approx$ 2.4 - 2.5 Å). There is some disagreement, of course, since usually the calculated cell parameters are different from the experimental ones.

In this context, one should note that the strategy of an energy landscape exploration via generating super cells as starting point for threshold runs allows us to find at least

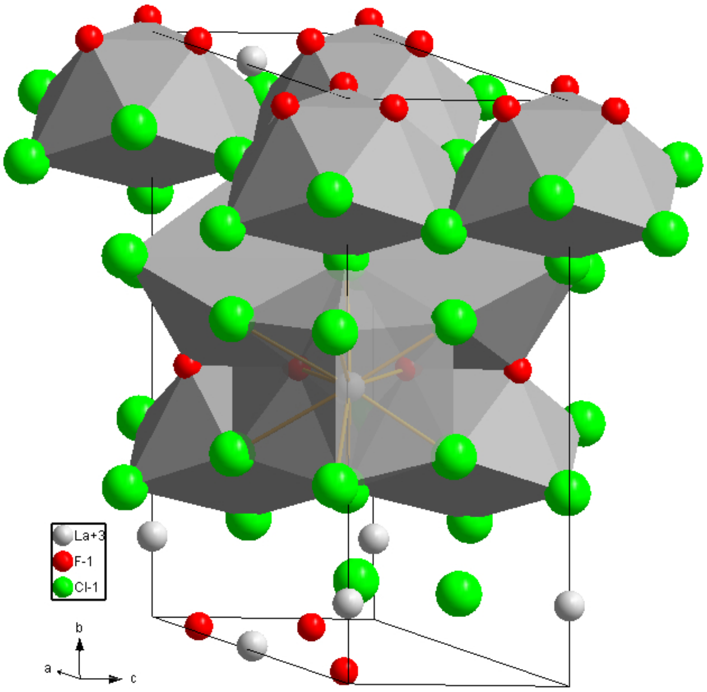

Figure 8.3: The $LaFCl_2$-Type91 structure candidate. The cell parameters and atom positions are listed in Table 8.1.

some new structure candidates with a large number of formula units[3] (and atoms) in the primitive cell, which could not be obtained during a standard simulated annealing run. Of course, this does not exclude the possibility, that some important local minima have been missed, but nevertheless this approach allows us to investigate the energy landscape in more detail.

Other quasi-binary lanthanum halide systems

Figures 8.4 - 8.7 depict the information about the low-temperature region of the remaining five phase diagrams derived from the landscape exploration and *ab initio* energy minima studies. As well as in case of the LaF_3-$LaCl_3$ system, the top part of a figure indicates by a solid line, at which composition new possible stable compounds are expected, together with the experimentally known binary compounds; metastable compounds correspond to dashed lines. The bottom part of the figures shows the convex hulls for the quasi-binary lanthanum halide system at T = 0 K, obtained in the present work.

All modifications present as corners on the convex hull for the three *ab initio* methods can be considered as serious candidates for thermodynamically stable phases at least at 0 K, being stable with respect to the binary compounds and neighboring phases. Thus, in the case of the LaF_3-$LaBr_3$ system promising structure candidates exist for compositions 2:1 and 1:2, and in the case of the $LaBr_3$-$LaCl_3$ system for compositions: 3:1, 1:1 and 1:3, respectively. Similarly in the $LaBr_3$-LaI_3 and $LaCl_3$-LaI_3 systems thermodynamically stable structure candidates lie on the convex hull for compositions 3:1, 2:1, 1:2 and 1:3. Here, one should mention that in the case of the Hartree-Fock calculations the compounds with compositions 1:1 also lie on the convex hull for both these systems. However, since DFT calculations with both the B3LYP and the LDA-VBH and also three additional functionals (to clarify this issue, we performed additional calculations for all modifications in all three systems containing iodide with three other functionals: BECKE-PWGGA, LDA-LYP and LDA-PWGGA) do not favour the candidates with this composition, we suggest that the 1:1 compounds are not stable but only metastable. Finally, in the case of the LaF_3-LaI_3 system, stable structures with compositions 2:1, 1:2 and 1:3 should exist. We note that for all structure candidates the equilibrium volume per formula unit was the largest (smallest) when calculated using the HF approximation (DFT with the LDA-VBH functional), in agreement with the general expectations when using those *ab initio* methods.

---

[3] We performed calculations up to 8 formula units.

As we mentioned earlier, for some compositions we have found that the ranking of the structure candidates as a function of energy depended on the *ab initio* methods used, similar to the binary lanthanum halides. In some of these instances, we reach the limit of the accuracy of the *ab initio* methods, and thus without any other facts as guidance, it is not possible to choose between two candidates. However, these disagreements in the ranking are to a certain degree self-consistent: Whenever two structures yielded a different ranking, the HF-method always preferred the modification with the lower density and the DFT-calculation the one with higher density, respectively. Thus, in the tables 8.1 - 8.6 we listed for every composition in all systems under investigation the hypothetical modifications with the lowest energy according to at least one of the *ab initio* methods[4].

In principle, we cannot exclude the possibility that there might exist some additional relevant structure candidates, which our global explorations have failed to identify so far. Thus, one should consider the present results as a starting point for further investigations. From a theoretical point of view, the technique suggested in the previous section can be one of these steps. In particular for more complicated compositions, which have not been analyzed, stable modifications might exist that exhibit more atoms in the primitive unit cell than can be employed during the usual global optimization runs due to limits in computer time. But nevertheless, we can conclude that all the mixed lanthanum halides should exhibit at least some ordered crystalline phases at low temperatures, and that no solid solution-like phases are thermodynamically stable in the low-temperature region of the corresponding phase diagrams.

---

[4] The numbering of the modifications (e.g. $La_4F_9Cl_3$-Type10) in the tables and the figure captions refers to the order of appearance of local minimum structures in a given chemical system for a particular composition during the global energy landscape explorations.

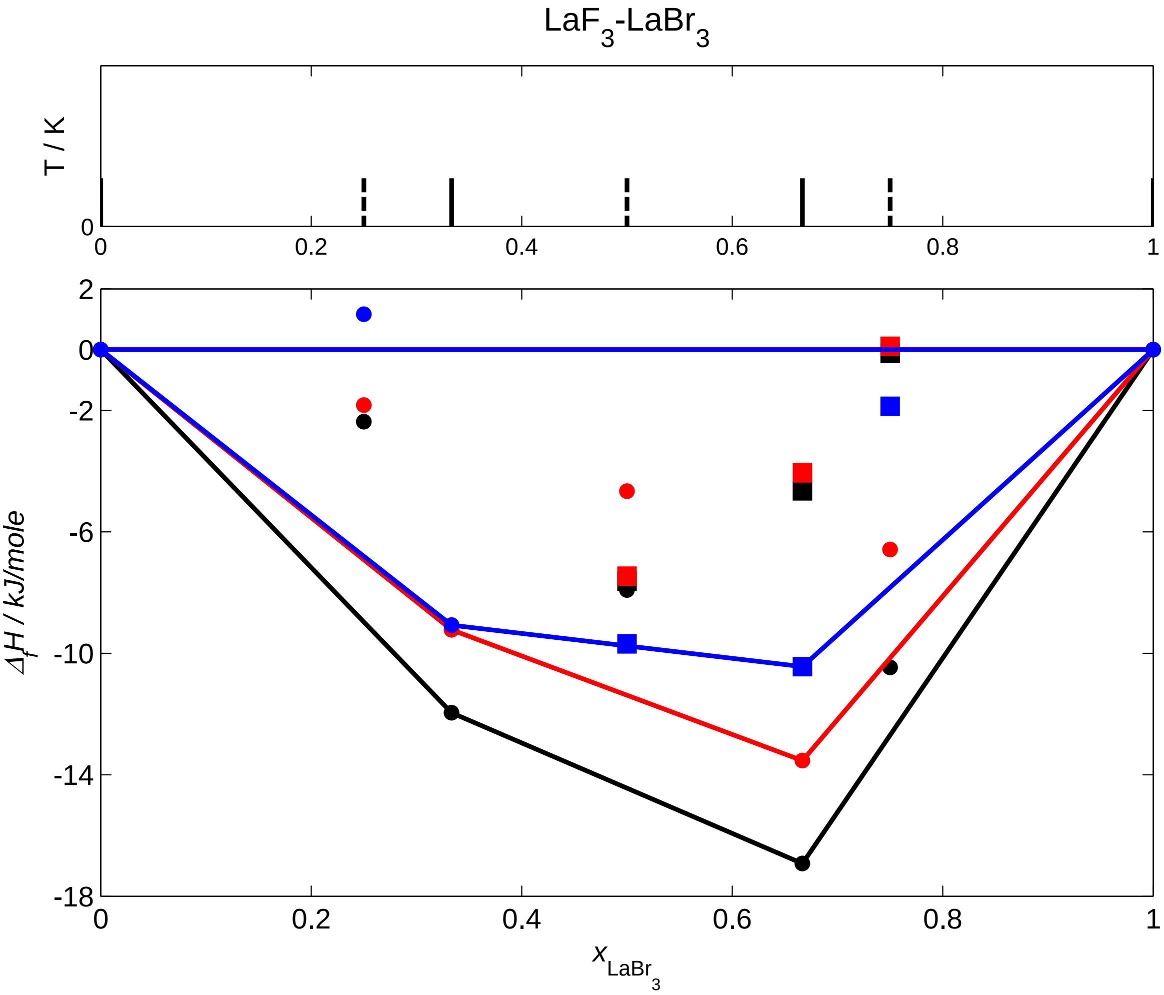

Figure 8.4: Top: Low-temperature phase diagram for the LaF_3-$LaBr_3$ system: solid lines and dashed lines indicate stable and metastable phases, respectively. Bottom: The ground state convex hull for the LaF_3-$LaBr_3$ system; the enthalpies of formation at 0 K are given with respect to the binary compounds. For notation c.f. Figure 8.1. Composition 3:1: circles $\widehat{=}$ $La_4F_9Br_3$-Type2; 2:1: circles $\widehat{=}$ LaF_2Br-Type17; 1:1: circles $\widehat{=}$ $La_2F_3Br_3$-Type21, squares $\widehat{=}$ $La_2F_3Br_3$-Type35; 1:2: circles $\widehat{=}$ $LaFBr_2$-Type28, squares $\widehat{=}$ $LaFBr_2$-Type69; 1:3: circles $\widehat{=}$ $La_4F_3Br_9$-Type28, squares $\widehat{=}$ $La_4F_3Br_9$-Type6 (see Table 8.2 for more detail).

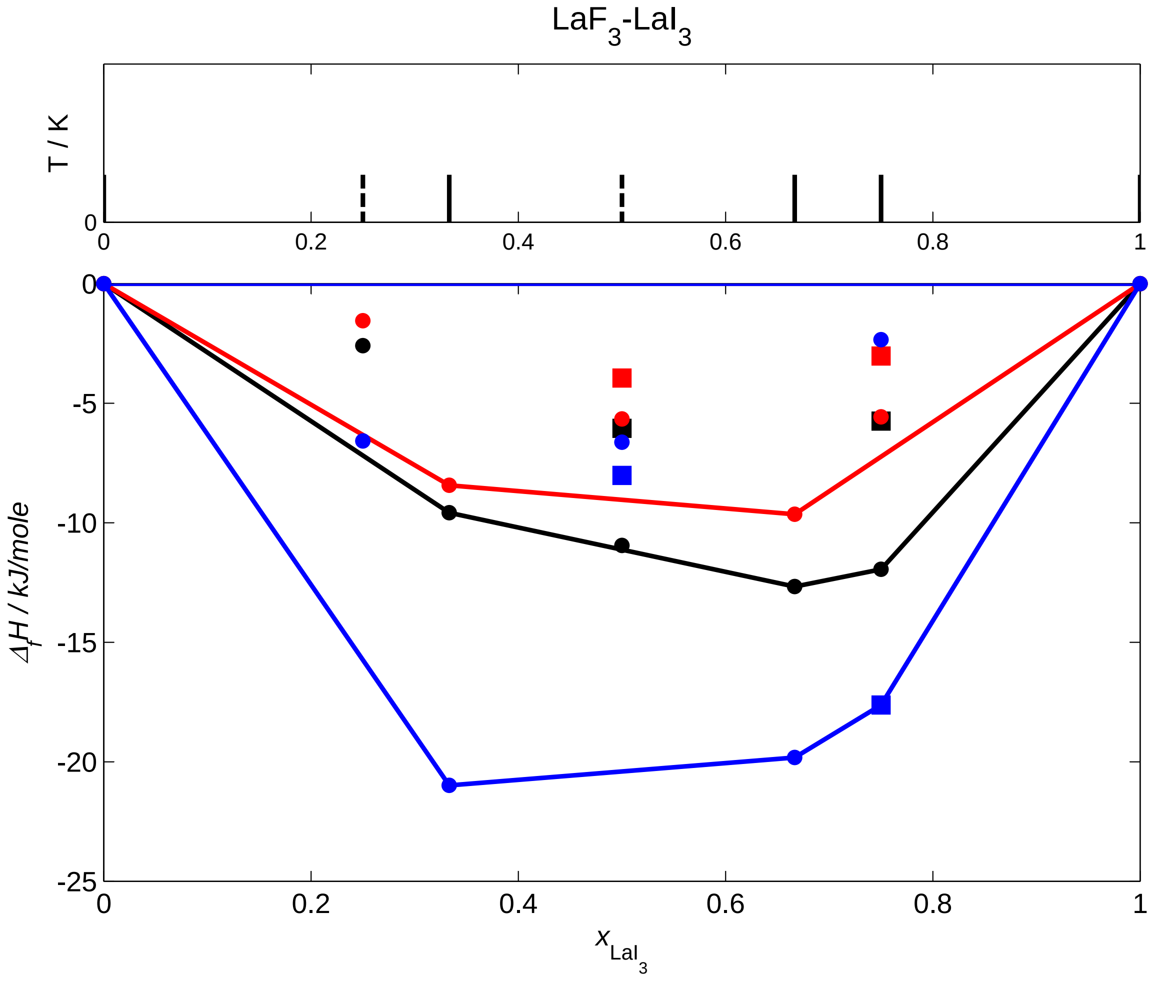

Figure 8.5: Top: Low-temperature phase diagram for the LaF_3-LaI_3 system: solid lines and dashed lines indicate stable and metastable phases, respectively. Bottom: The ground state convex hull for the LaF_3-LaI_3 system; the enthalpies of formation at 0 K are given with respect to the binary compounds. For notation c.f. Figure 8.1. Composition 3:1: circles $\widehat{=}$ $La_4F_9I_3$-Type30; 2:1: circles $\widehat{=}$ LaF_2I-Type13; 1:1: circles $\widehat{=}$ $La_2F_3I_3$-Type18, squares $\widehat{=}$ $La_2F_3I_3$-Type29; 1:2: circles $\widehat{=}$ $LaFI_2$-Type63; 1:3: circles $\widehat{=}$ $La_4F_3I_9$-Type7, squares $\widehat{=}$ $La_4F_3I_9$-Type10 (see Table 8.3 for more detail).

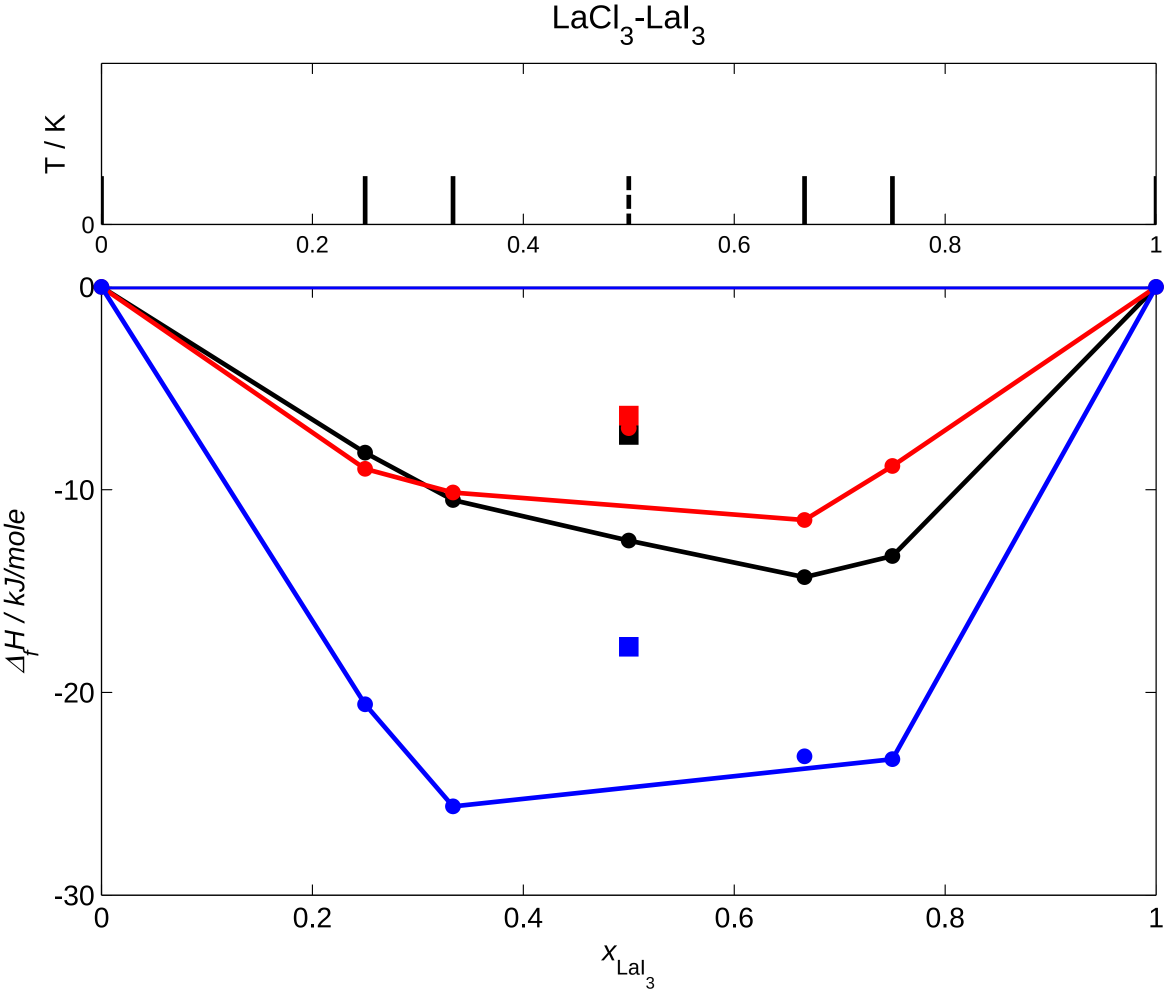

Figure 8.6: Top: Low-temperature phase diagram for the $LaCl_3$-LaI_3 system: solid lines and dashed lines indicate stable and metastable phases, respectively. Bottom: The ground state convex hull for the $LaCl_3$-LaI_3 system; the enthalpies of formation at 0 K are given with respect to the binary compounds. For notation c.f. Figure 8.1. Composition 3:1: circles $\widehat{=}$ $La_4Cl_9I_3$-Type4; 2:1: circles $LaCl_2I$-Type62 $\widehat{=}$; 1:1: circles $\widehat{=}$ $La_2Cl_3I_3$-Type3, squares $\widehat{=}$ $La_2Cl_3I_3$-Type33; 1:2: circles $\widehat{=}$ $LaClI_2$-Type50; 1:3: circles $\widehat{=}$ $La_4Cl_3I_9$-Type9 (see Table 8.5 for more detail).

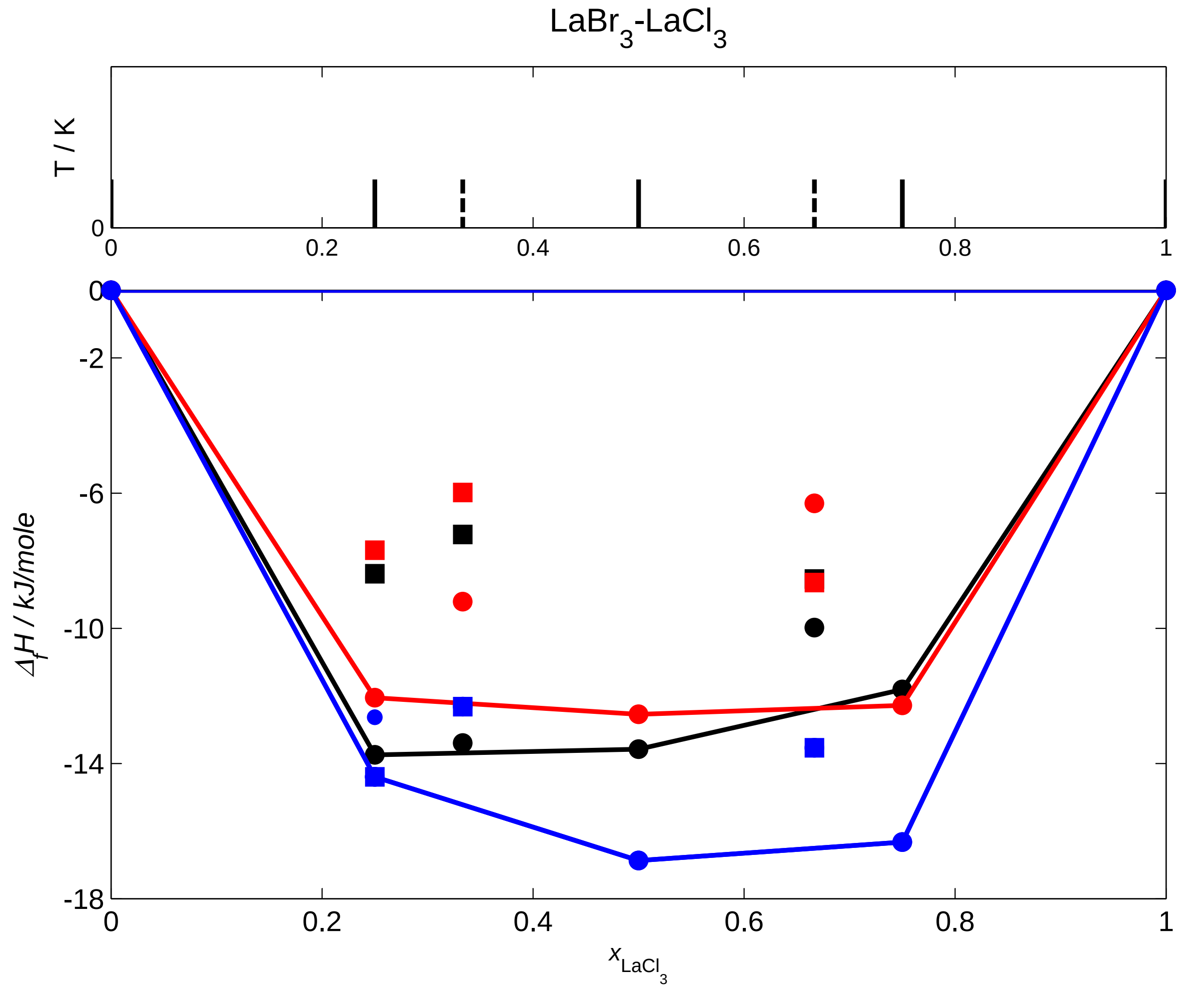

Figure 8.7: Top: Low-temperature phase diagram for the $LaBr_3$-LaI_3 system: solid lines and dashed lines indicate stable and metastable phases, respectively. Bottom: The ground state convex hull for the $LaBr_3$-LaI_3 system; the enthalpies of formation at 0 K are given with respect to the binary compounds. For notation c.f. Figure 8.1. Composition 3:1: circles $\widehat{=}$ $La_4Br_9I_3$-Type6, squares $\widehat{=}$ $La_4Br_9I_3$-Type2; 2:1: circles $\widehat{=}$ $LaBr_2I$-Type18, squares $\widehat{=}$ $LaBr_2I$-Type67; 1:1: circles $\widehat{=}$ $La_2Br_3I_3$-Type1, squares $\widehat{=}$ $La_2Br_3I_3$-Type37; 1:2: circles $\widehat{=}$ $LaBrI_2$-Type70, squares $\widehat{=}$ $LaBrI_2$-Type67; 1:3: circles $\widehat{=}$ $La_4Br_3I_9$-Type17, squares $\widehat{=}$ $La_4Br_3I_9$-Type13 (see Table 8.6 for more detail).

Table 8.2: Structure parameters, bulk moduli, minimum energies (in hartree / formula unit) at 0 K for ordered crystalline structure candidates for the LaF_3-$LaBr_3$ system after local optimization on DFT-LDA-VBH level.

Space group (no.) Crystal system, Type	Lattice constants a, b, c [Å]; α, β, γ [o]	Atom (Multip., Wyckoff lett.), Relative coordinates				V_{min}[$Å^3$] Bulk modulus [GPa]	E_{min}
		atom	x	y	z		
Pm (6)	$a = 7.26044$	La1(1b)	0.11663	1/2	0.24636	304.041	-33809.3828
monoclinic	$b = 4.09183$	La2(1b)	0.80352	1/2	0.74532	84.518	
$La_4F_9Br_3 - Type - 2$	$c = 10.77039$	La3(1a)	0.60561	0	0.21982		
	$\alpha = \gamma = 90$	La4(1a)	0.31746	0	0.77178		
	$\beta = 108.156$	F1(1a)	0.51038	0	0.99188		
		F2(1b)	0.15827	1/2	0.81205		
		F3(1b)	0.76727	1/2	0.17216		
		F4(1a)	0.31787	0	0.29070		
		F5(1b)	0.52770	1/2	0.82512		
		F6(1a)	0.96408	0	0.29386		
		F7(1b)	0.40251	1/2	0.17265		
		F8(1a)	0.96391	0	0.69747		
		F9(1a)	0.61577	0	0.70950		
		Br1(1a)	0	0	0		
		Br2(1b)	0.25975	1/2	0.54130		
		Br3(1b)	0.71829	1/2	0.45150		
$Pmmn$ (59)	$a = 6.02660$	La1(2a)	1/4	1/4	0.34166	156.216	-8430.8116
orthorhombic	$b = 4.14826$	F1(4f)	0.54582	1/4	0.60105	82.540	
$LaF_2Br - Type - 17$	$c = 6.24867$	Br1(2b)	1/4	3/4	0.90382		
	$\alpha = \beta = \gamma = 90$						
$Pmn2_1$ (31)	$a = 5.82107$	La1(2a)	0	0.73306	0	485.064	-16775.3627
orthorhombic	$b = 10.45040$	La2(2a)	0	0.29706	0.04779	47.741	
$La_2F_3Br_3 - Type - 21$	$c = 7.97377$	F1(4b)	0.25320	0.27625	0.27128		
	$\alpha = \beta = \gamma = 90$	F2(2a)	0	0.51427	0.00643		
		Br1(2a)	0	0.01317	0.04831		
		Br2(2a)	0	0.25238	0.64607		
		Br3(2a)	0	0.64794	0.40567		
Pm (6)	$a = 6.37413$	La1(1a)	0	0	0	357.333	-16775.4202
monoclinic	$b = 4.33414$	La2(1a)	0.95225	0	0.55789	72.728	
$La_2F_3Br_3 - Type - 35$	$c = 13.00228$	La3(1b)	0.63457	1/2	0.77341		
	$\alpha = \gamma = 90$	La4(1b)	0.39546	1/2	0.21587		
	$\beta = 95.8533$	F1(1b)	0.05948	1/2	0.10227		
		F2(1a)	0.27345	0	0.13945		
		F3(1b)	0.86841	1/2	0.63832		
		F4(1a)	0.70184	0	0.86548		
		F5(1b)	0.91539	1/2	0.91423		
		F6(1a)	0.67151	0	0.67396		
		Br1(1a)	0.73834	0	0.17965		
		Br2(1b)	0.73883	1/2	0.40769		
		Br3(1b)	0.44225	1/2	0.98201		
		Br4(1a)	0.22798	0	0.36442		
		Br5(1a)	0.16203	0	0.78385		
		Br6(1b)	0.31562	1/2	0.58451		
Cc (9)	$a = 9.22772$	La1(4a)	0.00258	0.81552	0.01992	453.011	-8344.6060
monoclinic	$b = 6.48750$	F1(4a)	0.00275	0.99807	0.27130	51.448	
$LaFBr_2 - Type - 28$	$c = 7.70515$	Br1(4a)	0.18204	0.54514	0.40984		
	$\alpha = \gamma = 90$	Br2(4a)	0.82820	0.54575	0.65619		
	$\beta = 100.8573$						
$P2_1$ (4)	$a = 5.90589$	La1(2a)	0.62804	0	0.60660	384.336	-8344.6102
monoclinic	$b = 6.91307$	La2(2a)	0.31256	0.50249	0.82466	65.835	
$LaFBr_2 - Type - 69$	$c = 9.44334$	F1(2a)	0.55944	0.18063	0.38669		
	$\alpha = \gamma = 90$	F2(2a)	0.42698	0.31686	0.61417		
	$\beta = 94.5499$	Br1(2a)	0.73024	0.24773	0.88366		
		Br2(2a)	0.27727	0.25396	0.10276		
		Br3(2a)	0.94874	0.51870	0.59019		
		Br4(2a)	0.20260	0.98858	0.76905		
$Amm2$ (38)	$a = 5.98538$	La1(4d)	0	0.12924	0.56609	1396.866	-33292.0932
orthorhombic	$b = 22.39540$	La2(4d)	0	0.10433	0.00163	30.500	
$La_4F_3Br_9 - Type - 14$	$c = 10.42087$	F1(2a)	0	0	0		
	$\alpha = \beta = \gamma = 90$	F2(4d)	0	0.86394	0.78910		
		Br1(4e)	1/2	0.12859	0.57565		
		Br2(4d)	0	0.90383	0.29054		
		Br3(4d)	0	0.23804	0.04701		
		Br4(2a)	0	0	0.65013		
		Br5(4e)	1/2	0.90150	0.99352		
Pm (6)	$a = 9.93207$	La1(1b)	0.46709	1/2	0.76564	434.786	-33292.1865
monoclinic	$b = 4.46754$	La2(1a)	0.97239	0	0.74223	56.033	
$La_4F_3Br_9 - Type - 6$	$c = 9.80293$	La3(1a)	0.47953	0	0.25128		
	$\alpha = \gamma = 90$	La4(1b)	0.98514	1/2	0.14489		
	$\beta = 91.6897$	F1(1a)	0	0	0		
		F2(1b)	0.05797	1/2	0.78305		
		F3(1b)	0.54028	1/2	0.18754		
		Br1(1a)	0.27011	0	0.69815		
		Br2(1a)	0.66518	0	0.63051		

continued on next page

continued from previous page

Space group (no.) Crystal system, Type	Lattice constants a, b, c [Å]; α, β, γ [$\circ$]	Atom (Multip., Wyckoff lett.), Relative coordinates				V$_{min}$[Å^3] Bulk modulus [GPa]	E$_{min}$
		atom	x	y	z		
		Br3(1a)	0.16835	0	0.28415		
		Br4(1b)	0.79325	1/2	0.89668		
		Br5(1b)	0.42835	1/2	0.46019		
		Br6(1b)	0.26070	1/2	0.01991		
		Br7(1b)	0.94868	1/2	0.49676		
		Br8(1a)	0.78807	0	0.23042		
		Br9(1a)	0.52494	0	0.95666		

Table 8.3: Structure parameters, bulk moduli, minimum energies (in hartree / formula unit) at 0 K for ordered crystalline structure candidates for the LaF_3-LaI_3 system after local optimization on DFT-LDA-VBH level.

Space group (no.) Crystal system, Type	Lattice constants a, b, c [Å]; α, β, γ [$\circ$]	Atom (Multip., Wyckoff lett.), Relative coordinates				V$_{min}$[Å^3] Bulk modulus [GPa]	E$_{min}$
		atom	x	y	z		
$Amm2$ (38)	$a = 4.19939$	La1(4d)	0	0.28880	0.88121	650.222	-33804.0560
$orthorhombic$	$b = 11.16907$	La2(2b)	1/2	0	0.18906	79.031	
$La_4F_9I_3 - Type - 30$	$c = 13.86304$	La3(2b)	1/2	0	0.76196		
	$\alpha = \beta = \gamma = 90$	F1(4e)	1/2	0.38049	0.83174		
		F2(4d)	0	0.88620	0.77243		
		F3(2a)	0	0	0.41620		
		F4(4d)	0	0.88726	0.22339		
		F5(4e)	1/2	0.16851	0.86929		
		I1(2a)	0	0	0		
		I2(4e)	1/2	0.30777	0.08482		
$Pmmn$ (59)	$a = 6.49124$	La1(2a)	1/4	1/4	0.12994	169.305	-8429.0357
$orthorhombic$	$b = 4.18578$	F1(4f)	0.55529	1/4	0.90048	73.556	
$LaF_2I - Type - 13$	$c = 6.23112$	I1(2b)	1/4	3/4	0.60363		
	$\alpha = \beta = \gamma = 90$						
$P2_1/c$ (14)	$a = 7.07639$	La1(4e)	0.73648	0.67267	0.33622	508.539	-16770.0354
$monoclinic$	$b = 6.82338$	F1(4e)	0.50024	0.57263	0.77885	44.849	
$La_2F_3I_3 - Type - 18$	$c = 12.01868$	F2(2a)	0	0	0		
	$\alpha = \gamma = 90$	I1(4e)	0.09087	0.01371	0.36386		
	$\beta = 118.8001$	I2(2b)	1/2	0	0		
$P2_1$ (4)	$a = 7.07678$	La1(2a)	0.64755	0	0.90277	476.067	-16770.0386
$monoclinic$	$b = 6.75310$	La2(2a)	0.14409	0.92952	0.40654	49.285	
$La_2F_3I_3 - Type - 29$	$c = 10.12532$	F1(2a)	0.74567	0.21318	0.74478		
	$\alpha = \gamma = 90$	F2(2a)	0	0.22880	0.44983		
	$\beta = 100.3172$	F3(2a)	0.53255	0.23383	0.04083		
		I1(2a)	0.50047	0.22369	0.38579		
		I2(2a)	0.97566	0.66934	0.88697		
		I3(2a)	0.24440	0.19963	0.75041		
$P2/c$ (15)	$a = 9.87443$	La1(4e)	0	0.67263	1/4	534.789	-8341.0406
$monoclinic$	$b = 6.73669$	F1(4b)	0	1/2	0	43.551	
$LaFI_2 - Type - 63$	$c = 8.17135$	I1(8f)	0.81333	0.01826	0.37274		
	$\alpha = \gamma = 90$						
	$\beta = 100.3104$						
$Amm2$ (38)	$a = 6.40948$	La1(4d)	0	0.36810	0.21391	1648.764	-33276.0639
$orthorhombic$	$b = 23.82931$	La2(4d)	0	0.59770	0.79917	25.590	
$La_4F_3I_9 - Type - 7$	$c = 10.79505$	F1(4d)	0	0.63142	0		
	$\alpha = \beta = \gamma = 90$	F2(2a)	0	0	0.29188		
		I1(4d)	0	0.59531	0.49798		
		I2(4e)	1/2	0.59441	0.80124		
		I3(2a)	0	0	0.63092		
		I4(4d)	0	0.26425	0.75756		
		I5(4e)	1/2	0.63218	0.20705		
Cm (8)	$a = 11.11218$	La1(4b)	0.14085	0.74605	0.47555	1158.203	-33276.1512
$monoclinic$	$b = 11.46707$	La2(2a)	0.80256	0	0.92062	40.264	
$La_4F_3I_9 - Type - 10$	$c = 9.09164$	La3(2a)	0.19343	0	0.10552		
	$\alpha = \gamma = 90$	F1(2a)	0	0	0		
	$\beta = 91.2866$	F2(4b)	0.12365	0.88188	0.29186		
		I1(4b)	0.89733	0.82428	0.65039		
		I2(2a)	0.75274	0	0.27028		
		I3(2a)	0.58812	0	0.65129		
		I4(4b)	0.66567	0.75374	0.95658		
		I5(4b)	0.91041	0.67062	0.26780		
		I6(2a)	0.21401	0	0.62368		

Table 8.4: Structure parameters, bulk moduli, minimum energies (in hartree / formula unit) at 0 K for ordered crystalline structure candidates for the $LaBr_3$-$LaCl_3$ system after local optimization on DFT-LDA-VBH level.

Space group (no.) Crystal system, Type	Lattice constants a, b, c [Å]; α, β, γ [$\circ$]	Atom (Multip., Wyckoff lett.), Relative coordinates				V$_{min}$[Å^3] Bulk modulus [GPa]	E$_{min}$
		atom	x	y	z		
Pm (6)	$a = 6.52089$	La1(1a)	0.17314	0	0.32405	491.639	-34371.0104
$monoclinic$	$b = 9.43690$	La2(1b)	0.10303	1/2	0.59011	48.594	
$La_4Br_9Cl_3 - Type - 3$	$c = 7.99019$	La3(1a)	0.62216	0	0.82164		
	$\alpha = \gamma = 90$	La4(1b)	0.67638	1/2	0.08447		

continued on next page

continued from previous page

Space group (no.)	Lattice constants	Atom (Multip., Wyckoff lett.),				V_{min}[Å^3]	E_{min}
Crystal system,	a, b, c [Å];	Relative coordinates				Bulk modulus	
Type	α, β, γ [○]	atom	x	y	z	[GPa]	
	$\beta = 90.8449$	Br1(2c)	0.30512	0.81460	0.62800		
		Br2(2c)	0.80923	0.31103	0.79161		
		Br3(2c)	0.98600	0.31151	0.28480		
		Br4(2c)	0.48268	0.18664	0.12327		
		Br5(1b)	0.51213	1/2	0.42700		
		Cl1(1a)	0	0	0		
		Cl2(1a)	0.79340	0	0.49792		
		Cl3(1b)	0.29233	1/2	0.91161		
Pm (6)	$a = 10.76111$	La1(1b)	0.07361	1/2	0.18020	463.163	-34371.0194
$monoclinic$	$b = 4.75842$	La2(1a)	0.57776	0	0.19165	52.279	
$La_4Br_9Cl_3 - Type - 6$	$c = 9.04515$	La3(1b)	0.60466	1/2	0.68632		
	$\alpha = \gamma = 90$	La4(1a)	0.10013	0	0.69837		
	$\beta = 90.1597$	Br1(1b)	0.48429	1/2	0.99530		
		Br2(1a)	0.27785	0	0.18775		
		Br3(1b)	0.89388	1/2	0.68966		
		Br4(1a)	0.98142	0	0.37597		
		Br5(1a)	0.69263	0	0.87994		
		Br6(1a)	0.39490	0	0.69313		
		Br7(1b)	0.18445	1/2	0.50250		
		Br8(1b)	0.49370	1/2	0.37875		
		Br9(1b)	0.77987	1/2	0.18356		
		Cl1(1a)	0	0	0		
		Cl2(1a)	0.67852	0	0.50473		
		Cl3(1b)	0.17345	1/2	0.87861		
$P4/mmm$ (123)	$a = 6.00141$	La1(1a)	0	0	0	203.817	-8704.1602
$tetragonal$	$c = 5.65892$	Br1(2f)	0	1/2	0	25.727	
$LaBr_2Cl - Type - 21$	$\alpha = \beta = \gamma = 90$	Cl1(1b)	0	0	1/2		
$Cmc2_1$ (36)	$a = 4.74211$	La1(4a)	0	0.23423	0	456.007	-8704.1993
$orthorhombic$	$b = 10.90598$	Br1(4a)	0	0.94155	0.00056	53.091	
$LaBr_2Cl - Type - 28$	$c = 8.81728$	Br2(4a)	0	0.64768	0.19110		
	$\alpha = \beta = \gamma = 90$	Cl1(4a)	0	0.66024	0.80982		
$P2_1$ (4)	$a = 6.02229$	La1(2a)	0.68599	0	0.99997	441.249	-17854.2028
$monoclinic$	$b = 8.26474$	La2(2a)	0.17671	0.75643	0.50547	55.521	
$La_2Br_3Cl_3 - Type - 30$	$c = 8.86574$	Br1(2a)	0.13948	0.15832	0.00222		
	$\alpha = \gamma = 90$	Br2(2a)	0.37380	0.80047	0.19154		
	$\beta = 90.5776$	Br3(2a)	0.35288	0.10115	0.50060		
		Cl1(2a)	0.87522	0.96386	0.31464		
		Cl2(2a)	0.88020	0.95746	0.68885		
		Cl3(2a)	0.38091	0.79659	0.80812		
$P2/m$ (10)	$a = 5.64209$	La1(1a)	0	0	0	191.269	-9149.9432
$monoclinic$	$b = 5.65528$	Br1(1c)	0	0	1/2	27.971	
$LaBrCl_2 - Type - 18$	$c = 6.00479$	Cl1(1b)	0	1/2	0		
	$\alpha = \gamma = 90$	Cl2(1d)	1/2	0	0		
	$\beta = 93.3628$						
$Cmcm$ (63)	$a = 4.65591$	La1(4c)	0	0.22851	1/4	426.288	-9149.9909
$orthorhombic$	$b = 10.67912$	Br1(4c)	0	0.94178	1/4	57.718	
$LaBrCl_2 - Type - 14$	$c = 8.57361$	Cl1(8f)	0	0.65582	0.44220		
	$\alpha = \beta = \gamma = 90$						
Pm (6)	$a = 8.14950$	La1(1a)	0.15090	0	0.47020	418.672	-37045.7690
$monoclinic$	$b = 8.71182$	La2(1a)	0.65369	0	0.81734	59.745	
$La_4Br_3Cl_9 - Type - 1$	$c = 5.89777$	La3(1b)	0.89982	1/2	0.33266		
	$\alpha = \gamma = 90$	La4(1b)	0.39274	1/2	0.95970		
	$\beta = 90.9011$	Br1(1a)	0	0	0		
		Br2(1b)	0.54966	1/2	0.49147		
		Br3(1a)	0.50052	0	0.29052		
		Cl1(2c)	0.19091	0.68835	0.26373		
		Cl2(2c)	0.85821	0.80856	0.52122		
		Cl3(2c)	0.69906	0.31189	0.01488		
		Cl4(1b)	0.06130	1/2	0.77813		
		Cl5(2c)	0.35577	0.80918	0.76816		

Table 8.5: Structure parameters, bulk moduli, minimum energies (in hartree / formula unit) at 0 K for ordered crystalline structure candidates for the $LaCl_3$-LaI_3 system after local optimization on DFT-LDA-VBH level.

Space group (no.)	Lattice constants	Atom (Multip., Wyckoff lett.),				V_{min}[Å^3]	E_{min}
Crystal system,	a, b, c [Å];	Relative coordinates				Bulk modulus	
Type	α, β, γ [○]	atom	x	y	z	[GPa]	
Pm (6)	$a = 8.51816$	La1(1b)	0.09807	1/2	0.32002	441.176	-37040.4181
$monoclinic$	$b = 8.52080$	La2(1b)	0.59589	1/2	0.01420	56.451	
$La_4Cl_9I_3 - Type - 4$	$c = 6.07866$	La3(1a)	0.83592	0	0.49980		
	$\alpha = \gamma = 90$	La4(1a)	0.35451	0	0.79645		
	$\beta = 90.5815$	Cl1(2c)	0.79860	0.30689	0.30352		
		Cl2(2c)	0.63897	0.81086	0.80357		
		Cl3(2c)	0.31379	0.30166	0.03010		
		Cl4(2c)	0.14239	0.19144	0.51360		
		Cl5(1a)	0.50952	0	0.34721		
		I1(1a)	0	0	0		
		I2(1b)	0.94930	1/2	0.82012		
		I3(1b)	0.44462	1/2	0.51812		
$Pmna$ (62)	$a = 8.59025$	La1(4c)	0.37688	1/4	0.09759	450.831	-9148.2169
$orthorhombic$	$b = 8.53386$	Cl1(8d)	0.66602	0.05834	0.10744	55.184	
$LaCl_2I - Type - 62$	$c = 6.14983$	I1(4c)	0.02738	1/4	0.90564		
	$\alpha = \beta = \gamma = 90$						

continued on next page

continued from previous page

Space group (no.)	Lattice constants	Atom (Multip., Wyckoff lett.),				V_{min}[Å^3]	E_{min}
Crystal system,	a, b, c [Å];	Relative coordinates				Bulk modulus	
Type	α, β, γ [$\circ$]	atom	x	y	z	[GPa]	
$Pmmm$ (47)	$a = 6.51460$	La1(2m)	0	0.73192	0	442.279	-17848.7567
$orthorhombic$	$b = 12.08639$	Cl1(2n)	0	0.72929	1/2	23.409	
$La_2Cl_3I_3 - Type - 3$	$c = 5.61710$	Cl2(1e)	0	1/2	0		
	$\alpha = \beta = \gamma = 90$	I1(1a)	0	0	0		
		I2(2o)	1/2	0.72613	0		
$P2_1/m$ (11)	$a = 8.58756$	La1(2e)	0.38267	1/4	0.05324	534.531	-17848.8288
$monoclinic$	$b = 9.62731$	La2(2e)	0.86467	1/4	0.44876	44.205	
$La_2Cl_3I_3 - Type - 33$	$c = 6.52787$	Cl1(2e)	0.11214	1/4	0.77664		
	$\alpha = \gamma = 90$	Cl2(4f)	0.34488	0.92242	0.83841		
	$\beta = 97.93$	I1(4f)	0.85613	0.95102	0.71134		
		I2(2e)	0.52511	1/4	0.61745		
$Pccn$ (56)	$a = 7.09230$	La1(4c)	1/4	1/4	0.90435	602.654	-8700.6314
$orthorhombic$	$b = 7.53198$	Cl1(4a)	0	0	0	37.186	
$LaClI_2 - Type - 50$	$c = 11.28163$	I1(8e)	0.03148	0.42821	0.16711		
	$\alpha = \beta = \gamma = 90$						
$C2$ (5)	$a = 10.48511$	La1(4c)	0.74949	0.24793	0.59878	1236.799	-34354.9457
$monoclinic$	$b = 10.22189$	La2(4c)	0.26556	0.25074	0.89033	36.015	
$La_4Cl_3I_9 - Type - 9$	$c = 11.53971$	Cl1(4c)	0.71415	0	0.49575		
	$\alpha = \gamma = 90$	Cl2(2a)	0	0.78236	0		
	$\beta = 90.0421$	I1(4c)	0.69981	0.04612	0.82399		
		I2(4c)	0.22170	0.44371	0.16678		
		I3(2a)	0	0.17830	0		
		I4(4c)	0.55278	0.28745	0.33622		
		I5(4c)	0.94604	0.21832	0.33953		

Table 8.6: Structure parameters, bulk moduli, minimum energies (in hartree / formula unit) at 0 K for ordered crystalline structure candidates for the $LaBr_3$-LaI_3 system after local optimization on DFT-LDA-VBH level.

Space group (no.)	Lattice constants	Atom (Multip., Wyckoff lett.),				V_{min}[Å^3]	E_{min}
Crystal system,	a, b, c [Å];	Relative coordinates				Bulk modulus	
Type	α, β, γ [$\circ$]	atom	x	y	z	[GPa]	
$P2/m$ (10)	$a = 13.65901$	La1(2m)	0.76373	0	0.62192	919.475	-33028.1568
$monoclinic$	$b = 6.00972$	La2(2m)	0.25372	0	0.86652	22.477	
$La_4Br_9I_3 - Type - 6$	$c = 12.49627$	Br1(2m)	0.99157	0	0.26862		
	$\alpha = \gamma = 90$	Br2(2n)	0.76993	1/2	0.62349		
	$\beta = 116.3154$	Br3(2m)	0.74266	0	0.37198		
		Br4(2n)	0.24959	1/2	0.86252		
		Br5(1d)	1/2	0	0		
		I1(2m)	0.76372	0	0.88236		
		I2(1g)	1/2	0	1/2		
Pm (6)	$a = 8.56977$	La1(1b)	0.40503	1/2	0.03113	520.771	-33028.3420
$monoclinic$	$b = 9.39647$	La2(1b)	0.90320	1/2	0.68687	46.393	
$La_4Br_9I_3 - Type - 2$	$c = 6.46881$	La3(1a)	0.64973	0	0.16290		
	$\alpha = \gamma = 90$	La4(1a)	0.16158	0	0.54513		
	$\beta = 91.2992$	Br1(2c)	0.85338	0.81408	0.48049		
		Br2(2c)	0.20026	0.68883	0.74024		
		Br3(2c)	0.36358	0.18453	0.24813		
		Br4(2c)	0.69191	0.30891	0.97236		
		Br5(1a)	0.48296	0	0.74125		
		I1(1a)	0	0	0		
		I2(1b)	0.05661	1/2	0.21975		
		I3(1b)	0.55854	1/2	0.49106		
$P4/mmm$ (123)	$a = 6.00520$	La1(1a)	0	0	0	234.776	-8256.5937
$tetragonal$	$c = 6.51025$	Br1(2f)	0	1/2	0	21.987	
$LaBr_2I - Type - 18$	$\alpha = \beta = \gamma = 90$	I1(1b)	0	0	1/2		
$Pmna$ (62)	$a = 8.69103$	La1(4c)	0.12405	1/4	0.07796	522.780	-8256.6439
$orthorhombic$	$b = 9.33154$	Br1(8d)	0.16894	0.93858	0.87431	46.554	
$LaBr_2I - Type - 67$	$c = 6.44606$	I1(4c)	0.96924	1/4	0.60948		
	$\alpha = \beta = \gamma = 90$						
$Pmmm$ (47)	$a = 6.00161$	La1(2q)	0	0	0.74000	486.904	-16511.4034
$orthorhombic$	$b = 6.50329$	Br1(1c)	0	0	1/2	20.997	
$La_2Br_3I_3 - Type - 1$	$c = 12.47506$	Br2(2s)	1/2	0	0.26160		
	$\alpha = \beta = \gamma = 90$	I1(2r)	0	1/2	0.73636		
		I2(1a)	0	0	0		
Pc (7)	$a = 7.05161$	La1(2a)	0	0.87917	0	599.842	-16511.4658
$monoclinic$	$b = 8.25471$	La2(2a)	0.55002	0.38529	0.99939	37.806	
$La_2Br_3I_3 - Type - 37$	$c = 12.40210$	Br1(2a)	0.36821	0.30392	0.51007		
	$\alpha = \gamma = 90$	Br2(2a)	0.67015	0.40766	0.33047		
	$\beta = 123.8081$	Br3(2a)	0.19840	0.80163	0.50554		
		I1(2a)	0.03789	0.42263	0.68995		
		I2(2a)	0.52158	0.91513	0.32044		
		I3(2a)	0.89315	0.90969	0.69388		
$P4_2/ncm$ (138)	$a = 7.49600$	La1(4e)	1/4	1/4	0.38754	662.694	-8254.8411
$tetragonal$	$c = 11.79379$	Br1(4d)	0	0	0	33.700	
$LaBrI_2 - Type - 70$	$\alpha = \beta = \gamma = 90$	I1(8i)	0.04897	0.04897	0.66770		
$Pmna$ (62)	$a = 8.75833$	La1(4c)	0.13285	1/4	0.48102	616.453	-8254.8481
$orthorhombic$	$b = 9.96216$	Br1(4c)	0.43966	1/4	0.67578	37.605	
$LaBrI_2 - Type - 67$	$c = 7.06521$	I1(8d)	0.83829	0.06478	0.31597		
	$\alpha = \beta = \gamma = 90$						

continued on next page

continued from previous page

Space group (no.) Crystal system, Type	Lattice constants a, b, c [Å]; α, β, γ [$\circ$]	Atom (Multip., Wyckoff lett.), Relative coordinates				V$_{min}$[Å^3] Bulk modulus [GPa]	E$_{min}$
		atom	x	y	z		
$Amm2$ (38)	$a = 6.49171$	La1(4d)	0	0.88191	0.98146	2048.711	-33017.4528
$orthorhombic$	$b = 25.36203$	La2(4d)	0	0.62683	0.96167	19.554	
$La_4Br_3I_9-Type-27$	$c = 12.44335$	Br1(2a)	0	0	0		
	$\alpha = \beta = \gamma = 90$	Br2(4d)	0	0.62827	0.72169		
		I1(4d)	0	0.11499	0.72222		
		I2(4e)	1/2	0.11556	0.98718		
		I3(4e)	1/2	0.62861	0.96497		
		I4(4d)	0	0.74583	0.47674		
		I5(2a)	0	0	0.44607		
Pm (6)	$a = 7.18885$	La1(1a)	0.34217	0	0.19372	630.008	-33017.5918
$monoclinic$	$b = 10.47912$	La2(1b)	0.29391	1/2	0.93785	35.803	
$La_4Br_3I_9-Type-13$	$c = 8.36435$	La3(1a)	0.80243	0	0.69260		
	$\alpha = \gamma = 90$	La4(1b)	0.85240	1/2	0.42328		
	$\beta = 91.0335$	Br1(1a)	0	0	0		
		Br2(1a)	0.14769	0	0.50174		
		Br3(1b)	0.64709	1/2	0.11950		
		I1(2c)	0.50091	0.81648	0.89976		
		I2(2c)	0.13824	0.31520	0.22304		
		I3(2c)	0.99388	0.68533	0.72820		
		I4(2c)	0.64449	0.18162	0.39250		
		I5(1b)	0.47062	1/2	0.60087		

8.4 Conclusion

To summarize, we have found, that the subsolidus regions in the quasi-binary lanthanum halide systems exhibit ordered crystalline phases and no solid solution-like phases appear to be thermodynamically stable. In each system, we found a number of compositions, where modifications exist that can be considered as thermodynamically stable with respect to the binaries and neighboring phases.

Part V

Summary

9 Summary

From the point of view of thermodynamic, materials are found as thermodynamically stable (equilibrium) or metastable phases. These can be characterized via functions of state that depend uniquely on the given state variables such as temperature, pressure and composition. The graphical representations of all thermodynamically stable phases that exist or co-exist at equilibrium is called the phase diagram of the chemical system as function of the thermodynamic variables.

Nowadays, phase diagrams continue to play a key role in material science and engineering. Usually, the phase diagrams are studied experimentally. However, in many instances, it is both very time-consuming and difficult to determine the full phase diagram from experiment only. This applies especially to the low-temperature parts, since the time scales on which equilibration to the thermodynamically stable phase takes place often exceed the time available for the experiment. Nevertheless, e.g. information about the existence of a thermodynamically stable crystalline phase that will form by very slow transformation processes from, say, a solid solution-like phase, is crucial for deciding whether this compound is suitable for practical applications. Recent years have seen a large increase in the number of theoretical studies to support and complement the experiments in deriving phase diagrams.

The goal of this thesis has been to develop a computational strategy to analyze and predict phase diagrams, with the main focus on the low-temperature parts. The crucial new aspect is the ability to predict, whether a solid solution or crystalline like compounds are present, without recourse to experimental data. The starting point of this method is the global exploration of the energy landscape of a given chemical system for several compositions and the subsequent analysis of thousands of crystal structures on the *ab initio* and thermodynamic level.

The first step of a general modular approach developed in this work is a global optimization on the enthalpy landscape using an empirical Coulomb plus Lennard-Jones potential for the potential energy contribution to the enthalpy. This is followed by a local optimization of all obtained structure candidates on the *ab initio* level (using several *ab initio* methods: Hartree-Fock plus at least one DFT method). The candidates with the lowest energy are selected and their enthalpies of formation are calculated. Of special importance is whether we observe a number of structurally related candidates with approximately same energy, where (part of the) atoms are randomly distributed over one of the sublattices of the structure. In this case we deal with a so-called structure family, and we expect a solid solution to occur at low temperatures. In contrast, when the structure candidates exhibit big differences in energy and belong to different structure types, then we expect ordered crystalline compounds to be present which can be thermodynamically stable, metastable or unstable. Finally, after this analysis the low-temperature parts of the phase diagrams are constructed.

The main part of the thesis has dealt with the application of the suggested approach to numerous chemical systems. The following chemical systems have been selected to be studied: quasi-binary alkali metal halides, quasi-binary lanthanum halides, quasi-binary and quasi-ternary semiconductors $A^{III}B^{V}$.

In the case of the quasi-binary alkali metal halides, 20 systems were studied. For 14 of these systems (NaCl-LiCl, NaBr-LiBr, NaCl-KCl, KBr-NaBr, KCl-RbCl, KBr-RbBr, MBr-MI (M = Li, Na, K, Rb or Cs) and MBr-MCl (M = Li, Na or K)) it was predicted that solid solutions should be present as the thermodynamically stable phase. Based on the obtained data for the enthalpies of formation the locations of the corresponding miscibility gaps were calculated, and a good agreement with experimental data (where available) was found. The remaining 6 systems (CsX-LiX (X = F, Cl, Br or I) and LiX-RbX (X = Cl or Br)) were predicted to contain ordered crystalline phases, again in agreement with experimental observations. Besides the experimentally known phases, several new ones were predicted as possible candidates for synthesis.

The low temperature parts of the phase diagrams of the quasi-binary lanthanum halides (LaX_3-LaY_3, (X, Y = F, Cl, Br or I)) have not been investigated experimentally, up to now. The exploration of the energy landscape and the further analysis of the various structure candidates found have shown that the low-temperature parts of all six systems should exhibit ordered crystalline phases. Several possible candidates were proposed as thermodynamically stable modifications.

In a third project, the low temperature part of the phase diagrams of the quasi-ternary semiconductors AlSb-GaSb-InSb and AlAs-GaAs-InAs were investigated. In the literature, the liquid/solid equilibria for the quasi-binary semiconductors $(AA')^{III}B^{V}$ have been well studied, but no investigations of the low-temperature regions of the phase diagrams have been reported. In this thesis, the energy landscapes of the quasi-binary semiconductor MM'As and MM'Sb (M, M' = Al, Ga or In) plus the two quasi-ternary systems AlSb-GaSb-InSb and AlAs-GaAs-InAs were explored globally. The analysis of the computed data have shown that a solid solution-like phase should be thermodynamically stable in all systems. Based on these data the locations of the miscibility gaps were calculated and the low-temperature parts of the six quasi-binary and two quasi-ternary phase diagrams were predicted.

Part VI

Zusammenfassung

10 Zusammenfassung

Grundsätzlich können im Sinne der chemischen Thermodynamik Stoffe im Gleichgewicht oder im Ungleichgewicht (metastabil) vorliegen. Die Gleichgewichtszustände sind eindeutig durch den Satz der jeweils eingestellten Zustandsvariablen festgelegt und durch die Zustandsfunktionen beschrieben. Eine Darstellung des Phasenbestandes im Gleichgewicht in der Abhängigkeit von den Zustandsvariablen wird als Phasen- oder Zustandsdiagramm bezeichnet.

Phasendiagramme spielen eine Schlüsselrolle in den Material- und Ingenieurwissenschaften. Traditionell werden Phasendiagrammen experimentell bestimmt. Dieses ist in aller Regel ein zeitaufwendiges und auch oft schwieriges Unterfangen. Letzteres trifft vor allem auf den Bereich niedriger Temperaturen zu, da sich das thermodynamische Gleichgewicht hier nur sehr langsam einstellt und die für das Experiment zur Verfügung stehende Zeit eher nicht ausreicht. Gleichwohl sind auch solche Zustände von Bedeutung, und Informationen über eine thermodynamisch stabile kristalline Phase, die durch einen sehr langsamen Transformationsprozess aus einem Mischkristall entsteht, sind sehr wichtig bei der Entscheidung, ob diese Phase für praktische Anwendungen brauchbar ist oder nicht. In den letzten Jahren nahm die Zahl der theoretischen Arbeiten, die zum Ziel hatten, die experimentell bestimmten Phasendiagramme zu komplettieren, stark zu.

Das Ziel dieser Dissertation ist es, eine computergestützte Strategie zu entwickeln, mit der Phasendiagramme berechnet werden können, wobei die jeweiligen Niedertemperaturbereiche besonders im Fokus stehen. Hierbei kann es beispielweise darum gehen vorherzusagen, ob ein Mischkristall oder ausgeordnete kristalline Verbindungen vorliegen.

Der Ausgangspunkt des hier entwickelten Verfahrens ist eine Untersuchung der globalen Energielandschaft des zu charakterisierenden chemischen Systems für verschiedene Zusammensetzungen. Anschließend folgt eine Nachoptimierung der gefundenen existierenden Strukturen (einige Tausende) auf *ab initio* Ebene sowie deren thermodynamischen Analyse.

Der allgemeine modulare Ansatz, wie er im Rahmen dieser Arbeit entwickelt wird, umfasst im ersten Schritt die globale Suche nach Minima der Enthalpielandschaft eines chemischen Systems. Dabei wird ein empirisches Potential, das einen Coulomb- und einen Lennard-Jones-Term umfasst, für die Berechnung des Beitrags der potentiellen Energie zur Enthalphie verwendet. Danach erfolgt auf *ab initio* Ebene eine lokale Optimierung aller beobachteter Stukturkandidaten, wobei mehrere *ab initio* Verfahren, zum Beispiel Hartree-Fock und mindestens eine DFT Methode, zur Anwendung kommen.

Die Strukturen mit der niedrigsten Energie werden ausgewählt und deren Bildungsenthalphien berechnet. Von besonderer Wichtigkeit ist, ob eine Anzahl strukturell verwandter Kandidaten mit der ungefähr gleichen Energie beobachtet werden, bei denen ein Teil der Atome in vielfältiger Weise über ein Untergitter der gleichen Basisstruktur verteilt sind. In diesen Fällen haben wir es mit einer sogenannten Strukturfamilie zu tun, und wir erwarten einen Mischkristall bei niedrigen Temperaturen. Sind die Kandidaten jedoch unterschiedlicher Struktur und weisen sie einen großen Energieunterschied auf, liegen individuelle kristalline Verbindungen vor, welche thermodynamisch stabil oder metastabil sein können. Aus den erhaltenen Bildungenthalpien und -entropien wird der Sub-solidus Bereich des Phasendiagramm berechnet.

Der Hauptteil der Doktorarbeit beschäftigt sich mit der Anwendung des vorgestellten Ansatzes auf verschiedene chemische Systeme: quasi-binäre Alkalimetallhalogenide, quasi-binäre Lanthanhalogenide, sowie quasi-binäre und quasi-ternäre $A^{III}B^{V}$ Halbleiter.

Im Fall der quasi-binären Alkalimetallhalogenide wurden 20 Systeme untersucht. Für 14 dieser Systeme (NaCl-LiCl, NaBr-LiBr, NaCl-KCl, KBr-NaBr, KCl-RbCl, KBr-RbBr, MBr-MI (M = Li, Na, K, Rb oder Cs) und MBr-MCl (M = Li, Na oder K)) wurde das Auftreten von festen Lösungen und Mischungslücken vorhergesagt. Die berechneten Zustandsfelder stimmen gut mit den (unvollständig) vorliegenden experimentellen Werten überein. In den verbliebenen 6 Systemen (CsX-LiX (X = F, Cl, Br oder I) und LiX-RbX (X = Cl oder Br)) wurden geordnete kristalline Phasen vorhergesagt, was sich ebenfalls mit den experimentellen Beobachtungen deckt. Neben bereits bekannten ternären Verbindungen wurden mehrere neue als mögliche Synthesekandidaten vorhergesagt.

Die Niedertemperaturbereiche in den Phasendiagrammen der quasi-binären Lanthanhalogenide (LaX_3-LaY_3, (X, Y = F, Cl, Br or I)) sind bislang nicht experimentell untersucht. Die hier durchgeführte Untersuchung der Energielandschaft sowie die weiteren Analysen der gefundenen Strukturkandidaten legen nahe, dass in allen sechs Systemen geordnete kristalline Verbindungen existieren sollten. Verschiedene dieser Kandidaten wurden als thermodynamisch stabile Modifikationen berechnet.

In einem dritten Projekt wurden die Niedertemperaturbereiche der Phasendiagramme von den quasi-ternären Halbleitern AlSb-GaSb-InSb und AlAs-GaAs-InAs untersucht. Die bisherige Literatur der quasi-binären Halbleiter vom Typ $(AA')^{III}B^{V}$ beschäftigt sich ausgiebig mit dem Gleichgewicht zwischen dem flüssigen und festen Zustand. Untersuchungen der Niedertemperaturbereiche der Phasendiagramme sind jedoch unbekannt. In dieser Doktorarbeit wurden die Energielandschaften der quasi-binären Halbleiter MM'As und MM'Sb (M, M' = Al, Ga und In) sowie die der zwei quasi-ternären Systeme AlSb-GaSb-InSb und AlAs-GaAs-InAs global untersucht. Die Analyse der berechneten Daten zeigt, dass in allen Systemen eine thermodynamisch stabile feste Lösung vorliegt. Basierend auf diesen Daten wurden die Mischungslücken berechnet und die Niedertemperaturbereiche der sechs quasi-binären und der zwei quasi-ternären Phasendiagramme vorhergesagt.

Appendix

A Quasi-binary alkali halogenide systems

A.1 Alkali halogenides: auxiliary data

A.1.1 General data

Table A.1: Ionic radii of atoms $r(q)$ ([Å]) and charges q used in the present work for the global landscape explorations of the alkali halide systems.

	Li	Na	K	Rb	Cs
q	$+1$	$+1$	$+1$	$+1$	$+1$
$r(q)$	0.78	0.98	1.41	1.49	1.65
	Cl	Br	I		
q	-1	-1	-1		
$r(q)$	1.81	1.96	2.2		

Table A.2: Summary of basis set optimizations (135).

Element	Basis set name	Shell no	Shell type	Exponent
NaCl-LiCl, NaBr-LiBr and NaCl-KCl				
Li	6-1G	2	sp	0.5197
Na	8-511G	3	sp	0.5468
		4	sp	0.2361
		3	d	0.4319
K	86-511G	-	-	-
Cl	86-311G	4	sp	0.320
		5	sp	0.125
Br	[HAYWLC]-31	-	-	-
LiBr-LiCl				
Li	6-11G	2	sp	0.528
		2	sp	0.1745
Br	[HAYWLC]-31	4	sp	0.0999
Cl	86-311G	3	sp	0.3117
		3	d	0.1172
NaBr-NaCl				
Na	8-511G	3	sp	0.5390
		3	sp	0.2021
		3	d	0.2675
Br	[HAYWLC]-31	4	sp	0.1006
Cl	86-311G	3	sp	0.3144
		3	d	0.1217
KBr-KCl				
K	86-511G	4	sp	0.3949
		4	sp	0.2170
		4	d	0.3774
Br	[HAYWLC]-31	4	sp	0.0989
Cl	86-311G	3	sp	0.317

continued on next page

continued from previous page

Element	Basis set name	Shell no	Shell type	Exponent
		3	d	0.1178
		KBr-NaBr		
K	86-511G	4	sp	0.3949
		4	sp	0.2170
		3	d	0.3774
Na	8-511G	3	sp	0.5390
		3	sp	0.2021
		3	d	0.2675
Br	[HAYWLC]-31	4	sp	0.0989
		KCl-RbCl		
K	86-511G	4	sp	0.3941
		4	sp	0.2212
		3	d	0.4218
Rb	ECP28MWB	5	p	0.3262
		5	p	0.134
		4	d	0.2967
Cl	86-311G	3	sp	0.3154
		3	sp	0.1156
		KBr-RbBr		
K	86-511G	4	sp	0.3949
		4	sp	0.2170
		3	d	0.3774
Rb	ECP28MWB	5	p	0.3248
		5	p	0.1328
		4	d	0.3032
Br	[HAYWLC]-31	4	sp	0.0975
		LiCl-RbCl		
Li	6-11G	2	sp	0.5315
		2	sp	0.2088
Rb	ECP28MWB	5	p	0.3262
		5	p	0.134
		4	d	0.2967
Cl	86-311G	3	sp	0.3154
		3	d	0.1156
		LiBr-RbBr		
Li	6-11G	2	sp	0.528
		2	sp	0.1745
Rb	ECP28MWB	5	p	0.3248
		5	p	0.1328
		4	d	0.3032
Br	[HAYWLC]-31	4	sp	0.0975
		LiBr-LiI		
Li	6-11G	2	sp	0.5258
		2	sp	0.1585
Br	[HAYWLC]-31	4	sp	0.0999
I	[HAYWLC]-31	5	sp	0.0885
		NaBr-NaI		
Na	8-511G	3	sp	0.5397
		3	sp	0.2097
		3	d	0.2301
Br	[HAYWLC]-31	4	sp	0.1006
I	[HAYWLC]-31	5	sp	0.0889
		KBr-KI		
K	86-511G	4	sp	0.39638
		4	sp	0.2169
		4	d	0.4750
Br	[HAYWLC]-31	4	sp	0.0989
I	[HAYWLC]-31	5	sp	0.0885
		RbBr-RbI		
Rb	ECP28MWB	5	p	0.3255
		5	p	0.1347
		5	d	0.3147
Br	[HAYWLC]-31	4	sp	0.0975
I	[HAYWLC]-31	5	sp	0.088
		CsBr-CsI		
Cs	ECP46MWB	6	p	0.2810
		6	p	0.1162
		6	d	0.2538
Br	[HAYWLC]-31	4	sp	0.0966
I	[HAYWLC]-31	5	sp	0.0873
		CsF-LiF		
Cs	ECP46MWB	6	p	0.2823
		6	p	0.1124
		5	d	0.2678
Li	6-11G	2	sp	0.5147
		2	sp	2.0376
F	7-311G	2	sp	0.4378
		2	sp	0.1469
		CsCl-LiCl		
Cs	ECP46MWB	6	p	0.2817
		6	p	0.1158
		5	d	0.2467
Li	6-11G	2	sp	0.5315

continued on next page

continued from previous page

Element	Basis set name	Shell no	Shell type	Exponent
		2	sp	0.2088
Cl	86-311G	3	sp	0.3168
		3	d	0.1139
CsBr-LiBr				
Cs	ECP46MWB	6	p	0.2814
		6	p	0.1161
		5	d	0.2527
Li	6-11G	2	sp	0.528
		2	sp	0.1745
Br	[HAYWLC]-31	4	sp	0.0966
CsI-LiI				
Cs	ECP46MWB	6	p	0.2810
		6	p	0.1162
		5	d	0.2538
Li	6-11G	2	sp	0.5258
		2	sp	0.1585
I	[HAYWLC]-31	5	sp	0.0873

A.1.2 The CsX-LiX systems, where X = F, Cl, Br or I

Table A.3: Summary of basis set optimizations (135).

Element	Basis set name	Shell no	Shell type	Exponent
CsF-LiF				
Cs	ECP46MWB	6	p	0.2823
		6	p	0.1124
		5	d	0.2678
Li	6-11G	2	sp	0.5147
		2	sp	2.0376
F	7-311G	2	sp	0.4378
		2	sp	0.1469
CsCl-LiCl				
Cs	ECP46MWB	6	p	0.2817
		6	p	0.1158
		5	d	0.2467
Li	6-11G	2	sp	0.5315
		2	sp	0.2088
Cl	86-311G	3	sp	0.3168
		3	d	0.1139
CsBr-LiBr				
Cs	ECP46MWB	6	p	0.2814
		6	p	0.1161
		5	d	0.2527
Li	6-11G	2	sp	0.528
		2	sp	0.1745
Br	[HAYWLC]-31	4	sp	0.0966
CsI-LiI				
Cs	ECP46MWB	6	p	0.2810

continued on next page

continued from previous page				
Element	Basis set name	Shell no	Shell type	Exponent
		6	p	0.1162
		5	d	0.2538
Li	6-11G	2	sp	0.5258
		2	sp	0.1585
I	[HAYWLC]-31	5	sp	0.0873

A.1.3 The LiX-RbX systems, where X = Cl or Br

Table A.4: Summary of basis set optimizations (135).

Element	Basis set name	Shell no	Shell type	Exponent
		LiCl-RbCl		
Li	6-11G	2	sp	0.5315
		2	sp	0.2088
Rb	ECP28MWB	5	p	0.3262
		5	p	0.134
		4	d	0.2967
Cl	86-311G	3	sp	0.3154
		3	d	0.1156
		LiBr-RbBr		
Li	6-11G	2	sp	0.528
		2	sp	0.1745
Rb	ECP28MWB	5	p	0.3248
		5	p	0.1328
		4	d	0.3032
Br	[HAYWLC]-31	4	sp	0.0975

Table A.5: Structure parameters, bulk moduli, minimum energies, and energy differences (ΔE) between the structure candidate and the candidate with the lowest energy (in hartree / formula unit) at 0 K for ordered crystalline structure candidates for the LiCl-RbCl system after local optimization on Hartree-Fock level. The candidates with the lowest energy are listed in Table 6.17 for all compositions investigated. The candidates given in the table below are metastable with respect to decomposition into neighboring phases, but stable with respect to decomposition into the binary compounds LiCl and RbCl.

Space group (no.)	Lattice constants	Atom (Multip., Wyckoff lett.),				V_{min}[Å^3]	E_{min}
Crystal system,	a, b, c [Å];	Relative coordinates				Bulk modulus	(ΔE)
Type	α, β, γ [$\circ$]	atom	x	y	z	[GPa]	
Composition: $LiRb_2Cl_3$							
$C2/m$ (12)	$a = 18.13828$	Li1(4i)	0.63917	0	0.04907	801.831	-1433.9753
monoclinic	$b = 4.81380$	Rb2(4i)	0.69044	0	0.68565	15.115	(0.0005)
$LiRb_2Cl_3 - Type2$	$c = 9.54180$	Rb3(4i)	0.03665	0	0.26558		
	$\alpha = \gamma = 90$	Cl4(2b)	0	1/2	0		
	$\beta = 105.75560$	Cl5(4i)	0.15716	0	0.94587		
		Cl6(4i)	0.31751	0	0.68720		
		Cl7(2d)	0	1/2	1/2		
$P-62m$ (189)	$a = 7.66526$	Li1(1a)	0	0	0	223.737	-1433.9732
hexagonal	$c = 4.39697$	Rb2(2d)	1/3	2/3	1/2	12.954	(0.0026)
$LiRb_2Cl_3 - Type3$	$\alpha = \beta = 90$	Cl3(3f)	0.30648	0	0		
	$\gamma = 120$						
$Pmn2_1$ (31)	$a = 4.65467$	Li1(2a)	0	0.93526	0.72634	425.905	-1433.9756
orthorhombic	$b = 13.50468$	Rb2(2a)	0	0.41339	0.18568	14.200	(0.0002)
$LiRb_2Cl_3 - Type4$	$c = 6.77547$	Rb3(2a)	0	0.78520	0.18396		
	$\alpha = \beta = \gamma = 90$	Cl4(2a)	0	0.39903	0.68532		
		Cl5(2a)	0	0.02957	0.42338		
		Cl6(2a)	0	0.76348	0.67963		
Pc (7)	$a = 4.89897$	Li1(2a)	0.55316	0.35658	0.45393	404.519	-1433.9725
monoclinic	$b = 10.55458$	Rb2(2a)	0.05575	0.99313	0.70277	14.937	(0.0023)
$LiRb_2Cl_3 - Type5$	$c = 7.82550$	Rb3(2a)	0.05337	0.63633	0.43659		
	$\alpha = \gamma = 90$	Cl4(2a)	0.55516	0.87789	0.44712		
	$\beta = 91.34070$	Cl5(2a)	0.05284	0.26725	0.46325		
		Cl6(2a)	0.55267	0.49241	0.19671		
Cm (8)	$a = 16.23643$	Li1(2a)	0.19756	0	0.57831	844.369	-1433.9723
monoclinic	$b = 4.39525$	Li2(2a)	0.35714	0	0.12999	14.216	(0.0025)
$LiRb_2Cl_3 - Type6$	$c = 12.03593$	Rb3(2a)	0.46482	0	0.44466		
	$\alpha = \gamma = 90$	Rb4(2a)	0.80502	0	0.86148		
	$\beta = 100.56230$	Rb5(2a)	0.64474	0	0.19207		
		Rb6(2a)	0.03279	0	0.82047		
		Cl7(2a)	0.45613	0	0.99912		
		Cl8(2a)	0.63149	0	0.66807		
		Cl9(2a)	0.21381	0	0.01297		
		Cl10(2a)	0.11831	0	0.39355		
		Cl11(2a)	0.34874	0	0.65699		
		Cl12(2a)	0.86460	0	0.23773		
Cm (8)	$a = 23.93524$	Li1(2a)	0.06471	0	0.36636	775.099	-1433.9757
monoclinic	$b = 4.28356$	Li2(2a)	0.76236	0	0.07644	15.423	(0.0001)
$LiRb_2Cl_3 - Type7$	$c = 7.84493$	Rb3(2a)	0.58937	0	0.87871		
	$\alpha = \gamma = 90$	Rb4(2a)	0.41353	0	0.22039		
	$\beta = 105.49290$	Rb5(2a)	0.23786	0	0.55626		
		Rb6(2a)	0.41358	0	0.72104		
		Cl7(2a)	0.62225	0	0.44012		
		Cl8(2a)	0.82348	0	0.38165		
		Cl9(2a)	0.82799	0	0.88768		
		Cl10(2a)	0.99844	0	0.55317		
		Cl11(2a)	0.00436	0	0.06034		
		Cl12(2a)	0.20491	0	0.01163		
Composition: $LiRb_3Cl_4$							
$P2_1/m$ (11)	$a = 12.09866$	Li1(2e)	0.37840	1/4	0.41208	557.555	-1917.4138
monoclinic	$b = 4.61585$	Rb2(2e)	0.40064	1/4	0.81228	14.954	(0.0056)
$LiRb_3Cl_4 - Type2$	$c = 9.98685$	Rb3(2e)	0.88185	1/4	0.36325		
	$\alpha = \gamma = 90$	Rb4(2e)	0.83276	1/4	0.86548		
	$\beta = 91.39710$	Cl5(2e)	0.61215	1/4	0.44589		
		Cl6(2e)	0.39394	1/4	0.14810		
		Cl7(2e)	0.15516	1/4	0.39525		
		Cl8(2e)	0.12452	1/4	0.99046		

Table A.6: Structure parameters, bulk moduli, minimum energies, and energy differences (ΔE) between the structure candidate and the candidate with the lowest energy (in hartree / formula unit) at 0 K for ordered crystalline structure candidates for the LiBr-RbBr system after local optimization on Hartree-Fock level. The candidates with the lowest energy are listed in Table 6.18 for all compositions investigated. The candidates given in the table below are metastable with respect to decomposition into neighboring phases, but stable with respect to decomposition into the binary compounds LiBr and RbBr.

Space group (no.) Crystal system, Type	Lattice constants a, b, c [Å]; α, β, γ [$\circ$]	Atom (Multip., Wyckoff lett.), Relative coordinates				V_{min}[Å^3] Bulk modulus [GPa]	E_{min} (ΔE)
		atom	x	y	z		
Composition: Li_2RbBr_3							
$P2_1/m$ (11)	$a = 4.74302$	Li1(2e)	0.47321	1/4	0.91578	401.460	-77.9531
monoclinic	$b = 5.98327$	Li2(2e)	0.06278	1/4	0.19188	14.020	(0.0004)
$Li_2RbBr_3 - Type2$	$c = 14.22902$	Rb1(2e)	0.37155	1/4	0.62417		
	$\alpha = \gamma = 90$	Br1(2e)	0.12816	1/4	0.37961		
	$\beta = 96.17360$	Br2(2e)	0.94323	1/4	0.82447		
		Br3(2e)	0.53291	1/4	0.10108		
$C2/m$ (12)	$a = 7.54472$	Li1(8j)	0.23041	0.80812	0.74844	781.919	-77.9495
monoclinic	$b = 13.28055$	Rb1(4i)	0.71304	0	0.75693	14.035	(0.004)
$Li_2RbBr_3 - Type3$	$c = 7.81077$	Br1(4g)	0	0.72869	0		
	$\alpha = \gamma = 90$	Br2(4h)	0	0.28261	1/2		
	$\beta = 92.43130$	Br3(4i)	0.19361	0	0.75214		
$Imm2$ (44)	$a = 5.90418$	Li1(4d)	0	0.18835	0.33648	385.073	-77.9504
orthorhombic	$b = 14.71978$	Rb1(2b)	0	1/2	0.31625	14.727	(0.0031)
$Li_2RbBr_3 - Type4$	$c = 4.43081$	Br1(4d)	0	0.69421	0.82560		
	$\alpha = \beta = \gamma = 90$	Br2(2a)	0	0	0.26558		
$Pmmn$ (59)	$a = 5.89517$	Li1(4e)	1/4	0.05698	0.24898	387.616	-77.9515
orthorhombic	$b = 14.04437$	Rb1(2b)	1/4	3/4	0.23439	14.521	(0.002)
$Li_2RbBr_3 - Type5$	$c = 4.68170$	Br1(4e)	1/4	0.94881	0.75022		
	$\alpha = \beta = \gamma = 90$	Br2(2a)	1/4	1/4	0.33902		
Composition: $Li_2Rb_3Br_5$							
$Imm2$ (44)	$a = 24.99243$	Li1(4c)	0.71086	0	0.57580	832.983	-151.7345
orthorhombic	$b = 4.65157$	Rb2(4c)	0.39184	0	0.94289	11.105	(0.006)
$Li_2Rb_3Br_5 - Type2$	$c = 7.16520$	Rb3(2a)	0	0	0.94015		
	$\alpha = \beta = \gamma = 90$	Br4(4c)	0.21311	0	0.29869		
		Br5(4c)	0.39252	0	0.43760		
		Br6(2a)	0	0	0.44167		
$C2$ (5)	$a = 7.28878$	Li1(4c)	0.13744	0.72883	0.91739	831.531	-151.7330
monoclinic	$b = 7.36539$	Rb2(4c)	0.08391	0.21442	0.73638	11.114	(0.0075)
$Li_2Rb_3Br_5 - Type3$	$c = 15.54286$	Rb3(2b)	0	0.71025	1/2		
	$\alpha = \gamma = 90$	Br4(2b)	0	0.20987	1/2		
	$\beta = 94.76530$	Br5(4c)	0.90802	0.70595	0.26139		
		Br6(4c)	0.25794	0.06587	0.93812		
$C2$ (5)	$a = 7.29321$	Li1(4c)	0.13694	0.23262	0.41750	831.694	-151.7330
monoclinic	$b = 7.36245$	Rb2(4c)	0.91696	0.74653	0.76356	11.110	(0.0075)
$Li_2Rb_3Br_5 - Type4$	$c = 15.54395$	Rb3(2a)	0	0.24866	0		
	$\alpha = \gamma = 90$	Br4(4c)	0.74190	0.89567	0.56199		
	$\beta = 94.82080$	Br5(2a)	0	0.74981	0		
		Br6(4c)	0.90847	0.25503	0.76122		
Cm (8)	$a = 7.15368$	Li1(4b)	0.64356	0.20920	0.33524	785.986	-151.7327
monoclinic	$b = 26.06444$	Rb2(4b)	0.09963	0.88546	0.64513	11.654	(0.0078)
$Li_2Rb_3Br_5 - Type5$	$c = 4.50180$	Rb3(2a)	0.55298	0	0.86622		
	$\alpha = \gamma = 90$	Br4(2a)	0.08151	0	0.13059		
	$\beta = 110.54820$	Br5(4b)	0.54068	0.88613	0.36059		
		Br6(4b)	0.90452	0.21605	0.04786		
Cm (8)	$a = 7.91439$	Li1(4b)	0.51415	0.21519	0.97145	759.695	-151.7395
monoclinic	$b = 25.04511$	Rb2(2a)	0.48170	0	0.37506	11.880	(0.001)
$Li_2Rb_3Br_5 - Type6$	$c = 4.46226$	Rb3(4b)	0.99660	0.88254	0.97727		
	$\alpha = \gamma = 90$	Br4(2a)	0.97105	0	0.45897		
	$\beta = 120.80630$	Br5(4b)	0.89724	0.23224	0.36496		
		Br6(4b)	0.45645	0.11449	0.85894		
Composition: $LiRb_2Br_3$							
$Pmc2_1$ (26)	$a = 5.38571$	Li1(2b)	1/2	0.84434	0.91429	583.181	-94.3165
orthorhombic	$b = 11.91691$	Rb2(2a)	0	0.52970	0.64013	11.447	(0.0029)
$LiRb_2Br_3 - Type2$	$c = 9.08650$	Rb3(2a)	0	0.86166	0.35114		
	$\alpha = \beta = \gamma = 90$	Br4(2b)	1/2	0.37558	0.86562		
Cm (8)	$a = 25.74231$	Li1(2a)	0.92230	0	0.66032	933.614	-94.3122
monoclinic	$b = 4.52394$	Li2(2a)	0.24965	0	0.94916	12.028	(0.0072)
$LiRb_2Br_3 - Type3$	$c = 8.38985$	Rb1(2a)	0.42008	0	0.16700		
	$\alpha = \gamma = 90$	Rb2(2a)	0.58663	0	0.81505		
	$\beta = 107.14940$	Rb3(2a)	0.58555	0	0.30822		
		Rb4(2a)	0.75069	0	0.47576		
		Br1(2a)	0.00094	0	0.48044		
		Br2(2a)	0.81465	0	0.93642		
		Br3(2a)	0.17645	0	0.13808		

continued on next page

continued from previous page

Space group (no.)	Lattice constants	Atom (Multip., Wyckoff lett.),				V$_{min}$[Å^3]	E$_{min}$
Crystal system,	a, b, c [Å];	Relative coordinates				Bulk modulus	(ΔE)
Type	α, β, γ [$\circ$]	atom	x	y	z	[GPa]	
		Br4(2a)	0.99949	0	0.97674		
		Br5(2a)	0.36151	0	0.51101		
		Br6(2a)	0.17005	0	0.63488		
Cm (8)	a = 17.17879	Li1(2a)	0.34124	0	0.14280	1008.594	-94.3121
monoclinic	b = 4.67022	Li2(2a)	0.18786	0	0.58430	11.043	(0.0073)
$LiRb_2Br_3 - Type4$	c = 12.77285	Rb1(2a)	0.01222	0	0.81020		
	$\alpha = \gamma = 90$	Rb2(2a)	0.45704	0	0.44855		
	β = 100.18770	Rb3(2a)	0.62997	0	0.18047		
		Rb4(2a)	0.80172	0	0.86130		
		Br1(2a)	0.35074	0	0.66520		
		Br2(2a)	0.44614	0	0.00013		
		Br3(2a)	0.09895	0	0.37866		
		Br4(2a)	0.62194	0	0.67040		
		Br5(2a)	0.84152	0	0.26301		
		Br6(2a)	0.19493	0	0.99990		
Cm (8)	a = 19.70191	Li1(2a)	0.65005	0	0.01252	964.102	-94.3171
monoclinic	b = 4.94459	Li2(2a)	0.35193	0	0.93863	11.664	(0.0023)
$LiRb_2Br_3 - Type5$	c = 10.31705	Rb1(2a)	0.96245	0	0.70884		
	$\alpha = \gamma = 90$	Rb2(2a)	0.68576	0	0.64596		
	β = 106.41430	Rb3(2a)	0.31542	0	0.30847		
		Rb4(2a)	0.03893	0	0.24688		
		Br1(2a)	0.31819	0	0.65440		
		Br2(2a)	0.83388	0	0.05326		
		Br3(2a)	0.68329	0	0.29371		
		Br4(2a)	1/2	0	0.47110		
		Br5(2a)	0.49994	0	0.97579		
		Br6(2a)	0.15515	0	0.87594		
Composition: $LiRb_3Br_4$							
$P2_1/m$ (11)	a = 10.36559	Li1(2e)	0.89933	1/4	0.41947	750.087	-131.2113
monoclinic	b = 9.84495	Rb2(2e)	0.46524	1/4	0.50042	9.978	(0.0016)
$LiRb_3Br_4 - Type2$	c = 7.35076	Rb3(4f)	0.75892	0.00088	0.98342		
	$\alpha = \gamma = 90$	Br4(4f)	0.24263	0.96505	0.51231		
	β = 90.65350	Br5(2e)	0.99873	1/4	0.09749		
		Br6(2e)	0.49562	1/4	0.99895		
$Pmn2_1$ (31)	a = 14.00384	Li1(2a)	0	0.80186	0.43544	706.531	-131.2051
orthorhombic	b = 7.12363	Rb2(4b)	0.24999	0.76002	0.88552	10.578	(0.0078)
$LiRb_3Br_4 - Type3$	c = 7.08243	Rb3(2a)	0	0.28268	0.89834		
	$\alpha = \beta = \gamma = 90$	Br4(2a)	0	0.78098	0.85422		
		Br5(2a)	0	0.20885	0.39846		
		Br6(4b)	0.29208	0.26199	0.88638		
$Cmc2_1$ (36)	a = 14.07191	Li1(4a)	0	0.08105	0.55473	1431.126	-131.2071
orthorhombic	b = 14.24443	Rb2(4a)	0	0.35396	0.11832	10.406	(0.0058)
$LiRb_3Br_4 - Type4$	c = 7.13969	Rb3(8b)	0.75067	0.12193	0.11731		
	$\alpha = \beta = \gamma = 90$	Br4(8b)	0.21055	0.87121	0.11957		
		Br5(4a)	0	0.60554	0.11878		
		Br6(4a)	0	0.90489	0.68641		
$P2_1$ (4)	a = 8.56114	Li1(2a)	0.03401	0.50764	0.59998	724.677	-131.2058
monoclinic	b = 5.31544	Rb2(2a)	0.41894	0.79306	0.12969	10.528	(0.0071)
$LiRb_3Br_4 - Type5$	c = 15.94570	Rb3(2a)	0.57173	0.24467	0.60824		
	$\alpha = \gamma = 90$	Rb4(2a)	0.91625	0.32021	0.13740		
	β = 92.93400	Br5(2a)	0.59082	0.25711	0.27221		
		Br6(2a)	0.25016	0.30381	0.00102		
		Br7(2a)	0.80559	0.75549	0.50875		
		Br8(2a)	0.92057	0.32723	0.73426		
$P2_1$ (4)	a = 7.10561	Li1(2a)	0.95514	0.55920	0.89168	713.447	-131.2038
monoclinic	b = 7.13187	Rb2(2a)	0.99814	0.11792	0.64626	10.463	(0.0091)
$LiRb_3Br_4 - Type6$	c = 14.08012	Rb3(2a)	0.50581	0.60958	0.63309		
	$\alpha = \gamma = 90$	Rb4(2a)	0.50774	0.57964	0.12837		
	β = 90.86670	Br5(2a)	0.54587	0.57955	0.88010		
		Br6(2a)	0.99389	0.14733	0.90615		
		Br7(2a)	0.49755	0.10694	0.61756		
		Br8(2a)	0.99104	0.11575	0.31934		
$P2_1$ (4)	a = 15.52462	Li1(2a)	0.60616	0.02475	0.54322	689.621	-131.2114
monoclinic	b = 8.63870	Rb2(2a)	0.13881	0.77134	0.81702	10.659	(0.0015)
$LiRb_3Br_4 - Type7$	c = 5.17515	Rb3(2a)	0.40328	0.03126	0.96225		
	$\alpha = \gamma = 90$	Rb4(2a)	0.86321	0.77642	0.18396		
	β = 96.47830	Br5(2a)	0.67138	0.02010	0.06880		
		Br6(2a)	0.77555	0.52498	0.64429		
		Br7(2a)	0.50210	0.27711	0.50068		
		Br8(2a)	0.95054	0.02414	0.71600		
$Ama2$ (40)	a = 9.13183	Li1(4b)	1/4	0.00094	0.59994	1346.202	-131.2037
orthorhombic	b = 12.97403	Rb2(4a)	0	0	0.13896	11.005	(0.0092)
$LiRb_3Br_4 - Type8$	c = 11.36260	Rb3(8c)	0	0.22182	0.86908		
	$\alpha = \beta = \gamma = 90$	Br4(4a)	0	0	0.47180		
		Br5(4b)	1/4	0.78955	0.13129		
		Br6(4b)	1/4	0	0.83181		
		Br7(4b)	1/4	0.20977	0.13169		
$C2$ (5)	a = 6.13585	Li1(2b)	0	0.73578	1/2	621.716	-131.2042
monoclinic	b = 6.13866	Rb2(4c)	0.35973	0.98394	0.72942	11.859	(0.0087)
$LiRb_3Br_4 - Type9$	c = 16.71271	Rb3(2a)	0	0.48327	0		
	$\alpha = \gamma = 90$	Br4(4c)	0.92990	0.98347	0.86487		
	β = 99.01920	Br5(4c)	0.79615	0.98614	0.59864		
Pm (6)	a = 7.23352	Li1(1b)	0.25389	1/2	0.81225	365.622	-131.2102

continued on next page

continued from previous page

Space group (no.) Crystal system, Type	Lattice constants a, b, c [Å]; α, β, γ [∘]	Atom (Multip., Wyckoff lett.), Relative coordinates atom	x	y	z	V$_{min}$[Å^3] Bulk modulus [GPa]	E$_{min}$ (ΔE)
monoclinic	b = 10.41021	Rb2(2c)	0.82179	0.74070	0.50725	10.143	(0.0027)
$LiRb_3Br_4 - Type10$	c = 4.87111	Rb3(1a)	0.32821	0	0.11809		
	$\alpha = \gamma = 90$	Br4(2c)	0.33772	0.72911	0.63699		
	β = 94.60650	Br5(1a)	0.82649	0	0.01624		
		Br6(1b)	0.93141	1/2	0.01790		
Pm (6)	a = 8.56079	Li1(1b)	0.61951	1/2	0.00904	336.667	-131.2057
monoclinic	b = 4.66425	Rb2(1a)	0.07900	0	0.12352	11.010	(0.0072)
$LiRb_3Br_4 - Type11$	c = 8.51507	Rb3(1a)	0.60174	0	0.52284		
	$\alpha = \gamma = 90$	Rb4(1a)	0.09281	0	0.61928		
	β = 98.03350	Br5(1b)	0.86553	1/2	0.81834		
		Br6(1a)	0.45070	0	0.92659		
		Br7(1b)	0.29340	1/2	0.40864		
		Br8(1b)	0.80339	1/2	0.29165		
Cm (8)	a = 31.20721	Li1(2a)	0.87595	0	0.47646	1368.479	-131.2070
monoclinic	b = 5.27125	Li2(2a)	0.75836	0	0.98503	10.959	(0.0059)
$LiRb_3Br_4 - Type12$	c = 8.35569	Rb3(2a)	0.98681	0	0.83503		
	$\alpha = \gamma = 90$	Rb4(2a)	0.63509	0	0.72968		
	β = 95.37360	Rb5(2a)	0.50138	0	0.36246		
		Rb6(2a)	0.26147	0	0.49349		
		Rb7(2a)	0.12532	0	0.19461		
		Rb8(2a)	0.36239	0	0.01047		
		Br9(2a)	0.93527	0	0.20005		
		Br10(2a)	0.55541	0	0.00848		
		Br11(2a)	0.81299	0	0.75528		
		Br12(2a)	0.81044	0	0.25156		
		Br13(2a)	0.21408	0	0.92139		
		Br14(2a)	0.41385	0	0.61467		
		Br15(2a)	0.06634	0	0.55146		
		Br16(2a)	0.68393	0	0.37799		

B Quasi-binary and quasi-ternary semiconductors

B.1 Semiconductors: $A^{III}B^{V}$: auxiliary data

Table B.1: Ionic radii of atoms $r(q)$ ([Å]) and charges q used in the present work for the global landscape explorations of the semiconductor A^3B^5 systems.

	Al	Ga	In	As	Sb
q	$+3$	$+3$	$+3$	-3	-3
$r(q)$	0.57	0.62	0.8	2.3	2.4

C Quasi-binary lanthanum halogenide systems

C.1 Lanthanum halides: auxiliary data

Table C.1: Ionic radii of atoms $r(q)$ ([Å]) and charges q used in the present work for the global landscape explorations of the lanthanum halide systems.

	La	F	Cl	Br	I
q	$+3$	-1	-1	-1	-1
$r(q)$	1.22	1.33	1.81	1.96	2.2

Table C.2: Summary of basis set optimizations (135).

Element	Basis set name	Shell no	Shell type	Exponent
F	7-311G	2	sp	0.4378
		2	sp	0.1469
Cl	86-311G	3	sp	0.3168
		3	d	0.1139
Br	[HAYWLC]-31	4	sp	0.0966
I	[HAYWLC]-31	5	sp	0.0873

D List of publications

J.C. Schön and I.V. Pentin and M. Jansen,
"Ab initio computation of low-temperature phase diagrams exhibiting miscibility gaps",
Phys. Chem. Chem. Phys **8**, 1778 **(2006)**.

I.V. Pentin and J.C. Schön and M. Jansen,
"Ab initio prediction of low-temperature phase diagrams in the systems KBr-NaBr, KX-RbX, and LiX-RbX (X = Cl, Br)",
J. Chem. Phys. **126**, 124508 **(2007)**.

J.C. Schön and I.V. Pentin and M. Jansen,
"Ab initio computation of low-temperature phase diagrams of the alkali metal iodide-bromides: MBr_xI_{1-x} *(0≤x≤1), where M = Li, Na, K, Rb or Cs"*,
J. Phys. Chem. B **111**, 3943 **(2007)**.

J.C. Schön and I.V. Pentin and M. Jansen,
"Ab initio prediction of low-temperature phase diagrams in the systems MBr-MCl (M = Li, Na, K)",
J. Solid State Science **10**, 455 **(2008)**.

I.V. Pentin and J.C. Schön and M. Jansen,
"Ab initio prediction of low-temperature phase diagrams in the systems CsX-LiX (X = F, Cl, Br, I)",
J. Solid State Science 10 , 804 **(2008)**.

Bibliography

Bibliography

[1] A. Pelton, Phase diagrams, in *Physical Metallurgy, 3rd ed.*, edited by R. W. Cahn and P. Haasen, North-Holland, New York, 1983.

[2] A. M. N. Saunders, *CALPHAD: a comprehensive guide*, New York: Pergamon, Oxford, 1998.

[3] P. Dörner, L. J. Gauckler, H. Krieg, H. L. Lukas, and G. Petzow, Calphad **3**, 241 (1979).

[4] G. Petzow, E. T. Henig, U. Kattner, and H. L. Lukas, Z. Metallkd. **75**, 3 (1984).

[6] L. Kaufman and H. Nesor, Physica B **150**, 99 (1988).

[5] F. H. Hayes, H. L. Lukas, G. Effenberg, and G. Petzow, Z. Metallkd. **77**, 749 (1986).

[8] L. M. Foster and J. F. Woods, J. Electrochem. Soc. **118**, 1175 (1971).

[7] E. Irle et al., Z. Metallkd. **78**, 535 (1987).

[9] I. Ansara et al., Calphad **18**, 177 (1994).

[10] P. Dörner, E. T. Henig, H. Krieg, H. L. Lukas, and G. Petzow, Calphad **4**, 241 (1980).

[11] L. Kaufman, Calphad **2**, 55 (1978).

[12] A. V. der Ven, M. Aydinol, G. Ceder, G. Kresse, and J. Hafner, Phys. Rev. B **58**, 2975 (1998).

[13] B. Burton et al., Z. Metallkd. **92**, 514 (2001).

[14] D. Fuks, S. Dorfman, S. Piskunov, and E. Kotomin, Phys. Rev. B **71**, 014111 (2005).

[15] S. Shang and A. J. Böttger, Acta Materialia **53**, 255 (2005).

[16] D. Nguyen-Manh, M. Y. Lavrentiev, and S. L. Dudarev, Comp. Ren. Phys. **9**, 379 (2008).

[17] R. Hirschl, J. Hafner, and Y. Jeanvoine, J. Phys. Condens. Matter **13**, 3545 (2001).

[18] L. Kaufman, P. Turchi, W. Huang, and Z.-K. Liu, Calphad **25**, 419 (2001).

[19] H. Ohtani, M. Yamano, and M. Hasebe, CALPHAD **28**, 177 (2004).

[20] S. H. Zhou et al., Mat. Sc. Eng. **397**, 288 (2005).

[21] J. Houserova, J. Vrestal, and M. Sob, CALPHAD **29**, 133 (2005).

[22] X. Wang, S. Scandolo, and R. Car, Phys. Rev. Letters **95**, 185701 (2005).

[23] S. Mehta, G. D. Price, and D. Alfé, J. Chem. Phys. **125**, 194507 (2006).

[24] J. Shen et al., Rare Metals **25**, 481 (2006).

[25] G. Ghosh, S. Delsante, G. Borzone, M. Asta, and R. Ferro, Acta Mater. **54**, 4977 (2006).

[26] W. Xiong, Y. Du, X. Lu, J. C. Schuster, and H. Chen, Intermetallics **15**, 1401 (2007).

[27] S. P. Ong, L. Wang, B. Kang, and G. Ceder, Chem. Mater. **20**, 1798 (2008).

[28] R. Arroyave, D. Shin, and Z.-K. Liu, Acta Mat. **53**, 1809 (2005).

[29] Y. Wang et al., Calphad **28**, 79 (2004).

[30] G. Ghosh and M. Asta, Acta Mat. **53**, 3225 (2005).

[31] G. Rubin and A. Finel, J. Phys. Condens. Matter **7**, 3139 (1995).

[32] B. Winkler, C. J. Pickard, V. Milman, and G. Thimm, Chem. Phys. Lett. **337**, 36 (2001).

[33] S. Curtarolo, D. Morgan, K. Persson, J. Rodgers, and G. Ceder, Phys. Rev. Letters **91**, 135503 (2003).

[34] S. M. Woodley, Struct. Bond. **110**, 95 (2004).

[35] M. Launay and R. Dronskowski, Z. Naturforsch. **60b**, 437 (2005).

[36] S. Curtarolo, D. Morgan, and G. Ceder, Calphad **29**, 163 (2005).

[37] S. Curtarolo, A. N. Kolmogorov, and F. H. Cocks, Calphad **29**, 155 (2005).

[38] B. Alling et al., Phys. Rev. B **75**, 045123 (2007).

[39] ICSD-Fiz-Karlsruhe, Inorganic crystal structure database, http://icsdweb.fiz-karlsruhe.de, 2005.

[40] M. Jansen, Angew. Chem. Int. Ed. **41**, 3747 (2002).

[41] J. C. Schön and M. Jansen, Angew. Chem. Int. Ed. Eng. **35**, 1286 (1996).

[42] J. C. Schön and M. Jansen, Z. Kristallogr. **216**, 307 (2001).

[43] M. Jansen, The deductive approach to chemistry, a paradigm shift, in *Turning points in Solid-State, Materials and Surface Science*, edited by K. M. Harris and P. Edwards, page 22, RSC Publishing, Cambridge, UK, 2008.

[44] J. C. Schön and M. Jansen, Comp. Mater. Sci. **4**, 43 (1995).

[45] M. A. C. Wevers, J. C. Schön, and M. Jansen, J. Solid State Chem. **136**, 223 (1998).

[46] M. Jansen and J. C. Schön, Z. Anorg. Allg. Chem. **624**, 533 (1998).

[47] J. C. Schön, Z. Anorg. Allg. Chem. **630**, 2354 (2004).

[48] J. C. Schön, Ž. Čančarević, and M. Jansen, J. Chem. Phys. **121**, 2289 (2004).

[49] H. Putz, J. C. Schön, and M. Jansen, Z. Anorg. Allg. Chem. **625**, 1624 (1999).

[50] H. Putz, J. C. Schön, and M. Jansen, Comp. Mater. Sci. **11**, 309 (1998).

[51] J. C. Schön, M. A. C. Wevers, and M. Jansen, Solid State Sci. **2**, 449 (2000).

[52] G. Voronin, Russian J. Phys. Chem. **77**, 1874 (2003).

[53] M. O'Keefe and A. Navrotsky, *Structure and Bonding in Crystal, Vols. I and II*, Academic Press, London, 1981.

[54] M. Jansen, Abh. Rhein. Westf. Akad. Wiss. **N420**, 7 (1996).

[55] J. C. Schön and M. Jansen, Z. Kristallogr. **216**, 307 (2001).

[56] J. C. Schön and M. Jansen, Z. Kristallogr. **216**, 361 (2001).

[57] J. Callaway, *Quantum Theory of the Solid State*, Academic Press, New York, 1974.

[58] K. Doll, J. C. Schön, and M. Jansen, Phys. Chem. Chem. Phys. **9**, 6128 (2007).

[59] J. C. Schön and P. Sibani, J. Phys. A: Math. Gen. **31**, 8165 (1998).

[60] J. C. Schön and M. Jansen, in *Pauling's Legacy: Modern Modeling of the Chemical Bond*, edited by Z. Maksic and W. Orville-Thomas, pages 103–127, Elsevier, Amsterdam, 1999.

[61] R. A. Buckingham, Proc. Roy. Soc. London A **168**, 264 (1938).

[62] M. Born and K. Huang, *Dynamical Theory of Crystal Lattices*, Oxford University Press, London, 1954.

[63] B. G. Dick and A. W. Overhauser, Phys. Rev. **112**, 90 (1958).

[64] K. Fischer, H. Blitz, R. Habernkorn, and W. Weber, Phys. Stat. Solidi B **54**, 285 (1972).

[65] U. Schröder, Solid State Commun. **4**, 347 (1966).

[66] V. Nusslein and U. Schröder, Phys. Stat. Solidi B **21**, 309 (1967).

[67] R. G. Gordon and Y. S. Kim, J. Chem. Phys. **56**, 3122 (1972).

[68] A. J. Cohen and R. G. Gordon, Phys. Rev. B **14**, 4593 (1976).

[69] C. Muhlhauser and R. Gordon, Phys. Rev. B **23**, 900 (1981).

[70] C. Muhlhauser and R. Gordon, Phys. Rev. B **24**, 2147 (1981).

[71] L. L. Boyer et al., Phys. Rev. Lett. **54**, 1940 (1985).

[72] M. J. Mehl, R. J. Hemley, and L. L. Boyer, Phys. Rev. B **33**, 8685 (1986).

[73] R. E. Cohen, Geophys. Res. Lett. **14**, 37 (1987).

[74] G. H. Wolf and M. S. T. Bukowinski, Phys. Chem. Min. **15**, 209 (1988).

[75] M. D. Jackson and R. G. Gordon, Phys. Chem. Min. **16**, 212 (1988).

[76] O. V. Ivanov and E. G. Maksimov, Phys. Rev. Lett. **69**, 108 (1992).

[77] D. J. Lacks and R. G. Gordon, Phys. Rev. B **48**, 2889 (1993).

[78] H. T. Stokes, L. L. Boyer, and M. J. Mehl, Phys. Rev. B **54**, 7729 (1996).

[79] L. L. Boyer, H. T. Stokes, and M. J. Mehl, Ferroelec. **194**, 1173 (1997).

[80] R. E. Cohen, First-principles theory of crystalline sio_2, in *MSA Reviews in Mineralogy; Silica: Physical Behavior, Geochemistry, and Materials Applications*, edited by P. Heaney, C. Prewitt, and G. Gibbs, volume 29, pages 369–402, Mineralogical Society of America, Washington, D.C., 1994.

[81] L. Stixrude, R. E. Cohen, and R. J. Hemley, Theory of minerals at high pressures, in *MSA Reviews in Mineralogy; Ultrahigh-Pressure Mineralogy*, edited by R. Hemley, volume 37, pages 639–671, Mineralogical Society of America, Washington, D.C., 1998.

[82] B. B. Karki, L. Stixrude, and R. M. Wentzcovitch, Reviews of Geophysics **39**, 507 (2001).

[83] C. Mellot-Draznieks et al., Chem. Eur. J. **8**, 4102 (2002).

[84] R. Horst, P. M. Pardalos, and N. V. Thoai, *Introduction to Global Optimization, Second Edition*, Kluwer Academic Publishers, 2000.

[85] P. Y. Papalambros and D. J. Wilde, *Principles of Optimal Design: Modeling and Computation*, Cambridge University Press., Cambridge, 2000.

[86] S. Boyd and L. Vandenberghe, *Convex Optimization*, Cambridge University Press., Cambridge, 2004.

[87] http://www.wikipedia.org/, 2008.

[88] A. Schrijver, On the history of combinatorial optimization (till 1960), in *Handbook of discrete optimization*, edited by K. Aardal, G. L. Nemhauser, and R. Weismantel, page 1, Elsevier, Amsterdam, 2005.

[89] S. Kirkpatrick, C. D. Gelatt Jr., and M. P. Vecchi, Science **220**, 671 (1983).

[90] V. Czerny, J. Optim. Theo. Appl. **45**, 41 (1985).

[91] K. Hamacher and W. Wenzel, Phys. Rev. E **59**, 938 (1999).

[92] W. Wenzel and K. Hamacher, Phys. Rev. Lett. **82**, 3003 (1999).

[93] P. Salamon, P. Sibani, and R. Frost, Facts, conjectures and improvements for simulated annealing, in *SIAM Monographs on Mathematical Modeling and Computation*, edited by J. E. Flaherty, Society for Industrial and Applied Mathematics, Philadelphia, USA, 2002.

[94] A. Neumaier, Complete search in continuous global optimization and constrain satisfaction, in *Acta Numerica 2004*, edited by A. Iserles, pages 271–369, Cambridge University Press., Cambridge, 2004.

[95] R. Motwani and P. Raghavan, *Randomized Algorithms*, Cambridge University Press., Cambridge, 1995.

[96] N. Metropolis, A. W. Rosenbluth, M. N. Rosenbluth, A. H. Teller, and E. Teller, J. Chem. Phys. **21**, 1087 (1953).

[97] S. Geman and D. Geman, IEEE T. Pattern Anal **6**, 721 (1984).

[98] J. H. Holland, *Adaptation in Natural and Artificial Systems*, Univ. Mich. Press, Ann Arbor, 1975.

[99] L. Davis, *Genetic Algorithms and Simulated Annealing*, Pitman, London, 1987.

[100] D. E. Goldberg, *Genetic Algorithms in Search, Optimization, and Machine Learning*, Addison-Wesley Publishing Company, Reading. M.A., 1989.

[101] J. C. Schön, Ber. Bunsenges. **100**, 1388 (1996).

[102] J. C. Schön, H. Putz, and M. Jansen, J. Phys.: Cond. Matt. **8**, 143 (1996).

[103] F. Harary, *Graph Theory*, Addison-Wesley Publishing Company, Reading. M.A., 1969.

[104] R. M. Martin, *Electronic structure. Basic theory and practical methods*, Cambridge, United Kingdom, 2004.

[105] L. H. Thomas, Proc. Cambridge Phil. Roy. Soc. **23**, 542 (1927).

[106] E. Fermi, Rend. Accad. Naz. Lincei **6**, 602 (1927).

[107] P. A. M. Dirac, Proc. Cambridge Phil. Soc. **26**, 376 (1930).

[108] R. Dovesi, Total energy and related properties, in *Quantum-Mechanical Ab-initio Calculation of the Properties of Crystalline Materials*, edited by C.Pisani, volume 67 of *Lecture Notes in Chemistry*, Springer-Verlag, Berlin Heidelberg New York, 1996.

[109] C. Pisani, editor, *Quantum-Mechanical Ab-initio Calculation of the Properties of Crystalline Materials*, volume 67 of *Lecture Notes in Chemistry*, Springer-Verlag, Berlin Heidelberg New York, 1996.

[110] R. Dovesi, B. Civalleri, R. Orlando, C. Roeti, and V. R. Sounders, Ab initio quantum simulation in solid state chemistry, in *Reviews in Computational Chemistry*, edited by K. B. Lipkowitz, R. Larter, and T. R. Cundari, volume 21, Wiley-VCH, John Wiley & Sons, Inc., Weinheim, New York, 2005.

[111] R. Dovesi et al., Z. Kristallogr. **220**, 571 (2005).

[112] A. D. Becke, J. Chem. Phys. **98**, 5648 (1993).

[113] C. Lee, W. Yang, and R. G. Parr, Phys. Rev. B **37**, 785 (1988).

[114] P. J. Stephens, F. J. Devlin, C. F. Chabalowski, and M. J. Frisch, J. Phys. Chem. **98**, 11623 (1994).

[115] J. A. Pople and R. K. Nesbet, J. Chem. Phys. **22**, 571 (1954).

[116] M. D. Towler, An introductory guide to Gaussian basis sets in solid-state electronic structure calculations, European Summer School "*Ab initio* modeling in solid state chemistry", Torino, Italy, 2000.

[117] V. R. Saunders et al., *CRYSTAL2003*, Univ. Torino, Torino, 2003.

[118] O. Redlich and A. T. Kister, Ind. Eng. Chem. **40**, 345 (1948).

[119] J. C. Schön and M. Jansen, in *Mat. Res. Soc. Symp. Proc. Vol 848: Solid State Chemistry of Inorganic Materials V*, edited by J. Li, N. E. Brese, M. G. Kanatzidis, and M. Jansen, MRS, Warrendale, 2005.

[120] J. Schön, Ž. P. Čančarević, A. Hannemann, and M. Jansen, J. Chem. Phys. **128**, 194712 (2008).

[121] S. Elliott, *Physics of Amorphous Materials*, Longman Scientific & Technical, Essex, 1990.

[122] R. Hundt, J. C. Schön, and M. Jansen, J. Appl. Cryst. **39**, 6 (2006).

[123] V. R. Saunders et al., *CRYSTAL2006*, Univ. Torino, Torino, 2006.

[124] R. Hundt, J. C. Schön, A. Hannemann, and M. Jansen, J. Appl. Cryst. **32**, 413 (1999).

[125] A. Hannemann, R. Hundt, J. C. Schön, and M. Jansen, J. Appl. Cryst. **31**, 922 (1998).

[126] R. Hundt, KPLOT: A Program for Plotting and Investigation of Crystal Structures, University of Bonn, Germany, 1979.

[127] Ž. Čančarević, J. C. Schön, and M. Jansen, Progress in Materials Science and Processes (Mat. Sci. Forum) **453**, 71 (2004).

[128] F. D. Murnaghan, Proc. Nat. Acad. Sci. **30**, 244 (1944).

[129] http://www.factsage.com.

[130] http://www.thermocalc.com/.

[131] http://www.npl.co.uk/server.php?show=ConWebDoc.1226;
http://www.mtdata.software.com/.

[132] http://www.computherm.com/pandat.html/.

[133] Y. Liebold-Ribeiro, D. Fischer, and M. Jansen, Angew. Chem. Int. Ed. **47**, 4428 (2008).

[134] J. Sangster and A. Pelton, J. Phys. Chem. Ref. Data **16**, 509 (1987).

[135] Ž. Čančarević, J. C. Schön, and M. Jansen, Chem. Asian J. **3**, 561 (2008).

[136] Available on web-site http://www.crystal.unito.it/Basis_Sets/ptable.html.

[137] A. S. Arabadzhan and A. G. Bergman, Russ. J. Inorg. Chem. **7**, 1152 (1962).

[138] D. S. Coleman and P. D. A. Lacy, Mater. Res. Bull. **2**, 935 (1967).

[139] A. D. Pelton, A. Gabriel, and J. Sangster, J. Chem. Soc. Faraday Trans. 1 **81**, 1167 (1985).

[140] S. Zhemchuzhnyi and F. Rambach, Z. Anorg. Chem. **65**, 403 (1910).

[141] W. Schaefer, Neues Jahrb. Mineral. Geol. Palaeontol. Abh. Abt. A **43**, 132 (1920).

[142] D. Doornhof, H. V. Wijk, and H. Hoonk, Thermochim. Acta **76**, 171 (1984).

[143] Nguyen-Ba-Chanh, J. Chim. Phys. **61**, 1428 (1964).

[144] Y. Vesin and S. Zakovryashin, Solid State Commun. **31**, 635 (1979).

[145] J. C. Schön, I. V. Pentin, and M. Jansen, Phys. Chem. Chem. Phys **8**, 1778 (2006).

[146] Y. Kondo, H. Muramatsu, W. A. Matthews, N. Toriyama, and M. Hirota, J. Atm. Chem. **6**, 235 (1988).

[147] S. Gupta, S. Patnaik, S. Chaklanobis, and S. Shahi, Solid State Ionics **31**, 5 (1988).

[148] D. Fischer, Ž. Čančarević, J. C. Schön, and M. Jansen, Z. Anorg. Allg. Chem. **630**, 156 (2004).

[149] M. Hovi, Annales Academiae Scientiarum Fennicae, Series A6: Physica **315** (1969).

[150] M. Ahtee and H. Koski, Annales Academiae Scientiarum Fennicae, Series A6: Physica **297** (1968).

[151] B. Thomas and L. Wood, J. Am. Chem. Soc. **57**, 822 (1936).

[152] M. Ahtee, Annales Academiae Scientiarum Fennicae, Series A6: Physica **313**, 1 (1969).

[153] T. Swamy, K. Subhadra, and D. Sirdeshmukh, Pramana - J. Phys. **43**, 33 (1994).

[154] Y. G. Vlasov, B. L. Seleznev, and E. A. Elchin, Zh. Neorg. Khim. **17**, 3069 (1872).

[155] Ž. Čančarević, J. C. Schön, and M. Jansen, Progress in Materials Science and Processes (Mat. Sci. Forum) **494**, 61 (2005).

[156] R. Tomoshige, H. Kenbishi, M. Kodama, and T. Matsushita, J. Cer. Soc. Japan **103**, 828 (1995).

[157] Y. Kimura, Y. Saito, T. Nakada, and C. Kaito, Phys. Low-Dim. Struct. **1-2**, L1 (2000).

[158] C. Zangmeister, J. Turner, and J. Pemberton, Geophys. Res. Let. **28**, 995 (2001).

[159] A. Asif and M. Butt, J. Mat. Sc. **42**, 2862 (2007).

[160] W. J. M. van der Kemp, J. G. Blok, A. C. G. van Genderen, P. J. van Ekeren, and H. A. J. Oonk, Thermochim. Acta **196**, 301 (1993).

[161] P. W. Bridgman, Proc. Am. Acad. Arts Sci **76**, 1 (1945).

[162] J. H. Burns and W. R. Busing, Inorg. Chem. **4**, 1510 (1965).

[163] H. C. Gaebell, G. Meyer, and R. Hoppe, Z. Anorg. Allg. Chem. **498**, 94 (1983).

[164] E. Korreng, Z. Anorg. Chem. **91**, 194 (1915).

[165] H. C. Gaebell and G. Meyer, Z. Anorg. Allg. Chem. **513**, 15 (1984).

[166] G. Meyer and H. C. Gaebell, Mat. Research Bull. **18**, 1353 (1983).

[167] G. Meyer and H. C. Gaebell, Mat. Research Bull. **18**, 1353 (1983).

[168] I. V. Pentin, J. C. Schön, and M. Jansen, J. Chem. Phys. **126**, 124508 (2007).

[169] J. Schön, M. Jansen, and P. Salamon, in preparation (2008).

[170] P. Sibani and P. Schriver, Phys. Rev. B **59**, 6667 (1994).

[171] P. Sibani, Physica A **258**, 249 (1998).

[172] O. Gropen, Methods in computational chemistry, volume 2, New York, 1988.

[173] W. Ermler, R. Ross, and P. Christiansen, Advan. Quantum Chem. **19**, 139 (1988).

[174] T. Leininger et al., Chem. Phys. Lett. **255**, 274 (1996).

[175] Z. Muszynski and N. G. Riabcev, J. Cryst. Growth **36**, 335 (1976).

[176] L. M. Foster, J. E. Scardefield, and J. F. Woods, J. Electrochem. Soc. **119**, 765 (1972).

[177] J. C. Woolley and B. A. Smith, Proc. Phys. Soc. B London **70**, 153 (1957).

[178] J. C. Woolley and B. A. Smith, Proc. Phys. Soc. B London **72**, 214 (1958).

[179] H. J. van Hook and E. S. Lenker, Trans. Met. Soc. AIME **227**, 220 (1963).

[180] E. E. Matyas, Phys. Stat. Solidi **42**, K129 (1977).

[181] J. F. Miller, H. L. Goering, and R. C. Himes, J. Electrochem. Soc. **107**, 527 (1960).

[182] R. L. Aulombard and A. Joullie, Mater. Res. Bull. **14**, 349 (1979a).

[183] K. Ishida, T. Shumiya, H. Ohtani, M. Hasebe, and T. Nishizawa, J. Less-Comm Met. **143**, 279 (1988).

[184] N. A. Goryunova, *The chemistry of diamond-like semiconductors*, MIT, Cambridge, 1965.

[185] G. B. Blom and T. S. Plaskett, J. Electrochem. Soc. **118**, 1831 (1971).

[186] C. Li, J. B. Li, Z. Du, L. Lu, and W. Zhang, J. Phase Eq. **22**, 26 (2001).

[187] R. Schmid-Fetzer, Bull. Alloy Ph. Diag. **10**, 527 (1989).

[188] R. C. Sharma and M. Srivastava, Calphad **16**, 387 (1992).

[189] R. C. Sharma and M. Srivastava, Calphad **16**, 409 (1992).

[190] Y. Jianrong and A. Watson, Calphad **18**, 165 (1994).

[191] L. G. Ferreira, S. H. Wei, and A. Zunger, Phys. Rev. B **40**, 3197 (1989).

[192] S. H. Wei, L. G. Ferreira, and A. Zunger, Phys. Rev. B **41**, 8240 (1990).

[193] L. Kaufman, J. Nell, K. Taylor, and F. Hayes, Calphad **5**, 185 (1981).

[194] G. B. Stringfellow, J. Phys. Chem. Solids **33**, 665 (1972).

[195] M. B. Panish and M. Ilegems, Prog. Solid State Chem. **7**, 39 (1972).

[196] J. Y. Shen et al., Calphad **19**, 215 (1995).

[197] I. V. Bodnar, Vesti Akad. Nauk B. SSR. SER. Khim. Nauk. **5**, 49 (1975).

[198] V. T. Bublik and V. N. Leikin, Phys. Stat. Sol. **46**, 365 (1978).

[199] K. Ishida, H. Tokunaga, H. Ohtani, , and T. Nishizawa, J. Crys. Growth **98**, 140 (1989).

[200] G. B. Stringfellow, J. Appl. Phys. **54**, 404 (1983).

[201] W. H. Zachariasen, Acta Cryst. **1**, 265 (1948).

[202] O. Janka and T. Schleid, Z. Anorg. Allg. Chem. **634**, 31 (2008).

[203] E. Buis et al., Nucl. Instr. and Meth. in Phys. Res. A **580**, 902 (2007).

[204] O. Selles, M. Fasoli, A. Vedda, M. Martini, and A. Gourier, Phys. Stat. Sol. C **4**, 1004 (2007).

[205] K. Ahn, R. Kremer, H. Mattausch, and A. Simon, J. Alloys and Comp. **303-304**, 257 (2000).

[206] M. D. Towler, TCM CRYSTAL basis set library, (http://www.tcm.phy.cam.ac.uk/mdt26/crystal.html)., 1996.

Formalia

Eidesstattliche Versicherung

Ich versichere hiermit an Eides Statt, dass ich die vorliegende Arbeit selbständig verfasst und die verwendeten Hilfsmittel angegeben habe.

Lebenslauf

Persönliche Angaben

Name: Pentin Ilya Vladimirovich

Geburtsdatum: 01. 04. 1982

Geburtsort: Moskau

Familienstand: ledig

Schulausbildung

1989 – 1996	Französische Grundschule 75 (1265), Moskau
1996 – 1999	Lyzeum 1533, Moskau

Studium

09/1999 – 01/2005	Diplom-Chemie an der Moskauer Staatliche Universität “M. W. Lomonosow”, Fakultät für Material-wissenschaft
09/2003 – 01/2005	Moskauer Staatliche Universität “M. W. Lomonosow”, Laboratorium für Chemische Thermodynamik: Diplomarbeit bei Prof. G.F. Voronin zun Thema “Zersetzung von Festköperlösungen der Cadmium-, Quecksilber- und Zink- Telluride ”
Seit 03/2005	MPI für Festköperforschung in Stuttgart: Anfertigung der Dissertation bei Prof. Martin Jansen zum Thema „Computational determination of low-temperature parts of the phase diagrams on ab initio level”.